The Dissertation Committee for Seong Jun Kim
certifies that this is the approved version of the following dissertation:

Numerical methods for highly oscillatory dynamical systems using multiscale structure

Committee:

Yen-Hsi Tsai, Supervisor

Björn Engquist

Kui Ren

Graeme Henkelman

Oscar Gonzalez

Numerical methods for highly oscillatory dynamical systems using multiscale structure

by

Seong Jun Kim, B.S.

DISSERTATION

Presented to the Faculty of the Graduate School of

The University of Texas at Austin

in Partial Fulfillment

of the Requirements

for the Degree of

DOCTOR OF PHILOSOPHY

THE UNIVERSITY OF TEXAS AT AUSTIN

August 2013

Dedicated to my family.

Acknowledgments

First and foremost, I am greatly indebted to my advisor, Yen-Hsi Richard Tsai, for his guidance, dedication, and patience throughout my study in Austin. His brilliance, keen insight and enthusiasm about Mathematics always kept me inspired and moved me forward. It has been an honor and a joy to work with him, and I hope that we may continue to collaborate for many years to come.

I wish to thank Björn Engquist, Kui Ren, Graeme Henkelman, and Oscar Gonzalez for serving on my committee and for taking the time to speak with me on many occasions. Special thanks to my collaborator, Gil Ariel, for the many helpful conversations we had about numerical treatments for dynamical and stochastic systems. I also thank Gil for arranging my visit to Tel Aviv and for being a tremendous mentor while I was there. His suggestions contributed greatly to the computational part of this thesis.

In addition, my graduate student colleagues helped me a lot, both mathematically and personally. I wish to thank the members of the Junior numerical analysis group. Thanks also to Korean students, Jinhyuk Choi, Kyudong Choi and Yoonsang Lee for their kind assistance during the life in Austin. I also feel fortunate to be a part of the graduate community at the Department of Mathematics which has enriched my professional life through

varied and memorable experiences. I would like to give a big thank to Dan Knopf and Sandra Catlett for their administrative support.

Lastly, I would like to thank my parents and my brother for the encouragement and support.

Numerical methods for highly oscillatory dynamical systems using multiscale structure

Publication No. _____

Seong Jun Kim, Ph.D.
The University of Texas at Austin, 2013

Supervisor: Yen-Hsi Tsai

The main aim of this thesis is to design efficient and novel numerical algorithms for a class of deterministic and stochastic dynamical systems with multiple time scales. Classical numerical methods for such problems need temporal resolution to resolve the finest scale and become, therefore, inefficient when the much longer time intervals are of interest. In order to accelerate computations and improve the long time accuracy of numerical schemes, we take advantage of various multiscale structures established from a separation of time scales.

This dissertation is organized into four chapters: an introduction followed by three chapters, each based on one of three different papers. The framework of the heterogeneous multiscale method (HMM) is considered as a general strategy both for the design and the analysis of multiscale methods.

In Chapter 2, we consider a new class of multiscale methods that use a technique related to the construction of a Poincaré map. The main idea is to construct effective paths in the state space whose projection onto the slow subspace shows the correct dynamics. More precisely, we trace the evolution of the invariant manifold $\mathcal{M}(t)$, identified by the level sets of slow variables, by introducing a slowly evolving effective path which crosses $\mathcal{M}(t)$. The path is locally constructed through interpolation of neighboring points generated from our developed map. This map is qualitatively similar to a Poincaré map, but its construction is based on the procedure which solves two split equations successively backward and forward in time only over a short period. This algorithm does not require an explicit form of any slow variables.

In Chapter 3, we present efficient techniques for numerical averaging over the invariant torus defined by ergodic dynamical systems which may not be mixing. These techniques are necessary, for example, in the numerical approximation of the effective slow behavior of highly oscillatory ordinary differential equations in weak near-resonance. In this case, the torus is embedded in a higher dimensional space and is given implicitly as the intersection of level sets of some slow variables, e.g. action variables. In particular, a parametrization of the torus may not be available. Our method constructs an appropriate coordinate system on lifted copies of the torus and uses an iterated convolution with respect to one-dimensional averaging kernels. Non-uniform invariant measures are approximated using a discretization of the Frobenius-Perron operator. These two numerical averaging strategies play a central role

in designing multiscale algorithms for dynamical systems, whose fast dynamics is restricted not to a circle, but to the tori. The efficiency of these methods is illustrated by numerical examples.

In Chapter 4, we generalize the classical two-scale averaging theory to multiple time scale problems. When more than two time scales are considered, the effective behavior may be described by the new type of slow variables which do not have formally bounded derivatives. Therefore, it is necessary to develop a theory to understand them. Such theory should be applied in the design of multiscale algorithms. In this context, we develop an iterated averaging theory for highly oscillatory dynamical systems involving three separated time scales. The relevant multiscale algorithm is constructed as a family of multilevel solvers which resolve the different time scales and efficiently computes the effective behavior of the slowest time scale.

Table of Contents

List of Tables

List of Figures

Chapter 1

Introduction

Multiscale problems, with different dominant behaviors across multiple time or length scales, are becoming increasingly prevalent in various areas of research such as mechanics, astronomy, chemistry, molecular dynamics and numerical analysis. The fundamental motivation for the study of such problems is the desire to understand, qualitatively, the long time (macroscopic) behavior of solutions of stiff differential equations. The theory of numerical methods for stiff equations has been widely discussed by many authors, and much of the computational efforts have concentrated on implicit methods. Such efforts focus on enlarging the region of absolute stability, but implicit methods themselves require solving a nonlinear equation accurately at each time step, which requires expensive cost with very small stiff parameters. From a different viewpoint with the former, we have found that in many situations the long time behavior of the stiff systems can be described adequately by an effective model that does not require small time steps. Keeping this in mind, we proceed with the coupling of different models in different scales. This kind of philosophy will be applied to our overall methods that surpass a single scale.

Two examples of multiscale problems discussed below exhibit different

behaviors as the scales involved changed. One example from chemical kinetics is the enzyme-substrate reaction. The laws of mass action and mass conservation describe the evolution of concentration via a dynamical system, in which the initial part of the trajectories approaches the attractor in a transient way. Thus, from a computational point of view, time steps should be sufficiently small enough to resolve the transient when explicit solvers are used. Another example, pointed out by G. Dahlquist, is the drift path of a mechanical alarm clock due to its shaking and rattling when it is in motion on a hard surface. Fast vibrations are present for all times and may interact to give contributions to the slower movement.

There are various analytical techniques to address multiscale problems. Using the tools of asymptotic analysis, we can introduce averaging and homogenization methods based on multiscale expansion. Matched asymptotics is a systematic way of approximating solutions to problems whose solutions have rapid behavior in localized regions. In the study of global properties of a dynamical system, important mathematical theories are the ergodic theory, the Liouville theorem, the Poincaré-Bendixon theorem and the KAM theory.

The motivation for developing numerical algorithms for a class of highly oscillatory dynamical systems came independently from the long time computation of oscillatory Hamiltonian systems. There is an active field of study known as geometric integrations which preserve geometric properties of the exact flow of a differential equation. As an example, symplectic integrators conserve the energy, and they have at most a linear error growth for inte-

grable systems [55]. However, this theory breaks down in the presence of high oscillations, when the product of the highest frequency with the step size is not small enough. Detailed reviews and further references can be found in [21, 59, 62, 83],[55, 78, 95] and [27].

In this thesis, we present essential techniques for constructing numerical multiscale methods for highly oscillatory ordinary differential equations (ODEs) and stochastic differential equations (SDEs), including non-Hamiltonian systems that are not solvable by the standard geometric integrators. These techniques reduce the computational effort so that the long time behavior of dynamical systems can be performed using a personal computer in acceptable time.

1.1 Why are multiscale problems difficult to simulate?

In most of the cases, the solution of a differential equation cannot be explicitly given in a closed form by functions that can be evaluated directly. We therefore must rely on numerical computations that approximate the solution of a differential equation to any desired accuracy.

The common feature of the multiscale problem we are interested in is the separation of scales., i.e., the number $0 < \epsilon \ll 1$ has been used to parametrize the scales involved. In highly oscillatory dynamical systems to be considered, the fastest time scale involves oscillations with frequencies at the order of ϵ, which means that oscillations' quasi-period is a function of ϵ. The computational time domain is $[0, \epsilon^{-m}T]$ with $m \geq 0$, T independent

of ϵ. As an example, a highly oscillatory solution in Hamiltonian systems typically arises when the potential energy is given by a sum of $U + V_\epsilon$, where the Hessian of V_ϵ has positive eigenvalues in terms of ϵ^{-1} that are much larger compared with those of U. It is immediately evident that problems with highly oscillatory solutions are much more difficult to simulate since the fast oscillations are present for all times and may interact to give contributions to the slow behaviors.

Traditional numerical algorithms for dynamical systems can be categorized into one-step methods, e.g. the Euler method and the Runge-Kutta method, and multi-step methods, e.g. the Adams methods and methods using the backward differentiation formulas. Major limitations of the traditional algorithms are high computational costs and not being guaranteed convergence of long time simulation. Much of the following sections are devoted to these issues.

1.1.1 High computational complexity

An important aspect of numerical analysis is the determination of the computational complexity of a given algorithm. With traditional numerical methods, very small time steps would be required for the reasons of both accuracy and stability requirement. In particular, the local truncation error which measures the accuracy of the method is given in the power of $\epsilon^{-1}h$. For stability, the set of values $C\epsilon^{-1}h$ with $C \in \mathbb{C}$ should be contained in the region of absolute stability which may be a bounded set in the complex plane.

In other words, the integrator imposes restrictions on the step size h to be of order ϵ. This fact implies that the computational complexity is at least of the order of ϵ^{-m-1} for the computational time domain $[0, \epsilon^{-m}T]$. Note that this previous estimate is only a lower bound for the actual computational cost. The situation is even worse in practice.

With this notion, it is clear that a sensible method generates accurate approximation with a complexity sublinear to ϵ^{-m-1}. In this context, the proposed methods in Chapter 2-4 will focus on this sublinear scaling complexity.

1.1.2 Exponential error growth in long time simulation

This section is devoted to the analysis of the error growth in the numerical integration by the traditional algorithms to stiff differential equations. We study the global error bound without considering round-off error. Let x_n denote an approximation to the solution $x(t_n)$ at t_n. In nonstiff problems, the classical results for the linear multistep methods [76] and for the Runge-Kutta methods [56] can be expressed as

$$\left|x_{T/h} - x(T)\right| \leq Ch^p \left(e^{LT} - 1\right) \tag{1.1.1}$$

where a method has an order p with the step size h, C and L are positive constants, and a calculation is established over the time interval $[0, T]$. The error bound (1.1.1) implies that the global error decreases as h goes to 0 for a fixed T. However, due to the exponential dependence on the final time T, the error may be exponentially and explosively amplified in a long time simulation.

On the consideration of stiff problems, errors from the fast timescale are accumulated intensively. The corresponding error bound is given by

$$\left|x_{T/h} - x(T)\right| \leq C\epsilon^{-1}h^p\left(e^{\epsilon^{-1}LT} - 1\right). \tag{1.1.2}$$

Therefore as ϵ shrinks, the much smaller h should be used to guarantee the convergence. To make it worse, if the computation is conducted over the longer time interval $[0, \epsilon^{-m}T]$, the term $e^{\epsilon^{-1-m}LT}$ becomes extremely large. This leads to unacceptable inaccuracies, regardless of the size of h. An important reason is that bounds on the stability factors grow exponentially with time in general, for much the same reason that general a priori error bounds grow exponentially except for the geometric integrators which have only linear growth for the applicable equations.

Of course the bounds in (1.1.1) and (1.1.2) are nearly always excessively conservative. However, the bounds are helpful in our understanding of how local errors propagate differently between nonstiff and stiff problems.

1.2 Systematic construction of multiscale methods

By explicitly taking advantage of the separation of scales, multiscale methods become much more efficient than solving the full scale problem. *One way to improve long time numerical integrations is to utilize geometric structures in the system of interest.*

For convenience, it is preferable to change the time variable so the slowest time scale of interest is independent of the small parameter ϵ. Accordingly,

the computational domain $[0, \epsilon^{-m}T]$ is rescaled to $[0, T]$ by replacing t by $\epsilon^{-m}t$ where T is the final time which is independent of ϵ. We aim at the computation of the effective long time properties of the dynamical system,

$$\frac{d}{dt}x = \sum_{i=0}^{m+1} \epsilon^{-i} f_i(x), \quad x(0) = x_0 \in \mathcal{D}_0 \subset \mathbb{R}^d, \tag{1.2.3}$$

where we assume that the solution of (1.2.3) remains in a domain $\mathcal{D}_0 \subset \mathbb{R}^d$ which is bounded independent of ϵ for all $t \in [0, T]$. For fixed ϵ and initial condition x_0, the solution of (1.2.3) is denoted $x(t; \epsilon; x_0)$.

In many situations, one is interested only in a set of slowly changing quantities that are derived from the solutions of the given stiff system (1.2.3). Slow variables ξ of a dynamical system (1.2.3) can be defined as below when $m = 0$.

Definition 1.2.1. Let $x(t) \in \mathcal{D}_0$ denote the solution of (1.2.3). A smooth function $a(t)$ is to be *slow* if $|da/dt| \leqq C$ for some constant C independent of ϵ in $t \in [0, T]$. Moreover, a smooth function $\xi(x) : \mathcal{D}_0 \to \mathbb{R}$ is called a *slow variable* with respect to $x(t)$ if $\xi(t) = \xi(x(t))$ is slow.

Formally, slow variables of a dynamical system involving three or more time scales are defined as [7].

Definition 1.2.2. A smooth time dependent function $\alpha : [0, T] \mapsto \mathbb{R}$ is said to *evolve on the ϵ^k time scale in* $[0, T]$ for some integer k and for $0 < \epsilon \leq \epsilon_0$, if there exists a smooth function $\beta : [0, T] \mapsto \mathbb{R}$ and constants C_0 and C_1 such

that

$$\sup_{t\in[0,T]}\left|\frac{d}{dt}\beta(t)\right| \leq C_0\epsilon^{-k} \quad \text{and} \quad \sup_{t\in[0,T]}|\alpha(t)-\beta(t)| \leq C_1\epsilon.$$

Definition 1.2.3. A function $\xi(x)$ is said to *evolve on the ϵ^k time scale along the trajectories of* (4.1.6) *in* $[0,T]$ if the time dependent function $\xi(x(t;\epsilon,x_0))$ evolves on the ϵ^k time scale in $[0,T]$. For brevity, we will refer to variables that evolve on the ϵ^0 time scale as slow.

In Chapter 2, we propose a strategy to construct multiscale ODE/SDE methods in the case $m = 0$. In Chapter 4, we will deal with the case integer $k \geq 1$. We remark however that there of course exist dynamical systems whose multiscale features are not integer powers of ϵ, and these general systems will be discussed in Chapter 3. Throughout this section, we consider the case $m = 0$ for brevity.

In many problems, for autonomous systems, there exists a diffeomorphism $\Psi : x \to (\xi(x), \phi(x))$ of (1.2.3) from $\mathbb{R}^d$ onto $\mathbb{R}^{d-p} \times \mathcal{M}$ is constructed so that a corresponding slow-fast system is

$$\begin{cases} \dot{\xi} = g_0(\xi,\phi), & \xi(0) = \xi_0, \\ \dot{\phi} = \epsilon^{-1}g_1(\xi,\phi) + g_2(\xi,\phi), & \phi(0) = \phi_0, \end{cases} \tag{1.2.4}$$

and all smooth slow variables depends on ξ up to some bounded lower order perturbative terms. Moreover, the invariant manifold $\mathcal{M}$ is assumed to be defined as below.

Assumption 1. *The invariant manifold* $\mathcal{M}$ *is given as the level sets of* ξ_1,ξ_2,$\cdots$,ξ_{d-p} *which are slow variables with respect to* $x(t)$*. Thus, for each time* t*, we may identify the manifold as*

$$\mathcal{M}(t) = \cap_{j=1}^{p}\{z \in \mathbb{R}^d : \xi_j(z) = \xi_j \circ z(t)\}.$$

In this thesis, since we consider highly oscillatory dynamical systems, for fixed ξ*, the fast variable* ϕ *is restricted in the manifold* $\mathcal{M}$ *which is diffeomorphic to an* n *dimensional torus* $\mathbb{T}^p = \underbrace{S^1 \times S^1 \times \cdots \times S^1}_{p}$ *with* $d > p \geq 1$*. This is equivalent that for fixed* ξ*, the fast variable* ϕ *is restricted in the manifold* $\mathcal{M}$ *which is diffeomorphic to an* n *dimensional torus. In this context, we shall write* $(\xi, \phi) \in \mathbb{R}^{d-p} \times \mathbb{T}^p$ *with* $\xi \in \mathbb{R}^{d-p}$ *and* $\phi \in \mathbb{T}^p$*.*

Our main interest is to construct and analyze numerical solvers that integrate the system

$$\frac{d}{dt}\xi = F(\xi, D), \tag{1.2.5}$$

where D is the data that can be computed by solving (1.2.3) locally in time. ξ may be some function or functional of x and describes some effective behavior of (1.2.3) that is of relevance to the application. Since F is not explicitly available in many situations, we have set up a formal numerical discretization for (1.2.5) to evaluate F from short time histories of x with properly chosen initial conditions. Detailed explanations will be given in the following sections.

1.2.1 Abstract multiscale algorithm structure

The general philosophy of our algorithm is based on the heterogeneous multiscale method (HMM) for highly oscillatory ordinary differential equations [3, 36]. We are interested in the macroscopic behavior of a system which is specified by the variable ξ. However, the macroscopic model is not explicitly known in general. To solve the incomplete macroscale model, we extract the needed data from the microscale model for the state variable x, i.e., the macroscopic behavior of dynamical systems is captured with the help of the microscopic model.

Let's go back to our example considering the drift path of a mechanical alarm clock since that provides us with a better understanding of the motivation behind the HMM. The main difference with the other example from chemical kinetics is that the fast variable oscillates rapidly instead of approaching a fixed manifold for each slow variable ξ. Formally, the equation of motion for an active alarm clock may be given by

$$\begin{cases} \xi' &= \phi, \\ \phi' &= \epsilon^{-1} g_1(\xi, \phi), \end{cases} \tag{1.2.6}$$

where the slow variable ξ is the displacement and the fast variable ϕ is the velocity. It seems that the slowly changing quantity ξ depends only locally in time on the fast oscillations. Thus, using a very informal argument, we expect that the averaged effect of the velocity is locally felt on the slow time scales. In this context, it is reasonable to devise a scheme that tracks the slow quantities by measuring the effects of the fast solutions only locally in time. Thus, we

will discuss how to correctly track the dynamics for those slowly changing quantities by computing fast oscillations only in very short time intervals.

We will generalize the scope of this type of algorithms by providing a more general systematic analysis that is applicable to a much wider class of applications including some systems from molecular dynamics. In the HMM framework [3, 5, 42], we assume a macroscopic model

$$F(\xi, D) = 0, \;\; \xi \in \Omega_{(M)} \tag{1.2.7}$$

which may not be explicitly given, but can be evaluated with a help of a given microscopic model,

$$f(x, d) = 0, \;\; x \in \Omega_{(m)} \tag{1.2.8}$$

where x are the microscopic variables. $D = D(x)$ and $d = d(\xi)$ denote the set of data or auxiliary conditions that further couple the macro- and microscopic models. Model (1.2.7) is formally discretized at a macroscopic scale, and the adopted numerical scheme dictates when the necessary information $D(x)$ should be acquired from solving (1.2.8), locally on the microscopic scale with auxiliary conditions $d(\xi)$. As part of $d(\xi)$ and $D(x)$, the macro- and microscopic variables are related by reconstruction and compression operators:

$$\mathcal{R}(\xi, D_R) = x, \;\; \mathcal{Q}(x) = \xi, \;\; \mathcal{Q}(\mathcal{R}(\xi, D_R)) = \xi, \tag{1.2.9}$$

where D_R are the needed data that can be evaluated from x;

Errors of this type of schemes generally take the structure

$$\text{Error} = E_H + E_h + E_{HMM},$$

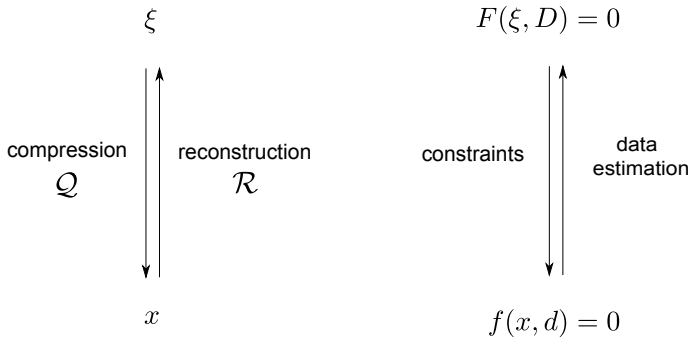

where E_H is the error of the macroscopic model (1.2.7), E_h is the errors from solving (1.2.8), and E_{HMM} contains the errors in the the multiscale model, including the passing of information through $\mathcal{R}$ and $\mathcal{Q}$. This approach has been used in a number of applications, such as contact line problems, epitaxial growth, thermal expansions, combustion [36], as well as homogenizations of wave propagation in long time intervals [41], and coupling network models for macroscopic multiphase flows in porous media [25, 26].

Figure 3.1 shows a typical structure of such a algorithm. In our context, an ODE solver for ξ lies on the upper axis and constructs approximations of ξ at the grid points depicted there. The fine meshes on the lower axis depict the very short evolutions of (1.2.3) with initial values determined by $\mathcal{R}(\xi(t_n))$. The reconstruction operator then takes each short time evolution of x and evaluates F and ξ. The algorithms in [34],[48], and [92] are also of a similar structure. As a simple example, the forward Euler scheme applied to (1.2.5) would appear to be

$$\xi_{n+1} = \xi_n + H \cdot F(\xi_n), \tag{1.2.10}$$

where F contains the passage of $\mathcal{Q}\Phi_t\mathcal{R}(\xi_n)$; reconstruction $\mathcal{R}$, evolution Φ_t,

and compression $\mathcal{Q}$, and H is the step size. If each evolution Φ_t of the full scale system (1.2.3) is reasonably short, the overall complexity of such type of solvers would be smaller than solving the stiff system (1.2.3) for all time, thereby gaining computational efficiency.

Essential questions that need to be resolved for each scheme include:

- If only the microscopic model is given, how to systematically derive a corresponding macroscopic model for the application in question? What are $\mathcal{R}$ and $\mathcal{Q}$?
- With the system for x, and a choice of $\xi(x)$, is F well-defined by the procedure defined above? If not, how can it be properly defined?
- How long should each evolution be computed?
- What do consistency, stability, and convergence mean?

For a fixed ϵ, all well known methods, assuming $\xi = x$, will converge as the step-size $H \to 0$, and there is no difference between stiff and non-stiff problems. In the related work [3, 5, 42], convergence for stiff problems ($\epsilon \ll H$) is defined by the following relation: For the error

$$E(H) = \max_{0 \le t_n \le T} (\sup_{0 < \epsilon < \epsilon_0(H)} |\xi(t_n) - \xi_n|), \tag{1.2.11}$$

we have that $E(H) \to 0$ as $H \to 0$. Here, $\epsilon_0(H)$ is a positive function of H, serving as an upper bound for the range of ϵ, and $\xi(t_n)$ and ξ_n denote respectively the analytical solution and the discrete solution at t_n.

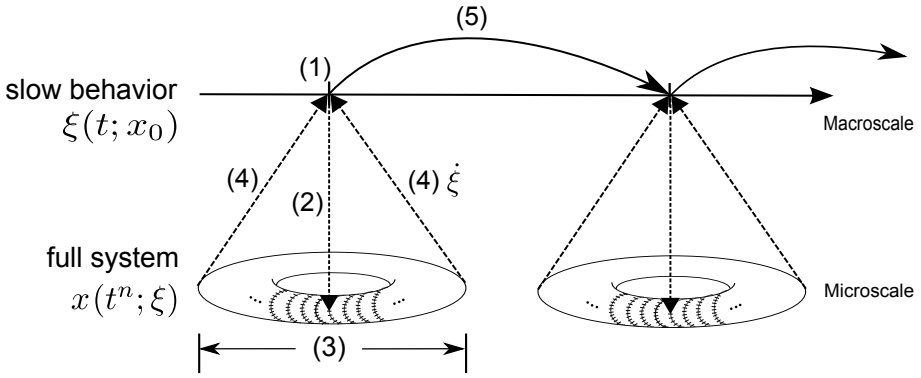

Figure 1.1: A typical structure of the proposed multiscale algorithm.

The above procedures algorithmically consist of the following three components:

1. Force estimation for the slow variable:

   (1) At $T = t_n$, ξ_n is given.

   (2) Reconstruction: at $T = t_n$, $\mathcal{R}(\xi_n) \mapsto x_n$.

   (3) Solve for the micro state variables: $x_n(t)$, for $t \in [t_n - \frac{\eta}{2}, t_n + \frac{\eta}{2}]$, with $x_n(t_n) = x_n$.

   (4) Compression and estimate force: $U_* = Q[x_n]$. Approximate $\xi'(t_n)$ using an appropriate data estimation.

2. Evolve the macro variables: (5) $\{U_n\} \cup \{U_*\} \to U_{n+1}$, $T = t_{n+1}$.

3. Repeat.

Several remarks can be made as follows. Computational efficiency lies in how long (3) is run and the complexity of (4). We assume that the trajectory

passing through $x_n \in \mathcal{D}_0$ are ergodic on some invariant manifold $\mathcal{M}(x_n) \subset \mathcal{D}_0$ which is given implicitly as the intersection of level sets of slow variables. Therefore, the fast variables in (1.2.4) are locally ergodic with respect to a family of measures μ drifted by slow variables, i.e., *the microscale model has some particular features that we can take advantage of.* The invariant manifold in (3) is described by the torus in Figure 3.1 since we consider highly oscillatory dynamical systems. For the data estimation in (4), we shall see in Chapter 2-4 that these slowly changing quantities may be evaluated conveniently by various averaging techniques with suitable kernels. An analytical motivation for these techniques will be given in the following section. Another challenge is that the torus may be embedded in a higher dimensional space and a parametrization of the torus is not available.

1.2.2 Averaging and ergodicity

Averaging and ergodic theories are parts of the theory of dynamical systems. We start with the definition of ergodicity.

Definition 1.2.4. A dynamical system is called ergodic if it has a unique invariant measure.

Let φ^t denote the solution operator for the fast equation (1.2.4).

Theorem 1.2.1. If g is integrable on a manifold $\mathcal{M}$ and the dynamics of ϕ is ergodic on $\mathcal{M}$ with the invariant measure μ, then the time average of a function

g exists for μ-a.e. $\phi \in \mathcal{M}$, and coincides with the space average

$$\lim_{T\to\infty} \frac{1}{T} \int_0^T g\left(\varphi^t(\phi_0)\right) dt = \int_{\mathcal{M}} g(\phi)\mu(d\phi).$$

See [11, 91, 93] for the proof. It is interesting to point out that time average converges to a value which is independent of the initial condition. Theorem 1.2.1 implies that it is equivalent to look at the distribution of ϕ either at a given moment in time or along one long time trajectory.

From a computational point of view, averaging methods inspire efficient numerical schemes for integrating the slow components of slow-fast systems (1.2.4) without fully resolving all fast oscillations in $[0, T]$. A wide range of applications require numerical averaging over the invariant measure of an ergodic dynamical system [11, 93].

1.2.2.1 Ordinary differential equations

We recall a class of system that has an explicit slow-fast grouping in the solution's components (1.2.4),

$$\begin{cases} \dot{\xi} = f(\xi, \phi), & \xi(0) = \xi_0, \\ \dot{\phi} = \epsilon^{-1} g_1(\xi, \phi) + g_0(\xi, \phi), & \phi(0) = \phi_0. \end{cases} \tag{1.2.12}$$

We assume that, for fixed ξ, the fast variable ϕ is locally ergodic on $\mathcal{M}$ with respect to a family of measures $\mu_\xi(d\phi)$ drifted by slow variables. In this case, the averaging theorem [90, 93] states that $\xi(t)$ converges to a solution of the

averaged equation as $\epsilon \to 0$. Formally, $\xi(t)$ is approximately described by the averaged equation:

$$\dot{\bar{\xi}} = \bar{f}(\bar{\xi}), \quad \bar{\xi}(0) = x_0 \tag{1.2.13}$$

where

$$\bar{f}(\bar{\xi}) = \int f(\bar{\xi}, \phi)\mu_{\bar{\xi}}(d\phi). \tag{1.2.14}$$

Furthermore, the approximation is of order ϵ in the sup norm, i.e.

$$\sup_{0 \le t \le T} |\xi(t) - \bar{\xi}(t)| = \mathcal{O}(\epsilon).$$

This elementary result has been generalized considerably to include, for example, chaotic and stochastic systems [12, 19, 20, 66, 69, 89, 91, 93].

It is immediately clear that (1.2.13) is more preferable to simulate the evolution of $\xi(t)$, provided one is able to compute analytically the force $\bar{f}(\bar{\xi})$. In general, this cannot be done because the dynamics of the fast variable ϕ is too complicated. The motivation for estimating the forces leads us to devise numerical methods equipped with multiscale integrations.

1.2.2.2 Stochastic differential equations

Another interesting example of a multiscale methodology is in the work of Vanden-Eijnden on stochastic systems or systems on long time scales for which the stochastic effects are important [101]. Stochastic processes and diffusion theory are the mathematical underpinnings of many scientific disciplines, including statistical physics, physical chemistry, molecular biophysics, communications theory, and many more [96]. This section reviews the basic

averaging theories of multiscale stochastic processes, mostly focusing on the advective time scale which is independent of ϵ. We will address the following question: how to characterize long-time behavior of SDEs?

We consider a slow-fast system of SDEs,

$$\begin{cases} dx = f(x,y)dt, & x(0) = x_0, \\ dy = \epsilon^{-1} g(x,y)dt + \epsilon^{-1/2}\beta(x,y)dW, & y(0) = y_0 \end{cases} \tag{1.2.15}$$

where $(x,y) \in \mathbb{R}^{d-p} \times \mathbb{R}^p$, dW is the standard Gaussian white noise, and $f(\cdot) \in \mathbb{R}^{d-p}$, $g(\cdot)$, $\beta(\cdot) \in \mathbb{R}^p$ are $\mathcal{O}(1)$ functions in ϵ. In other words, we have assumed that the phase space can be decomposed into slow variables x and fast ones y. Systems of (1.2.15) arise from molecular dynamics, chemical kinetics, material sciences, atmospheric and ocean sciences [37, 38, 101].

Similar to Section 1.2.2.1, we assumed that, for fixed $x = X$, the fast equation

$$dy = \epsilon^{-1} g(X,y)dt + \epsilon^{-1/2}\beta(X,y)dW \tag{1.2.16}$$

is ergodic. A stochastic process is called ergodic if it has a unique invariant measure. Then the probability distribution function of the solution y of (1.2.16), denoted $\rho^*(Y;X)$, satisfies two differential partial differential equations (PDEs). One with respect to the "forward variables" and one with respect to the "backward variables". The former is called the *Fokker-Planck equation* or the forward Kolmogorov equation, and the latter is called the backward Kolmogorov equation. See [96], [90] for more details.

The corresponding Fokker-Planck equation is given by

$$\frac{\partial \rho}{\partial t} + \epsilon^{-1}\frac{\partial (g(X,Y)\rho)}{\partial Y} = \epsilon^{-1}\frac{\beta^2(X,Y)}{2}\frac{\partial^2 \rho}{\partial Y^2}. \tag{1.2.17}$$

We point that the drift term in (1.2.16) shows up as an advection term for (1.2.17), that the standard Gaussian white noise in in (1.2.16) shows up as a diffusion term for (1.2.17), and that the computational cost remains due to the stiff parameter ϵ^{-1}.

An important theorem [69, 89] implies that the effective dynamics for the slow variable x is obtained by averaging the RHS of dx/dt with respect to the conditional equilibrium distribution of y:

$$\frac{d\bar{x}}{dt} = \bar{f}(\bar{x}), \quad \bar{x}(0) = x_0$$

where $\bar{f}(x) = \int f(x,y)\mu_x(dy) = \int f(x,y)\rho^*(y;x)dy$. The result of the procedure is a deterministic macroscopic equation in the limit of $\epsilon \to 0$,

$$\begin{cases} dx = f(x,y)dt, \\ dy = \epsilon^{-1}g(x,y)dt + \epsilon^{-1/2}\beta(x,y)dW, \end{cases} \longrightarrow \quad \frac{d\bar{x}}{dt} = \bar{f}(\bar{x}).$$

However, the microscopic system can be either deterministic or stochastic. We only require ergodicity of the fast dynamics, which result in the uniqueness of the steady state of the Fokker-Planck operator for each value of $x = X$. The challenge for numerical methods is to efficiently sample the invariant measure.

1.2.3 Averaging kernel

We review the well-known kernel averaging that evaluates slowly changing quantities in ODEs [3, 5, 6, 42] and SDEs [37, 101]. Performing averages over fast oscillations can be approximated in a convenient and computationally efficient way by convolution of dx/dt with appropriate compactly supported

kernels. Inside the convolution, the value of x is not exactly fixed but varies following the correct dynamics. This subtle change in the values of $x(t)$ allows for the kernel to capture the correct effective change of $x(t)$ in a longer time scale.

In the ODE case, we assume that for a fixed slow variable, the fast variable is restricted in the manifold $\mathcal{M}$ which is diffeomorphic to an one dimensional torus $\mathbb{T}^1$. The fast dynamics can be viewed as a complete rotation over a circle.

Let $\mathbb{K}^{p,q}$ denote the space of normalized C^q functions, supported on $[-1,1]$ that have p vanishing moments, i.e.,

$$\int_{[-1,1]} K(t)t^r dt = \begin{cases} 1, & r = 0, \\ 0, & 1 \leq r \leq p. \end{cases} \tag{1.2.18}$$

Furthermore, for $\eta > 0$, let K_η denote a scaling of $K(t)$ to $[-\eta, \eta]$,

$$K_\eta(t) = \frac{1}{\eta} K\left(\frac{t}{\eta}\right).$$

Then $\bar{f}$ in (1.2.13) can be obtained efficiently with the help of averaging kernel K.

Theorem 1.2.1. Let $f(t) = f(t, \epsilon^{-1}t)$, where $f(t,s)$ is 1-periodic in s and $\partial f(t,s)/\partial t^r$ is continuous for $r = 0, \cdots, p$. For any $K \in \mathbb{K}^{p,q}$, there exist nonnegative constants C_1 and C_2, independent of ϵ and η, such that

$$\left| K_\eta * f(t) - \bar{f}(t) \right| \leqq C_1 \eta^p + C_2 (\frac{\epsilon}{\eta})^q.$$

We refer to the proof of [42]. Two commonly used kernels are:

- Exponential kernel $K^{\exp} \in \mathbb{K}^{1,\infty}$,

$$K(t) = 422.11 \cdot \exp\left[5\left(t^2-1\right)^{-1}\right] \cdot \chi_{[-1,1]}(t).$$

- Cosine kernel $K^{\cos} \in \mathbb{K}^{1,1}$,

$$K(t) = \frac{1}{2}\left[1+\cos(\pi t)\right] \cdot \chi_{[-1,1]}(t).$$

In the SDE case, on the $\mathcal{O}(1)$ time scale (advective time scale), suppose that the dynamics for Y with $X = x$ fixed has an invariant probability measure $\mu_x(dy)$ and that the following limit exists,

$$\bar{f}(x) = \lim_{\epsilon \to 0} \int f(x,y)\mu_x(dy).$$

See the discussion in Section 1.2.2.2. Then, the averaged $\bar{f}(X_n)$ can be approximated by the following time and ensemble average [37, 101]:

$$\tilde{f}_n = \frac{1}{MN}\sum_{j=1}^{M}\sum_{m=1}^{N} f(X_n, Y_{n,m,j}) = \sum_{j=1}^{M} K(t_m) f(X_n, Y_{n,m,j})$$

where M is the number of replicas, N is the number of steps in the time averaging and the kernel function $K(\cdot)$ is defined by

$$K(t) = \frac{1}{M}\chi_{[0,t_M]}(t),$$

which is usually referred to as a naive kernel.

1.3 Related works

Detailed reviews and further references on this active field of geometric integration can be found in [21, 59, 62, 83],[55, 78, 95], and [27]. Another

approach based on asymptotic expansions in inverse powers of the oscillatory parameter is given in [28] and references within.

The impulse method [47] for Newtonian dynamics splits the force field into fast and slow parts. As with the conventional splitting strategy, the basic impulse algorithm then integrates alternately in time intervals of equal length, the fast equation and the slow equation; the integration for the fast equation starts with the solution generated by the slow equation, and vice versa. In the context of impulse method, it is assumed that the slow part of the vector field comes from long range interaction potential and is relatively costly to evaluate compared to the fast force.

FLAVORS [99] integrate the whole system and the split non-stiff system alternately as well. More precisely, during the integration, stiff forces in the given system are "turned on" over a microscopic time interval time and then "turned off" over a mesoscopic time step. As in the impulse method, the solution produced at the end of a microscopic interval by "turning on" the stiff force in the system is continued by serving as the initial condition for the whole system in the following mesoscopic time integration.

The equation-free approach [9, 68] is also very similar to that of the extended multi-grid method and HMM. Its basic strategy is to link simulations of the microscopic models on small spatio-temporal domains in order to mimic the behavior of a system at large scale. This is done by interpolation (in space) and extrapolation (in time) of ensemble-averaged macroscale variables obtained from the microscopic simulations. It consists of a set of

techniques including coarse bifurcation analysis, projective integrators, the gap-tooth scheme and the patch dynamics [68]. At an abstract level, equation-free is built on a three-stage lift-evolve- restrict coarse time-stepper procedure [68].

In the use of Young measures [12, 13], the situations in which the fast dynamics tend to fixed points, periodic solutions, or chaotic solutions can be treated in a unified manner. The general philosophy is to analyze the behavior of a fast dynamics drifted along with a slow movement by computing limit cycles as $\epsilon \to 0$, describing the invariant measures supported on them as a Young measure, and progressing via averaging with respect to which induces the equation for the slow dynamics.

The seamless multiscale method does not require changing a focus here and there between the macro- and micro-states of the system [39]. The main idea is to artificially modify the time scale of the microscale problem, and solve the macroscale model and the modified microscale model simultaneously, i.e., the macro- and the micro-solvers runs with its own time-step, and both are not identical. The accuracy and efficiency are generally comparable to those of HMM.

In this paper, we will be concentrated on the case that for fixed x, the fast variable y is restricted in the manifold $\mathcal{M}$ which is diffeomorphic to an n dimensional torus $\mathbb{T}^p = (S^1)^n$ with $p > 1$.

1.4 Overview

In the following chapters, a multiscale method for computing the effective behavior of a class of highly oscillatory ODEs and SDEs is presented. we are also concerned with the analysis of efficient numerical methods for the dynamical system with disparate time scales. Consider the computation of the effective long time properties of the dynamical system;

$$\frac{d}{dt}x = \sum_{i=0}^{m+1} \epsilon^{-i} f_i(x), \quad x(0) = x_0 \in \mathcal{D}_0 \subset \mathbb{R}^d, \tag{1.4.19}$$

and a corresponding slow-fast system;

$$\begin{cases} \dot{\xi} = g_0(\xi, \phi), & \xi(0) = \xi_0, \\ \dot{\phi} = \epsilon^{-1} g_1(\xi, \phi) + g_2(\xi, \phi), & \phi(0) = \phi_0 \end{cases} \tag{1.4.20}$$

where the slow variable ξ is in $\mathbb{R}^{d-p}$ and the fast variable ϕ is restricted in the manifold $\mathcal{M}$ which is diffeomorphic to $\mathbb{T}^p = S^p$ for each fixed ξ.

In Chapter 2, we propose a new strategy to construct multiscale methods for ODE/SDE in the case $m = 0$ and $p = 1$. In particular, we consider dynamical systems, in which an underlying diffeomorphism $\Psi : x \to (\xi(x), \phi(x))$ of (1.4.19) from $\mathbb{R}^d$ onto $\mathbb{R}^{d-1} \times \mathbb{T}^1$ is implicitly given.

In Chapter 3, efficient techniques for numerical averaging over a higher dimension torus ($m = 1$, $p > 1$) will be given. A torus is defined by ergodic dynamical systems which may not be mixing. These thechniques are necessary, for example, in the numerical approximation of the effective behavior of highly oscillatory ordinary differential equations in near resonance. Dynamical systems whose multiscale features are not integer powers of ϵ will be discussed.

In Chapter 4, we generalize the framework of averaging kernels presented in Section 1.2.3 to include three or more time scales. In particular, we deal with the case integer $m = 1$ and an underlying diffeomorphism $\Psi : x \to (\xi(x), \phi_1(x), \phi_2(x))$ of (1.4.19) from $\mathbb{R}^d$ onto $\mathbb{R}^{d-2} \times \mathbb{T}^1 \times \mathbb{T}^1$ is implicitly given. An equation in a generalized form of (1.4.20) is analyzed by an iterated averaging techniques, and we devise a numerical method using tiered applications of HMM.

Chapter 2

BF HMM: A multiscale method using a Poincaré map type technique

We introduce and analyze a new class of multiscale methods that use a developed map which is qualitatively similar to a Poincaré map. The proposed algorithms construct effective paths in the state space whose projection onto the slow subspace shows the correct dynamics. The path is locally constructed through interpolation of neighboring points generated from our developed map. Its construction is based on the procedure which splits the full system so that the split equations satisfies the requirement and solves two split equations successively backward and forward in time only over a short period. This algorithm does not require an explicit form of any slow variables.

The main idea of this paper is summarized in the following three points: (1) The given highly oscillatory system is regarded as a system with lower order perturbation. The solutions of the corresponding system without the lower order perturbation are assumed to stay on some invariant manifolds; (2) We construct an effective path by comparing the solutions of the equations with and without lower order perturbation. This path discloses information about how the solutions of the given perturbed system traverse through the

invariant manifolds of the unperturbed system; and (3) A novel on-the-fly filtering technique is applied for achieving high order accuracy beyond other approaches that rely only on dynamical system's self-averaging property.

Most of the results in this chapter are published in [1]. Finally, we emphasize that the proposed HMM methods are not limited to the few simple schemes that we will present here.

2.1 The BF HMM scheme

We consider the computation of the effective long time properties of a class of dynamical system, formally written in the form

$$\frac{d}{dt}x^\epsilon = \epsilon^{-1} f_1(x^\epsilon) + f_0(x^\epsilon, t; \epsilon), \tag{2.1.1}$$

with initial condition $x^\epsilon(0) = x_0 \in \mathcal{D}_0 \subset \mathbb{R}^d$.

Assumption 2. *The trajectory passing through $y_0 \in \mathcal{D}_0$ of the unperturbed equation*

$$\frac{d}{dt}y = \epsilon^{-1} f_1(y), \tag{2.1.2}$$

are ergodic on some invariant manifold $\mathcal{M}(y_0) \subset \mathcal{D}_0$. Furthermore, for points in $\mathcal{D}_0$, the Jacobian of f_1 has only purely imaginary eigenvalues bounded away from 0, independent of ϵ.

Assumption 3. *The invariant manifolds $\mathcal{M}$ of (2.1.2) can be identified by the level sets of $\xi_1, \xi_2, \cdots, \xi_k$ with $k < d$ which are slow variables with respect to $x^\epsilon(t)$.*

Thus, for each time t, we may identify the manifold

$$\mathcal{M}(t) = \cap_{j=1}^{k} \{z \in \mathbb{R}^d : \xi_j(z) = \xi_j \circ x^\epsilon(t)\},$$

and if we solve (2.1.1) and (2.1.2) with the same initial condition lying on $\mathcal{M}(t)$, it is then possible to track $\mathcal{M}(t)$ by comparison of $x^\epsilon(t)$ and $y(t)$ without explicitly knowing the slow variables. Thus the evolution of the slow variables, or equivalently, that of $\mathcal{M}(t)$, can be tracked at least locally in state space by a path $\gamma(s)$ which crosses $\mathcal{M}(t)$ at $s = t$. Note that such γ is not unique and we shall construct one in the state space such that for any slow variable ξ, and finite time interval, γ satisfies the following conditions:

1. (Consistency) $\xi \circ \gamma(t) = \xi \circ x^\epsilon(t)$;
2. (Effectiveness) $\left|\frac{d^{(j)}\gamma}{dt^{(j)}}\right| \leq C$, for $1 \leq j \leq k$ for some positive integer k.

We shall refer γ as an effective path of the given dynamical system.

It has been observed in [5] that such a path can be constructed using an effectively closed system of explicitly identified slow variables. Furthermore, the constructed path is orthogonal to the level sets of the slow variables in the limit as $\epsilon \to 0$. *Our new algorithm does not require explicit form of any slow variables.* Instead, our new algorithm compares short time solutions of (2.1.1) and (2.1.2) to generate a sequence of points whose interpolation defines an approximation of γ. In the following algorithms, γ is not necessarily orthogonal to the level sets of slow variables. As we shall see further below, the more sophisticated form of our algorithm requires both the forward and

backward in time solutions of (2.1.1) and (2.1.2). Thus, we shall call our algorithms BF HMMs for brevity.

2.1.1 The basic scheme

Our basic algorithm is illustrated in Figure 2.1 and summarized below. This first algorithm does not involve any solution of the equations involved backward in time, but we shall still call it a BF HMM. We remark here that Algorithm 1 described below shares a similar strategy is that proposed in [8] for a different problem.

Algorithm 1. *(Forward Euler BF HMM)*

1. (Forward Euler macro-solver) Compute γ_{n+1} from γ_n at $t_n = nH$.

   $$\gamma_{n+1} = y_n(\Delta) + HF_n,$$

   where

   $$F_n := \frac{x_n(\Delta) - y_n(\Delta)}{\Delta},$$

   and $x_n(\Delta)$ and $y_n(\Delta)$ are evaluated from the micro-solver.

2. (Micro-solver) At $t_n = nH$, solve

   $$\frac{d}{dt}x_n = \epsilon^{-1} f_1(x_n) + f_0(x_n, t_n; \epsilon), \quad x_n(0) = \gamma_n,$$

   and

   $$\frac{d}{dt}y_n = \epsilon^{-1} f_1(y_n), \quad y_n(0) = \gamma_n,$$

   for $t \in [t_n, t_n + \Delta]$ with $0 < \epsilon \ll \Delta \ll H$.

3. Repeat.

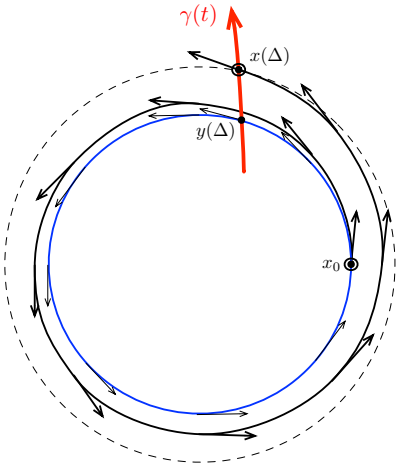

Figure 2.1: $\gamma(\Delta) := x(\Delta)$,$\gamma(0) := y(\Delta)$, and $\gamma(-\Delta) := x(-\Delta; y(\Delta))$.

Example 1. Our simple example to demonstrate the consistency of the Forward Euler BF HMM is an expanding spiral [3] in $\mathbb{C}$.

$$\frac{d}{dt}x^\epsilon = i\epsilon^{-1}x^\epsilon + x^\epsilon, \quad x^\epsilon(0) = x_0 \tag{2.1.3}$$

with $x_0 > 0$ independent of ϵ. We transform x^ϵ into (ξ, θ) where $\xi = |x^\epsilon|$ and $\theta = \arg(x^\epsilon)$, and obtain

$$\begin{cases} \dot{\xi} = \xi, & \xi(0) = |x_0|, \\ \dot{\theta} = \epsilon^{-1}, & \theta(0) = \arg(x_0). \end{cases} \tag{2.1.4}$$

By Definition **3.1.1**, ξ is a slow variable. In Step 1, we assume that all micro simulations of x and y are exact over $[t_n, t_n + \Delta]$, $\Delta \ll H$. Then the local truncation error in approximating a slow variable ξ is given by

$$\begin{aligned} \left|\xi \circ x^\epsilon(t_{n+1}) - \xi \circ \left(y_n(\Delta) + H\frac{x_n(\Delta) - y_n(\Delta)}{\Delta}\right)\right| &= \left|e^{t_n+H} - e^{t_n}\left(1 + H\frac{e^\Delta - 1}{\Delta}\right)\right| \\ &= \left|e^{t_n}\left(\frac{H^2 - \Delta H}{2} + \cdots\right)\right| \\ &\leq CH^2 \end{aligned}$$

for some positive constant C. Thus to leading order in H^2, Forward Euler BF HMM yields a correct $\gamma(t)$ for the slow variable ξ.

2.1.2 Higher order schemes

In this section we describe the construction of high order accurate BF HMMs with sublinear complexity in constant time intervals. In Algorithm 1, forward Euler scheme is used to compute the effective path γ that passes through $y(\Delta)$. A lower order approximation of $d\gamma/dt$ when it crosses $y(\Delta)$ is approximated by F_n, which is a linear approximation. Thus, higher order BF HMMs require higher order approximation of $d\gamma/dt$. In order to do that, we systematically solve (2.1.1) and (2.1.2) both forward and backward in time to obtain points lying on an effective path that crosses a chosen point. Below, we outline this general procedure:

- The chosen macroscopic integrator is used to construct an effective path γ that crosses a chosen point γ_0^*, which may either be given by the macroscopic integrator directly, or come from solving (2.1.2) for a short time. The values of $\frac{d}{dt}\gamma$ at various quadrature points needed by the macro-integrator are computed as below.

- From the initial condition $\gamma(t^*) =: \gamma_0^*$. A sequence of points in the state space, denoted by γ_k^*, $k = 0, \pm 1, \cdots, \pm p$, is generated by the microscopic solver solving (2.1.1) and (2.1.2) for short time intervals of length Δ. The generation of γ_k^* will be described in detail later.

- $\frac{d}{dt}\gamma(t)$ is approximated by $\frac{d}{dt}\gamma^*_\Delta(t)$ for $t \in [t^* - p\Delta,\, t^* + p\Delta]$, where $\gamma^*_\Delta(t)$ is an interpolation of γ^*_k at $t = t^* + k\Delta$.

For simplicity of presentation, we only describe the procedure for $k > 0$. Assume that the value of $\gamma(t^*)$ is given, we start by defining $\gamma^*_0 := \gamma(t^*)$.

- For $k = 0, 1, \cdots, p-1$,

    1. Solve equation (2.1.1) for x^ϵ using γ^*_k as the initial condition at $t = k\Delta$, and obtain the solution at time $(k+1)\Delta$, denoted by $x^\epsilon(\Delta; \gamma^*_k)$.

    2. Solve equation (2.1.2) for y backward in time, from $t = (k+1)\Delta$ to $k\Delta$, with the condition $x(\Delta; \gamma^*_k)$. Denote the solution at $t = k\Delta$ by $y(-\Delta; \gamma^*_k)$.

- Define $\gamma^*_{k+1} := y(-\Delta; \gamma^*_k)$.

The procedure for $k < 0$ involves first solving y backward in time, and then solving x^ϵ forward in time. This type of construction involving forward-backward flow can be recognized using the diagram shown in Figure 2.2. In Figure 2.26, we show two projections of γ thus constructed for the stellar orbits problem. See Section **2.2.2** for the stellar orbits model.

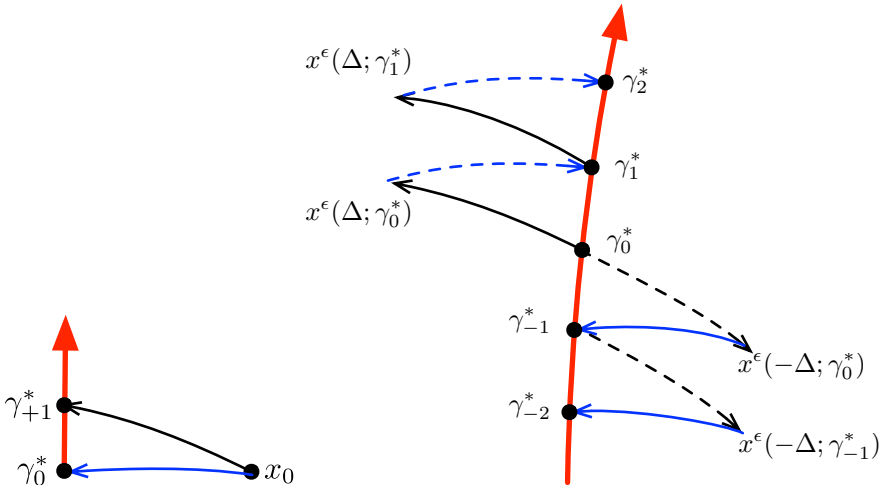

Figure 2.2: An illustration of the BF HMM construction for approximating an effective path that passes through γ_0^*. This construction will take place at every microscopic simulation in a BF HMM algorithm. Mappings that involve backward in time solutions of either (2.1.1) and (2.1.2) are depicted by the dashed arrow curves. (Left) This diagram summarizes the evaluation of F_n in Algorithm 1. Together with the chosen Forward Euler macro-solver, the structure corresponds to the HMM structure shown in the left subfigure of Figure 1. (Right) Blue curves symbolizes mappings that involve the solutions of (2.1.2). The red curve depicts the trajectory of the computed effective path.

2.1.2.1 A sampling issue

In a typical application, the slow variables along $x^\epsilon(t)$ will possess $\mathcal{O}(\epsilon)$ oscillations around a smooth average; i.e. one cannot expect that $|\frac{d^\nu}{dt^\nu}\xi \circ x^\epsilon|$ be bounded uniformly in ϵ for $\nu \geq 2$. Since slow variables are functions that do not depend on ϵ, the boundedness of $|\frac{d^\nu}{dt^\nu}\xi \circ x^\epsilon| = |\frac{d^\nu}{dt^\nu}\xi \circ \gamma|$ thus determines the boundedness of $\gamma^{(\nu)}(t)$. In other words, for most applications, the effective path $\gamma(t)$ constructed by the algorithm outlined above will have fast oscillations of

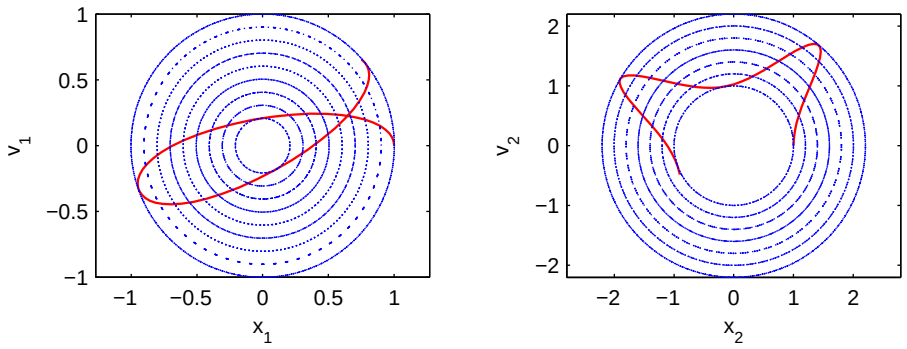

Figure 2.3: Projections of $\gamma(t)$ onto the x_1-v_1 and the x_2-v_2 planes, are shown by the solid curve. The level sets of the slow variables are shown by the dotted contours. γ is computed by a second order explicit Runge-Kutta method using macroscopic time step size $H = 0.25$, $\epsilon = 10^{-4}$. See Algorithm 2 for generating solid curves and Section 2.2.2 for the stellar orbits equation.

$\mathcal{O}(\epsilon)$ amplitudes. This poses some restriction to the lengths of Δ and the macroscopic step size, H.

Nevertheless, the $O(\epsilon)$ oscillations will be sampled very irregularly by the interpolation points γ_k^* and will typically lead to an $O(\epsilon/\Delta)$ error in the approximation of $d\bar{\xi}/dt$ regardless of how many points we interpolate. This limitation of the accuracy can be lifted by a novel filtering technique described in the following section, or by additional knowledge of the periodicities of the fast oscillations in $\xi \circ x^\epsilon(t)$.

2.1.2.2 A novel on-the-fly filtering approach

As we see from the discussion in Section 2.1.2.1, the bottleneck in the accuracy of this new algorithm is a consequence of the small-amplitude fast oscillations in $\xi \circ x^\epsilon(t)$. The accuracy of the proposed algorithm can be im-

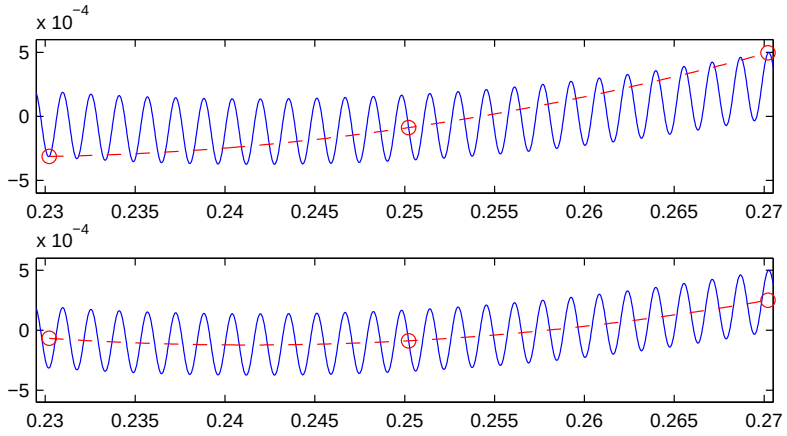

Figure 2.4: The blue curves are the trajectories of $\xi_1 \circ x^\epsilon(t)$ with $\epsilon = 10^{-3}$, showing fast oscillations with small amplitudes. The top plot shows the result obtained without the new filtering. The bottom plot is obtained with the new filtering.

proved if γ_k sample the smooth average $\bar{\xi}$ instead. Since we assume no explicit knowledge about the slow variables, $\bar{\xi}$ must be computed *intrinsically.*

Our idea is to average the vector field defined by the dynamical system "on-the-fly". More precisely, we propose to replace (2.1.1) by a filtered equation

$$\frac{d}{dt}\tilde{x} = \frac{1}{\epsilon} f_1(\tilde{x}) + K_\Delta(t) f_0(\tilde{x}, t; \epsilon), \tag{2.1.5}$$

with the identical initial condition as x^ϵ; i.e. $\tilde{x}(t^*) = x^\epsilon(t^*)$. In the forward in time simulations for time interval $t^* \le t \le t^* + \Delta$, the filter $K_\Delta(t)$ will vanish outside of that interval. Similarly, in the backward in time simulations, the filter will be supported on the interval $t^* - \Delta \le t \le t^*$. We will develop the appropriate filters so that the smooth average $\bar{\xi}(t)$ of $\xi \circ x^\epsilon(t)$ is approximated accurately by $\xi \circ \tilde{x}(t)$ at $t = t^* \pm \Delta$.

The mechanism of this approach for linear equations can be understood by comparing

$$x' = \frac{i}{\epsilon}x + c(t, \frac{t}{\epsilon})x,$$

and the corresponding filtered equation in the interval $0 \leq t \leq \Delta$. Analysis of this new approach for more general nonlinear systems will be reported in a forthcoming paper. With $x = e^{\frac{i}{\epsilon}t}w$ and $\tilde{x} = e^{\frac{i}{\epsilon}t}\tilde{w}$, we have

$$w' = c(t, \frac{t}{\epsilon})w, \quad \text{and } \tilde{w}' = K_\Delta(t)c(t, \frac{t}{\epsilon})\tilde{w}.$$

Suppose $c(t, t/\epsilon) = \bar{c}(t) + \alpha(t/\epsilon)$, where α is a periodic function with zero average. Then

$$w(t) = w_0 \exp(\int_0^t \bar{c}(s)ds + \int_0^t \alpha(\frac{s}{\epsilon})ds) = w_0 \exp(\int_0^t \bar{c}(s)ds) + \mathcal{O}(\epsilon), \quad (2.1.6)$$

$$\tilde{w}(t) = w_0 \exp(\int_0^t K_\Delta(s)\bar{c}(s)ds + \int_0^t K_\Delta(s)\alpha(\frac{s}{\epsilon})ds). \quad (2.1.7)$$

In this example, the lower order term containing α in the right hand side of (2.1.6) causes the sampling issue mentioned above. Thus, our main objective is to build high order schemes that compute the smooth part of w; i.e.

$$\bar{w}(t) := w_0 \exp(\int_0^t \bar{c}(s)ds).$$

In the algorithm that we outlined above, *we only need that the value of* $\tilde{w}(t)$ *to be close to* $\bar{w}(t)$ *at* $t = \Delta$*, the filter* K_Δ *performs two specific types of approximations corresponding to the integrals involving* $\bar{c}$ *and* α*.*

The theory of averaging out oscillations that appear in the integral for $\alpha(t/\epsilon)$ is developed in [42]. It requires that K_Δ is compactly supported in the

interval $[0, \Delta]$, and the effectiveness of averaging out the oscillations in α is determined by the regularity of K_Δ at $s = 0$ and Δ; i.e.

$$\frac{d^k}{dt^k} K_\Delta(0) = \frac{d^k}{dt^k} K_\Delta(\Delta) = 0, k = 0, 1, \ldots, q, \tag{2.1.8}$$

and then integration by parts yields

$$\left| \int_0^\Delta K_\Delta(s) \alpha(\frac{s}{\epsilon}) ds \right| \leq \mathrm{C} \cdot \frac{\epsilon^q}{\Delta^{q-1}}. \tag{2.1.9}$$

High order accurate approximation of the integration of $\bar{c}$ requires different conditions. Taylor expansion of $\bar{c}(t)$ around $t = \Delta$ gives $\bar{c}(t) = \bar{c}(\Delta) + (t - \Delta)\bar{c}'(\Delta) + ...$ and

$$\int_0^\Delta \bar{c}(s) ds = \sum_j \frac{\bar{c}^{(j)}(\Delta)}{j!} \int_0^\Delta (s - \Delta)^j ds,$$

$$\int_0^\Delta K_\Delta(s) \bar{c}(s) ds = \sum_j \frac{\bar{c}^{(j)}(\Delta)}{j!} \int_0^\Delta K_\Delta(s) (s - \Delta)^j ds.$$

Thus for this type of problems, we may require what we called *the quadrature moment conditions for the filter* K_Δ:

$$\int_0^\Delta K_\Delta(\Delta - s) s^j ds = \int_0^\Delta s^j ds, j = 0, 1, 2, \cdots, p. \tag{2.1.10}$$

We thus have the error

$$\left| \int_0^\Delta K_\Delta(\Delta - s) \bar{c}(s) ds - \int_0^\Delta \bar{c}(s) ds \right| \leq C \Delta^{p+1}.$$

For convenience of presentation below, let $\tilde{\mathbb{K}}^{p,q}(I)$ denote the space of normalized C^q functions, supported on $I = [0, 1]$ that have p moments specified

by

$$\int_I K(1-t)t^r dt = \int_I t^r dt = \frac{1}{r+1}, 0 \le r \le p. \tag{2.1.11}$$

For $\Delta > 0$, $K_\Delta(t)$ denotes a rescaling of K as $K_\Delta(t) = K(\Delta^{-1}t)$.

We remark that with $\Delta = \mathcal{O}(\epsilon)$, the estimate in (2.1.9) shows that it is more important to use a filter with higher regularity, as it directly impacts on how the error $|\frac{d^j}{dt^j}\xi \circ \tilde{x} - \frac{d}{dt}\bar{\xi}|$ depends on ϵ, and consequently, how the sizes of Δ and the step size H for the macro-solver should be chosen.

Figure 2.4 demonstrates a scenario for the stellar orbits example. In it, the blue curves correspond to the the values of the slow variable $\xi_1 \circ \mathbf{x}(t)$ defined in Section 2.2.2. The red circles show the values of $\xi_1(\gamma_k)$ at times $t_n + k\Delta$, and the dotted red curves are the quadratic interpolants of these values. The bottom plot in Figure 2.4 is obtained with the strategy to be discussed below.

Algorithm 2. *Midpoint rule BF HMM*

1. (Midpoint rule macro-solver) Compute γ_{n+1} from γ_n at $t_n = nH$.

$$\begin{aligned} \gamma_{n+\frac{1}{2}} &= \gamma_n + \frac{H}{2}\mathcal{F}_{HMM}(\gamma_n, t_n), \\ \gamma_{n+1} &= \gamma_n + H\mathcal{F}_{HMM}(\gamma_{n+\frac{1}{2}}, t_n + \frac{H}{2}) \end{aligned}$$

   where $\mathcal{F}_{HMM}$ is defined below.

2. (Micro-solver) Evaluation of $\mathcal{F}_{HMM}(\gamma_0^*, t^*)$. With a chosen filter $K_\Delta \in \tilde{\mathbb{K}}^{p,q}([0,\Delta])$, $p, q \ge 1$, and $\Delta > 0$:

(a) (Forward solution of the perturbed equation) Solve

$$\frac{d}{dt}\tilde{x} = \epsilon^{-1} f_1(\tilde{x}) + K_\Delta(t - t^*) f_0(\tilde{x}, t; \epsilon), \quad \tilde{x}(t^*) = \gamma_0^*$$

for $t \in [t^*, t^* + \Delta]$. Denote the solution at $t = t^* + \Delta$ by $\tilde{x}(\Delta; \gamma_0^*)$.

(b) (Backward solution of the perturbed equation) Solve

$$\frac{d}{dt}\tilde{x} = \epsilon^{-1} f_1(\tilde{x}) + K_\Delta(t - t^*) f_0(\tilde{x}, t; \epsilon), \quad \tilde{x}(t^*) = \gamma_0^*$$

for $t \in [t^* - \Delta, t^*]$. Denote the solution at $t = t^* - \Delta$ by $\tilde{x}(-\Delta; \gamma_0^*)$.

(c) (Forward solution of the unperturbed equation) Solve

$$\frac{d}{dt} y_F = \epsilon^{-1} f_1(y_F), \quad y_F(t^* - \Delta) = \tilde{x}(-\Delta; \gamma_0^*)$$

for $t \in [t^* - \Delta, t^*]$. Denote the solution $y_F(t^*)$ by γ_{-1}^*.

(d) (Backward solution of the unperturbed equation) Solve

$$\frac{d}{dt} y_B = \epsilon^{-1} f(y_B), \quad y_B(t^* + \Delta) = \tilde{x}(\Delta; \gamma_0^*)$$

for $t \in [t^*, t^* + \Delta]$. Denote the solution $y_F(t^*)$ by γ_1^*.

(e) Evaluate $\mathcal{F}_{HMM}$:

$$\mathcal{F}_{HMM}(\gamma_0^*, t^*) := \frac{\gamma_1^* - \gamma_{-1}^*}{2\Delta}.$$

3. Repeat.

Algorithm 3. *(Explicit s-stage Runge Kutta BF HMM)*

1. (Macro-solver: An explicit s-stage m-th order Runge-Kutta method defined by the Butcher's tableau involving the coefficients $(a_{i,j})$, b_i, and c_j, $1 \leq i, j \leq s$.)

   Computes γ^{n+1} from the given value γ^n at $t = t_n$.

$$\gamma^{n+1} = \gamma^n + H \sum_{i=1}^{s} b_i k_i,$$

   where

$$k_j = \mathcal{F}_{HMM}(\gamma^n + H \sum_{\ell=1}^{j-1} a_{j\ell} k_\ell, t_n + c_j H), \quad j = 1, 2, \cdots, s.$$

   The values of $\mathcal{F}_{HMM}$ are computed from microscopic simulations.

2. (Micro-solver) Evaluate $\mathcal{F}_{HMM}(\gamma_0^*, t^*)$ at the given values of γ_0^* and t^*.

   Let $S_{t^*}^{\Delta}$ be the operator that maps a given initial data at $t = t^*$ to the solution of the filtered perturbed equation (2.1.5) to $t^* + \Delta$, and let $\tilde{S}_{t^*}^{\Delta}$ be the operator that has the analogous function for the unperturbed equation (2.1.2). Define

$$\gamma_j^* := \left(\tilde{S}_{t^*+\Delta}^{-\Delta} S_{t^*}^{\Delta} \right)^j \gamma_0^*,$$

$$\gamma_{-k}^* := \left(\tilde{S}_{t^*-\Delta}^{\Delta} S_{t^*}^{-\Delta} \right)^k \gamma_0^*.$$

   Let $\gamma_\Delta(t)$ be an interpolant of γ_j at $t^* + j\Delta$. Then

$$\mathcal{F}_{HMM}(\gamma_0^*, t^*) := \frac{d}{dt} \gamma_\Delta(t^*).$$

2.1.2.3 Analysis of the filtering effect

We will now explain the rationale and mechanism behind the new filtering technique. By transforming x into $(\xi, \phi) \in \mathbb{R}^{d-1} \times S^1$, we have the following slow-fast system

$$\begin{cases} \dot{\xi} = f_0(\xi, \phi), & \xi(0) = \xi_0, \\ \dot{\phi} = \epsilon^{-1} g_1(\xi, \phi) + g_2(\xi, \phi), & \phi(0) = \phi_0. \end{cases} \tag{2.1.12}$$

$$\dot{\bar{x}} = \bar{f}_0(\bar{x}) = \frac{1}{T} \int_0^T f_0(\bar{x}, s) ds, \ \bar{x}(0) = x_0, \tag{2.1.13}$$

$$\dot{y} = K_\Delta(t) f_0^\epsilon(y, \frac{t}{\epsilon}), \ y(0) = x_0, \tag{2.1.14}$$

In this section, we needs to analyze $e = \bar{x} - y$ at $t = \Delta$.

Notation. We use the notation $f^{[k]}(t)$ for k-th order integral of f and $f^{(s)}(t)$ to denote $\frac{d^s f}{dt^s}$, and use $\tilde{K}^{p,q}$ to denote a function in $\tilde{\mathbb{K}}^{p,q}([0,1])$.

Theorem 2.1.1. Suppose that (1) $f_0^\epsilon(x, \frac{t}{\epsilon}) = \bar{f}_0(x) + \alpha(\frac{t}{\epsilon})$ (or one can simplify the setting as $f_0^\epsilon(t, \frac{t}{\epsilon}) = \bar{f}_0(t) + \alpha(\frac{t}{\epsilon})$), (2) the effective force $\bar{f}_0$ is in C^{p+1}, and (3) $K^{(q+1)}(\frac{t}{\Delta})$ and $\alpha^{[q+1]}(\frac{t}{\epsilon})$ exist and bounded over $t \in [0, \Delta]$. We define $e = \bar{x} - y$. Then for any $K \in \tilde{\mathbb{K}}^{p,q}(I)$, and $t \in [0, \Delta]$, the following inequality holds

$$|e(t)| \leq C\Delta. \tag{2.1.15}$$

Moreover, at $t = \Delta(= C_\Delta \epsilon)$,

$$|e(\Delta)| \leq C_1 \left(C_\Delta \epsilon\right)^{\min\{2,p+2\}} + C_2 \frac{\max\limits_{0\leq i\leq q+1} ||K^{(i)}(t)||_{L^\infty([0,1])}}{(C_\Delta)^q} \epsilon \tag{2.1.16}$$

holds.

Proof. Using equations (2.1.15) and (2.1.16),

$$\begin{aligned}
\dot{e} &= \bar{f}_0(e+y) - K_\Delta(t) f_0(y, \frac{t}{\epsilon}), \\
e(t) &= \int_0^t \bar{f}_0(e+y) - \bar{f}_0(y) ds + \int_0^t \bar{f}_0(y) - K_\Delta(s) f_0(y, \frac{t}{\epsilon}) ds, \\
|e(t)| &\leq \int_0^t \left|\bar{f}_0(e+y) - \bar{f}_0(y)\right| ds + \left| \int_0^t \bar{f}_0(y) - K_\Delta(s) f_0(y, \frac{t}{\epsilon}) ds \right| \\
&\leq L \int_0^t |e(s)| ds + \underbrace{\left| \int_0^t \bar{f}_0(y) - K_\Delta(s) f_0(y, \frac{t}{\epsilon}) ds \right|}_{=A(t)}.
\end{aligned}$$

where L is a Lipschitz constant of $\bar{f}_0$. Then using Gronwall's lemma

$$\begin{aligned}
|e(t)| &\leq A(t) + \int_0^t A(s) \cdot L e^{\int_s^t L dr} ds \\
&= A(t) + \int_0^t A(s) \cdot L e^{L(t-s)} ds.
\end{aligned}$$

For $t \in [0, \Delta]$,

$$|e(t)| \leq C_1 \Delta + L e^{L\Delta} C_2 \Delta^2.$$

Therefore,

$$|e(t)| \leq C\Delta \tag{2.1.17}$$

for a generic constant $C > 0$. Moreover, especially, $t = \Delta$,

$$|e(\Delta)| \leq A(\Delta) + \int_0^\Delta A(s) \cdot Le^{L(\Delta-s)} ds. \tag{2.1.18}$$

Firstly, note that $\left|\int_0^\Delta A(s) \cdot Le^{L(\Delta-s)} ds\right| \leq C\Delta^2$. For simplicity, we change the y dependence in f to t dependence. Since $f_0(t, \frac{t}{\epsilon}) = \bar{f}_0(t) + \alpha(\frac{t}{\epsilon})$ where α is a periodic function with zero average,

$$\begin{aligned} A(\Delta) &= \left|\int_0^\Delta \bar{f}_0(s) - K_\Delta(s) f_0(s, \frac{s}{\epsilon}) ds\right| \\ &\leq \left|\int_0^\Delta \bar{f}_0(s) - K_\Delta(s)\bar{f}_0(s) ds\right| + \left|\int_0^\Delta K_\Delta(s)\alpha(\frac{s}{\epsilon}) ds\right| \\ &\leq C_1\Delta^{p+2} + C_2 \max_{0\leq i\leq q+1} ||K^{(i)}(t)||_{L^\infty([0,1])} \frac{\epsilon^{q+2}}{\Delta^{q+1}}. \end{aligned} \tag{2.1.19}$$

Note that at the moment of estimating $\left|\int_0^\Delta K_\Delta(s)\alpha(\frac{s}{\epsilon}) ds\right|$ for $K \in \tilde{K}^{p,q}$,

$$\begin{aligned} \int_0^\Delta K_\Delta(s)\alpha(\frac{s}{\epsilon}) ds &= (-1)^q \frac{\epsilon^q}{\Delta^q} \int_0^\Delta K^{(q)}(\frac{s}{\Delta})\alpha^{[q]}(\frac{s}{\epsilon}) ds \\ &= (-1)^q \frac{\epsilon^{q+1}}{\Delta^q} \left[K^{(q)}(\frac{s}{\Delta})\alpha^{[q+1]}(\frac{s}{\epsilon})\right]_{s=0}^\Delta \\ &\quad + (-1)^{q+1} \frac{\epsilon^{q+1}}{\Delta^{q+1}} \int_0^\Delta K^{(q+1)}(\frac{s}{\Delta})\alpha^{[q+1]}(\frac{s}{\epsilon}) ds \\ &= (-1)^{q+1} \frac{\epsilon^{q+1}}{\Delta^{q+1}} \int_0^\Delta K^{(q+1)}(\frac{s}{\Delta})\alpha^{[q+1]}(\frac{s}{\epsilon}) ds. \end{aligned}$$

$$\begin{aligned} \left|\int_0^\Delta K_\Delta(s)\alpha(\frac{s}{\epsilon}) ds\right| &\leq \frac{\epsilon^{q+1}}{\Delta^{q+1}} \max_{0\leq i\leq q+1} ||K^{(i)}(t)||_{L^\infty([0,1])} \int_0^\Delta \left|\alpha^{[q+1]}(\frac{s}{\epsilon})\right| ds \\ &= C_2 \frac{\epsilon^{q+1}}{\Delta^q} \max_{0\leq i\leq q+1} ||K^{(i)}(t)||_{L^\infty([0,1])}. \end{aligned}$$

Putting (2.1.18) and (2.1.19) together,

$$|e(\Delta)| \leq C_1 \Delta^{\min\{2,p+2\}} + C_2 \epsilon \frac{\max\limits_{0\leq i\leq q+1} ||K^{(i)}(t)||_{L^\infty([0,1])}}{(C_\Delta)^q} \tag{2.1.20}$$

where $\Delta = C_\Delta \epsilon$. □

Here we verify the error bound of (2.1.20) implemented in two test problems. A result shows that the error bound is correct, but it is not sharp. The first test problem is given by

$$\begin{cases} \dot{y} = K_\Delta(t)\left(y + \cos(\eta)\right), \\ \dot{\eta} = \frac{1}{\epsilon} \end{cases} \quad vs \quad \begin{cases} \dot{\bar{x}} = \bar{x}, \\ \dot{\eta} = 0 \end{cases}$$

with an initial condition $[1, 0.5]^t$.

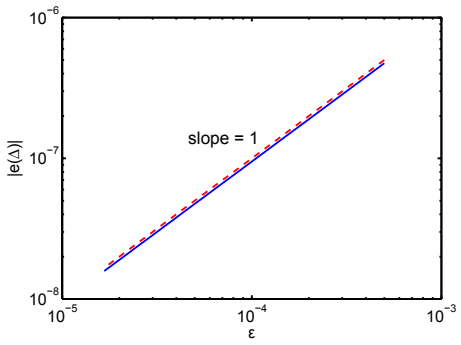

(a) [Various ϵ] $\Delta = 40\epsilon$, $\tilde{K}^{1,3}$

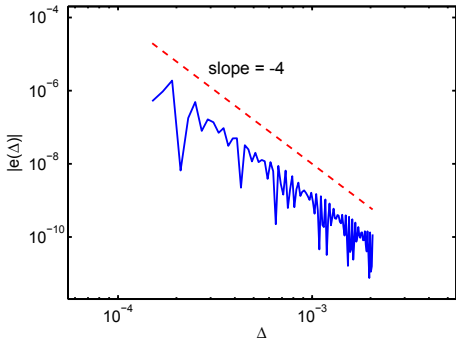

(b) [Various Δ] $\epsilon = 10^{-5}$. $\Delta = (2k+5)\epsilon$, $k = [5:100]$, $\tilde{K}^{1,3}$. As Δ increases, $|e(\Delta)|$ decreases as a rate of $\frac{1}{(C_\Delta)^{q+1}}$.

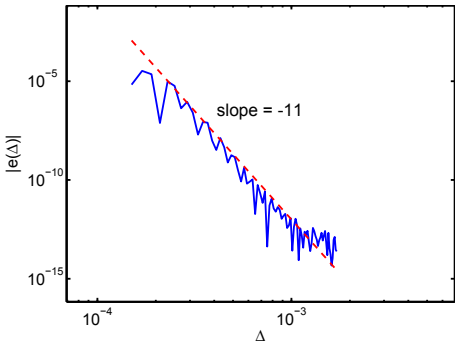

(c) [Various Δ] $\epsilon = 10^{-5}$. $\Delta = (2k+5)\epsilon$, $k = [5:80]$, $\tilde{K}^{1,10}$

Figure 2.5: Plot of $|e(\Delta)|$. It is hard to see $\mathcal{O}(\Delta^2)$ rate numerically since $(C_\Delta)^2$ and $\frac{1}{(C_\Delta)^{q+1}}$ are competing each other.

Another test problem is more complicated than the former.

$$\begin{cases} \dot{y} = K_\Delta(t)\left(\cos(y) + \cos\left(2\pi\sin(\eta)\right)\right), \\ \dot{\eta} = \frac{1}{\epsilon} \end{cases} \quad vs \quad \begin{cases} \dot{\bar{x}} = \cos(\bar{x}) + C, \\ \dot{\eta} = 0 \end{cases}$$

with an initial condition $[1, 0.5]^t$. The constant $C \approx 0.2203$ is analytically computed using Maple 15.

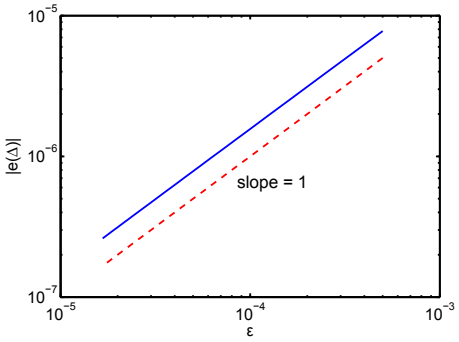

(a) [Various ϵ] $\Delta = 30\epsilon$, $\tilde{K}^{3,2}$

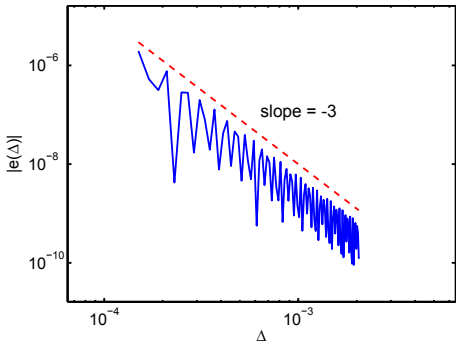

(b) [Various Δ] $\epsilon = 10^{-5}$. $\Delta = (2k+5)\epsilon$, $k = [5:100]$, $\tilde{K}^{3,2}$. As Δ increases, $|e(\Delta)|$ decreases as a rate of $\frac{1}{(C_\Delta)^{q+1}}$.

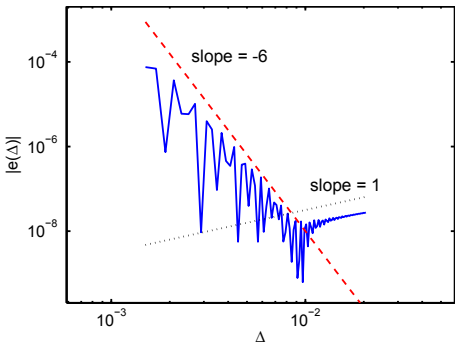

(c) [Various Δ] $\epsilon = 10^{-4}$. $\Delta = (2k+5)\epsilon$, $k = [5:100]$, $\tilde{K}^{3,5}$. When $\Delta \sim 100\epsilon$, the leading order term has been changed to $C_1\Delta^{\min\{2,p+2\}}$ but note that $100^2 = \epsilon^{-1}$ so we see the 1st order of ϵ.

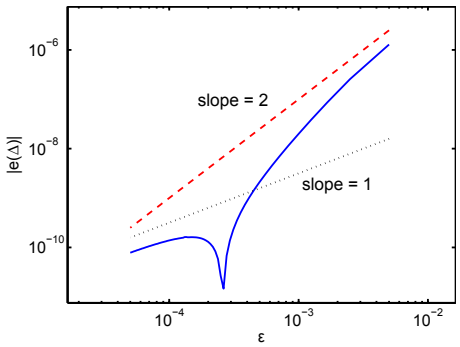

(d) [Various ϵ] $\Delta = 150\epsilon$, $\tilde{K}^{3,5}$. When $\epsilon \in [0.16 \cdot 10^{-3}, 0.3 \cdot 10^{-3}]$, the leading order term has been changed to $C_2 \frac{\max_{0\le i\le q+1} ||K^{(i)}(t)||_{L^\infty([0,1])}}{(C_\Delta)^{q+1}}\epsilon$.

Figure 2.6: Plot of $|e(\Delta)|$.

2.1.2.4 Formal accuracy estimate

Here we summarize errors produced by Algorithm 3.

- Global error in macro-simulation: Using an α-th order method with step size H, is given by H^α.

- Global error in each micro-simulation: Using a β-th order method with step size h, we solve equations for $x(t)$ and $y(t)$ over micro interval Δ. The global error is of order $\frac{\Delta h^\beta}{\epsilon^{\beta+1}}$.

- Filtering errors, by which we refer to the errors made in constructing γ_k^*. Using a filter $K_\Delta(t) \in \tilde{\mathbb{K}}^{p,q}$ with $p, q \geq 1$, we have a residual from averaging the oscillations of order $\frac{\epsilon^q}{\Delta^{q-1}}$, and quadrature error of order at most Δ.

- Error in approximation of $\gamma'(t)$ via interpolation: interpolating $n+1$ points by an n-th degree polynomial leads to an error of order Δ^n.

In our setup for the multiscale problems, we consider a regime: $0 \leq t \leq T$, $\epsilon \to 0$, $T \sim \mathcal{O}(1)$, $\Delta \sim \mathcal{O}(\epsilon)$, and $H \sim \mathcal{O}(1)$, assuming that $\bar{\xi}(t)$ has ν derivatives bounded uniformly independent of ϵ, and $\nu \geq \alpha$. In this regime, the dominating error terms would be that from micro-solver $\mathcal{O}(h/\epsilon)^\beta$, the filtering errors $\mathcal{O}(\epsilon)$, and the error from the macro-solver $\mathcal{O}(H^\alpha)$.

2.1.3 A new structure of the BF HMM

2.1.3.1 Difficulties with the case

We begin with a motivating example, in which the Forward Euler BF HMM is not appropriate to compute the slow behavior in a multiscale fashion.

Example 2. Consider the following nonlinear equation in Cartesian coordinates,

$$\dot{x} = \frac{ix|x|}{\epsilon} + \frac{x}{|x|} + \frac{\mathrm{Re}(x)x}{|x|^2}, \quad x(0) = 1 \tag{2.1.21}$$

whose slow-fast system is given by

$$\begin{cases} \dot{\xi} = 1 + \cos(\phi), & \xi(0) = 1, \\ \dot{\phi} = \frac{\xi}{\epsilon}, & \phi(0) = 0. \end{cases} \tag{2.1.22}$$

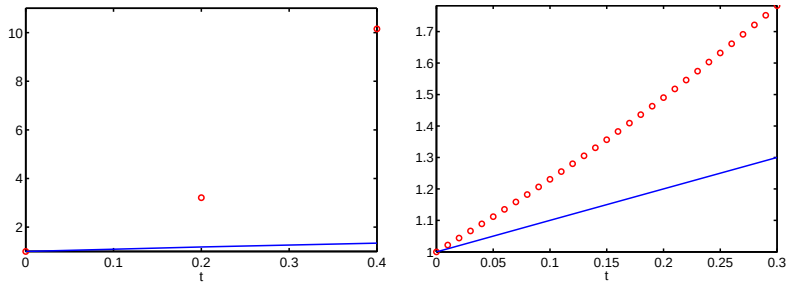

Figure 2.7: (Example 2) Plots of $\xi \circ x(t)$. Forward Euler BF HMM with linear interpolation, $\epsilon = 10^{-4}$ and $\Delta = 30\epsilon$ are used. The solid lines correspond to the direct numerical simulation (DNS) solution. Circles are the results of BF HMM. (Left) $H = 0.2$. (Right) $H = 0.01$. Circles eventually converge to the DNS solution as $H \to 0$.

One of the subtle points in applying the Forward Euler BF HMM to (2.1.22) is that the equation of the fast variable depends on ξ. From the Assumption 5, the slow variable is almost stationary when we solve an unperturbed equation backward and forward in time over Δ amount of time. In this situation, a large difference between $\phi(\Delta)$ from the full equation and the unperturbed equation may exist and this results in inaccurate or even erroneous approximation of the evolution of slow variable over a Δ period (See Figure 2.8).

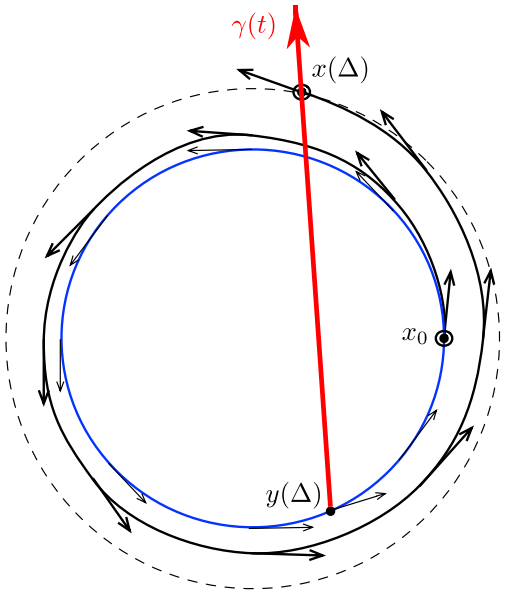

Figure 2.8: An illustration of the erroneous approximation due to the difference in ϕ. The path $\gamma(t)$ overestimates the evolution of the slow variable.

This is not a contradiction to the convergence of the BF HMM since the slow behavior of (2.1.22) can be correctly computed using the Forward Euler BF HMM with very small $H = \mathcal{O}(\epsilon)$. However, the computational cost now becomes linear to ϵ^{-1} which is same as the traditional methods. In order to overcome this limitation, the BF HMM with symmetric structure is presented in the following section.

2.1.3.2 BF HMMs with z-structure

In this section, we describe the construction of the BF HMM with a new structure which has a shape of "z". Thus, we shall call the proposed algorithms BF HMM with z-structure for brevity. This has a symmetric structure and

can be summarized as below.

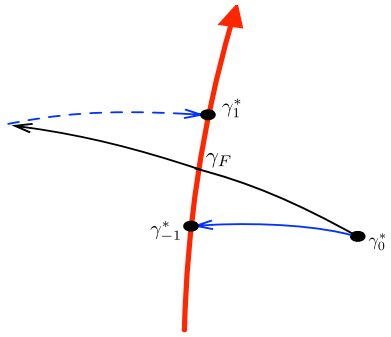

Figure 2.9: An illustration of the BF HMM construction with z-structure.

Algorithm 4. *Forward Euler BF HMM with z-structure*

1. (Forward Euler macro-solver) Compute γ_{n+1} from γ_n at $t_n = nH$.

$$\gamma_{n+1} = \gamma_{-1}^* + H\mathcal{F}_{HMM}(\gamma_n, t_n)$$

   where $\mathcal{F}_{HMM}$ is defined below.

2. Evaluation of $\mathcal{F}_{HMM}(\gamma_0^*, t^*)$. With a chosen filter $K_\Delta \in \tilde{\mathbb{K}}^{p,q}([0,\Delta])$, $p, q \geq 1$, and $\Delta > 0$:

   (a) (Forward solution of the perturbed equation) Solve

$$\frac{d}{dt}\tilde{x} = \epsilon^{-1} f_1(\tilde{x}) + K_\Delta(t - t^*) f_0(\tilde{x}, t; \epsilon), \quad \tilde{x}(t^*) = \gamma_0^*$$

   for $t \in [t^*, t^* + 2\Delta]$. Denote the solution at $t = t^* + 2\Delta$ by $\tilde{x}(2\Delta; \gamma_0^*)$.

   (b) (Forward solution of the unperturbed equation) Solve

$$\frac{d}{dt}\tilde{x} = \epsilon^{-1} f_1(\tilde{x}) + K_\Delta(t - t^*) f_0(\tilde{x}, t; \epsilon), \quad \tilde{x}(t^*) = \gamma_0^*$$

   for $t \in [t^*, t^* + \Delta]$. Denote the solution at $t = t^* + \Delta$ by γ_{-1}^*.

(c) (Backward solution of the unperturbed equation) Solve

$$\frac{d}{dt}y_B = \epsilon^{-1}f(y_B), \quad y_B(t^* + 2\Delta) = \tilde{x}(2\Delta; \gamma_0^*)$$

for $t \in [t^* + \Delta, t^* + 2\Delta]$. Denote the solution $y_F(t^* + \Delta)$ by γ_1^*.

(d) Evaluate $\mathcal{F}_{HMM}$:

$$\mathcal{F}_{HMM}(\gamma_0^*, t^*) := \frac{\gamma_1^* - \gamma_{-1}^*}{2\Delta}.$$

To analyze the BF HMM with z-structure, we consider a system of the form:

$$\begin{cases} \dot{\xi} = g(\xi, \phi), & \xi(0) = \xi_0, \\ \dot{\phi} = \frac{1}{\epsilon}f_1(\xi) + f_0(\xi, \phi), & \phi(0) = \phi_0. \end{cases} \tag{2.1.23}$$

The corresponding unperturbed equation is chosen as

$$\begin{cases} \dot{\xi}_u = 0, & \xi_u(0) = \xi_0, \\ \dot{\phi}_u = \frac{1}{\epsilon}f_1(\xi_u), & \phi_u(0) = \phi_0. \end{cases} \tag{2.1.24}$$

Theorem 2.1.2. We assume that f_0 and g are periodic with respect to the fast variable ϕ with a period 1. Then, the following estimation holds: $|\phi(\gamma_1^*) - \phi(\gamma_F^*)| = \mathcal{O}(\frac{\Delta^2}{\epsilon})$ and $\left|\phi(\gamma_1^*) - \phi(\gamma_{-1}^*)\right| = \mathcal{O}(\frac{\Delta^3}{\epsilon})$.

Proof. Thanks to the on-the-fly filtering approach, we can write $g(\xi, \phi)$ as $\bar{g}(\bar{\xi})$ with (f_0 also). For simplicity, we drop tilde. For γ_1^*,

$$\begin{cases} \xi^+ = \xi_0 + \int_0^\Delta g(\xi^F)dt, \\ \phi^F(\Delta) = \phi_0 + \int_0^\Delta \frac{1}{\epsilon}f_1(\xi^F)dt + \int_0^\Delta f_0(\xi^F)dt, \\ \phi^+ = \phi_0 + \int_0^\Delta \frac{1}{\epsilon}f_1(\xi^F)dt + \int_0^\Delta f_0(\xi^F)dt - \frac{\Delta}{\epsilon}f_1(\xi^+) - \Delta f_0(\xi^+). \end{cases}$$

For γ_{-1}^*,

$$\begin{cases} \xi^- = \xi_0 - \int_0^\Delta g(\xi^B)dt, \\ \phi^B(-\Delta) = \phi_0 - \int_0^\Delta \frac{1}{\epsilon} f_1(\xi^B)dt - \int_0^\Delta f_0(\xi^B)dt, \\ \phi^- = \phi_0 - \int_0^\Delta \frac{1}{\epsilon} f_1(\xi^B)dt - \int_0^\Delta f_0(\xi^B)dt + \frac{\Delta}{\epsilon} f_1(\xi^-) + \Delta f_0(\xi^-). \end{cases}$$

In the step evaluating $\mathcal{F}_{HMM}(\gamma_0^*, t^*)$,

$$\xi^+ - \xi^- = \int_0^\Delta g(\xi^F)dt + \int_0^\Delta g(\xi^B)dt$$

which is exactly capturing the evolution of ξ over $[-\Delta, \Delta]$. On the other hand,

$$\begin{aligned} \phi^+ - \phi^- &= \int_0^\Delta \frac{1}{\epsilon} f_1(\xi^F)dt - \frac{\Delta}{\epsilon} f_1(\xi^+) + \int_0^\Delta f_0(\xi^F)dt - \Delta f_0(\xi^+) \\ &\quad \int_0^\Delta \frac{1}{\epsilon} f_1(\xi^B)dt - \frac{\Delta}{\epsilon} f_1(\xi^-) + \int_0^\Delta f_0(\xi^B)dt - \Delta f_0(\xi^-) \end{aligned}$$

where $\xi^+ = \xi_0 + \int_0^\Delta g(\xi^F)dt$ and $\xi^- = \xi_0 - \int_0^\Delta g(\xi^B)dt$. By considering $\xi^F(t) = \xi_0 + \int_0^t g(\xi^F)ds$ and $\xi^B(t) = \xi_0 - \int_0^t g(\xi^B)ds$, for $\mathcal{O}(\frac{1}{\epsilon})$ terms

$$\begin{aligned} &\epsilon\left(\phi^+ - \phi^-\right) = \\ &\quad \left\{\int_0^\Delta f_1\left(\xi_0 + \int_0^t g(\xi^F)ds\right)dt - \Delta f_1\left(\xi_0 + \int_0^\Delta g(\xi^F)dt\right)\right\} \\ &\quad + \left\{\int_0^\Delta f_1\left(\xi_0 - \int_0^t g(\xi^B)ds\right)dt - \Delta f_1\left(\xi_0 - \int_0^\Delta g(\xi^B)dt\right)\right\} \\ &\quad = \left\{\int_0^\Delta \left(f_1(\xi_0) + \int_0^t g(\xi^F)ds \cdot \dot{f}_1(\xi_0)\right)dt - \Delta f_1(\xi_0) - \Delta \int_0^\Delta g(\xi^F)dt\dot{f}_1(\xi_0)\right\} \\ &\quad + \left\{\int_0^\Delta \left(f_1(\xi_0) - \int_0^t g(\xi^B)ds \cdot \dot{f}_1(\xi_0)\right)dt - \Delta f_1(\xi_0) + \Delta \int_0^\Delta g(\xi^F)dt\dot{f}_1(\xi_0)\right\} + \mathcal{O}(\Delta^3). \end{aligned}$$

Thus, we have cancellation due to the z-structure;

$$\begin{aligned} \epsilon\left(\phi^+ - \phi^-\right) &= \left\{\int_0^\Delta \left(\int_0^t g(\xi^F)ds \cdot \dot{f}_1(\xi_0)\right)dt - \Delta \int_0^\Delta g(\xi^F)dt \cdot \dot{f}_1(\xi_0)\right\} \\ &\quad + \left\{-\int_0^\Delta \left(\int_0^t g(\xi^B)ds \cdot \dot{f}_1(\xi_0)\right)dt + \Delta \int_0^\Delta g(\xi^F)dt \cdot \dot{f}_1(\xi_0)\right\} + \mathcal{O}(\Delta^3). \end{aligned}$$

By considering $\xi^F(s) = \xi_0 + s\dot{\xi}^F(0) + \frac{s^2}{2}\dot{\xi}^F(0) + \cdots$ and $\xi^B(s) = \xi_0 + s\dot{\xi}^B(0) + \frac{s^2}{2}\dot{\xi}^B(0) + \cdots$, one can show that

$$\epsilon\left(\phi^+ - \phi^-\right) = \mathcal{O}(\Delta^3)$$

and this completes the proof. □

In Figure 2.10, we show a result computed by the same BF HMM algorithm with Figure 2.7 but having z-structure and demonstrate the efficiency by choosing H independent of ϵ.

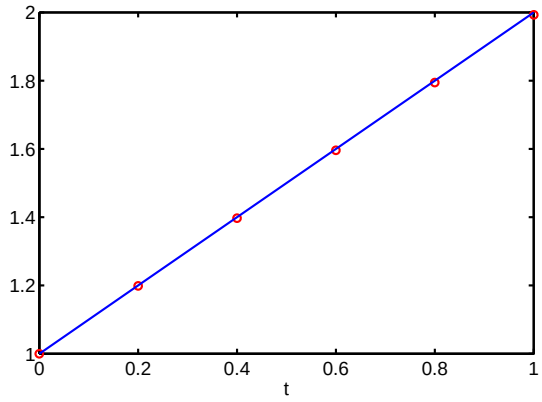

Figure 2.10: (Example 2) Plot of $\xi \circ x(t)$ over $t \in [0, 1]$. Circles are results of the Forward Euler BF HMM with z-structure. The maximal difference between γ_1^* and γ_{-1}^* over $t \in [0, 1]$ is $0.144 \cdot 10^{-5}$. However, in the Forward Euler BF HMM with linear interpolation, the maximal difference is 0.045 when $H = 0.01$.

For a scheme with a high order accuracy, another interesting example is presented. Consider the following nonlinear equation in slow-fast coordinates,

$$\begin{cases} \dot{\xi}_1 = -\frac{\xi_2^2}{10} + \xi_1 + \sin(\xi_2) + \cos(3\phi), & \xi_1(0) = 1, \\ \dot{\xi}_2 = \xi_1\sqrt{\xi_2} + \sin(\phi), & \xi_2(0) = 0.5, \\ \dot{\phi} = \frac{\xi_1^2 + \xi_2}{\epsilon} + \xi_2, & \phi(0) = 0. \end{cases}$$

whose averaged system is given by

$$\begin{cases} \dot{\xi}_1 = 0, & \xi_1(0) = 1, \\ \dot{\xi}_2 = 0, & \xi_2(0) = 0.5, \\ \dot{\phi} = \frac{\xi_1^2 + \xi_2}{\epsilon}, & \phi(0) = 0. \end{cases}$$

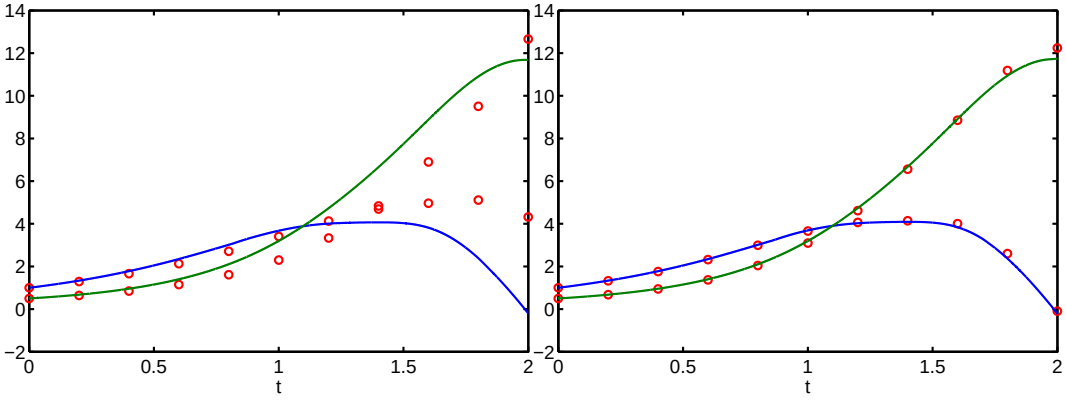

Figure 2.11: Plot of $\xi_i \circ x(t)$ over $t \in [0, 2]$. Circles are results of the Forward Euler BF HMM (Left) and the Midpoint rule BF HMM with z-structure (Right). Parameters are $\epsilon = 10^{-4}$, $\Delta = 50\epsilon$ and $H = 0.2$. A kernel in $\tilde{\mathbb{K}}^{1,4}$ is used.

2.2 Numerical examples

In this section, we apply our BF HMM algorithm described in Section 2.1 to ODE systems and compare it with other methods.

2.2.1 Nonlinear expanding spiral

Consider the following nonlinear equation in the complex plane

$$\dot{x} = i\epsilon^{-1} x|x| + (\sin x + \mathrm{Re}(x) \cdot x)\,|x|^{-2}, \tag{2.2.25}$$

with the initial value $x(0) = 1$. As in Example 1, the dynamics of $x(t)$ can be analyzed by the corresponding system of slow and fast variables:

$$\begin{cases} \dot{\xi} = \cos\theta + \xi^{-2} \left\{ \cos\theta \sin(\xi\cos\theta)\cosh(\xi\sin\theta) + \sin\theta\cos(\xi\cos\theta)\sinh(\xi\sin\theta) \right\}, \\ \dot{\theta} = \epsilon^{-1}\xi + \xi^{-3} \left\{ \cos\theta\cos(\xi\cos\theta)\sinh(\xi\sin\theta) - \sin\theta\sin(\xi\cos\theta)\cosh(\xi\sin\theta) \right\}. \end{cases} \tag{2.2.26}$$

with initial conditions $\xi(0) = 1$ and $\theta(0) = 0$. We see immediately from Definition **3.1.1** that ξ is a slow variable. Note that (2.2.26) is never used in our algorithm; we use ξ in (2.2.26) only to show that the results computed by the algorithm is correct. The averaged equation for the slow variable ξ is

$$\dot{\bar{\xi}} = \bar{\xi}^{-1}, \quad \bar{\xi}(0) = 1. \tag{2.2.27}$$

In this example, we used Algorithm 2, the Midpoint rule macro-solver and ODE45 micro-solver with quadratic polynomial interpolation for γ to compute the solution; however, in each micro-simulation, the micro-solver integrates the filtered equation

$$\dot{x}_n = i\epsilon^{-1} x_n |x_n| + K_\Delta(t - t_n) \left\{ (\sin x_n + \mathrm{Re}(x_n) \cdot x_n) |x_n|^{-2} \right\}, \;\; t_n \le t \le t_n + \Delta,$$

with the parameters in Table 2.1. The estimation errors for each different value of Δ with respect to $\epsilon = 10^{-4}$ and 10^{-5} are illustrated in Figure 2.12. Without the filtering technique, the resulting errors are highly oscillatory due to the sampling issue discussed in Section 2.1.2.1.

In Table 2.2, we show the effect of kernels on accuracy in the approximations of the slow variable ξ. Since the error tends to be dominated by the step size H of the macroscopic solver, taking a kernel with one-moment and one-regularity condition is enough to prevent the sampling error.

Table 2.1: (Section 2.2.1) BF HMM parameters for Section 2.2.1

T	H	Δ	h	Micro solver	RelTol, AbsTol(ODE45)	Macro solver
4	1/6	40ϵ	$\epsilon/30$	ODE45	10^{-13}, 10^{-10}	Midpoint rule

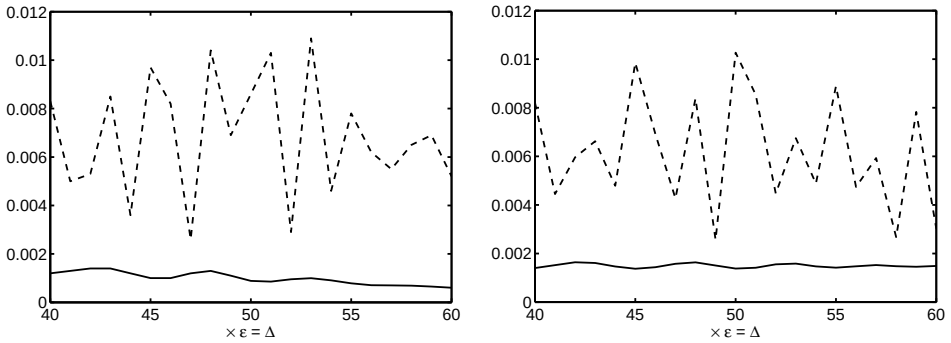

(a) $\epsilon = 10^{-4}$ (b) $\epsilon = 10^{-5}$

Figure 2.12: (Section 2.2.1) Plot of an estimation error $||\bar{\xi}(\cdot) - \xi \circ \gamma(\cdot)||_{L^\infty}$ with different Δ's over $t \in [0, 4]$. The dotted lines are the errors *without* the new filtering. A kernel $K \in \tilde{\mathbb{K}}^{1,1}$ is used.

Table 2.2: Table of $||\bar{\xi}(\cdot) - \xi \circ \gamma(\cdot)||_{L^\infty([0,4])}$ with various kernels $\tilde{\mathbb{K}}^{p,q}$.

(a) $H = 0.2$, $\epsilon = 10^{-4}$, $\Delta = 40\epsilon$

	$q=1$	2	3
$p=1$	2.00(-3)	1.84(-3)	1.99(-3)
w/o filtering	6.76(-3)		

(b) $H = 0.2$, $\epsilon = 10^{-5}$, $\Delta = 40\epsilon$

	$q=1$	2	3
$p=1$	2.21(-3)	2.03(-3)	2.15(-3)
w/o filtering	5.82(-3)		

(c) $H = 0.02$, $\epsilon = 10^{-4}$, $\Delta = 40\epsilon$

	$q=1$	2	3
$p=1$	2.14(-4)	2.79(-4)	1.92(-4)
w/o filtering	8.12(-4)		

(d) $H = 0.02$, $\epsilon = 10^{-5}$, $\Delta = 40\epsilon$

	$q=1$	2	3
$p=1$	4.85(-5)	6.13(-5)	9.05(-6)
w/o filtering	1.16(-3)		

2.2.2 A simplified model for stellar orbits in a galaxy

The following extensively analyzed system is taken from the theory of stellar orbits in a galaxy (see [65, 67]):

$$\begin{cases} r_1'' + a^2 r_1 &= \epsilon r_2^2, \\ r_2'' + b^2 r_2 &= 2\epsilon r_1 r_2, \quad 0 < \tilde{t} < T/\epsilon. \end{cases}$$

Here $r_1(0,\epsilon) = r_2(0,\epsilon) = 1, r_1'(0,\epsilon) = r_2'(0,\epsilon) = 0$; r_1 stands for the radial displacement of the orbit of a star from a reference circular orbit, and r_2 stands for the deviation of the orbit from the galactic plane. The time variable $\tilde{t}$ actually denotes the angle of the planets in a reference coordinate system. After a rescaling of time, the system can be written in the following form

$$\mathbf{x}' = \epsilon^{-1} \begin{bmatrix} 0 & a & 0 & 0 \\ -a & 0 & 0 & 0 \\ 0 & 0 & 0 & b \\ 0 & 0 & -b & 0 \end{bmatrix} \mathbf{x} + \begin{bmatrix} 0 \\ x_2^2/a \\ 0 \\ 2x_1x_2/b \end{bmatrix}, \quad \mathbf{x}(0) = \begin{bmatrix} 1 \\ 0 \\ 1 \\ 0 \end{bmatrix}, \tag{2.2.28}$$

where $\mathbf{x} = [x_1, v_1, x_2, v_2]^{\mathrm{t}}$. One seeks approximation of the effective properties that takes place in a constant time interval. When $a = 2$ and $b = 1$, resonance of oscillatory modes take effect in the lower order term. Using the numerical algorithm proposed in [5], three functionally independent slow variables are identified to be

$$\xi_1 = x_1^2 + v_1^2, \quad \xi_2 = x_2^2 + v_2^2, \quad \xi_3 = x_1x_2^2 + 2v_1x_2v_2 - x_1v_2^2. \tag{2.2.29}$$

where $\xi_i : \mathbb{R}^4 \to \mathbb{R}$, $i = 1, 2, 3$.

In Figure 2.2.2, we present a result computed by our method and compare it with the results computed by FLAVORS [99] with two different sets of parameters. Figure 2.13a shows the BF HMM Mid-ODE45 (Midpoint rule macro-solver and ODE45 micro-solver with quadratic polynomial interpolation for γ) result computed with the parameters tabulated in Table 2.3 and a kernel $K \in \tilde{\mathbb{K}}^{1,4}$. The resulting error in the slow variables is $\max_{i=1,2,3} ||\xi_i(\cdot) - \xi_i \circ \gamma(\cdot)||_{L^\infty([0,14])} = 0.049$. The computational time on a one-year old desktop is about 7s.

In Figure 2.13b, we show the result computed by FLAVORS with the parameters within the recommended regimes. To be more precise, as stated in [99], the required conditions for FLAVORS are as follows:

$$\Delta \ll \epsilon \ll H \ll 1 \text{ and } \left(\frac{\Delta}{\epsilon}\right)^2 \ll H \ll \frac{\Delta}{\epsilon}. \tag{2.2.30}$$

In [99], the proposed empirical choice is given by $\Delta = \gamma\epsilon$, $H = \gamma\frac{\Delta}{\epsilon}$ where γ is small (0.1, for instance). Figure 2.13b is from their empirical choice $\Delta = \gamma\epsilon$, $H = \gamma\frac{\Delta}{\epsilon}$ where $\gamma = 0.1$. We obtained $\max_{i=1,2,3} ||\xi_i(\cdot) - \xi_i \circ \tilde{\mathbf{x}}(\cdot)||_{L^\infty([0,14])}$=0.56. The computational time on the same machine is about 3.1s.

In Figure 2.13c, we show the result computed by FLAVOR by a set of parameters which do not fall in the recommendation. With the parameters shown in the Figure, we obtained $\max_{i=1,2,3} ||\xi_i(\cdot) - \xi_i \circ \tilde{\mathbf{x}}(\cdot)||_{L^\infty([0,14])}$=0.23. The computational time is about 8.4s.

Table 2.3: (Section 2.2.2) BF HMM parameters for Section 2.2.2

ϵ	T	h	Δ	H	Micro solver	RelTol	Macro solver
10^{-4}	14	$\epsilon/30$	15ϵ	0.25	ODE45	10^{-4}	Midpoint rule

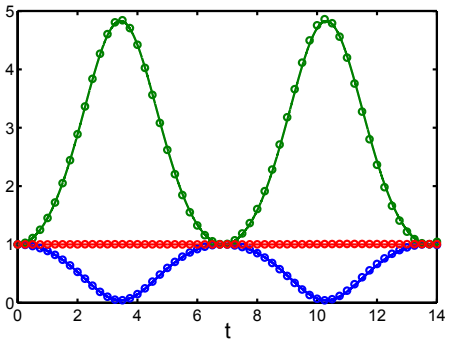

(a) BF HMM Mid-ODE45 with $\Delta = 7\epsilon$, $H = 0.25$.

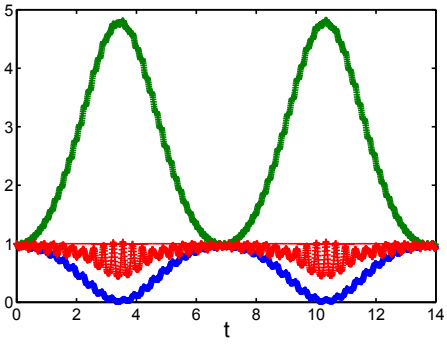

(b) FLAVORS Mid-ODE45 with $\Delta = \gamma\epsilon$, $H = \gamma\frac{\Delta}{\epsilon}$, $\gamma = 0.1$.

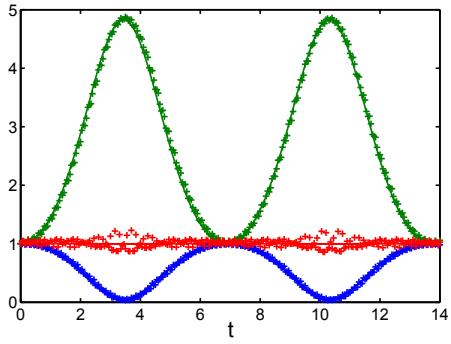

(c) FLAVORS Mid-ODE45 with $\Delta = 20\epsilon$, $H = 0.05$.

Figure 2.13: (Section 2.2.2) The dynamics of the slow variables ξ_1, ξ_2 and ξ_3 in (2.2.28). Subfigures (b) and (c) FLAVORS fail to preserve the geometrical structure of the flow.

2.2.3 The Fermi-Pasta-Ulam problem

The Fermi-Pasta-Ulam problem is a dynamical system which reveals highly unexpected behavior. We consider a chain of $2k+1$ springs connected with alternating soft $k+1$ nonlinear and stiff k linear springs, and both ends are soft ones and fixed. This problem has been a test bed for evaluating the long-time performance of geometric integrators [55]. The model is derived from the following Hamiltonian:

$$H(p,q) = \frac{1}{2}\sum_{i=1}^{2k} p_i^2 + \frac{1}{4}\epsilon^{-2}\sum_{i=1}^{k}(q_{2i} - q_{2i-1})^2 + \sum_{i=1}^{k}(q_{2i+1} - q_{2i})^4. \tag{2.2.31}$$

Using the change of variables given in [5], we have the following equations of motion

$$\begin{cases} \dot{y}_i = u_i, \\ \dot{x}_i = \epsilon^{-1} v_i, \\ \dot{u}_i = -(y_i - \epsilon x_i - y_{i-1} - \epsilon x_{i-1})^3 + (y_{i+1} - \epsilon x_{i+1} - y_i - \epsilon x_i)^3, \\ \dot{v}_i = -\epsilon^{-1} x_i + (y_i - \epsilon x_i - y_{i-1} - \epsilon x_{i-1})^3 + (y_{i+1} - \epsilon x_{i+1} - y_i - \epsilon x_i)^3. \end{cases} \tag{2.2.32}$$

Both fixed ends yield $y_0 = x_0 = y_{k+1} = x_{k+1} = 0$ and we choose $k = 3$ for an illustration. Initial conditions are $y_1 = x_1 = u_1 = 1$ and zero otherwise. Total energies of the stiff springs are given by

$$I_i = x_i^2 + v_i^2, \quad i = 1, 2, 3 \tag{2.2.33}$$

where $I_i : \mathbb{R}^{12} \to \mathbb{R}$. See [16, 17, 54] and references therein for some recent progress. With ϵ denoting the time scale of the fast oscillations, the nontrivial energy transfer take place in the very long ϵ^{-1} time scale. Even if one could afford the long computational time, it is unclear if the computational results retain enough effective accuracy. The FPU is a good model problem to study the proposed new algorithm for computation in $\mathcal{O}(\epsilon^{-1})$ timescale. This section is intended to deal with the multiple time scales (> 2) using a two-scale method. In Section 2.5, focusing on this Fermi-Pasta-Ulam (FPU) problem, we will propose a three-scale version of the BF HMM.

Figure 2.29 shows the energy exchange of the stiff springs over $T = \epsilon^{-1}$, with $\epsilon = 2 \cdot 10^{-3}$. We compare the results computed by the BF HMM Verlet-ODE45 (Verlet macro-solver and ODE45 micro-solver with quadratic polynomial interpolation for γ) with those by an exponential integrator with Deuflhard's filter functions [30, 55] with the stepsize $h = 5 \cdot 10^{-7}$, which we used as a reference solution. We point out here that in order to obtain a reliable reference numerical solution, the aforementioned step size is needed. Furthermore, we had to use 128-bit precision for the variables in our computation in order to retain reasonable significant digits at time T in our computation with the exponential integrator. The BF HMM result is computed with the parameters given in Table 2.9, and with the filter $K^{cos} \in \tilde{\mathbb{K}}^{1,1}$ for the filtered equation that corresponds to (4.7.79). In this setup, the BF HMM runs approximately 30,000 times faster. The difference in the stiff springs' total energy between the HMM solution and the reference solution measured in the supremum norm is $\max_{i=1,2,3} ||I_i(\cdot) - I_i \circ \gamma(\cdot)||_{L^\infty([0,\epsilon^{-1}])} = 0.027$.

In Figure 2.15, with $\epsilon = 5 \cdot 10^{-3}$, we show a result computed by the same BF HMM algorithm for longer time and demonstrate the stability of our algorithm in a longer time interval. See Table 2.10 for simulation parameters.

Table 2.4: (Section 2.2.3) BF HMM parameters for Figure 2.29.

ϵ	T	h	Δ	H	Micro solver	RelTol	Macro solver
$2 \cdot 10^{-3}$	ϵ^{-1}	$\epsilon/10$	$6\pi\epsilon$	$1/3$	ODE45	10^{-7}	Verlet

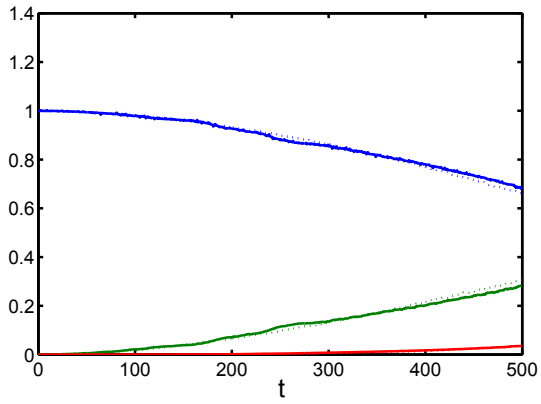

Figure 2.14: (Section 2.2.3) The solid lines correspond to the direct numerical simulation (DNS) solution with an exponential integrator. Dotted lines correspond to the HMM.

Table 2.5: (Section 2.2.3) BF HMM parameters for Figure 2.15.

ϵ	T	h	Δ	H	Micro solver	RelTol	Macro solver
$5 \cdot 10^{-3}$	$7 \cdot \epsilon^{-1}$	$\epsilon/10$	15ϵ	0.3	ODE45	10^{-7}	Verlet

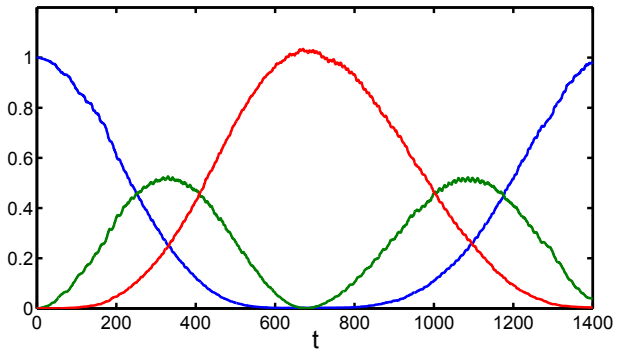

Figure 2.15: (Section 2.2.3) Long time simulation by BF HMM Verlet-ODE45 to $T = 7\epsilon^{-1}$.

2.3 Stochastic differential equations

We will consider the BF HMM for SDEs on the $\mathcal{O}(1)$ time scale (advective time scale).

2.3.1 Slow-fast systems

We start with the simple case in which state variables are split into slow and fast variables.

$$\begin{cases} dX = f(X,Y)dt, & X(0) = X_0, \\ dY = \frac{1}{\epsilon}g(X,Y)dt + \frac{1}{\sqrt{\epsilon}}h(Y)dW, & Y(0) = Y_0. \end{cases}$$

As explained in Section 1.2.2.2, in the limit $\epsilon \to 0$, the dynamics of X can be approximated by the effective equation

$$dX = F(X)dt,$$

where

$$F(X) = \int f(X,y)\mu_X(dy).$$

Our basic algorithm is summarized below.

Algorithm 5. *(SDE Forward Euler BF HMM)*

1. (Micro-solver full equation) Solve

$$\begin{cases} dX = f(X,Y)dt, \\ dY = \frac{1}{\epsilon}g(X,Y)dt + \frac{1}{\sqrt{\epsilon}}h(Y)dW, \end{cases}$$

with the initial condition (X_n, Y_n), forward in time over Δ amount of time. Denote the solution at $t = t_n + \Delta$ by (X^1_Δ, Y^1_Δ).

2. (Micro-solver unperturbed equation) Solve

$$\begin{cases} dX = 0dt, \\ dY = \frac{1}{\epsilon}g(X,Y)dt + \frac{1}{\sqrt{\epsilon}}h(Y)dW, \end{cases}$$

with the initial condition (X_n, Y_n), forward in time over Δ amount of time where the random variable for dW is previously used in step 1. Denote the solution at $t = t_n + \Delta$ by (X^0_Δ, Y^0_Δ).

3. (Forward Euler macro-solver) Compute (X_{n+1}, Y_{n+1}) using (X^1_Δ, Y^1_Δ) and (X^0_Δ, Y^0_Δ),

$$(X_{n+1}, Y_{n+1}) = (X^1_\Delta, Y^1_\Delta) + \frac{H-\Delta}{\Delta}\left\{(X^1_\Delta, Y^1_\Delta) - (X^0_\Delta, Y^0_\Delta)\right\}. \qquad (2.3.34)$$

We apply our Algorithm 5 to stochastic systems. Consider the following test problem

$$\begin{cases} dX = -(X-Y)dt, & X(0) = 1, \\ dY = -\frac{1}{\epsilon}(X^2+Y)dt + \sqrt{\frac{1}{\epsilon}}YdW, & Y(0) = 1. \end{cases}$$

The BF HMM result is computed with the parameters given in Table 2.6. In this setup, the BF HMM runs approximately 400 times faster. Figure 2.16 compares the results computed by the proposed HMM with those by the Euler method [79]. The sample averages of X against t are plotted with a solid line (Euler) and circles (BF HMM). We estimate the errors of the method by comparing the standard deviation of sample paths.

Table 2.6: BF HMM parameters

ϵ	T	h	Δ	H	Micro solver	Macro solver
10^{-4}	3	$\epsilon/30$	30ϵ	0.1	Forward Euler	Forward Euler

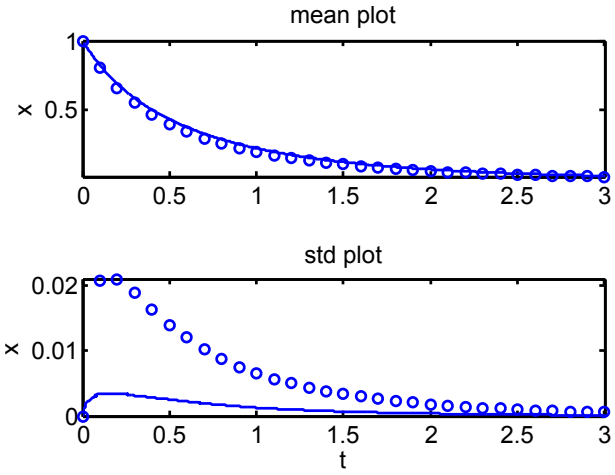

Figure 2.16: Circles are the results of the BF HMM. Solid lines are DNS solutions using Forward Euler with $h = \epsilon/30$. 500 independent paths are taken.

2.3.2 SDEs with hidden slow variables

In this section, we consider a system which is not split into the fast and slow coordinates. Let $X \in \mathbb{R}^d$,

$$dX = \frac{1}{\epsilon} f_2(X)dt + \sqrt{\frac{1}{\epsilon}} f_1(X)dW + f_0(X)dt, \quad X(0) = X_0. \tag{2.3.35}$$

Our basic algorithm for the generic system (2.3.35) is summarized below.

Algorithm 6. *(Forward Euler BF HMM)*

1. (Micro-solver full equation) Solve

$$dX = \frac{1}{\epsilon} f_2(X)dt + \sqrt{\frac{1}{\epsilon}} f_1(X)dW + f_0(X)dt, \quad X(0) = X_n$$

forward in time over Δ amount of time. Denote the solution at $t = t_n + \Delta$ by X^1_Δ.

2. (Micro-solver unperturbed equation) Solve

$$dX = \frac{1}{\epsilon} f_2(X)dt + \sqrt{\frac{1}{\epsilon}} f_1(X)dW, \quad X(0) = X_n$$

forward in time over Δ amount of time where the random variable for dW is previously used in step 1. Denote the solution at $t = t_n + \Delta$ by X^0_Δ.

3. (Forward Euler macro-solver) Compute X_{n+1} using X^1_Δ and X^0_Δ,

$$X_{n+1} = X^1_\Delta + \frac{H-\Delta}{\Delta}\left\{X^1_\Delta - X^0_\Delta\right\}. \tag{2.3.36}$$

We apply our BF HMM algorithm described above. We start with the following slow-fast system

$$\begin{cases} dX = -(Y-2)dt, & X(0) = 3, \\ dY = \frac{1}{\epsilon}(X-Y)dt + \sqrt{\frac{1}{\epsilon}}Y dW, & Y(0) = 1. \end{cases} \tag{2.3.37}$$

Intuitively, it is clear that when ϵ is small, the X variable in the RHS of dY does not change much before Y reaches local equilibrium in a time scale of $\mathcal{O}(\epsilon)$. In addition, the effective equation for X is obtained by averaging the RHS of dX in (2.3.37) with respect to the conditional equilibrium distribution of Y.

$$\dot{\bar{X}} = -(\bar{X}-2), \quad \bar{X}(0) = 3.$$

In order to have a stochastic system with hidden slow variables, we change (2.3.37) to polar coordinates

$$\begin{cases} R = \sqrt{X^2+Y^2}, \\ \theta = \tan^{-1}(\frac{Y}{X}). \end{cases}$$

The equations for R and θ are found from Ito's formula. We write

$$\begin{cases} dR = \left(2\cos(\theta) - R\cos(\theta)\sin(\theta)\right)dt \\ \qquad +\frac{1}{2\epsilon}\left(2R\cos(\theta)\sin(\theta) - 2R - R\cos(\theta)^4 + 3R\cos(\theta)^2\right)dt + \frac{R}{\sqrt{\epsilon}}\sin(\theta)^2 dW, \\ d\theta = \frac{1}{\epsilon}\left(\cos(\theta)^3\sin(\theta) - 2\cos(\theta)\sin(\theta) + \cos(\theta)^2\right)dt \\ \qquad +\sqrt{\frac{1}{\epsilon}}\cos(\theta)\sin(\theta)dW + \left(-\frac{2}{R}\sin(\theta) + 1 - \cos(\theta)^2\right)dt. \end{cases} \tag{2.3.38}$$

where both dW should be integrated with the same random number in each step. Therefore, in (2.3.38) there is a hidden slow variable. Accordingly, we choose an unperturbed equation as

$$\begin{cases} dR = \frac{1}{2\epsilon}\left(2R\cos(\theta)\sin(\theta) - 2R - R\cos(\theta)^4 + 3R\cos(\theta)^2\right)dt + \frac{R}{\sqrt{\epsilon}}\sin(\theta)^2 dW, \\ d\theta = \frac{1}{\epsilon}\left(\cos(\theta)^3\sin(\theta) - 2\cos(\theta)\sin(\theta) + \cos(\theta)^2\right)dt + \sqrt{\frac{1}{\epsilon}}\cos(\theta)\sin(\theta)dW. \end{cases}$$

Figure 2.17 shows the results computed by the Forward Euler BF HMM with those by the Euler method. With the parameters given in Table 2.6, the BF HMM runs approximately 600 times faster with a comparable standard deviation. The sample averages of X against t are plotted with a solid line (Euler) and circles (BF HMM).

Table 2.7: BF HMM parameters

ϵ	T	h	Δ	H	Micro solver	Macro solver
10^{-4}	2	$\epsilon/1000$	20ϵ	0.1	Forward Euler	Forward Euler

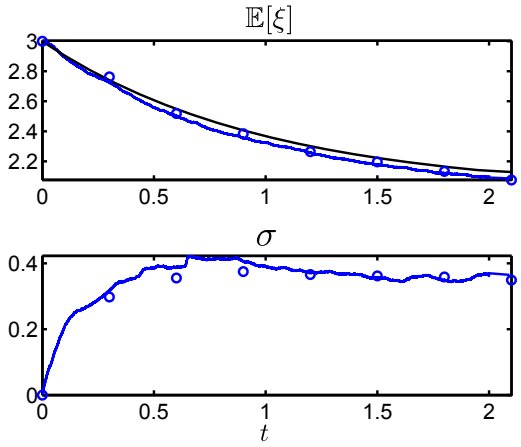

Figure 2.17: Plot of $R \circ X(t)$ over $t \in [0, 2]$. The dynamics of the slow variable R. Circles are results of the Forward Euler BF HMM. A dotted line (DNS solution) is computed using Forward Euler with $h = \epsilon/1000$. A solid line is an averaged solution $\bar{X}$. 500 independent paths are taken.

2.4 Further discussions on the splitting

In the recent, we have attempted to construct general strategies for the BF HMM. The main question is how to split a given equation into perturbed and unperturbed parts in order to compute the effective dynamics. This is indeed the central issue of the BF HMM. Our presentation here is very much motivated by the spring double pendulum (Section 2.4.1) and the modified stellar orbit problem (Section 2.4.2).

2.4.1 The stiff spring double pendulum

We consider a highly oscillatory solution in Hamiltonian systems. As discussed in Section 1.1, the potential energy is given by a sum of $U + V_\epsilon$ in stiff spring double pendulum. Two mass points $x_i = (x_{i1}, x_{i2})$ of mass 1 are serially attached to a point of suspension (origin) by two massless stiff springs with length l_i and spring constants $\left(\frac{1}{\epsilon}\right)^2$, for $i = 1, 2$. See Figure 2.18. We consider the motion of two mass points. In cartesian coordinates, the Hamiltonian is given by

$$H(x, y) = \frac{1}{2} y^T y + U(x) + V_\epsilon(x),$$

where $U(x) = x_{12} + x_{22}$ is a smooth potential energy, and

$$V_\epsilon(x) = \frac{1}{2}(\frac{1}{\epsilon})^2(||x_1|| - l_1)^2 + \frac{1}{2}(\frac{1}{\epsilon})^2(||x_1 - x_2|| - l_2)^2$$

is the oscillatory energy. Then the Hamiltonian system in the (x, y) coordinate reads as

$$\begin{cases} \dot{x} = y, & x(0) = x_0, \\ \dot{y} = -\nabla_x U(x) - \nabla_x V_\epsilon(x), & y(0) = y_0, \end{cases} \tag{2.4.39}$$

where $\nabla_x U(x) = [0, 1, 0, 1]^t$ and

$$\nabla_x V(x) = \begin{bmatrix} \frac{1}{\epsilon^2}\frac{(||x_1||-1)x_{11}}{||x_1||} + \frac{1}{\epsilon^2}\frac{(||x_1-x_2||-1)(x_{11}-x_{21})}{||x_1-x_2||} \\ \frac{1}{\epsilon^2}\frac{(||x_1||-1)x_{12}}{||x_1||} + \frac{1}{\epsilon^2}\frac{(||x_1-x_2||-1)(x_{12}-x_{22})}{||x_1-x_2||} \\ -\frac{1}{\epsilon^2}\frac{(||x_1-x_2||-1)(x_{11}-x_{21})}{||x_1-x_2||} \\ -\frac{1}{\epsilon^2}\frac{(||x_1-x_2||-1)(x_{12}-x_{22})}{||x_1-x_2||} \end{bmatrix}. \tag{2.4.40}$$

An initial condition is given as for the coordinate $x = (\sqrt{0.5}, -\sqrt{0.5}, 0, -\sqrt{2} + 5\epsilon)^t$, and for the momentum $y = [0, 0, 0, 0]^t$.

We perform the canonical transformation using angles $q_0 = (q_{01}, q_{02})^t$ and elongations $q_1 = (q_{11}, q_{12})^t$, see Figure 2.18, and get the Hamiltonian of the form

$$H(p, q) = \frac{1}{2} p^T M(q)^{-1} p + U(q) + \frac{1}{2\epsilon^2} q_1^T q_1 \tag{2.4.41}$$

with a symmetric positive definite matrix $M(q)$. In Figure 2.19, we depict the dynamics of (2.4.39) in the (p, q) coordinate.

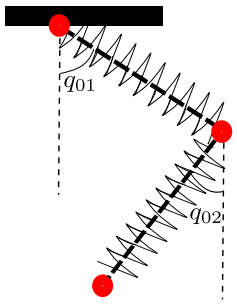

Figure 2.18: Spring double pendulum

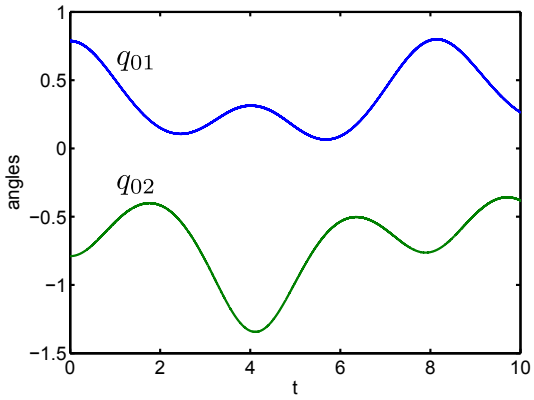

Figure 2.19: Dynamics of the angle q_{01} and q_{02} of the spring double pendulum. $\epsilon = 10^{-3}$.

Next we discuss how the slow variables, i.e., angles, can be approximated using the BF HMM. First of all, we consider the natural splitting in the (x, y) coordinate:

$$\begin{cases} \dot{x}_u = 0, \\ \dot{y}_u = -\nabla_{x_u} V_\epsilon(x_u), \end{cases} \tag{2.4.42}$$

where the subscript u means the unperturbed equation. Shown in Figure 2.20 is an example of the numerical results produced using Midpoint rule BF HMM with z-structure. One can see that after a limited number of steps, the BF HMM does not approximate the correct dynamics. Although we tested several combinations of the unperturbed equation, BF HMMs either diverge or approximate wrong dynamics. The existence of an adequate splitting of (2.4.39) in the (x, y) coordinate is still an open question. However, the BF HMM is applicable in the (p, q) coordinate with a

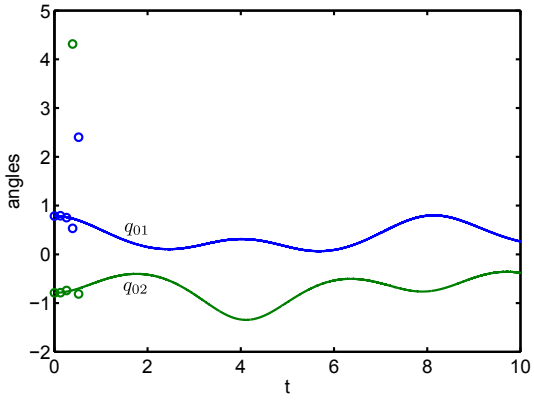

Figure 2.20: Results of the BF HMM are depicted as circles. The BF HMM blows up as $|q_{01}| \geq 10^4$ after only 5 steps. $\epsilon = 10^{-3}$ and $\Delta = 30\epsilon$.

special technique described below. Before launching into a discussion about this, we would like to see how they behave differently in terms of estimating $\mathcal{F}_{HMM}(\cdot, \cdot)$. In Figure 2.21, we plot two trajectories of p_{11} and p_{12}, describing a process of evaluating $\mathcal{F}_{HMM}(\gamma_0, t_0)$ with Midpoint rule BF HMM with z-structure. See Figure 2.9. At $t = 0$, we solve the unperturbed equation over Δ amount of time (for γ^*_{-1}), and at the same time, the perturbed equation is solved over 2Δ amount. Finally, with this initial condition, we solve the unperturbed equation during Δ time (for γ^*_1). The solid lines show the result obtained from splitting in the (x, y) coordinate, i.e., splitting with (2.4.39) and (2.4.42). On the other hand, the dotted lines are from splitting in the (p, q) coordinates. The exact solutions of p_{11} and p_{12} are oscillating in the $\mathcal{O}(\epsilon)$ time scale with bounded amplitudes (< 3). This figure shows that splitting in (x, y) is much more unstable than the one in (p, q). See the sharp drop of p_{11} in the backward solution of (x, y) splitting at $t = 2\Delta$ and the sharp increases of p_{12} in the forward/backward solutions of the unperturbed equation.

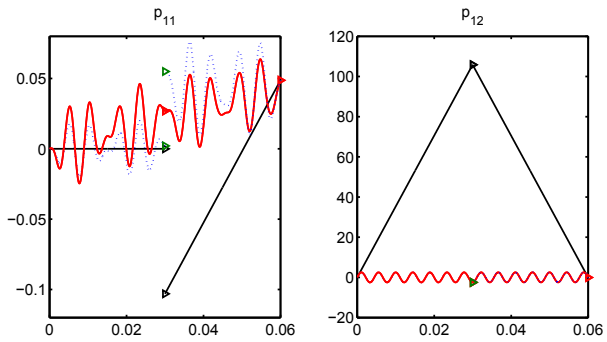

Figure 2.21: Comparison of two splittings in (x, y) and (p, q). The solid black lines show the result obtained from splitting in (x, y). The dotted blue lines are obtained from splitting in (p, q) with a special choice of unperturbed equation. Each γ^* is described by a triangle. $\mathcal{F}_{HMM}(\gamma_0, t_0)$ for p_{11} from (x, y) is indeed the opposite sign with the one from (p, q).

Now let me explain splitting in the (p, q) coordinate. Keeping the system with (2.4.41) as the full equation, we choose a nontrivial unperturbed equation associated with the Hamiltonian $H_u(p, q) = \frac{1}{2}p^T M(q)^{-1}p + \frac{1}{2\epsilon^2}q_1^T q_1$ and artificially set the RHS of $\dot{q}_{01}$,$\dot{q}_{02}$, $\dot{p}_{01}$ and $\dot{p}_{01}$ equal to 0. Indeed, $q_{01}(t)$, $q_{02}(t)$ and their momenta are kept fixed in backward-forward simulations in time. In fact, this seems to be special to the system, but freezing only such four variables result in the correct simulation. See Table 2.8 and Figure 2.22 for the numerical results.

Table 2.8: (Section 2.4.1) BF HMM parameters

T	H	Δ	h	Micro solver	RelTol, AbsTol(ODE45)	Macro solver
5	0.2	30ϵ	$\epsilon/30$	ODE45	10^{-8}, 10^{-8}	Midpoint rule

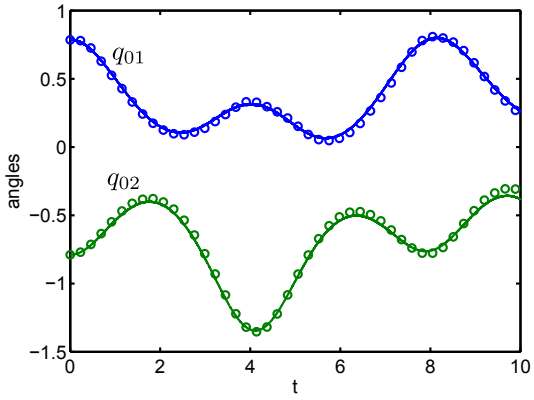

Figure 2.22: (Section 2.4.1) The dynamics of the slow variables (angles). Circles are results of the BF HMM Mid-ODE45 with z-structure. $\epsilon = 10^{-3}$ is used. DNS solutions are integrated using Stormer-Verlet with small step size $h = \epsilon^2/20$.

2.4.2 A modified model for stellar orbits in a galaxy (incorrect unperturbed equation)

In many problems, there always exists uncertainty to determine an unperturbed equation from the full equation. We will discuss some of the issues that have been motivated using the stellar orbit problem. Unlike the equations that we discussed previously, the problems presented here are artificially developed for the purpose. In Section 2.2.2, we considered the following equation

$$\mathbf{x}' = \epsilon^{-1} \begin{bmatrix} 0 & a & 0 & 0 \\ -a & 0 & 0 & 0 \\ 0 & 0 & 0 & b \\ 0 & 0 & -b & 0 \end{bmatrix} \mathbf{x} + \begin{bmatrix} 0 \\ x_2^2/a \\ 0 \\ 2x_1x_2/b \end{bmatrix}, \quad \mathbf{x}(0) = \begin{bmatrix} 1 \\ 0 \\ 1 \\ 0 \end{bmatrix}, \tag{2.4.43}$$

where $\mathbf{x} = [x_1, v_1, x_2, v_2]^{\mathrm{t}}$. As described earlier, when $a = 2$ and $b = 1$, resonance of oscillatory modes take effect in the lower order term, and the equation,

$$\mathbf{x}_u' = \epsilon^{-1} \begin{bmatrix} 0 & a & 0 & 0 \\ -a & 0 & 0 & 0 \\ 0 & 0 & 0 & b \\ 0 & 0 & -b & 0 \end{bmatrix} \mathbf{x}_u, \tag{2.4.44}$$

is chosen as an unperturbed equation. As a summary, an ODE system is formally given in the following form

$$\dot{\mathbf{x}} = \epsilon^{-1} A\mathbf{x} + f(\mathbf{x}), \quad \mathbf{x}(0) = \mathbf{x}_0 \tag{2.4.45}$$

and the unperturbed equation is chosen as

$$\dot{\mathbf{x}} = \epsilon^{-1} A\mathbf{x}.$$

We may modify (2.4.45) and consider

$$\dot{\mathbf{x}} = \epsilon^{-1}(A + B\epsilon)\mathbf{x} + f(\mathbf{x}), \quad \mathbf{x}(0) = \mathbf{x}_0 \tag{2.4.46}$$

where a matrix B is independent of ϵ. With

$$\dot{\mathbf{x}} = \epsilon^{-1}(A + B\epsilon)\mathbf{x}$$

as the unperturbed equation, we will see how the BF HMM works. First, we refer to the change of variables explained in [5]. The ODE (2.4.43) takes the form

$$\begin{aligned}
\dot{\xi}_1 &= (2a)^{-1}\sqrt{\xi_1}\xi_2 \left[2\sin(a\phi_1) + \sin(a\phi_1 + 2b\phi_2) + \sin(a\phi_1 - 2b\phi_2)\right], \\
\dot{\xi}_2 &= b^{-1}\sqrt{\xi_1}\xi_2 \left[\sin(a\phi_1 + 2b\phi_2) - \sin(a\phi_1 - 2b\phi_2)\right], \qquad (2.4.47) \\
\dot{\phi}_1 &= -\epsilon^{-1} + \xi_2(4a^2\sqrt{\xi_1})^{-1} \left[2\cos a\phi_1 + \cos(a\phi_1 + 2b\phi_2) + \cos(a\phi_1 - 2b\phi_2)\right], \\
\dot{\phi}_2 &= -\epsilon^{-1} + \sqrt{\xi_1}(2b^2)^{-1} \left[2\cos a\phi_1 + \cos(a\phi_1 + 2b\phi_2) + \cos(a\phi_1 - 2b\phi_2)\right] \qquad (2.4.48)
\end{aligned}$$

When $a = 2$ and $b = 1$, the leading order term in $\theta = a\phi_1 - 2b\phi_2$ is canceled exactly and resonance of oscillatory modes take effect in the lower order term. The interesting situation is when $a = 2 + k\epsilon$ and $b = 1$ with $k = \mathcal{O}(1)$. In this case, $a\phi_1 - 2b\phi_2 = \mathcal{O}(1)$, and the slow behaviors described by ξ_1, ξ_2 and ξ_3 are very different from the one we have seen. See (Left) in Figure 2.23.

In addition, with the unperturbed equation 2.4.2, we show that the BF HMM approximates the totally wrong dynamics. See (Right) in Figure 2.23.

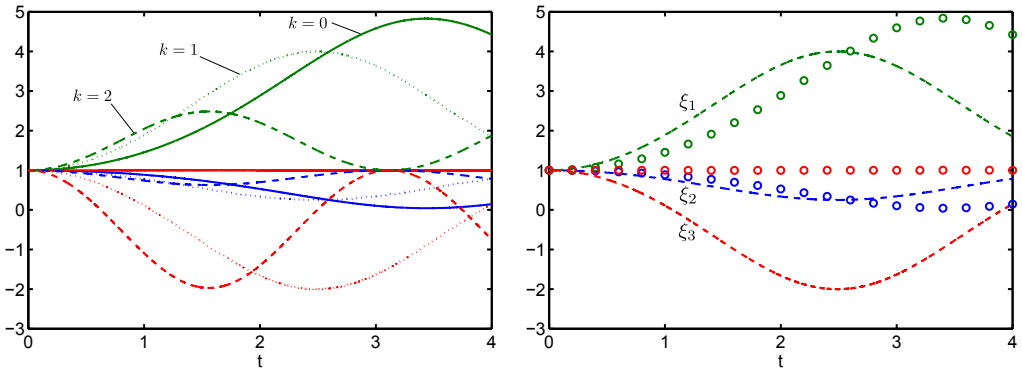

Figure 2.23: Dynamics of the modified stellar orbit problem. (Left) As k increases, the dynamics of ξ_1, ξ_2 becomes stationary around the initial condition, and ξ_3 highly oscillates. (Right) $a = 2 + \epsilon$, $b = 1$, $\epsilon = 10^{-4}$, BF HMM approximates wrong dynamics. BF HMM parameters are $\Delta = 30\epsilon$ and $H = 0.2$.

2.4.2.1 Analysis

Let $\theta = a\phi_1 - 2b\phi_2$ be the resonant mode.

When $a = 2$, and $b = 1$, the effective equation of (2.4.48) is

$$\begin{aligned} \dot{\xi}_1 &= (2a)^{-1}\sqrt{\xi_1}\xi_2\left[\sin(\theta)\right], \\ \dot{\xi}_2 &= b^{-1}\sqrt{\xi_1}\xi_2\left[-\sin(\theta)\right], \\ \dot{\theta}_{a=2} &= -0 + a\xi_2(4a^2\sqrt{\xi_1})^{-1}\left[\cos(\theta)\right] - 2b\sqrt{\xi_1}(2b^2)^{-1}\left[\cos(\theta)\right]. \end{aligned} \tag{2.4.49}$$

On the other hand, when $a = 2 + k\epsilon$, and $b = 1$, the effective equation of (2.4.48) is

$$\begin{aligned} \dot{\tilde{\xi}}_1 &= (2a)^{-1}\sqrt{\tilde{\xi}_1}\tilde{\xi}_2\left[\sin(\tilde{\theta})\right], \\ \dot{\tilde{\xi}}_2 &= b^{-1}\sqrt{\tilde{\xi}_1}\tilde{\xi}_2\left[-\sin(\tilde{\theta})\right], \\ \dot{\tilde{\theta}}_{a=2+k\epsilon} &= -k + a\tilde{\xi}_2(4a^2\sqrt{\tilde{\xi}_1})^{-1}\left[\cos(\tilde{\theta})\right] - 2b\sqrt{\tilde{\xi}_1}(2b^2)^{-1}\left[\cos(\tilde{\theta})\right]. \end{aligned} \tag{2.4.50}$$

Suppose that we choose the unperturbed equation as

$$\mathbf{x}_u' = \epsilon^{-1} \begin{bmatrix} 0 & a & 0 & 0 \\ -a & 0 & 0 & 0 \\ 0 & 0 & 0 & b \\ 0 & 0 & -b & 0 \end{bmatrix} \mathbf{x}_u \tag{2.4.51}$$

and that we solve for $\mathbf{x}_u$ over $t \in [0, \Delta]$. Then $\theta_{a=2}(\mathbf{x}_u(\Delta)) = 0$ but $\tilde{\theta}_{a=2+k\epsilon}(\mathbf{x}_u(\Delta)) = -k\Delta$.[1]The BF HMM with (2.4.51) always calculate the slow dynamics of (2.4.49). We see what happens in Forward Euler BF HMM with the unperturbed equation (2.4.51). We will focus on evaluating of $\tilde{\theta}^{BF}_{t=t_1}$ which MUST be close to $\tilde{\theta}(t_1)$. Recall that $a = 2 + k\epsilon$, $b = 1$. When we solve the unperturbed equation (2.4.51) over $[0, \Delta]$,

$$\xi_{1,u}(\Delta) - \xi_1(0) = 0, \quad \xi_{2,u}(\Delta) - \xi_2(0) = 0, \quad \theta_u(\Delta) - \theta(0) = -k\Delta.$$

Please see [1] on the bottom. On the other hand, when we solve the full equation (2.4.50) over $[0, \Delta]$,

$$\begin{aligned} \tilde{\xi}_1(\Delta) - \xi_1(0) &= \int_0^\Delta (2a)^{-1} \sqrt{\tilde{\xi}_1} \tilde{\xi}_2 \sin(\tilde{\theta}) dt, \\ \tilde{\xi}_2(\Delta) - \xi_2(0) &= -\int_0^\Delta b^{-1} \sqrt{\tilde{\xi}_1} \tilde{\xi}_2 \sin(\tilde{\theta}) dt, \\ \tilde{\theta}(\Delta) - \theta(0) &= -k\Delta + \int_0^\Delta \left\{ a\tilde{\xi}_2 (4a^2 \sqrt{\tilde{\xi}_1})^{-1} \cos(\tilde{\theta}) - 2b\sqrt{\tilde{\xi}_1} (2b^2)^{-1} \cos(\tilde{\theta}) \right\} dt. \end{aligned}$$

Without tilde notation is reserved for the solution of (2.4.49). In moving to the next

[1]The corresponding unperturbed equations are given by

$$\dot{\xi}_{1,u} = 0, \quad \dot{\xi}_{2,u} = 0, \quad \dot{\theta}_u|_{a=2+k\epsilon} = a\dot{\phi}_1 - 2b\dot{\phi}_2 = -(k\epsilon)\frac{1}{\epsilon} = -k.$$

step using $\mathcal{F}^{HMM}(\cdot,\cdot)$, we have

$$\begin{aligned}
\frac{\tilde{\xi}_1(\Delta)-\xi_{1,u}(\Delta)}{\Delta} &= \frac{1}{\Delta}\int_0^\Delta (2a)^{-1}\sqrt{\tilde{\xi}_1}\tilde{\xi}_2\sin(\tilde{\theta})dt,\\
\frac{\tilde{\xi}_2(\Delta)-\xi_{2,u}(\Delta)}{\Delta} &= -\frac{1}{\Delta}\int_0^\Delta b^{-1}\sqrt{\tilde{\xi}_1}\tilde{\xi}_2\sin(\tilde{\theta})dt, \qquad (2.4.52)\\
\frac{\tilde{\theta}(\Delta)-\theta_u(\Delta)}{\Delta} &= -k+k+\frac{1}{\Delta}\int_0^\Delta \left\{a\tilde{\xi}_2(4a^2\sqrt{\tilde{\xi}_1})^{-1}\cos(\tilde{\theta})-2b\sqrt{\tilde{\xi}_1}(2b^2)^{-1}\cos(\tilde{\theta})\right\}dt.
\end{aligned}$$

We are now ready to compare $\theta_{t=t_1}\approx\theta(t_1)$ and $\tilde{\theta}^{BF}_{t=t_1}$ using the Forward Euler BF HMM. Note that $a_\theta=2$, $a_{\tilde{\theta}}=2+k\epsilon$, $b_\theta=b_{\tilde{\theta}}=1$.

$$\begin{aligned}
|\theta_{t=t_1}-\tilde{\theta}^{BF}_{t=t_1}| &\leq |\theta(\Delta)-\tilde{\theta}(\Delta)|\\
&\quad+\frac{H}{\Delta}\int_0^\Delta\left|\frac{\xi_2}{4\sqrt{\xi_1}}\cos(\theta)-\frac{(2+k\epsilon)\tilde{\xi}_2}{4(2+k\epsilon)^2\sqrt{\tilde{\xi}_1}}\cos(\tilde{\theta})\right|dt\\
&\quad+\frac{H}{\Delta}\int_0^\Delta\left|\sqrt{\xi_1}\cos(\theta)-\sqrt{\tilde{\xi}_1}\cos(\tilde{\theta})\right|dt\\
&\leq |\theta(\Delta)-\tilde{\theta}(\Delta)|+\frac{H}{\Delta}\int_0^\Delta\left\{C_1|\theta-\tilde{\theta}|+\mathcal{O}(k\epsilon)\right\}dt+\frac{H}{\Delta}\int_0^\Delta C_2|\theta-\tilde{\theta}|dt+\mathcal{O}(H\Delta)
\end{aligned}$$

using Lipschitz continuity of cosine function and slowly evolving of slow variables $\xi_1,\xi_2,\tilde{\xi}_1,\tilde{\xi}_2$ over $t\in[0,\Delta]$.

$$\begin{aligned}
|\theta_{t=t_1}-\tilde{\theta}^{BF}_{t=t_1}| &\leq |\theta(\Delta)-\tilde{\theta}(\Delta)|+\frac{H}{\Delta}\int_0^\Delta C_1|\theta-\tilde{\theta}|dt+\frac{H}{\Delta}\int_0^\Delta C_2|\theta-\tilde{\theta}|dt+\mathcal{O}(Hk\epsilon)+\mathcal{O}(H\Delta)\\
&\leq |\theta(\Delta)-\tilde{\theta}(\Delta)|+2\max\{C_1,C_2\}\frac{H}{\Delta}\int_0^\Delta|\theta-\tilde{\theta}|dt+\mathcal{O}(Hk\epsilon)+\mathcal{O}(H\Delta)\\
&\leq ||\theta-\tilde{\theta}||_{L^\infty[0,\Delta]}+2\max\{C_1,C_2\}\frac{H}{\Delta}\Delta||\theta-\tilde{\theta}||_{L^\infty[0,\Delta]}+\mathcal{O}(Hk\epsilon)+\mathcal{O}(H\Delta)\\
&= (1+2\max\{C_1,C_2\}H)\,||\theta-\tilde{\theta}||_{L^\infty[0,\Delta]}+\mathcal{O}(Hk\epsilon)+\mathcal{O}(H\Delta)\\
&= \max\{\mathcal{O}(k\Delta),\mathcal{O}(Hk\epsilon),\mathcal{O}(H\Delta)\}
\end{aligned}$$

This is erroneous since resulting approximation $\tilde{\theta}^{BF}_{t=t_1}$ using BF HMM is close to $\theta(t_1)$ not $\tilde{\theta}(t_1)$.

2.4.2.2 Correct unperturbed equations

Indeed, these exists an unperturbed equation which enables the BF HMM to behave correctly. We will discuss it and present new numerical results. In order

to cancel $-k$ in (2.4.52),

$$\theta(\Delta) = a\phi_1 - 2\tilde{b}\phi_2 = (2+k\epsilon)(-\frac{\Delta}{\epsilon}) - 2\tilde{b}(-\frac{\Delta}{\epsilon}) = \left\{2 + k\epsilon - 2\tilde{b}\right\}(-\frac{\Delta}{\epsilon}) = 0$$

$$\Longrightarrow \tilde{b} = 1 + \frac{k}{2}\epsilon.$$

Thus the corrected unperturbed equation is

$$\frac{d}{dt}\mathbf{x}_u^{new} = \epsilon^{-1}\begin{bmatrix} 0 & a & 0 & 0 \\ -a & 0 & 0 & 0 \\ 0 & 0 & 0 & b+\frac{k}{2}\epsilon \\ 0 & 0 & -b-\frac{k}{2}\epsilon & 0 \end{bmatrix}\mathbf{x}_u^{new} \tag{2.4.53}$$

so that $\theta_{a=2+k\epsilon}(\mathbf{x}_u^{new}(\Delta)) = 0$, or simply one can choose

$$\frac{d}{dt}\mathbf{x}_u^{new} = \epsilon^{-1}\begin{bmatrix} 0 & a-k\epsilon & 0 & 0 \\ -a+k\epsilon & 0 & 0 & 0 \\ 0 & 0 & 0 & b \\ 0 & 0 & -b & 0 \end{bmatrix}\mathbf{x}_u^{new}. \tag{2.4.54}$$

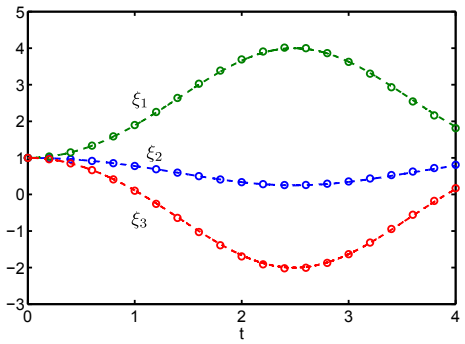

Figure 2.24: BF HMM approximates the dynamics of (2.4.49). Circles are depicting the results of BF HMM Mid-ODE45 with taking (2.4.54) as an unperturbed equation. Parameters $\Delta = 30\epsilon$, $H = 0.2$, and $a = 2+\epsilon$ and $b = 1$ are used.

To sum up, when we have the following equation

$$\dot{\mathbf{x}} = \epsilon^{-1}(A + B\epsilon)\mathbf{x} + f(\mathbf{x}), \quad \mathbf{x}(0) = \mathbf{x}_0 \tag{2.4.55}$$

where a matrix B is independent of ϵ, the correct unperturbed equation should be chosen as

$$\dot{\mathbf{x}} = \epsilon^{-1}A\mathbf{x}.$$

2.5 Three scale BF HMM and the FPU problem

The FPU is a good model problem to study a three-scale algorithm for computation in longer timescale. There are two main challenges in the FPU problem:

1. inaccurate computation of the direct numerical simulation even with very small step size, and
2. multiple scales(> 2) behavior.

We point out that in order to obtain a reliable reference numerical solution, the aforementioned step size is needed. In the following numerical simulations, an exponential integrator with Deuflhard's filter functions [30, 55] with very small stepsize $h \leq \epsilon/20000$ is used as a reference solution. Furthermore, the truncation error, introduced by attempting to represent a number using a finite string of digits, is accumulated due to the many steps. We had to use the extended precision for the variables in our computation at time T with the exponential integrator in order to retain reasonable significant digits. See Figure 2.25.

Several numerical methods have been reported as being applied to the FPU problem. However, the existing results are mainly based upon the two-scale method and the corresponding computational cost is $\mathcal{O}(\epsilon^{-1})$. Thus the running time increases with smaller ϵ. Therefore, it is meaningful to break through the need of $\mathcal{O}(\epsilon^{-1})$ steps in the two-scale algorithm and to devise a multiple-scale algorithm so that the much longer time scale $\mathcal{O}(\epsilon^{-1})$ behavior can be approximated in a truly multiscale fashion.

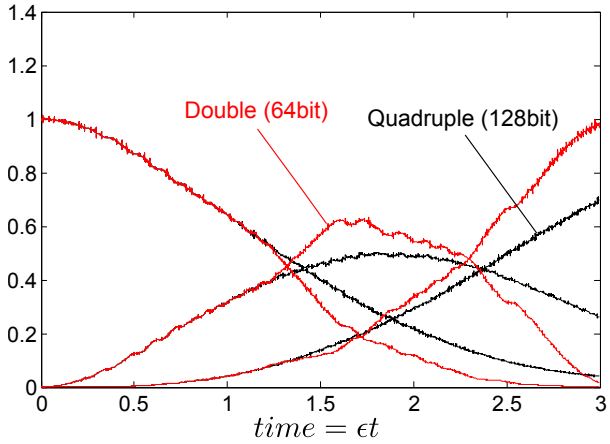

Figure 2.25: A slow energy exchange among the three stiff springs ($k = 3$) takes place on the ϵ^{-1} time scale. Deuflhard's trigonometric method with step size $h = \epsilon/20000$ is used. High precision computation leads more surely to the correct results. However, implementing quadruple precision shows performance drop by a factor 100 compared to double precision.

For convenience in the explanation, we rescale the time so that the slowest time of interest is independent of ϵ. Accordingly, the three time scales $\mathcal{O}(\epsilon^2)$, $\mathcal{O}(\epsilon)$ and $\mathcal{O}(1)$ will be considered. We consider the computation of the effective long time properties of a class of dynamical system, formally written in the form

$$\frac{d}{dt}x^\epsilon = \epsilon^{-2}f_2(x^\epsilon) + \epsilon^{-1}f_1(x^\epsilon) + f_0(x^\epsilon;\epsilon) \tag{2.5.56}$$

with initial condition $x^\epsilon(0) = x_0 \in \mathcal{D}_0 \subset \mathbb{R}^d$. It is assumed that a unique bounded solution exists for each x_0 in a time segment $[0, T]$. Both the bound and T are independent of ϵ.

2.5.1 Introduction - slow variables

Let's start this section with the corresponding time derivative of total energies of the k stiff springs in the rescaled FPU model (4.7.79); for $i = 1, 2, \cdots, k$,

$$\begin{aligned} I_i' &= 2\epsilon^{-1}v_i\left\{(y_i - \epsilon x_i - y_{i-1} - \epsilon x_{i-1})^3 + (y_{i+1} - \epsilon x_{i+1} - y_i - \epsilon x_i)^3\right\} \\ &= 2\epsilon^{-1}v_i\left\{(y_i - y_{i-1})^3 + (y_{i+1} - y_i)^3\right\} - 6v_i\left\{(y_{i-1} - y_i)^2(x_{i-1} + x_i)\right. \\ &\quad \left. +(y_i - y_{i+1})^2(x_i + x_{i+1})\right\} + \cdots \end{aligned}$$

It is important to point out that the time derivative of $I_i(t)$ is formally unbounded along the trajectory for $0 < \epsilon \leq \epsilon_0$. When more than two time scales are considered, such type of slow variables exists and we should take this into account on building multiscale algorithms. We refer to [2, 7] for more detailed discussions. In applying the BF HMM in Section 2.5.2, it is necessary to have that the average of the singular $\mathcal{O}(\epsilon^{-1})$ part in I_i' is effectively very small. This will be addressed in Proposition 2.5.1. Indeed, it can be shown that the average of $v_i \left\{(y_i - y_{i-1})^3 + (y_{i+1} - y_i)^3\right\}$ on any segment of length $\mathcal{O}(\epsilon)$ and larger is of order ϵ. Therefore, the averaged I_i' is bounded independent of ϵ and I_i evolves on the $\mathcal{O}(1)$ time scale, rather than the expected $\mathcal{O}(\epsilon)$.

We first need to define slow variables. Formally, slow variables of a dynamical system involving three or more time scales are defined as below [7].

Definition 2.5.1. A smooth time dependent function $\alpha : [0, T] \mapsto \mathbb{R}$ is said to evolve on the ϵ^k time scale in $[0, T]$ for some integer k and for $0 < \epsilon \leq \epsilon_0$, if there exists a smooth function $\beta : [0, T] \mapsto \mathbb{R}$ and constants C_0 and C_1 such that

$$\sup_{t\in[0,T]} \left| \frac{d}{dt}\beta(t) \right| \leq C_0\epsilon^{-k} \quad \text{and} \quad \sup_{t\in[0,T]} |\alpha(t) - \beta(t)| \leq C_1\epsilon.$$

This motivates the following definition for a variable, $\xi(x^\epsilon)$, that evolves on the ϵ^k time scale along the solutions of (2.5.56).

Definition 2.5.2. A function $\xi(x)$ is said to evolve on the ϵ^k time scale along the trajectories of (2.5.56) in $[0, T]$ if the time dependent function $\xi(x(t; \epsilon, x_0))$ evolves on the ϵ^k time scale in $[0, T]$. For brevity, we will refer to variables that evolve on the ϵ^0 time scale as slow.

In a sequence of papers, [2, 5], we have introduced multiscale algorithms which use a set of slow variables for computing the effective behavior. The set of slow variables should be identified by a procedure either analytically derived, or numerically determined.

2.5.2 Introduction - BF HMM

The BF HMM [1] which utilizes the construction of the effective paths $\Gamma(t)$ indicates that in order to generate a consistent approximation of a slow variable for $\mathcal{O}(1)$ time interval, one only needs to locally create neighboring points of $\Gamma(t)$ on a short time segment of order ϵ. Furthermore, if the dynamics on the intermediate $\mathcal{O}(\epsilon)$ time scale is again oscillatory (i.e. periodic), another effective path $\gamma(t)$ tracking the

evolution of the slow variables on the ϵ time scale can be also constructed similarly on a time segment of order ϵ^2. The previous discussion on constructing effective paths $\Gamma(t)$ and $\gamma(t)$ motivates a three-scale numerical method which applies the previous two-scale BF HMM algorithm hierarchically to multiple (> 2) timescale systems. This three-scale BF HMM shares a similar strategy described in [2, 7], which implements a two-level solver recursively, but the BF HMM has an important advantage over the former. *It does not require an explicit form of any slow variables.*

In order for the BF HMM to be applicable to the three-scale problems, following two assumptions are required.

Assumption 4. *The trajectory passing through $z_0 \in \mathcal{D}_0$ of the unperturbed equation*

$$\frac{d}{dt}z = \epsilon^{-2} f_2(z), \tag{2.5.57}$$

are ergodic on some invariant manifold $\mathcal{M}(z) \subset \mathcal{D}_0$. Furthermore, for points in $\mathcal{D}_0$, the Jacobian of f_2 has only purely imaginary eigenvalues bounded away from 0, independent of ϵ.

Assumption 5. *The trajectory passing through $y_0 \in \mathcal{D}_1$ of the slightly perturbed equation*

$$\frac{d}{dt}y = \epsilon^{-2} f_2(y) + \epsilon^{-1} f_1(y), \tag{2.5.58}$$

are ergodic on some invariant manifold $\mathcal{M}(y_0) \subset \mathcal{D}_1$.

The BF HMM to be constructed should evaluate the effective rate of change of $x(t)$. For three-scale problems, the evolution of the slow variables can be recovered from the manifold $\mathcal{M}(t)$ over $t \in [0, T]$. Let Δ_i and h_i denote the range of integration and step size used in resolving $\mathcal{O}(\epsilon^i)$ time behavior, respectively. The main idea of our approach is to track $\mathcal{M}(t)$ by an effective path $\Gamma(s)$ which crosses $\mathcal{M}(t)$ at $s_n = t_n = nh_0$, $n = 0, 1, 2, \cdots$ and is slowly evolving. The path Γ is locally constructed through interpolation of Γ_j^*, $j = 0, \pm 1, \pm 2, \cdots$. Our algorithm defines two Poincare-type mappings

$$\Gamma_{j+1}^* = P\Gamma_j^*, j = 0, 1, \cdots$$

and

$$\Gamma_{j-1}^* = Q\Gamma_j^*, j = 0, -1, -2, \cdots .$$

The procedure for constructing Γ_j^* involves applying the two-scale BF HMM on each pair of two equations over Δ_1 amount of time interval with forward-backward steps over Δ_2 with step size h_2 and advancing to the h_1 time intervals. As an illustration,

in Figure 2.26, we show two projections of Γ constructed for the FPU problem. See Section 2.2.3 for the FPU model. Note that such $\Gamma(t)$ is not unique and we shall construct one in the state space such that for any slow variable ξ, and finite time interval, Γ satisfies the following conditions:

1. $\xi \circ \Gamma(t_n) = \xi \circ x^\epsilon(t_n)$, at $t_n = nh_0$, $n = 0, 1, 2, \cdots$;
2. $\left| \frac{d^{(j)}\Gamma}{dt^{(j)}} \right| \leq C$, for $1 \leq j \leq k$ for some positive integer k.

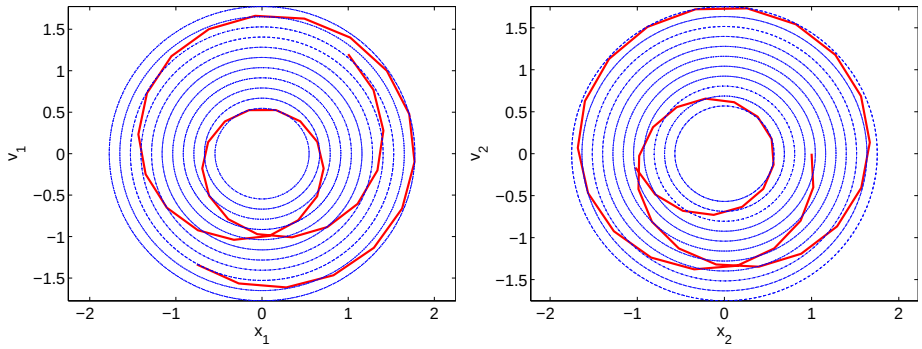

Figure 2.26: Projections of $\Gamma(t)$ onto the x_1-v_1 and the x_2-v_2 planes, are shown by the solid curve. The level sets of the total energies of the stiff springs are shown by the dotted contours. $\Gamma(t)$ is computed by a second order Verlet method using macroscopic time step size $h_0 = 0.25$, $\epsilon = 10^{-3}$. See Algorithm 7 for generating solid curves and Section 2.2.3 for the FPU equation.

Our basic algorithm is summarized below. Recall that Δ_i and h_i denote the range of integration and step size used in resolving $\mathcal{O}(\epsilon^i)$ time behavior, i-th tier, respectively.

Algorithm 7. *Three scale Forward Euler BF HMM*

1. (Forward Euler 0th-tier solver) Compute Γ_{n+1} from Γ_n at $t_n = nh_0$.

$$\Gamma_{n+1} = \Gamma_n + h_0 \mathcal{F}^0_{HMM}(\Gamma_n, t_n)$$

   where $\mathcal{F}^0_{HMM}$ is defined below.

2. (Forward Euler 1st-tier solver) Evaluation of $\mathcal{F}^0_{HMM}(\Gamma^*_0, t^*)$ with Δ_1, $h_1 > 0$.

(a) (Forward solution of the perturbed equation) Compute

$$\gamma_{n+1} = \gamma_n + h_1 \mathcal{F}^1_{HMM}(\gamma_n, t_n),\ n = 0, 1, 2, \cdots, \Delta_1/h_1 - 1,$$

where $\mathcal{F}^1_{HMM}$ is defined in Step 3 (a). Denote the point γ_{Δ_1/h_1} by Γ^*_1.

(b) (Forward solution of the unperturbed equation) Compute

$$\tilde{\gamma}_{n+1} = \tilde{\gamma}_n + h_1 \tilde{F}^1_{HMM}(\tilde{\gamma}_n, t_n),\ n = 0, 1, 2, \cdots, \Delta_1/h_1 - 1$$

where $\tilde{F}^1_{HMM}$ is defined in Step 3 (b). Denote the point $\tilde{\gamma}_{\Delta_1/h_1}$ by Γ^*_0

(c) Evaluate $\mathcal{F}^0_{HMM}$:

$$\mathcal{F}^0_{HMM}(\Gamma^*_0, t^*) := \frac{\Gamma^*_1 - \Gamma^*_0}{\Delta_1}.$$

3. (Forward Euler 2nd-tier solver) Evaluation of $\mathcal{F}^1_{HMM}(\Gamma^*_0, t^*)$ and $\tilde{\mathcal{F}}^1_{HMM}(\Gamma^*_0, t^*)$ with a chosen Filter $K_\Delta \in \tilde{K}^{p,q}([0, \Delta])$, $p, q \geq 1$, and Δ_2, $h_2 > 0$.

(a) Evaluation of $\mathcal{F}^1_{HMM}(\Gamma^*_0, t^*)$

i. (Forward solution of the perturbed equation) Solve

$$\frac{d}{dt}\tilde{x} = \epsilon^{-2} f_2(\tilde{x}) + K_{\Delta_2}(t - t^*)\left\{\epsilon^{-1} f_1(\tilde{x}) + f_0(\tilde{x}; \epsilon)\right\}, \quad \tilde{x}(t^*) = \Gamma^*_0$$

for $t \in [t^*, t^* + \Delta_2]$. Denote the solution at $t = t^* + \Delta_2$ by γ^*_1.

ii. (Forward solution of the unperturbed equation) Solve

$$\frac{d}{dt} z = \epsilon^{-2} f_2(z), \quad z(t^*) = \Gamma^*_0$$

for $t \in [t^*, t^* + \Delta_2]$. Denote the solution at $t = t^* + \Delta_2$ by γ^*_0.

iii. Evaluate $\mathcal{F}^1_{HMM}(\Gamma^*_0, t^*)$:

$$\mathcal{F}^1_{HMM}(\Gamma^*_0, t^*) := \frac{\gamma^*_1 - \gamma^*_0}{\Delta_2}.$$

(b) Evaluation of $\tilde{\mathcal{F}}^1_{HMM}(\Gamma^*_0, t^*)$

i. (Forward solution of the perturbed equation) Solve

$$\frac{d}{dt}\tilde{y} = \epsilon^{-2} f_2(\tilde{y}) + K_{\Delta_2}(t - t^*)\left\{\epsilon^{-1} f_1(\tilde{y})\right\}, \quad \tilde{y}(t^*) = \Gamma^*_0$$

for $t \in [t^*, t^* + \Delta_2]$. Denote the solution at $t = t^* + \Delta_2$ by $\tilde{\gamma}^*_1$.

ii. (Forward solution of the unperturbed equation) Solve

$$\frac{d}{dt}z = \epsilon^{-2} f_2(z), \quad z(t^*) = \Gamma_0^*$$

for $t \in [t^*, t^* + \Delta_2]$. Denote the solution at $t = t^* + \Delta_2$ by $\tilde{\gamma}_0^*$.

iii. Evaluate $\tilde{\mathcal{F}}^1_{HMM}(\Gamma_0^*, t^*)$

$$\tilde{\mathcal{F}}^1_{HMM}(\Gamma_0^*, t^*) := \frac{\gamma_1^* - \gamma_0^*}{\Delta_2}.$$

This type of construction involving forward flows can be recognized using the diagram shown in Figure 2.27.

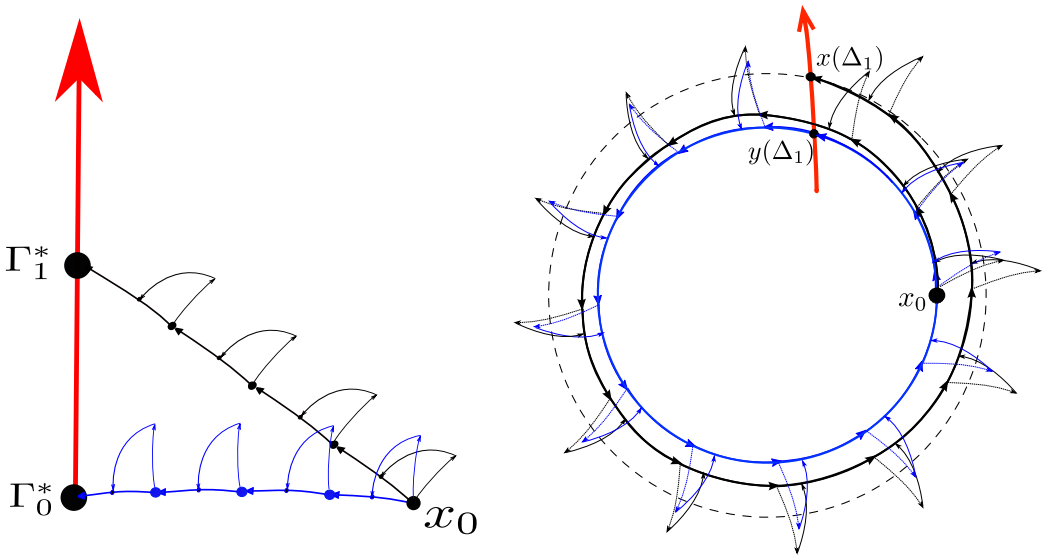

Figure 2.27: An illustration of the BF HMM construction for approximating an effective path that passes through Γ_0^*. This diagram summarizes the three-scale version of Forward Euler BF HMM. This first algorithm does not involve any solution of the equations involved backward in time, but we shall still call it a BF HMM.

The next two remarks are concerned with some issues about the extensions; (i) Algorithm 7 is easily generalized to the second order Midpoint rule or Verlet BF HMM using the similar strategy proposed in [1], and (ii) motivated and proved in the review of BF HMM with symmetric z-structure, if the leading force of the

fast variable depends on the slow variable, we should be careful in determining the size of steps in the macroscopic level and the structure of $\gamma^*_{\pm j}$, $j = 0, 1, 2, \cdots$. For example, see Figure 2.28 for an illustration of the Verlet BF HMM with z-structure.

2.5.3 BF HMM and FPU

Our three-scale algorithm for the FPU is illustrated in Figure 2.28 and summarized below. Aiming at approximating $\mathcal{O}(1)$ behavior, we locally construct the effective path $\Gamma(t)$ whose projection onto the slow manifolds shows the correct dynamics at $t_n = nh_0$, $n = 0, 1, 2, \cdots$. In the FPU model (4.7.79), we choose two pairs of the perturbed-unperturbed equations for evaluating $\mathcal{F}^1_{HMM}$ and $\tilde{\mathcal{F}}^1_{HMM}$ in Step 3 of Algorithm 7:

- (Evaluating $\mathcal{F}^1_{HMM}$) Perturbed equation:

$$\begin{cases} \dot{y}_i = \epsilon^{-1} u_i, \\ \dot{x}_i = \epsilon^{-2} v_i, \\ \dot{u}_i = -\epsilon^{-1}(y_i - \epsilon x_i - y_{i-1} - \epsilon x_{i-1})^3 + \epsilon^{-1}(y_{i+1} - \epsilon x_{i+1} - y_i - \epsilon x_i)^3, \\ \dot{v}_i = -\epsilon^{-2} x_i + \epsilon^{-1}(y_i - \epsilon x_i - y_{i-1} - \epsilon x_{i-1})^3 + \epsilon^{-1}(y_{i+1} - \epsilon x_{i+1} - y_i - \epsilon x_i)^3. \end{cases} \tag{2.5.59}$$

- (Evaluating $\tilde{\mathcal{F}}^1_{HMM}$) Perturbed equation:

$$\begin{cases} \dot{y}_i = \epsilon^{-1} u_i, \\ \dot{x}_i = \epsilon^{-2} v_i, \\ \dot{u}_i = -\epsilon^{-1}(y_i - y_{i-1})^3 + \epsilon^{-1}(y_{i+1} - y_i)^3, \\ \dot{v}_i = -\epsilon^{-2} x_i + \epsilon^{-1}(y_i - y_{i-1})^3 + \epsilon^{-1}(y_{i+1} - y_i)^3. \end{cases} \tag{2.5.60}$$

- Unperturbed equation in both:

$$\begin{cases} \dot{y}_i = 0, \\ \dot{x}_i = \epsilon^{-2} v_i, \\ \dot{u}_i = 0, \\ \dot{v}_i = -\epsilon^{-2} x_i. \end{cases} \tag{2.5.61}$$

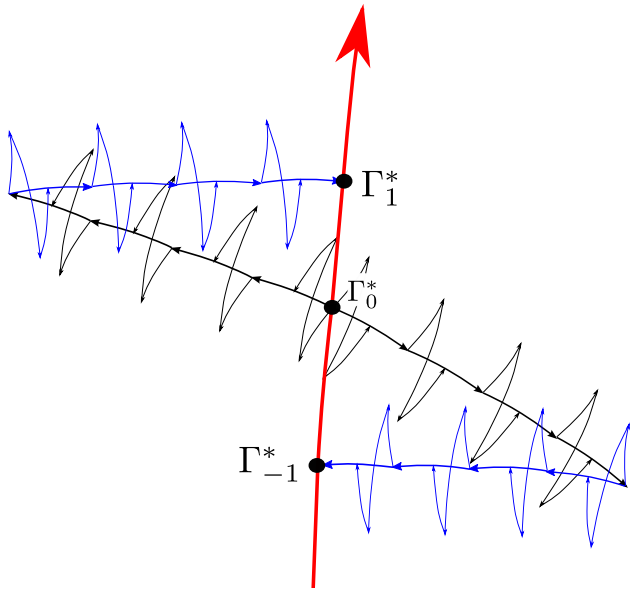

Figure 2.28: An illustration of the Verlet BF HMM with z-structure construction for approximating an effective path of the FPU problem. Black arrow lines are describing Step 2 (a) - construction of γ with $\mathcal{F}^1_{HMM}$ and blue arrow lines are corresponding with Step 2 (b) - construction of $\tilde{\gamma}$ with $\tilde{\mathcal{F}}^1_{HMM}$.

Figure 2.29 shows the energy exchange of the stiff springs over $T = 10$ with $k = 2$ and $\epsilon = 5 \cdot 10^{-3}$. We compare the results computed by the BF HMM Verlet-Verlet-ODE45 (Verlet $\mathcal{O}(1)$, Verlet $\mathcal{O}(\epsilon)$ and ODE45 $\mathcal{O}(\epsilon^2)$ time scale solvers with quadratic polynomial interpolation for γ and $\tilde{\gamma}$) with those by an exponential integrator with Deuflhard's filter functions [30, 55] with the stepsize $h = \epsilon/20000$, which we used as a reference solution. The initial conditions are $[y_1, x_1, u_1, v_1, y_2, x_2, u_2, v_2] = [1, 1, 0, 1.2, 1, 1, 1, 0]$. The BF HMM result is computed with the parameters given in Table 2.9, and with the filter $K^{cos} \in \tilde{\mathbb{K}}^{1,1}$ for the filtered equation that corresponds to (4.7.79). In this setup, the BF HMM runs approximately 45 times faster.

In Figure 2.30, with $\epsilon = 10^{-3}$, we show a result computed by the same BF HMM algorithm for three stiff springs $k = 3$ and demonstrate the stability of our algorithm in this case. The convergence for the reference solution is not verified, and thus solid lines are not reliable. Typical initial conditions are $y_1 = u_1 = v_1 = 1$ and zero otherwise. See Table 2.10 for simulation parameters.

Table 2.9: BF HMM parameters for Figure 2.29.

$\epsilon = 10^{-3}$	h_i	Δ_i	Method
0th tier	$1/4$	-	Verlet
1st tier	$\epsilon/10$	$4\pi\epsilon$	Verlet
2nd tier	$\epsilon^2/20$	$15\epsilon^2$	ODE45 (Reltol=10^{-7})

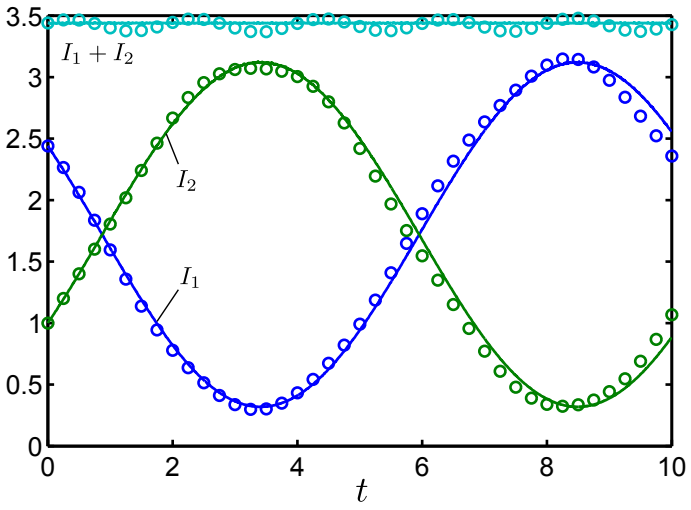

Figure 2.29: The solid lines correspond to the direct numerical simulation (DNS) solution with an exponential integrator. Circles correspond to the HMM.

Table 2.10: BF HMM parameters for Figure 2.30.

$\epsilon = 5 \cdot 10^{-3}$	h_i	Δ_i	Method
0th tier	$1/4$	-	Verlet
1st tier	$\epsilon/10$	$4\pi\epsilon$	Verlet
2nd tier	$\epsilon^2/20$	$15\epsilon^2$	ODE45 (Reltol=10^{-7})

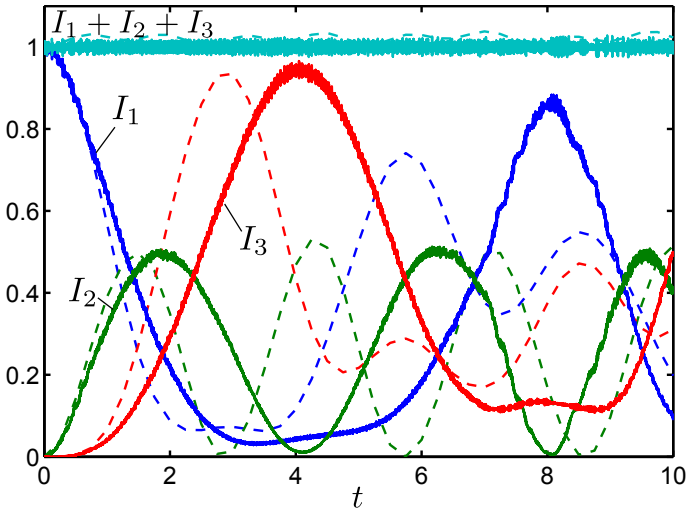

Figure 2.30: The solid lines correspond to the direct numerical simulation (DNS) solution with an exponential integrator which is not convergent. Dashed lines correspond to the HMM.

We will discuss the applicability of the BF HMM to the FPU model. More precisely, we will show that the specific choice of perturbed and unperturbed equation pairs proposed in Section 2.5.3 satisfies Assumption 4 and 5.

The next proposition says that if $\epsilon^{-2} f_2(x^\epsilon)$ in (2.5.56) is linear and has a special form, the time integration of $x^\epsilon(t)$ is bounded by in terms of ϵ.

Proposition 2.5.1. For $k > 0$, suppose that $x(t) = [x_{11}(t), x_{12}(t), x_{13}(t), x_{14}(t), \cdots, x_{k1}(t), x_{k2}(t), x_{k3}(t), x_{k4}(t)]^T \in \mathbb{R}^{4k}$ satisfies the following initial value problem,

$$x' = \epsilon^{-m}\Omega x + \sum_{i=-m+1}^{M} \epsilon^i F_i(x), \quad x(0) = x_0 \tag{2.5.62}$$

where $\Omega = \begin{bmatrix} A & 0 & \cdots & 0 \\ 0 & A & \cdots & 0 \\ \vdots & \vdots & \ddots & \vdots \\ 0 & 0 & \cdots & A \end{bmatrix}$ is a block diagonal matrix with $A = \begin{bmatrix} 0 & 0 & 0 & 0 \\ 0 & 0 & 0 & 1 \\ 0 & 0 & 0 & 0 \\ 0 & -1 & 0 & 0 \end{bmatrix}$, F_i's are bounded independent of ϵ, and $M > -m+1$. Then there exist constants $C > 0$ and $T > 0$ independent of ϵ such that

$$\max_{i=1,\cdots,k} \left\{ \left| \int_0^T x_{i2}(s)ds \right| + \left| \int_0^T x_{i4}(s)ds \right| \right\} \leq C \max\{\epsilon T, \epsilon^m\}.$$

If $F_i = 0$, then paired (x_{12}, x_{14}), $(x_{22}, x_{24}), \cdots$, (x_{k2}, x_{k4}) are decoupled harmonic oscillators with frequencies $2\pi\epsilon^m$, and the amplitude of its time integration over any time interval is $\mathcal{O}(\epsilon^m)$.

Proof. It is assumed that a unique bounded solution exists for each x_0 in a time segment $[0, T]$. Both the bound and T are independent of ϵ. Without loss of generality, we consider the case $k = 1$. Using the change of variables,

$$w = \cos(\epsilon^{-m}t)x_{12} + \sin(\epsilon^{-m}t)x_{14}, \quad v = -\sin(\epsilon^{-m}t)x_{12} + \cos(\epsilon^{-m}t)x_{14},$$

we have

$$\begin{aligned} w' &= -\epsilon^{-m}\sin(\epsilon^{-m}t)x_{12} + \cos(\epsilon^{-m}t)x'_{12} + \epsilon^{-m}\cos(\epsilon^{-m}t)x_{14} + \sin(\epsilon^{-m}t)x'_{14} \\ &= \sum_{i=-m+1}^{M} \epsilon^i \left\{ \cos(\epsilon^{-m}t)F_i^{(2)}(x) + \sin(\epsilon^{-m}t)F_i^{(4)}(x) \right\}, \end{aligned}$$

and similarly for v',

$$v' = \sum_{i=-m+1}^{M} \epsilon^i \left\{ -\sin(\epsilon^{-m}t)F_i^{(2)}(x) + \cos(\epsilon^{-m}t)F_i^{(4)}(x) \right\}.$$

The time integration of x_{12} over $[0, t]$ is

$$\begin{aligned} \int_0^t x_{12}(s)ds &= \int_0^t \cos(\epsilon^{-m}s)w(s)ds - \int_0^t \sin(\epsilon^{-m}s)v(s)ds \\ &= \epsilon^m \left[\sin(\epsilon^{-m}s)w(s)\right]_{s=0}^t - \epsilon^m \int_0^t \sin(\epsilon^{-m}s)w'(s)ds \\ &\quad + \epsilon^m \left[\cos(\epsilon^{-m}s)v(s)\right]_{s=0}^t - \epsilon^m \int_0^t \cos(\epsilon^{-m}s)v'(s)ds \\ &= -\int_0^t \sum_{i=-m+1}^{M} \epsilon^{m+i} \left\{ \sin(\epsilon^{-m}s)\cos(\epsilon^{-m}s)F_i^{(2)}(x) + \sin^2(\epsilon^{-m}s)F_i^{(4)}(x) \right\} ds \\ &\quad - \int_0^t \sum_{i=-m+1}^{M} \epsilon^{m+i} \left\{ -\sin(\epsilon^{-m}s)\cos(\epsilon^{-m}s)F_i^{(2)}(x) + \cos^2(\epsilon^{-m}s)F_i^{(4)}(x) \right\} ds + \mathcal{O}(\epsilon^m) \\ &= -\int_0^t \left\{ \sum_{i=-m+1}^{M} \epsilon^{m+i} F_i^{(4)}(x) \right\} ds + \mathcal{O}(\epsilon^m). \end{aligned}$$

where $\mathcal{O}(\epsilon^m)$ is valid for T independent of ϵ. Therefore, the leading order of the RHS is determined by $i = -m + 1$ and the last term. There exists a constant $C_1 > 0$ such that

$$\left| \int_0^T x_{12}(s) ds \right| \leq C_1 \max\{\epsilon T, \epsilon^m\}, \tag{2.5.63}$$

and similarly one can show that for $C_2 > 0$,

$$\left| \int_0^T x_{14}(s) ds \right| \leq C_2 \max\{\epsilon T, \epsilon^m\}. \tag{2.5.64}$$

The proof of the proposition follows by putting together (2.5.63) and (2.5.64) together. □

By the above proposition, the singular part in the derivative of total energies in the rescaled FPU model (4.7.79),

$$I_i' = 2\epsilon^{-1} v_i \left\{ (y_i - y_{i-1})^3 + (y_{i+1} - y_i)^3 \right\} + \mathcal{O}(1), \tag{2.5.65}$$

is integrated on any segment of length $\mathcal{O}(\epsilon)$ and larger is of order ϵ. Note that v_i's are identified with x_{i4}. Therefore, the averaged I_i' is bounded independent of ϵ and I_i is a slow variable which evolves on the $\mathcal{O}(1)$ time scale.

Remark 2.5.1. It should be pointed out that we only consider the integration of linear expression of $x_{i2}(t)$ and $x_{i4}(t)$ in Proposition 2.5.1. If a nonlinear expression is considered, resonance phenomena can be occurred. For instance, in the stellar orbit problem [5], the time derivative of the slow variable is given by

$$\xi_1' = 2a^{-1} v_1 x_2^2,$$

and both v_1 and x_2 are evolving on ϵ time scale. Using the assumption that $x_2^2(t)$ is bounded by M for $t \in [0, T]$ and the above proposition, one can insist that there exist $C > 0$ so that

$$|\xi_1(t) - \xi_1(0)| \leq 2a^{-1} M \int_0^t v_1(s) ds \leq C\epsilon. \tag{2.5.66}$$

However, (2.5.66) is correct as long as resonance does not occur. With a specific choice of the constants, due to the nonlinear terms, the stellar orbit system can be in resonance, and ξ_1 evolves on the $\mathcal{O}(1)$ time scale. □

We shall now start the analysis of the three-scale BF HMM on the FPU problem. The main idea is to trace the evolution of the invariant manifold $\mathcal{M}(t)$ by constructing $\Gamma(t)$. Two things should be clarified:

1. (Necessary condition for the unperturbed equation on the 1st tier) The evolution of I_i along the trajectories of the following unperturbed equation,

$$\begin{cases} \dot{y}_i = \epsilon^{-1} u_i, \\ \dot{x}_i = \epsilon^{-2} v_i, \\ \dot{u}_i = -\epsilon^{-1}(y_i - y_{i-1})^3 + \epsilon^{-1}(y_{i+1} - y_i)^3, \\ \dot{v}_i = -\epsilon^{-2} x_i + \epsilon^{-1}(y_i - y_{i-1})^3 + \epsilon^{-1}(y_{i+1} - y_i)^3, \end{cases} \tag{2.5.67}$$

over $\Delta_1 = \mathcal{O}(\epsilon)$ amount of time interval is effectively stationary. Therefore, a comparison with I_i along the trajectories of the following perturbed equation

$$\begin{cases} \dot{y}_i = \epsilon^{-1} u_i, \\ \dot{x}_i = \epsilon^{-2} v_i, \\ \dot{u}_i = -\epsilon^{-1}(y_i - \epsilon x_i - y_{i-1} - \epsilon x_{i-1})^3 + \epsilon^{-1}(y_{i+1} - \epsilon x_{i+1} - y_i - \epsilon x_i)^3, \\ \dot{v}_i = -\epsilon^{-2} x_i + \epsilon^{-1}(y_i - \epsilon x_i - y_{i-1} - \epsilon x_{i-1})^3 + \epsilon^{-1}(y_{i+1} - \epsilon x_{i+1} - y_i - \epsilon x_i)^3. \end{cases} \tag{2.5.68}$$

implicitly captures the evolution of I_i over $[t_n, t_n + \Delta_1]$.

2. (Difference in fast variables between Γ_1^* and Γ_0^*) When a singular part of the force of fast variables depends on the slow variable, for the accuracy, the step sizes h_0 and h_1 may be restricted, e.g., h_1 should be chosen $\mathcal{O}(\epsilon^2)$ not $\mathcal{O}(\epsilon)$ as desired. In the 1st tier, only one fast variable is in $\mathcal{O}(\epsilon^{-2})$ and its derivative is independent of slow variables. Thus, we can choose $h_1 = \mathcal{O}(\epsilon)$. On the other hand, in the 0th tier, all the degrees of freedom which are related to the soft springs: y_i and u_i, $i = 1, 2, \cdots, k$, are the fast variables. We shall show that

$$\max_{i=1,\cdots,k} \left\{ \left| y_i^{\Gamma_1^*} - y_i^{\Gamma_0^*} \right|, \left| u_i^{\Gamma_1^*} - u_i^{\Gamma_0^*} \right| \right\} = \mathcal{O}(\epsilon^2) \tag{2.5.69}$$

where $y_i^{\Gamma_0^*}$,$y_i^{\Gamma_1^*}$, $u_i^{\Gamma_0^*}$ and $u_i^{\Gamma_1^*}$ are the values of y_i and u_i at $t = \Delta_1$ related with Γ_j^*, $j = 0, 1$, respectively. Therefore, one can choose h_0 independent of ϵ since the errors from the deviation in fast variables are not amplified; e.g., for the fast variable y_i,

$$\mathcal{F}^0_{HMM}(\Gamma_n, t_n) := \frac{y_i^{\Gamma_1^*} - y_i^{\Gamma_0^*}}{\Delta_1} = \mathcal{O}(\epsilon). \tag{2.5.70}$$

Proof. 1. is immediate from Proposition 2.5.1. Indeed, in (2.5.67),

$$I_i' \;=\; 2\epsilon^{-1} v_i \left\{ (y_i - y_{i-1})^3 + (y_{i+1} - y_i)^3 \right\},$$

and

$$|I_i(t_n+\Delta_1)-I_i(t_n)| \le 2\epsilon^{-1}M\left|\int_{t_n}^{t_n+\Delta_1} v_i(s)ds\right| \le 2\epsilon^{-1}M\mathcal{O}(\epsilon\Delta_1)=\mathcal{O}(\epsilon)$$

for $\Delta_1=\mathcal{O}(\epsilon)$.

2. We begin with the observation that the RHS of y_i' and u_i' in (2.5.67) has the form

$$\begin{cases} y_i' = \epsilon^{-1}u_i, \\ u_i' = \epsilon^{-1}F_1(y_{i-1},y_i,y_{i+1}), \end{cases} \tag{2.5.71}$$

and in (2.5.68),

$$\begin{cases} y_i' = \epsilon^{-1}u_i, \\ u_i' = \epsilon^{-1}F_1(y_{i-1},y_i,y_{i+1}) + x_{i-1}F_0(y_{i-1},y_i) + x_iG_0(y_{i-1},y_i,y_{i+1}) + x_{i+1}H_0(y_i,y_{i+1}) + \mathcal{O}(\epsilon). \end{cases} \tag{2.5.72}$$

By Proposition 2.5.1, $\left|\int_0^t x_i(s)ds\right| \le \mathcal{O}(\epsilon t)$. Therefore, by Gronwall's inequality applied to the solutions of (2.5.71) and (2.5.72),

$$\left|y_i^{\gamma_n}-y_i^{\tilde{\gamma}_n}\right| \le \mathcal{O}(\epsilon^2), \text{ and } \left|u_i^{\gamma_n}-u_i^{\tilde{\gamma}_n}\right| \le \mathcal{O}(\epsilon^2),\ n=0,1,\cdots,\Delta_1/h_1-1.$$

Then 2. follows since $\Gamma_1^* := \gamma_{\Delta_1/h_1}$ and $\Gamma_0^* := \tilde{\gamma}_{\Delta_1/h_1}$. □

Chapter 3

Numerical averaging over embedded tori invariant under non-mixing dynamics

3.1 Introduction

A large number of multiscale numerical methods are based on numerical averaging or homogenization with respect to a fast or fine-scale process. In many applications in which the effective averaged equation cannot be obtained analytically, special multiscale numerical methods can give an approximate numerical solution. Given that the microscopic scale is rapidly mixing, the literature suggests a large variety of efficient methods which are called multiscale algorithms, mainly alternating between the computation on the fine scale and progressing with the slow dynamics on the large scale. However, the fine scale dynamics of ergodic systems which are not mixing may be more difficult to approximate the slow behavior since the fast process may take relatively long before eventually relaxing to the equilibrium distribution. The difficulty lies in the fact that the fast dynamics may be ergodic with respect to a low-dimensional manifold that is non-trivially embedded in phase space. Furthermore, the frequencies of the fast oscillations may not be known.

One important class of highly oscillatory systems arises naturally as integrable Hamiltonian systems that can be expressed in terms of action-angle variables

[11]. For integrable systems, phase space can be described in terms of n action variables and n corresponding angle coordinates. Systems with constant frequencies, that is, with frequencies independent of the action variables, undergo linear oscillations with respect to an n-torus, $\mathbb{T}^n$, that is described as the intersection of the level sets of the n action variables. If the frequencies composing the oscillations are independent over the rationals, then every trajectory is ergodic with respect to an n dimensional invariant manifold, $\mathcal{M}$, that is diffeomorphic to $\mathbb{T}^n$ and is embedded in $\mathbb{R}^{2n}$. Otherwise, additional constants of motion related to resonances exist and the trajectories are ergodic with respect to a torus of lower dimension [5, 11].

For rapidly mixing dynamics, as an example, the equation-free approach is to link simulations of the microscopic models on small spatio-temporal domains in order to mimic the behavior of a system at large scale [9, 68]. This involves averaging over microscopic time or number of realizations if an ensemble of simulations has been used. Moreover, by simultaneously evolving several initial conditions time averaging can be combined with ensemble averaging [37, 39, 101]. The advantage of using these methods hinges on efficiently averaging out the fast oscillations. For periodic system, averaging can be accelerated using convolution with respect to specially constructed one-dimensional averaging kernels [2, 3, 5–7, 42, 97]. However, for the best of our knowledge, these methods have not been extended to fast oscillations which are ergodic on a high-dimensional torus.

Under suitable circumstances, non-mixing dynamics can be approximated in the use of Young measures [12, 13]. The situations in which the fast dynamics tend to fixed points or periodic solutions can be treated in a unified manner. The

general philosophy is to analyze the behavior of a fast dynamics drifted along with a slow movement by computing limit cycles as $\epsilon \to 0$, describing the distributions supported on them as a Young measure, and progressing via averaging with respect to which induces the equation for the slow dynamics. However, since we know that the limit solution is periodic but we do not know in advance what the period is, in [13] the DFT is applied repeatedly on a subsequent longer sequences of the fast dynamics until one gets a satisfactory harmonic signal. In this way we discover an approximate period and an approximation of the limit cycle. The problem, then, is that for high dimensional limit cycles with non-mixing dynamics, one should consider very long sequences to get the correct distributions.

We now go back to the hamiltonian systems. A small perturbation on the integrable systems can create a drift in the action variables which is slow compared to the oscillations. In applications, one is often interested only in the behavior of such slowly changing quantities. The averaging principle is the idea that the oscillation discarded in averaging generates only small oscillations/errors which are superimposed on the drift described by the averaged equation. Here the averaged equation is written as the closed form for the perturbed equation which contains only slowly changing variables, and its solution is an asymptotic approximation as $\epsilon \to 0$ for the original variables on the given interval. To this end, in the classical two-scale averaging theory [11] where the multiscale behavior is characterized by time scales of integer powers of ϵ and the fast motion is periodic, one needs to take an integration over the suitable manifold (torus). However, at present one of the difficulties in averaging is the absence of a convenient parametrization of the torus.

The main purpose of this paper is twofold: (1) we introduce the averaging theory for a model problem whose solutions possess slow variables or observables as well as fast oscillations with multi-frequencies that are almost rationally resonant, i.e., near-resonant. Our generalization is along the lines of the so called averaging over angles in the case of ϵ-dependent variable frequencies. To study the slow behavior of solutions, we first find out what resonances are relevant in a given system, and then determine an appropriate type of averages to be taken. Especially, the slow behavior of weak near-resonant systems should be approximated by averaging over the torus; and (2) efficient numerical techniques for averaging over a higher dimensional torus will be given. We demonstrate how classical two-scale methods [3, 5, 42] can be generalized in order to construct a consistent approximation of the effective slow dynamics in multi-frequency systems. The fast dynamics is invariant over a multidimensional torus rather than just the unit circle. We propose two algorithms. The first assumes that the invariant measure is uniform, whereas the second algorithm addresses the more challenging case of non-uniform invariant measures. To our knowledge, very few algorithms have been developed considering directly averaging in multi-frequency systems. We develop our algorithm using the framework of the heterogeneous multiscale method (HMM) for highly oscillatory ODEs and the discretization of the Frobenius-Perron operator.

3.1.1 Slow-fast systems on a torus

Our principal motivation is the numerical approximation of highly oscillatory ordinary differential equations (ODEs) in near resonance. Solutions of highly

oscillatory ODEs often involve a wide range of time scales. In this section, consider singularly perturbed systems of the form

$$\dot{x} = \epsilon^{-1} f_1(x) + f_0(x), \tag{3.1.1}$$

with initial condition $x(0) = x_0 \in U \subset \mathbb{R}^d$, where U is bounded uniformly in ϵ. The parameter $0 < \epsilon \leq \epsilon_0 \ll 1$ characterizes the separation of time scales: the fast scale involves oscillations with frequencies of order ϵ^{-1} while the computational time domain is $[0, T]$ with T independent of ϵ. Throughout the paper we assume that a unique uniformly bounded solution $x(t) \in \mathbb{R}^d$ exists and that $f_1,\ f_0$ are sufficiently smooth. Then, this generally implies that the computational complexity of direct non-multiscale methods is at least $\mathcal{O}(\epsilon^{-1})$.

One might be interested only in a set of slowly changing quantities ξ that are derived from the solutions of the given stiff system (3.1.1). In the case where ξ is a set of functions of x, they are commonly referred to as slow variables of the system. See [4, 5, 45, 50, 70–72]. For example, ξ could be the action variables of integrable Hamiltonian systems or the averaged kinetic energy of a particle system x. Formally, slow variables of a dynamical system can be defined as below. This definition also applies to near-resonant systems where the fast oscillation involves the order of a fractional power of ϵ time scale.

Definition 3.1.1. Let $x(t) \in U$ denote the solution of highly oscillatory dynamical systems (3.1.1) for some initial conditions. A smooth function $a(t)$ is to be **slow** if $|da/dt| \leqq C$ for some constant C independent of ϵ with $0 < \epsilon \leq \epsilon_0$ in $t \in [0, T]$.

Moreover, a smooth function $\xi(x) : \mathcal{D}_0 \to \mathbb{R}$ is called a **slow variable** with respect to $x(t)$ if $\xi(t) = \xi(x(t))$ is said to be slow.

In many problems, there exists a diffeomorphism $\Psi : x \to (\xi(x), \phi(x))$ separating slow and fast variables such that the dynamics satisfies an ODE of the form

$$\begin{cases} \dot{\xi} = g_0(\xi, \phi), & \xi(0) = \xi_0, \\ \dot{\phi} = \epsilon^{-1} g_1(\xi) + g_2(\xi, \phi), & \phi(0) = \phi_0, \end{cases} \tag{3.1.2}$$

where $\xi \in \mathbb{R}^{d-n}$, $\phi \in \mathbb{T}^n$, and ϵ is a small parameter. For fixed slow coordinates ξ, the fast variable ϕ is restricted in the manifold $\mathcal{M}$ which is diffeomorphic to an n-torus. The computational challenge is to get an approximate solution for ξ when the parameter ϵ is small, when the derivative of the fast dynamics may be large.

We further assume that, for fixed ξ, the dynamics for the unperturbed equation of ϕ, $\dot{\phi} = \epsilon^{-1} g_1(\xi, \phi)$, is ergodic with respect to $\mathbb{T}^n$ with an invariant measure $\mu_\xi(d\phi)$. Then, the theory of averaging [10, 11, 80, 93] implies that in the limit of $\epsilon \to 0$ and for sufficiently smooth right hand side, $\xi(t)$ converges to the solution of an averaged equation given by

$$\dot{\bar{\xi}} = G(\bar{\xi}), \quad \bar{\xi}(0) = \bar{\xi}_0 \tag{3.1.3}$$

where

$$G(\bar{\xi}) = \int g(\bar{\xi}, \phi) \mu_{\bar{\xi}}(d\phi).$$

Moreover, the approximation is of order ϵ in the sup norm, i.e.

$$\sup_{t \in [0,T]} \left| \xi(t) - \bar{\xi}(t) \right| \leq C\epsilon.$$

where $C > 0$ is a constant that typically depends T but is independent of ϵ. In particular, for $p = 1$, the fast dynamics can be considered as a rotation over a circle, and averages can be approximated using a convolution with the kernel. See [3, 5, 42] for related theories. A naive application of this approach to (3.1.2) when $p > 1$ may result is a drastically reduction in efficiency.

In the following, the average of a function g with respect to n fast variables, i.e., over an n-torus, and the solution of an averaged equation obtained by this averaging procedure are denoted by

$$\langle g \rangle_{\mathbb{T}^n} \ , \ \bar{x}_{\mathbb{T}^n}(t),$$

respectively. Note that the 1-torus is just the circle: $\mathbb{T}^1 = S^1$.

The major limitation is that the averaged equation (3.1.3) is not explicitly available in practice since without knowing μ, the right hand side is not computable. The current research builds upon two essential averages of a function f on $\mathcal{M}$ - space average, as was stated above, over an invariant measure μ which is absolutely continuous with respect to $\mathcal{M}$, and time averages which are obtained by starting at a particular point and averaging over an infinitely long time. The well known Birkhoff' ergodic theorem states that if f is a continuous function on $\mathcal{M}$ then the time and space averages of f are equal [11]. More precisely,

$$\lim_{S\to\infty} \frac{1}{S} \int_0^S f(\phi_0 + \mathbf{w}t)dt = \int_{\mathcal{M}} f(\boldsymbol{\phi})\mu(d\boldsymbol{\phi}) \quad \mu \ a.e., \tag{3.1.4}$$

where $\mathbf{w} = (w_1, \cdots, w_n)$ denote the frequencies of oscillation and $\boldsymbol{\phi} = (\phi_1, \cdots, \phi_n)$ denote angle variables. In other words, the space average can be replaced by the

time average. However, from a computational time point of view, it is important to investigate the rate of convergence of (3.1.4). This will be discussed in Section 3.1.3.

It is important to emphasize that in certain resonant circumstances and the time interval $[0, T]$ of interest, S happens to be much bigger than T in order to replace the RHS of (3.1.4). Then, the challenge is to study the global behavior of solutions during such insufficient time. The first step is to find out what resonances are relevant in this situation, and then to try to find the appropriate type of averages to be taken.

So far, we assumed that the multiscale behavior is characterized by time scales of integer powers of ϵ. There of course exist dynamical systems whose multiscale features are not integer powers of ϵ, e.g. in weakly coupled, nearly resonant harmonic oscillators. The following sections introduce and analyze the averaging method applied to this general class of systems.

3.1.2 Near-resonances

A variety of highly oscillatory dynamical systems involving more than two time scales can be found in many different areas. For example, the Fermi-Pasta-Ulam model [46] involves almost-periodic dynamics on the ϵ time scale, dynamics of the soft nonlinear springs on the time scale independent of ϵ, and the slow energy exchange between stiff springs on the ϵ^{-1} time scale; see e.g. [18, 55].

More recently, the near-resonance behavior of the FPU has been studied in [54] with the scaling among particle number, total energy and time interval. The

main tool employed there is a multiscale expansion, so called modulated Fourier expansion, whose coefficient functions are constructed from a modulation system based on the discrete Fourier transform. When the frequencies are in near-resonance, it leads to small denominators in the construction of the modulated Fourier expansion. Such a near-resonant situation is dealt with several lemmas that give a lower bound in terms of fractional powers of the time scales interested. See also [16, 17]. Note that the near-resonance phenomena associated with integer powers of ϵ is explained in terms of resonance horns or tongues [86].

To specify non-integer time scales, we introduce near-resonances in the following context. For simplicity, let us consider the following model problem in which the singular term is linear while the regular part is polynomial

$$\begin{cases} x' = f(x,y), & x(0) = x_0, \\ y' = i\epsilon^{-1}\Lambda y, & y(0) = y_0, \end{cases} \tag{3.1.5}$$

where $x \in \mathbb{C}^{d-n}$, $y \in \mathbb{C}^n$, f is a vector of polynomials in x and y and $\Lambda = \mathrm{diag}(\lambda_1(\epsilon), \ldots, \lambda_n(\epsilon))$, a diagonal $n \times n$ matrix with diagonal elements $\lambda_1, \cdots, \lambda_n \in \mathbb{R}$. The solution for y reads

$$y = y_0 e^{i\epsilon^{-1}\Lambda t}.$$

Substituting into (3.1.5),

$$x' = f\left(x, y_0 e^{i\epsilon^{-1}\Lambda t}\right), \quad x(0) = x_0. \tag{3.1.6}$$

The RHS of (3.1.6) consists of finite expressions of the form

$$e^{i\epsilon^{-1}(\sum k_i\lambda_i)t} p(x).$$

Choosing f a polynomial in both x and y implies that $p(x)$ is a polynomial in x with integers k_i. We assume that the numbers $\lambda_1, \cdots, \lambda_n$ are rationally independent, that is, $\sum w_i\lambda_i \neq 0$ for any integers $w_1, \cdots, w_n$ unless $w_1 = \cdots = w_n = 0$. Thus, trajectories of y are dense in $\mathbb{T}^n$ [63]. We distinguish two different terms:

1. Non resonant term: $\lambda_1, \lambda_2, \cdots, \lambda_n$ are rationally independent regardless of ϵ, that is, there exists $\gamma > 0$ independent of ϵ such that all of the terms satisfy $|\sum k_i\lambda_i| > \gamma$. Since no resonance occurs in the system, the solution $x(t)$ stays close to the initial value.

2. Near-resonant term: $\sum k_i\lambda_i(\epsilon) = \delta(\epsilon)$ for some terms where $\delta(\epsilon)$ is small positive. Depending on δ, we classify two kinds of near-resonances: weak near-resonances (subcritical) for $\delta = \mathcal{O}(\epsilon^q)$, $0 < q < 1$, and strong near-resonances (supercritical) for $\delta = \mathcal{O}(\epsilon^p)$, $p > 1$.

Therefore, near-resonance arises for instance if there exists an exponent of the form,

$$\epsilon^{-1} \sum k_i\lambda_i = \epsilon^{-1}\delta.$$

This terminology derives from the fact that the fast variable is in many applications the difference among angles. The near-resonances are equivalent to saying that the frequencies of the angles are about equal. If we take $\gamma(t) = \epsilon^{-1}t\sum k_i\lambda_i$ as those linear combinations of angles for $\lambda_1, \lambda_2, \cdots, \lambda_n$, the equation for γ is varying either slowly or quickly depending on the size of δ over the time interval independent of ϵ. In the case of weak near-resonance, γ is varying quickly as $\epsilon \to 0$ and considered as a fast variable, so we can take an average over γ. However, in strong near-resonance,

γ is varying slowly as $\epsilon \to 0$ and considered as a "new" slow variable. Hence we cannot average over γ. As a remark, if δ happens to be equal to ϵ, γ is stationary, and this immediately causes degeneration of the averaged equation: one cannot get (3.2.18).

We emphasize that depending on the near-resonances present and the time scale of interest, $x(t)$ should be approximated by the appropriate type of averaging procedures. If one uses the wrong kind of averaging, the corresponding averaged equation may exhibit the wrong effective dynamics. In Section 3.2, we shall show that an appropriate choice of the manifold over which one should take an average is related with the order of ϵ in δ. As an overview, when the system is in weak near-resonance and the $\mathcal{O}(1)$ time interval is considered, trajectories cover the invariant torus on an ϵ^r time scale $0 < r < 1$ and one needs to average over the invariant torus. On the other hand, when strong resonance occurs, the system is effectively in resonance for any time interval that is independent of ϵ, and the averaging over the entire torus cannot, generally speaking, correctly describe the motion. As a result, we only need to average the flow over a suitable submanifold which is a lower dimensional torus. In either case, the distance between the exact solution and the averaged solution should depend on the strength of the near-resonances.

3.1.3 No rate of convergence in time averages

Considering time average is certainly a simple way to compute a long-term distribution. Notice that an important aspect of near-resonance is that the rate of convergence of time averages may be very slow. There are thus drawbacks to

this simple approach when the dynamical systems are in near-resonances: (i) it is possible that orbits display statistically irrelevant behavior for lengthy periods of time before settling into a more regular mode. In this matter, by solving on ODE for a finite time, there is the risk that one is only observing this irrelevant behavior and not the true asymptotic behavior of the system; and (ii) in the literature concerning ergodic dynamical systems, it is not possible to prove any general positive result about the rate of convergence of (3.1.4) even if the convergence is guaranteed by the ergodic theorem. More examples and related theories are discussed in [74, 77], [15]. This section mainly focuses on the latter.

In ergodic systems, trajectories are dense in the invariant manifold for almost all initial conditions. Moreover, the proportion of time the system spend in any Borel set converges to the measure of that set. This corresponds to ergodicity in the sense of Boltzmann, which roughly speaking is the mean time that a particle of a ergodic system spends in some region and it is proportional to its probabilistic measure [33]. To be precise, let φ_t denote the flow map of a highly oscillatory dynamical system which is ergodic with respect to an invariant probability measure μ and the invariant manifold $\mathcal{M}$. Furthermore, let A denote a set in the Borel σ-algebra on $\mathcal{M}$, and denote the naive time averaging of a bounded measurable function $f(x)$ to time S by

$$\langle f \rangle_S = \frac{1}{S} \int_0^S f(\varphi_t(x_0)) dt \tag{3.1.7}$$

where x_0 is the initial condition. If we substitute $f = \chi_A$ in (3.1.7), then the mean occupancy of the set A in the interval $0 \leq t \leq S$ is given by $\mu_S(A) := \langle \chi_A \rangle_S$. For ergodic systems, the following equality holds

$$\mu(A) = \lim_{S\to\infty} \mu_S(A) \tag{3.1.8}$$

where A is a set in the Borel σ-algebra on $\mathcal{M}$. In an approximation to the invariant measure by the time averaging trajectories, since a numerical scheme should stop at some finite time S, there is a natural question: How large is S so that the time averaging is close to the invariant measure of the underlying dynamics?

We partially address the above question by establishing a connection to the discrete time ergodic theorem:

$$\lim_{S\to\infty} \langle f\rangle_S = \lim_{N\to 0} \frac{1}{N}\sum_{k=0}^{N-1} g(\varphi_1^k(x_0))$$

where $g(x)$ is given by $g(x) = \int_0^1 f(\varphi_t(x))dt$. The question is now equivalent to determining the appropriate size of N. In general, no positive theoretic answer to this is possible. For example, Krengel [73] has shown in a certain case that the rate of convergence can be arbitrarily slow. On the other hand, Halasz [58] proved that in some cases the convergence can be arbitrarily fast, that is close to the order of N^{-1}. Therefore, we cannot determine the rate of convergence of time averages and, accordingly, how much numerical integration needs to be taken for time average to replace the invariant measure.

3.1.4 Numerical methods

The general philosophy of our algorithm is based on the heterogeneous multiscale method (HMM) for highly oscillatory ordinary differential equations [2, 3, 5–

7, 42, 97]. We are interested in the macroscopic behavior of a system which is specified by the slow variable. The averaged equation is integrated in the macrosolver, but the equation is not explicitly known in general. To solve the incomplete macroscale model, we extract the needed data from the microscale model for the state variable, i.e., the macroscopic behavior of dynamical systems is captured with the help of the microscopic model. More precisely, the needed data in the macroscale system is obtained by the integration of the microscale system on reduced time segments and the evaluation of averages with respect to the fast variable. Figure 3.1 shows a typical structure of such a algorithm. In this description:

(1) A macroscale solver, depicted on the upper axis, integrates an averaged ODE for ξ.

(2) An initial value on the lower axis is determined by applying a reconstruction operator $\mathcal{R}(\xi(t_n))$.

(3) The full multiscale system, depicted on the lower axis, is solved on a reduced time segment.

(4) The effective drift of $\dot{\xi}$ is approximated using numerical averaging

The steps are repeated to the required time. This methodology has been applied in [3, 5, 42] for the relatively simple case in which the fast dynamics is periodic, and the invariant manifold is equivalent to a circle $\mathbb{T}^1$. The main goal of this paper, is to develop a general averaging method that can be applied to high dimensional tori. *The key concerns are that in systems that are not mixing, naive time averaging may be highly inefficient.* This issue is addressed in Section 3.1.3. Sections 3.3-3.5

discuss alternatives of the naive time averaging.

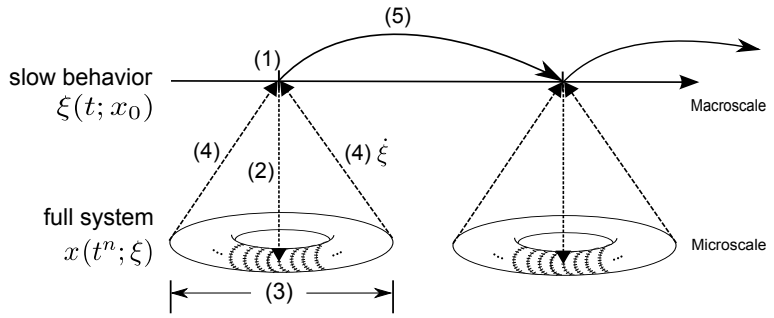

Figure 3.1: The HMM structure of the proposed multiscale algorithm.

3.1.5 Scope

The layout of the chapter is as follows. In Section 3.2, we introduce strong and weak near-resonances and review some relevant results from the theory of averaging. In Section 3.3, we propose our new algorithm for averaging over the torus where the flow has the uniform invariant measure. This is based on construction of orthogonal vector fields on the torus and successive use of averaging kernels. Section 3.4 presents the more general algorithm for approximating non-uniform invariant measures. The method is based on an appropriate discretization of the Frobenius-Perron operator. In order to avoid simulating long orbits, the invariant torus is divided into smaller cells, then the pullback of each cell is calculated numerically in order to approximate the area of intersection between cells and their pullback. Both algorithms are supported by numerical examples. Section 3.5 is devoted to numerical averaging method over the embedded torus with the absence of a convenient parametrization.

3.2 Strong and weak near resonances

We start by considering a class of system that has an explicit slow-fast grouping in the solution's components

$$\begin{cases} \dot{\xi} = g_0(\xi, \phi), & \xi(0) = \xi_0, \\ \dot{\phi} = \epsilon^{-1} g_1(\xi) + g_2(\xi, \phi), & \phi(0) = \phi_0, \end{cases} \tag{3.2.9}$$

where $\xi \in \mathbb{R}^{d-n}$ and $\phi \in \mathbb{T}^n$. ξ is assumed to be bounded independent of ϵ in a time segment $[0, T]$ also independent of ϵ. Here, $\phi \in \mathbb{T}^n$ means that ϕ is in $\mathbb{R}^n$ but the functions g_0 and g_2 are 1-periodic in each component of ϕ. The variables ξ and ϕ are referred to as the slow variable and the fast variable, respectively. See Definition 3.1.1. We shall discuss how averaged equations for the slowly evolving variables are chosen when the near-resonance is present in dynamical systems. It is already known that in the simplest case, $n = 1$, near-resonances cannot arise. Moreover, in this case efficient multiscale algorithms have been introduced in a sequence of papers [3, 5, 42] which use a convolution with a kernel for computing the effective slow behavior.

When $n > 1$, things are much complicated because the resonance module typically changes with respect to the value of ξ. Thus, we consider the simplest case of (3.2.9) where g_1 is ϵ-dependent constant and $g_2 = 0$. The following two frequency system will be considered thoroughly, and the results will be extended to the multi-frequency systems:

$$\begin{cases} \dot{\xi} = g(\xi, \phi_1, \phi_2), & \xi(0) = \xi_0, \\ \dot{\phi}_1 = \epsilon^{-1} \lambda_1, & \phi_1(0) = 0, \\ \dot{\phi}_2 = \epsilon^{-1} \lambda_2, & \phi_2(0) = 0, \end{cases} \tag{3.2.10}$$

where $(\xi, \phi_1, \phi_2) \in \mathbb{R}^{d-2} \times \mathbb{R} \times \mathbb{R}$, and g is assumed to be 1-periodic in both ϕ_1 and ϕ_2. ϵ-dependent variable frequencies λ_1 and λ_2 satisfy $|\lambda_2/\lambda_1| = 1 + \delta(\epsilon)$ so that fast dynamics is on a 2-torus.

The main role in near-resonant systems connected with the averaging procedure is played by the size of the dependence of δ on ϵ. The slow variable can be approximated using a specific averaging procedure with respect to the size of δ since when the system is in near-resonance, the trajectories cover an invariant torus at a different speed for a time interval independent of ϵ. In this case, there are only two averaging options since the fast dynamics has at most two dimensions: one is averaging over the "true" manifold, with respect to all fast variables, which is averaging over a 2-torus. The true manifold is defined by a 2-torus as shown by two fast variables. Another averaging is taken over one fast variable which is referred as averaging over a circle.

We plot the performance of these averagings in Figure 3.2 with various δ's. The left sub-figure depicts the exact solution $x(t)$ as the underlying near-resonance alters from weak to strong. It is observed that the exact solutions associated with $\delta = \epsilon^{1/3}$ (weak–bottom) and $\epsilon^{4/3}$, $\epsilon^{5/3}$, ϵ^2 (strong–up) shift from being close to the averaged solution $\bar{x}_{\mathbb{T}^2}(t)$ to being close to the averaged solution $\bar{x}_{\mathbb{T}^1}(t)$. On the other hand, the right sub-figure illustrates an asymptotic behavior of the strong near-resonant dynamics as ϵ shrinks to 0. See Example 3.2 for generating solid curves and for the equation.

The important consequence of these works is that only for weak near-resonant systems does the choice of averaging over 2-torus enable one to obtain a correct ap-

proximation for the slow variable with vanishing errors as $\epsilon \to 0$. Furthermore, for strong near-resonant systems, although the averaged equation over the true invariant manifold can still be defined, its solution is not a good approximation to the slow variables. From the results it is evident that the speed of covering of the flow and the strength of δ are closely related.

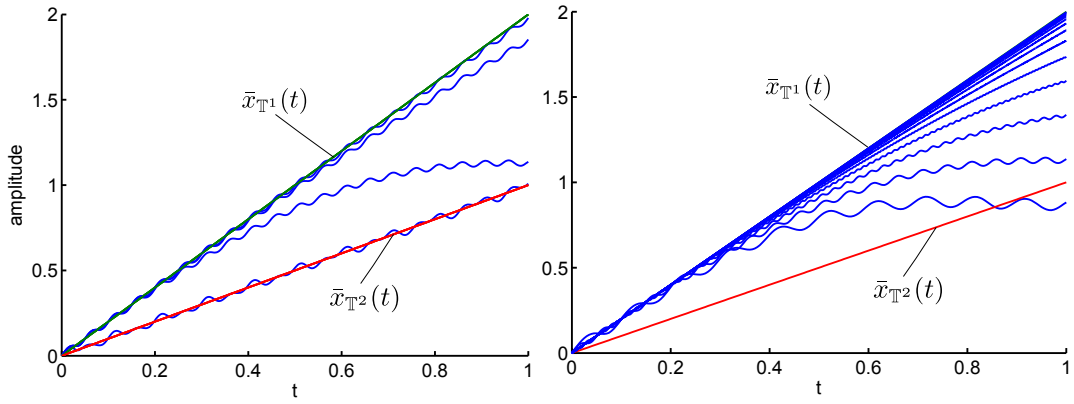

Figure 3.2: Dynamics of the slow variable $x(t)$. (Left) An amplitude of the exact solution $x(t)$ as δ changes among from bottom $\delta = \epsilon^{1/3}$ to up $\delta = \epsilon^2$. $\epsilon = 0.05$. (Right) The asymptotic behavior of the exact solution for $\epsilon = 10^{-i}/2^i$, $i = 1, \cdots, 14$ in strong near-resonance when $\delta = \epsilon^{4/3}$. As $\epsilon \to 0$, the exact dynamics converges to the solution obtained by averaging over a circle. The appropriate type of an averaged equation is different, depending on the near-resonances present. See Example 3.2.

Example 3 shows the subtle aspects of near-resonance phenomena at long-time approximation to the slow dynamics via averaging.

Example 3. We compare two averaging procedures for $x(t)$ in the following simple equation;

$$\begin{cases} \dot{x} = 1 + y_1 y_2 + 2y_1, & x(0) = 0, \\ \dot{y}_1 = i\epsilon^{-1}\lambda_1 y_1, & y_1(0) = 1, \\ \dot{y}_2 = i\epsilon^{-1}\lambda_2 y_2, & y_2(0) = 1, \end{cases} \tag{3.2.11}$$

where two frequencies are $\lambda_1 = 2\pi$ and $\lambda_2 = -2\pi(1 + \sqrt{2}\delta)$. The time interval of interest is $[0, T]$ independent of ϵ. We look at a decreasing sequence of ϵ so that $\sqrt{2}\delta$ is small irrational. Since λ_1 and λ_2 are noncommensurable, $(y_1(t), y_2(t))$ covers a 2-torus embedded in $\mathbb{C}^3$. The exact solution $x(t)$ is

$$x(t) = t + (4\pi\delta)^{-1}\sqrt{2}i\epsilon\left(e^{i\epsilon^{-1}(\lambda_1+\lambda_2)t} - 1\right) - \pi^{-1}i\epsilon\left(e^{i\epsilon^{-1}\lambda_1 t} - 1\right).$$

Depending on the strength of $\delta(\epsilon)$, the slow variable $x(t)$ should be approximated by different averaging procedures. We denote $\langle\cdot\rangle_{\mathbb{T}^1}$ as averaging over the lower dimensional torus which is defined, in this case, by a circle $\{(e^{it}, e^{-it}),\ 0 \le t < 2\pi\}$, and $\langle\cdot\rangle_{\mathbb{T}^2}$ as averaging over a 2-torus defined by $\{(e^{it_1}, e^{-it_2}),\ 0 \le t_1, t_2 < 2\pi\}$. Therefore, $\langle\cdot\rangle_{\mathbb{T}^1}$ is taking into account the resonance $\lambda_1 + \lambda_2 = 0$, whereas $\langle\cdot\rangle_{\mathbb{T}^2}$ is the independent averaging over two frequencies. A more advanced treatment may be found in [93].

The averaging over a circle produces an averaged equation for $x(t)$

$$\begin{cases} \frac{d}{dt}\bar{x}_{\mathbb{T}^1}(t) & = 1 + \langle y_1 y_2 + 2y_1\rangle_{S^1} = 1 + e^{i\gamma t}, \\ \frac{d}{dt}\gamma(t) & = \epsilon^{-1}(\lambda_1 + \lambda_2), \end{cases} \tag{3.2.12}$$

and by taking $\lambda_1 + \lambda_2 = 0$ to get a "closed" system for describing the slow motion, we have

$$\frac{d}{dt}\bar{x}_{\mathbb{T}^1}(t) = 2, \quad \bar{x}_{\mathbb{T}^1}(0) = 0. \tag{3.2.13}$$

An equation obtained from averaging over a 2-torus is

$$\frac{d}{dt}\bar{x}_{\mathbb{T}^2}(t) = 1 + \langle y_1 y_2 + 2y_1\rangle_{\mathbb{T}^2} = 1, \quad \bar{x}_{\mathbb{T}^2}(0) = 0. \tag{3.2.14}$$

To analyze the effect of the near-resonances, we introduce the errors to the exact solution

$$E_1 := \sup_{0\le t\le T} |x(t) - \bar{x}_{\mathbb{T}^1}(t)|, \quad E_2 := \sup_{0\le t\le T} |x(t) - \bar{x}_{\mathbb{T}^2}(t)|.$$

In the case of weak near-resonance, i.e., $\delta = \epsilon^q$, $q < 1$, averaging over $\mathbb{T}^1$ and $\mathbb{T}^2$ leads over time $t \in [0, T]$, T independent of ϵ, to the errors respectively

$$E_1 \approx \mathcal{O}(t) + \mathcal{O}\left(\epsilon^{1-q}\right), \quad E_2 \approx \mathcal{O}\left(\epsilon^{1-q}\right).$$

On the other hand, in strong near-resonance, i.e., $\delta = \epsilon^p$, $p > 1$, such averagings give the error from the exact solution as

$$E_1 \approx \mathcal{O}\left(\epsilon^{p-1}\right) + \mathcal{O}(\epsilon), \quad E_2 \approx \mathcal{O}(t) + \mathcal{O}\left(\epsilon^{p-1}\right).$$

See Table 3.1 for the summary of error estimation. □

Table 3.1: The error estimate between the exact solution and the approximated solution to (3.2.13) and (3.2.14). As $\epsilon \to 0$, $\bar{x}_{S^1}(t)$ gives a reasonable approximation for strong near-resonance, and $\bar{x}_{\mathbb{T}^2}(t)$ gives a reasonable approximation f for weak near-resonance.

Error $(0 \le t \le T)$	weak near-resonance	strong near-resonance
	$\delta = \mathcal{O}(\epsilon^q)$, $0 < q < 1$	$\delta = \mathcal{O}(\epsilon^p)$, $p > 1$
averaging over $\mathbb{T}^1$	$\mathcal{O}(t) + \mathcal{O}(\epsilon^{1-q})$	$\mathcal{O}(\epsilon^{\min\{1,p-1\}})$
averaging over $\mathbb{T}^2$	$\mathcal{O}(\epsilon^{1-q})$	$\mathcal{O}(t) + \mathcal{O}(\epsilon^{p-1})$

We describe an idea that will be important later: in near-resonant systems, there is the emergence of either a new slow variable (the dimension reduction in fast dynamics) or a new mesoscale variable. To be precise, in (3.2.12), the relative phase $\gamma(t)$ can be categorized as either a slow variable or a fast variable depending

on the size of δ. For example, in strong near-resonance where $\delta = \mathcal{O}(\epsilon^p)$, $p > 1$, it turns out that $\gamma(t)$ is a new slow variable to the system. Therefore, the dimension of fast dynamics is one rather than two as shown in (3.2.11). Moreover, in weak near-resonance, $\gamma(t)$ is regarded as a fast variable, but it evolves on the time scale between $\mathcal{O}(1)$ and $\mathcal{O}(\epsilon)$. We refer such intermediate time scale to a mesoscale, and thus the error estimates should be weakened from average principles given in [11, 93] to the order of ϵ/δ. In particular, see Theorem 3.2.1. This observation will be used to find an appropriate manifold where the averaging should be taken.

3.2.1 Averaging method for near-resonant systems

Averaging method for highly oscillatory dynamical systems is based on the ergodic property of the underlying fast process [10, 11, 93]; the geometry of the invariant manifold which is filled up by the trajectories, the distribution of such filling in the time scale of interest and most importantly, the presence of resonant frequencies. The last is critical since if the frequencies are resonant, then the phase trajectories must fill up a torus of lower dimension, and the averaging over the entire torus cannot correctly approximate the slow dynamics in general.

In this section, we will derive some basic results which are preliminary for our treatment of averaging a near-resonant system. Consider systems of the form

$$\begin{cases} x' = f(x, y), & x(0) = x_0, \\ y' = i\epsilon^{-1}\Lambda y, & y(0) = y_0, \end{cases} \tag{3.2.15}$$

where $x \in \mathbb{C}^{d-n}$, $y \in \mathbb{C}^n$, f is a vector of polynomials in x and y and $\Lambda = \mathrm{diag}(\lambda_1, \ldots, \lambda_n)$, a diagonal $n \times n$ matrix with diagonal elements $\lambda_1, \cdots, \lambda_n \in \mathbb{R}$.

As discussed in Section 3.1.2, the equation for x consists of expressions of the form

$$x' = e^{i\epsilon^{-1}(\sum k_i\lambda_i)t}p(x), \tag{3.2.16}$$

where the k_i are integers and $p(x)$ is a polynomial in x.

The averaging theory consists of replacing the systems of equations (3.2.16) by the averaged system

$$\bar{x}' = F(\bar{x}), \quad \bar{x}(0) = x_0 \tag{3.2.17}$$

for the approximate description of the evolution of the slow variables over $[0, T]$ where T is independent of ϵ.

Our aim is to describe a slow variable $x(t)$ in the original system by $\bar{x}(t)$ in the averaged one. To justify this recipe, we need to derive the RHS of the averaged equation (3.2.17) so that its solution ensures, in the formal sense,

$$\sup_{0\le t\le T} |x(t) - \bar{x}(t)| \to 0 \quad \text{as } \epsilon \to 0. \tag{3.2.18}$$

Since we are focusing on the case where the Fourier complex series for f are finite, there would be finitely many resonance manifolds. We thus begin by averaging in two-frequency systems since it shares the essential multiscale features with (3.2.15), and we will then extend the results to more general situations, multi-frequency systems. Away from the resonances, one can average $e^{i\epsilon^{-1}(\sum k_i\lambda_i)t}p(x)$ over either a circle or a n-torus since it does not effect on the effective slow behavior and thus should be discarded in averaging. Near the resonances, more detailed treatment is required since having small values of $\sum k_i\lambda_i$ may or may not effect on the slow behavior of x. Therefore, our main attention is devoted to the resonance exponent which goes to 0 as $\epsilon \to 0$.

3.2.1.1 Averaging in two-frequency systems

In two-frequency systems, by dividing one frequency by the other, the equation (3.2.16) can be equivalently rewritten as

$$x' = f\left(x, \epsilon^{-1}t, \epsilon^{-1}(\nu+\delta)t\right), \quad x(0) = x_0.$$

where ν is an integer. We assume that $f(x, t_1, t_2)$ is Lipschitz continuous in t_1, t_2 and x, and that f is 1-periodic in both t_1 and t_2. We will denote a generic positive constant by C whose value may change between expressions but is independent of ϵ.

Theorem 3.2.1. [Weak near-resonance in two frequencies] Suppose that there exists an exponent of the form $\sum k_i\lambda_i = \mathcal{O}(\epsilon^q)$ on the RHS of (3.2.16) where $0 < q < 1$. Consider the following averaged equation;

$$\xi' = \langle f\rangle_{\mathbb{T}^2}(\xi), \quad \xi(0) = x_0, \text{ where } \langle f\rangle_{\mathbb{T}^2}(\xi) = \int_0^1\int_0^1 f(\xi, t_1, t_2)dt_1dt_2.$$

Then there is a constant $C > 0$ such that

$$|x(t) - \xi(t)| \leqq C\epsilon^{1-q} \tag{3.2.19}$$

for $t \in [0, T]$ independent of ϵ.

Hence, when the system is in weak near-resonance, one can just average over all fast variables to get an averaged equation for the slow variable. For related numerical treatments, see Section 3.3-3.5.

Proof. This result follows from standard averaging techniques; see, e.g., [93]. In view of the expression $e^{i\epsilon^{-1}(\sum k_i\lambda_i)t}p(x)$, if there is no ϵ-dependent small value of

$\sum k_i\lambda_i$, then all of the fast variables are evolving on the ϵ time scale. Therefore, in this case, the result turns out to be $C\epsilon$. Otherwise, this estimate will be weakened as shown below. We consider the following slow-fast system for weak-near resonance,

$$\begin{cases} x' = f(x,y), & x(0) = x_0, \\ y' = i\epsilon^{-1}\Lambda y, & y(0) = y_0, \end{cases} \tag{3.2.20}$$

where $\Lambda = \text{diag}(\lambda, C\delta)$, a diagonal 2×2 matrix with diagonal elements $\lambda, C\delta \in \mathbb{R}$. λ is independent of ϵ. This is obtained by letting $y_2' = i\epsilon^{-1}\sum k_i\lambda_i y_2$ in (3.2.15). Therefore, in weak near-resonance, the new mesoscale variable appears by a linear combination of two angles. (3.2.20) can be written as

$$\begin{cases} x' = f(x,y), & x(0) = x_0, \\ y' = i\delta\epsilon^{-1}\Lambda' y, & y(0) = y_0, \end{cases}$$

where $\Lambda' = \text{diag}(\delta^{-1}\lambda, C)$. By letting this, we treat the case where the frequencies do not vanish, calling this the regular case [93]. This is the same form as (3.1.2), with $g_1 = \delta\epsilon^{-1}\Lambda'$, $g_2 = 0$ and with ϵ replaced $\epsilon\delta^{-1}$. Therefore, the results will have error $\mathcal{O}(\epsilon\delta^{-1})$ for the time interval independent of ϵ. 3.2.25 □

Theorem 3.2.2. [Strong near-resonance in two frequencies] Suppose that there exists an exponent of the form $\sum k_i\lambda_i = \mathcal{O}(\epsilon^p)$ on the RHS of (3.2.16) where $p > 1$. Suppose that its averaged equation is given by,

$$\xi' = \langle f \rangle_{\mathbb{T}^1}(\xi), \quad \xi(0) = x_0, \text{ where } \langle f \rangle_{\mathbb{T}^1}(\xi) = \int_0^1 f(\xi, t, \nu t)dt. \tag{3.2.21}$$

Then there is a constant $C > 0$ such that

$$|x(t) - \xi(t)| \leqq C\epsilon^{\min\{1,p-1\}} \tag{3.2.22}$$

for $t \in [0, T]$ independent of ϵ.

Proof. We let $\lambda = \nu + \delta$. Observe that

$$\begin{aligned} x(t) - x_0 &= \int_0^t f(x(\tau), \epsilon^{-1}\tau, \lambda\epsilon^{-1}\tau)d\tau \\ &= \int_{t_M}^t f(x(\tau), \epsilon^{-1}\tau, \lambda\epsilon^{-1}\tau)d\tau + \sum_{j=0}^{M-1} \int_{t_j}^{t_{j+1}} f(x(\tau), \epsilon^{-1}\tau, \lambda\epsilon^{-1}\tau)d\tau, \end{aligned}$$

where $t - t_M < \epsilon$. In each interval $t_j = \epsilon j \leqq \epsilon \leqq t_{j+1} = \epsilon(j+1)$,

$$\begin{aligned} \int_{t_j}^{t_{j+1}} f(x(\tau), \epsilon^{-1}\tau, \lambda\epsilon^{-1}\tau)d\tau &= \int_{\epsilon j}^{\epsilon(j+1)} f(x(t_j), \epsilon^{-1}\tau, \lambda\epsilon^{-1}\tau) + O(\epsilon)d\tau \\ &= \int_{\epsilon j}^{\epsilon(j+1)} f(x(t_j), \epsilon^{-1}\tau, \lambda\epsilon^{-1}\tau)d\tau + O(\epsilon^2) \\ &= \underbrace{\int_j^{j+1} f(x(t_j), t, \lambda t)\epsilon dt}_{I} + O(\epsilon^2). \end{aligned}$$

For each j, we can estimate I as

$$\begin{aligned} I &= \int_0^1 f(x(t_j), s+j, \lambda(s+j))\epsilon ds \\ &= \int_0^1 \left(f(x(t_j), s, \nu s) + \delta(s+j)\partial_{t_2} f(x(t_j), s, \xi)\right)\epsilon ds \end{aligned}$$

where $\xi \in [\nu s, \nu s + \delta(s+j)]$. Therefore, there exist constants $C_1, C_2 > 0$ such that

$$\left| \int_{t_j}^{t_{j+1}} f(x(\tau), \epsilon^{-1}\tau, \lambda\epsilon^{-1}\tau)d\tau - \epsilon \left\langle f \right\rangle_{\mathbb{T}^1} (x(t_j)) \right| \leq C_1(j + C_2)\epsilon\delta.$$

Note that for $T = O(1)$, $\epsilon M = O(1)$ and thus $M = O(\epsilon^{-1})$.

$$\begin{aligned}
\left| x(t) - x_0 - \int_0^t \langle f \rangle_{\mathbb{T}^1} (x(\tau)) d\tau \right| &\leq \left| x(t) - x_0 - \sum_{j=0}^{M-1} \int_{t_j}^{t_{j+1}} f(x(\tau), \epsilon^{-1}\tau, \lambda\epsilon^{-1}\tau) d\tau \right| \\
&\quad + \left| \sum_{j=0}^{M-1} \int_{t_j}^{t_{j+1}} f(x(\tau), \epsilon^{-1}\tau, \lambda\epsilon^{-1}\tau) d\tau - \epsilon \sum_{j=0}^{M-1} \langle f \rangle_{\mathbb{T}^1} (x(t_j)) \right| \\
&\quad + \left| \epsilon \sum_{j=0}^{M-1} \langle f \rangle_{\mathbb{T}^1} (x(t_j)) - \int_0^t \langle f \rangle_{\mathbb{T}^1} (x(\tau)) d\tau \right| \\
&\leq C \left(\epsilon + \delta + \frac{M(M-1)}{2} \epsilon\delta \right)
\end{aligned}$$

Therefore, this yields

$$\left| x(t) - x_0 - \int_0^t \langle f \rangle_{\mathbb{T}^1} (x(\tau)) d\tau \right| \leq C \left(\epsilon + \delta + \epsilon^{-1}\delta \right).$$

Since $y(t) - x_0 = \int_0^t \langle f \rangle_{\mathbb{T}^1} (y(\tau)) d\tau$, we have $|x(t) - y(t)| \leqq L \int_0^t |x(\tau) - y(\tau)| d\tau + C \left(\epsilon + \delta + \epsilon^{-1}\delta \right)$ where L is a Lipschitz constant from the first argument of f. By Gronwall's lemma, we have

$$|x(t) - y(t)| \leqq C \left(\epsilon + \delta + \epsilon^{-1}\delta \right) e^{Lt} \tag{3.2.23}$$

where $0 \leqq t \leqq T = O(1)$. □

For longer times, e.g, $T = \mathcal{O}(\epsilon^{-1})$, one has to average over a 2-torus since time is long enough for the flow to cover the torus and the averaged equation could be different. In numeric, one can use a technique using convolution with respect to specially constructed one-dimensional averaging kernels [2, 3, 5–7, 42, 97].

Remark 3.2.1. When $\sum k_i \lambda_i = \mathcal{O}(\epsilon)$, neither (3.2.19) nor (3.2.22) does give an desired approximation as (3.2.18). This immediately shows degeneration of the averaged equation.

3.2.1.2 Averaging in n-frequency systems, $n > 2$

When an n-frequency system is considered, it is necessary to reframe the averaging process in a more geometrical way that clarifies the role of δ. The difficulty is that if both weak and strong near-resonances occur, manifolds over which the averaging procedure is taken should be chosen adequately.

Let $\mathbf{k}$ denote an integer vector in $\mathbb{R}^n$, λ denote a frequency vector $(\lambda_1, \cdots, \lambda_n) \in \mathbb{R}^n$ which is a diagonal component of Λ, and define

$$\Lambda_w^{\perp} := \{\mathbf{k} | \mathbf{k} \cdot \lambda = k_1\lambda_1 + \cdots + k_n\lambda_n = \mathcal{O}(\epsilon^q),\ 0 < q < 1\}, \tag{3.2.24}$$

and

$$\Lambda_s^{\perp} := \{\mathbf{k} | \mathbf{k} \cdot \lambda = k_1\lambda_1 + \cdots + k_n\lambda_n = \mathcal{O}(\epsilon^p),\ p > 1\}. \tag{3.2.25}$$

The sets $\Lambda_w^{\perp}$ and $\Lambda_s^{\perp}$ are related to weak and strong near-resonances, respectively. Moreover, they are closed under addition and under multiplication by integers. Note that these operations should be independent of ϵ. Otherwise, it changes the asymptotic behavior of $\mathbf{k} \cdot \lambda$. For example, if we multiply by an integer$\sim \mathcal{O}(\epsilon^{-1})$, then the exponents on the RHS decrease by 1. To avoid this problem, one needs to make sure the finiteness of the Fourier series as assumed before. In the algebra literature, $\Lambda_w^{\perp}$ and $\Lambda_s^{\perp}$ are closely related to the annihilator module of λ.

In the case $\Lambda_w^{\perp}$ and $\Lambda_s^{\perp}$ are $\{\mathbf{0}\}$, by the classical averaging theorem [10, 80, 93], we need to average over n-torus. Thus, the corresponding averaged equation is

$$\xi' = \langle f \rangle_{\mathbb{T}^n}(\xi), \quad \xi(0) = x_0, \text{ where } \langle f \rangle_{\mathbb{T}^n}(\xi) = \int_{\mathbb{T}^n} f(\xi, \mathbf{t}) d\mathbf{t},$$

and its solution satisfies

$$|x(t) - \xi(t)| \leqq C\epsilon.$$

In the resonant case with $\Lambda_s^\perp = \{\mathbf{0}\}$, averaging over n-torus is also taken, and using Theorem 3.2.1, the error estimate between averaged and exact solutions would be

$$|x(t) - \xi(t)| \leqq C\epsilon^{\min\{1-q_1,\cdots,1-q_j\}}$$

where j is the number of different exponents in (3.2.24).

In the resonant case with $\Lambda_s^\perp \neq \{\mathbf{0}\}$, one cannot average over all fast variables since the associated averaged solution may not be close to the exact solution as $\epsilon \to 0$. Instead, average over particular angles should be considered as (3.2.21). This observation suggests that we transform the fast variables in (3.2.15) into the fast and "hidden" slow variables. This is called *the multiscale chart* in the context of [3, 7]. A brief idea is that there exist particular angles which are evolving slowly, and thus should be considered as slow variables. A numerical method for identifying new slow variables for the case in which the singular parts of the dynamics is linear is described in [5, 7]. Once we have the multiscale chart, the appropriate averaging can be taken and the error estimate between averaged and exact solutions would be

$$|x(t) - \xi(t)| \leqq C\epsilon^{\min\{p_1-1,p_2-1,\cdots,p_i-1,1-q_1,\cdots,1-q_j\}}$$

where i and j are the number of different exponents in (3.2.24) and (3.2.24), respectively. Note that in any cases, $i + j < n$ holds since at least one dimension

is reserved for describing fast dynamics of highly oscillatory dynamical systems [3]. Therefore except for the circumstance only strong near-resonances arise, $\Lambda_w^{\perp} = \{\mathbf{0}\}$, we need to average over a torus, and this motivates to devise efficient techniques for numerical averaging over a torus.

3.3 Numerical averaging over the torus : uniform invariant measure

We consider dynamical systems which are ergodic on the invariant manifold and the corresponding invariant measure is *uniform*. Our algorithm aims at speeding up the convergence of time averages in 3.1.4. In an analogy to molecular dynamics, this algorithm combines time averaging with ensemble averaging. There are three main components: (1) construct a global orthogonal coordinate system on a torus, (2) place a grid over the torus using the constructed coordinate system, and (3) compute suitable averages of the flows that start out from the grid nodes. This way, we can efficiently integrate over a torus via short time integration of the oscillatory system and iterative use of an efficient averaging kernel developed for averaging over circles. The orthogonal coordinate system on the torus is constructed by using a smooth invertible mapping of the dynamical system's flow direction and the normals of the torus to designated standard basis vectors in the embedding Euclidean space $\mathbb{R}^d$, and then properly pulling back the remaining basis vectors in $\mathbb{R}^d$ to the torus' tangle bundle.

In the following sections, for simplicity, we only consider the system whose fast variables are evolving on the manifold which is diffeomorphic to $\mathbb{T}^2$. Theoret-

ical results yield insight into the numerical method to average over $\mathbb{T}^2$. However, our algorithm can easily be extended to more general situations, where the torus considered is in the higher dimensions.

3.3.1 Preliminary setup and overview

We begin with an unperturbed Hamiltonian system whose two action variables are stationary over long time. In this case, the invariant manifold is embedded in a higher dimensional space and is given implicitly as the intersection of level sets of the action variables.

Consider a pair of undamped harmonic oscillators for $\mathbf{x} = [x_1, v_1, x_2, v_2]^T$,

$$\dot{\mathbf{x}}=\tfrac{1}{\epsilon} f(\mathbf{x}) = \epsilon^{-1} \begin{bmatrix} 0 & 1 & 0 & 0 \\ -1 & 0 & 0 & 0 \\ 0 & 0 & 0 & \lambda \\ 0 & 0 & -\lambda & 0 \end{bmatrix} \mathbf{x}, \quad \mathbf{x}(0) = \begin{bmatrix} 1 \\ 0 \\ 1 \\ 0 \end{bmatrix} \tag{3.3.26}$$

where $\lambda = 1 + \delta\sqrt{2}$ and $\delta = \epsilon^q$ with $0 < q < 1$. There are two slow variables $\xi_i : \mathbb{R}^4 \to \mathbb{R}^1$, $i = 1, 2$;

$$\xi_1 = x_1^2 + v_1^2,\ \xi_2 = x_2^2 + v_2^2.$$

and a manifold $\mathcal{M}$ is represented by

$$\mathcal{M}(t) = \cap_{i=1}^{2} \{z \in \mathbb{R}^d : \xi_i(z) = \xi_i \circ x(t)\}.$$

For a fixed $y \in \mathcal{M}$, we denote by

$$T_y\mathcal{M} = \{z \in \mathbb{R}^4 : \nabla\xi_i(y)z = 0, i = 1, 2\},$$

the tangent space of $\mathcal{M}$ at y. This is a linear space and has the same dimension 2 as the manifold $\mathcal{M}$. It follows from $f \perp \nabla\xi_i$ that the flow of (3.3.26) is in $T_y\mathcal{M}$,

i.e., (3.3.26) is a differential equation on the manifold $\mathcal{M}$ [53, 57]. Since $T_y\mathcal{M}$ has a dimension of 2, there exists another vector $\tau \in T_y\mathcal{M}$ so that

$$\{f, \tau, \nabla\xi_1, \nabla\xi_2\} \tag{3.3.27}$$

forms a set of orthogonal vectors at $y \in \mathcal{M}$. Formally, τ is a function from $\mathbb{R}^4$ to $\mathbb{R}^4$ and satisfies

$$\tau \perp \nabla\xi_i, \text{ and } \tau \perp f.$$

Therefore, we introduce a local coordinate systems where the fast and slow behaviors are separated. we can summary above as follows:

- at each point $y \in \mathcal{M}$, a local coordinate system is constructed,
- the slow behaviors are related to $\nabla\xi_1$ and $\nabla\xi_2$, but
- the fast behaviors are related to f and τ.

In the following section, we discuss a method to construct a local coordinate automatically. Since the other two fast variables can be regarded as angle coordinates, the manifold $\mathcal{M}$ is diffeomorphic to $\mathbb{T}^2$. To this reason, the manifold $\mathcal{M}$ will be referred to the torus $\mathbb{T}^2$. Such topological structure will be exploited for the construction of our numerical averaging method.

3.3.2 Construction of orthogonal vector fields on the torus

From above constructions, $\mathbb{T}^2$ embedded in $\mathbb{R}^4$ is given. At each point $\mathbf{x} \in \mathbb{T}^2$, two normal vectors $n_1 := \nabla\xi_1$ and $n_2 := \nabla\xi_2$ on $\mathbb{T}^2$, and a smooth vector field f

on $\mathbb{T}^2$ are provided. The main idea to construct an orthogonal coordinate system on the torus is a rotation map ψ which transforms n_1,n_2 and f into the selected standard basis vectors in the embedding Euclidean space $\mathbb{R}^4$. A new vector we try to find is obtained using the inverse transformation ψ^{-1} of an unassigned vector in standard basis. We identify this vector $\tau(\mathbf{x})$. To sum up, we fix an orientation of all vectors by taking the standard basis as a reference direction. Since every function is assumed to be sufficiently smooth, this construction is smooth as well. See Figure 3.3, 3.4 and Table 3.2 for an illustration.

orthogonal directions on $\mathbf{x} \in \mathcal{M}$	ψ	the standard basis
n_1 (given)	$\rightarrow$	e_1
n_2 (given)	$\rightarrow$	e_2
f (given)	$\rightarrow$	e_3
τ (needed)	$\leftarrow$	e_4

Table 3.2: Construction of orthogonal vector fields on the torus; pull e_4 back to the original coordinate and identify hidden direction τ. The transformation ψ is given by composition of various rotational matrices.

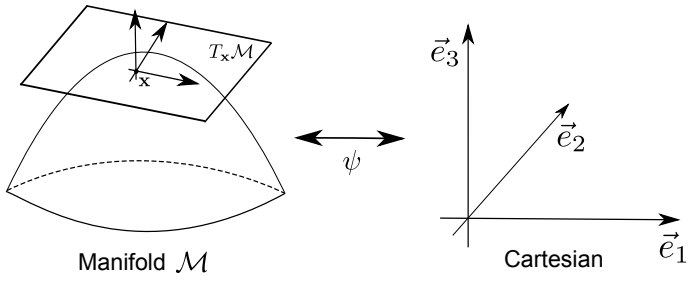

Figure 3.3: An illustration of defining a local coordinate system using transformation ψ.

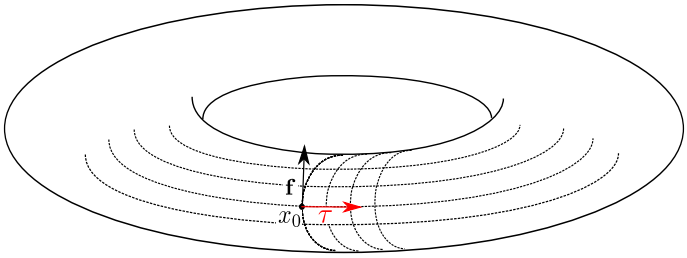

Figure 3.4: Construction of coordinate systems on the torus.

In the general case if we have a lower order perturbation forcing on the RHS of $\dot{\mathbf{x}}$, then when ϵ is very small, trajectories are lying very close to the invariant torus. However, for long enough time, they are drifted away and we need to track this *evolution of the invariant torus*. This can be done by advancing slow variables.

3.3.3 New averaging strategy - uniform invariant measure

In this section, we propose a new method to compute an average of a function on the manifold which is represented in Section 3.3.1. For the purpose of an explanation, we identify opposite faces of $I^2 = [0, 1]^2$ to represent the torus $\mathbb{T}^2$.

In the case of time averaging, we need to solve (3.3.26) for long enough time so that the trajectories cover I^2. The rate of convergence of time averaging applied to (3.3.26) depends on δ. As discussed in Section 3.1.3, For near-resonant systems, the convergence can be very slow and the error originated from the approximated solutions can be significant. For this reason, it is convenient to build new approaches for this problem. An alternative method of speeding up is to cover up the other dimension of the torus identified with τ. In Section 3.3.2, we construct a direction τ at each point $\mathbf{x} \in I^2$. We denote $\tau(t)$ as an integral curve of $\tau(\mathbf{x})$ by solving the

following autonomous system:

$$\dot{\tau}(t) = \tau(\mathbf{x}), \quad \tau(0) = \mathbf{x}. \tag{3.3.28}$$

Our numerical averaging method of g' over the invariant torus is as follows:

1. (Generating new initial conditions) Solve (3.3.28) over $[0, \eta_\tau]$ with stepsize $h_\tau = C\epsilon$. Denote the approximation at $t_n = nh_\tau$ as τ_n. We define $N := \eta_\tau / h_\tau$.

2. (N number of micro simulations) Solve (3.3.26) in $t \in [-\eta_1, \eta_1]$ with different initial conditions $\mathbf{x}_j(0) = \tau_j$, $j = 1, \cdots, N$. Denote the solution as $\mathbf{x}_j(t)$.

3. (Force estimation) Approximate g' by $\triangle g = K_\tau * [K_f * g'(\mathbf{x})]$ where K_f and K_τ are 1D averaging kernels along the direction of f and g respectively.

Figure 3.5 and 3.6 show a description of our algorithm.

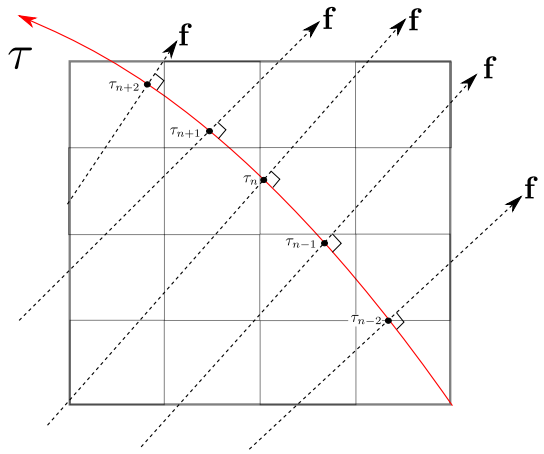

Figure 3.5: Averaging over 2-torus. Each small box refers to a torus.

The important aspect of our algorithm is to evaluate $g'(\mathbf{x})$ by numerical solutions of (3.1.1) on significantly reduced time intervals.

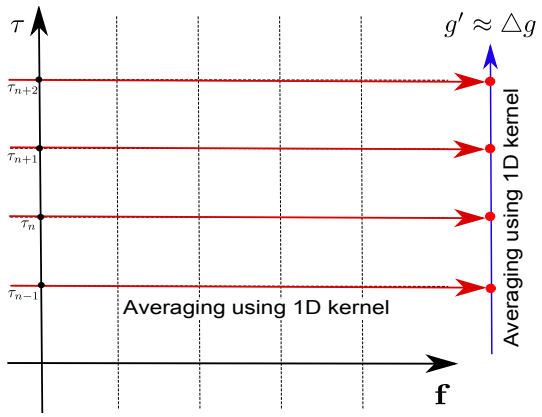

Figure 3.6: An illustration of the algorithm in the orthogonal coordinate system with f and τ . g' is approximated by $\triangle g = K_\tau * [K_f * g'(\mathbf{x})]$.

We point out that this algorithm has a very similar philosophy with a hierarchical HMM using iterated averages in Chapter 4. This will be further discussed in Chapter 5.

3.3.4 Examples

In this section, two different examples are presented. In Example 1, we compare our averaging strategy with time averaging. In Example 2, a two-scale HMM with the proposed averaging method as data estimation from microscale to macroscale systems is applied to an ODE system.

3.3.4.1 Example 1 (time averaging vs proposed method)

Consider (3.3.26) for $\mathbf{x} = [x_1, v_1, x_2, v_2]^T$,

$$\dot{\mathbf{x}} = \frac{1}{\epsilon} f(\mathbf{x}) = \frac{1}{\epsilon} \begin{bmatrix} v_1 \\ -x_1 \\ \lambda v_2 \\ -\lambda x_2 \end{bmatrix}, \quad \mathbf{x}(0) = \mathbf{x}_0,$$

where $\mathbf{x}_0 = [1, 0, 1, 0]^T$, $\lambda = 1 + \delta\sqrt{2}$ and $\delta = \epsilon^{\frac{1}{q}}$ with $q = 2$. In this section, we artificially choose the function g as $x_1^2 + v_1^2$ and compare the efficiency of $\frac{1}{S}\int_0^S g'(\varphi_t \mathbf{x})dt$ (time averaging) with our new method by considering $\bar{g}' = 0$ as an exact value. The results are summarized in Table 3.3.

Table 3.3: Comparison of time averaging with our method. Absolute errors are described using a max norm, $h_1 = \frac{\epsilon}{5}$ and time=sec.

S	$\frac{1}{S}\int_0^S g'(\varphi_t \mathbf{x})dt$	comp. time	comp. time	our method	η_1
42	0.0436	0.143	3.774	0.0437	30ϵ
149	0.0131	0.486	4.005	0.0132	40ϵ
550	0.0036	6.856	4.261	0.0036	50ϵ
2875	6.08e-04	34.84	4.457	5.85e-04	60ϵ
10000	1.75e-04	121.7	4.660	1.16e-04	70ϵ

3.3.4.2 Example 2 (HMM using averaging over the torus with proposed method)

Consider the following system describing two coupled harmonic oscillators whose hidden fast time dynamics is ergodic on $\mathbb{T}^2$.

$$\begin{cases} \dot{x}_1 = -2\pi\epsilon^{-1}x_2 - x_1^3 x_2^2 (x_1^2 + x_2^2)^{-3}, \\ \dot{x}_2 = 2\pi\epsilon^{-1}x_1 - y_2(x_1^2 + x_2^2)(y_1^2 + y_2^2)^{-1} - x_2^3 x_1^2 (x_1^2 + x_2^2)^{-3}, \\ \dot{y}_1 = -2\pi\lambda\epsilon^{-1}y_2 + y_1 x_2^2 (y_1^2 + y_2^2)^{-1}, \\ \dot{y}_2 = -2\pi\lambda\epsilon^{-1}y_1 + x_2 + y_4 x_2^2 (y_1^2 + y_2^2)^{-1}, \end{cases} \tag{3.3.29}$$

with initial conditions: $(x_1(0), x_2(0), y_1(0), y_2(0)) = (1, 0, 2, 0)$. To see how resonances occur, we replace (x_1, x_2) and (y_1, y_2) by the polar coordinates (r_1, θ_1) and (r_2, θ_2) respectively. We then get $\dot{\theta} = h(\theta)$ where $\theta \in \mathbb{T}^2$:

$$\begin{cases} \dot{\theta}_1 = \frac{1}{\epsilon} - \frac{r_1}{r_2}\frac{\cos 2\pi\theta_1 \sin 2\pi\theta_2}{2\pi}, \\ \dot{\theta}_2 = \frac{\lambda}{\epsilon} + \frac{r_1}{r_2}\sin 2\pi\theta_1 \cos 2\pi\theta_2. \end{cases} \tag{3.3.30}$$

In order to use our algorithm, we have to check two important questions: what is an invariant measure μ? given μ, is the flow $(\theta_1(t), \theta_2(t))$ ergodic on $\mathbb{T}^2$? In this case, we view (3.3.30) as a dynamical system on $\mathbb{T}^2$ where the vector field $h(\theta)$ is divergence-free , i.e., $\nabla \cdot h(\theta) = 0$. Consequently the Lebesgue measure is invariant for the ODE. Moreover, $h_1(\theta) \neq 0$ for all $\theta \in \mathbb{T}^2$ and the rotation number $\bar{h}_1/\bar{h}_2 = 1/\lambda$ is irrational. Thus $(\theta_1(t), \theta_2(t))$ is ergodic on $\mathbb{T}^2$. See [91] for more details.

we have a maximally slow chart (ξ_0, ξ_1) in which $\xi_i : \mathbb{R}^4 \to \mathbb{R}$ evolves on the ϵ^i time scale. The system admits two hidden slow variables on the ϵ^0 scale which are the squares of the amplitude of the harmonic oscillators, $I_1 = x_1^2 + x_2^2$ and $I_2 = y_1^2 + y_2^2$. The algorithm identifying slow variables is described in [5]. We indeed find that

$$\begin{aligned} \xi_0 &= \{I_1, I_2\}, \\ \xi_1 &= \varphi \in \mathbb{T}^2 \end{aligned}$$

where $I_1 = x_1^2 + x_2^2$ and $I_2 = y_1^2 + y_2^2$.

Table 3.4: Test parameters for 3-tier HMM

ϵ	λ	η_0	h_0	0 tier	η_τ	h_τ	τ tier	η_1	h_1	1 tier
10^{-4}	$1+\epsilon^{1/2}\sqrt{2}$	6	0.5	Midpoint	100	0.1	Midpoint	40ϵ	$\frac{\epsilon}{10}$	RK4

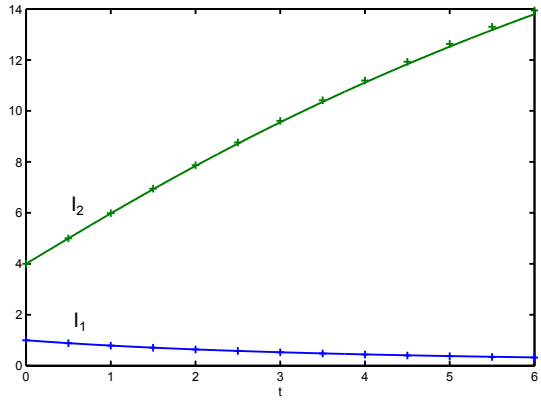

Figure 3.7: The dynamics of (4.6.77) on the ϵ^0 time scale. Plus signs are results of HMM.

3.4 Numerical averaging over the torus : nonuniform invariant measure

We consider an essentially different and more general situation with Section 3.3. We make no assumptions on the uniform measure of the ergodic flow and instead assume that the flow is ergodic on the manifold with non-uniform invariant measure.

Several remarks can be made to the previous approaches. Firstly, if the dynamical system is ergodic on an invariant manifold and the corresponding invariant measure is non-uniform, the flow density of such a dynamical system is not explicitly available in general, so we must consider a way to statistically estimate the density by looking at the flow. Secondly, the method presented in Section 3.3 needs to be modified since we we do not know which step size to use in the perpendicular direction. Accordingly, we cannot use the uniform step size h_τ in the algorithm of Section 3.3.3.

The underlying invariant measure is assumed to be absolutely continuous. In general, the existence of absolutely continuous invariant measure is not guaranteed. However, if a map is expanding, an absolutely continuous invariant measure is known to exist [77].

In this section, we present efficient techniques for the numerical approximation of nonuniform invariant measure supported on the torus. In particular, we construct a grid on the torus using the algorithm in Section 3.3.2 and develop numerical methods which allow us to approximate the invariant measure. The methods are based on an discretization of the Frobenius-Perron operator, and several numerical examples will be illustrated. See [29, 31, 32, 63] for more detailed theories.

3.4.1 Frobenius-Perron operator

We begin with recalling the following important theorem and assumption.

Theorem 3.4.1. If the flow is ergodic on the invariant manifold, then its corresponding invariant measure μ is unique for all time $t > 0$.

Assumption 6. *The corresponding invariant measure μ is absolutely continuous with respect to Lebesgue measure m.*

For fixed $t > 0$, let φ^t denote the solution operator for a dynamical system. An invariant measure μ is a probability measure on the Borel σ-algebra $\mathcal{B}(\mathbb{R}^n)$ such that

$$\mu(B) = \mu(\varphi^{-t}(B))$$

for all $B \in \mathcal{B}(\mathbb{R}^n)$ and $t > 0$. For example, the Dirac measure supported on a fixed point of the diffeomorphism of f and the Uniform measure supported on $\mathbb{R}$ of the irrational rotation map of f are typical invariant measures. For the notation, we denote for fixed η, f is identified with $\varphi^{\Delta t}$, and f^{-1} with $\varphi^{-\Delta t}$. Accordingly, for any point $x \in \mathbb{R}^d$, $f(x)$ is defined as the end point of microscale simulation over Δt amount of time by taking as x the initial condition.

Definition 3.4.1. Let $\mathcal{B}(\mathbb{R}^n)$ be the Borel σ-algebra and $\mathcal{A}$ be the space of probability measures on $\mathbb{R}^n$. The operator $P : \mathcal{A} \to \mathcal{A}$ defined by

$$(P\mu)(B) = \mu(f^{-1}(B)) \text{ for all } B \in \mathcal{B}(\mathbb{R}^n)$$

is called the Frobenius-Perron operator.

Note that $P\mu = \mu$ for all invariant measures $\mu \in \mathcal{A}$. The approximation procedure is to solve for an invariant measure for the Markov chain governed by P. Thus, computation of invariant measures is equivalent to calculating the fixed point of the Frobenius-Perron operator P. Now we describe a method to discretize the Frobenius-Perron operator and get an approximation density of the underlying invariant measure.

Let $\mathcal{B}_k = \{B_i\}_{i=1}^N$ denote the nested k-th disjoint space mesh refinement for the invariant manifold $\mathcal{M}(t)$. The sequence of refinements is constructed in such a way that the diameter

$$h_k := \text{diam}(\mathcal{B}_k) = \max_{B_i \in \mathcal{B}_k} \text{diam}(B_i)$$

converges to zero for $k \to \infty$. We let $\mathcal{A}_h$ be the space of density functions in terms of h which are constant on each B_i, $i = 1, \cdots, N$, i.e.,

$$\mathcal{A}_h = \left\{ u \in \mathbb{R}^N : u_i \geqq 0 \text{ and } \sum_{i=1}^{N} u_i = 1 \right\}.$$

By projecting the measure space $\mathcal{A}$ onto $\mathcal{A}_h$, the discretized Frobenius-Perron operator $P_h : \mathcal{A}_h \to \mathcal{A}_h$ is defined by

$$\sum_{i=1}^{N} u_i \frac{m(B_i \cap f^{-1}(B_j))}{m(B_i)} = v_j, \ j = 1, 2, \cdots, N. \tag{3.4.31}$$

In (3.4.31), $P_h u_h$ is described by a linear combination of all densities u_i with intersecting ratio $\frac{m(B_i \cap f^{-1}(B_j))}{m(B_i)}$ as coefficients. Accordingly we have in the matrix notation,

$$u_h P_h = v_h$$

where u_h,$v_h \in \mathcal{A}_h$ and $P_h = (p_{ij})$ with $p_{ij} := \frac{m(B_i \cap f^{-1}(B_j))}{m(B_i)}$ for $1 \leqq i, j \leqq N$. Indeed, P_h is a $N \times N$ transition matrix whose rows consist of nonnegative real numbers, with each row summing to 1. A stationary probability vector u_h is defined as a vector that does not change under application of the transition matrix P_h, that is, it is defined as a left eigenvector of the probability matrix P_h, associated with eigenvalue 1. The Perron–Frobenius theorem [85] ensures that every stochastic matrix has such a vector, and that the largest absolute value of an eigenvalue is always 1. Therefore, the invariant measure μ is approximated by a normalized left eigenvector $u_h \in \mathcal{A}_h$ of P_h associated with the eigenvalue 1. We denote this density by u_h, and have the approximation, $\mu(B_i) \approx (u_h)_i$.

Theorem 3.4.2. Let the flow f is ergodic on the invariant manifold and Assumption 6 is satisfied. Suppose that the partition $\{B_i\}$ of $\mathcal{M}$ consists of $\left(\frac{1}{h}\right)^d$ uniform hypercubes, that μ_h is an invariant vector for P and that the vector $\tilde{\mu}$ has components $\mu(B_i)$. Then there exists a constant $C > 0$ such that if h is sufficiently small,

$$||\tilde{\mu} - u_h||_{L^1} \leq Ch.$$

See Figure 3.10 for the numerical verification. For $d = 1$, one can find a related proof in [64].

3.4.1.1 Construction of p_{ij}

The crucial point in the computation of the discretize Frobenius-Perron operator is the efficient computation of the transition probabilities p_{ij}. We just have to approximate the Lebesgue measure of $B_i \cap f^{-1}(B_j)$. To do this, note that

$$m(B_i \cap f^{-1}(B_j)) = \int_{B_i} \chi_{f^{-1}(B_j)} dm.$$

Therefore,

$$p_{ij} = \frac{1}{m(B_i)} \int_{B_i} \chi_{f^{-1}(B_j)} dm. \tag{3.4.32}$$

We will discuss our proposed method to estimate (3.4.32) which is more efficient than the method based on Monte-Carlo method [61].

3.4.1.2 The complete algorithm for the density of an invariant measure

For simplicity, we identify n-torus with a hypercube $[0,1]^n$ in $\mathbb{R}^n$. The strategy for the approximation of an invariant measure supported on an invariant manifold is based on that f maps a hypercube to a convex polygon and the overlapped region is also defined by a convex polygon. In order to approximate the overlapped region, we note that one can decompose an n-dimensional polygon into unions of $n-$simplicies and the volume of an n-simplex in n-dimensional space with vertices $(v_0, v_1, \cdots, v_n)$ is given by

$$\frac{1}{n!} \left| \det \left(v_1 - v_0 \quad v_2 - v_0 \quad \cdots v_n - v_0 \right) \right|.$$

The algorithm is formulated as follows:

Algorithm 8. *Computing Multidimensional Absolutely Continuous Invariant Measures*

1. Discretize $[0,1]^n$ into $\left(\frac{1}{h}\right)^n$ uniform hypercubes $\{B_i\}_{i=1}^{\left(\frac{1}{h}\right)^n}$.
2. For all grid points $\{v_i\}$ in $[0,1]^n$, compute $\phi^\eta(\{v_i\})$ for $\eta(\approx h)$ amount of time.
3. For each $1 \leqq j \leqq \left(\frac{1}{h}\right)^n$, identify vertices of $\phi^\eta(B_j) \cap \{B_i\}_{i=1}^{\left(\frac{1}{h}\right)^n}$ and compute the volume of intersection area. $\rightarrow$Produce $\left(\frac{1}{h}\right)^n \times \left(\frac{1}{h}\right)^n$ stochastic matrix P.
4. Find the left eigenvector μ_h of P associated with eigenvalue 1.
5. μ_h gives an approximation of the invariant density ρ.

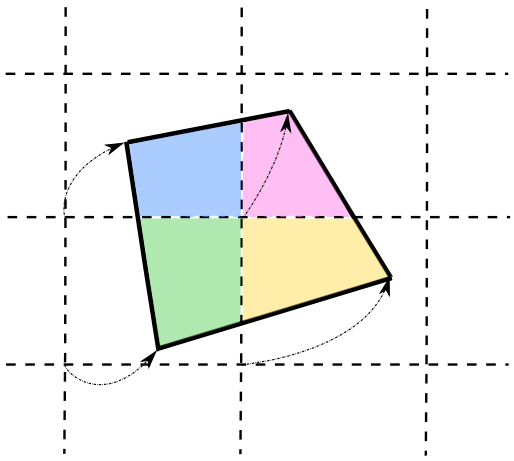

Figure 3.8: Computing $p_{ij} = \frac{m(f^{-1}(B_i) \cap B_j)}{m(B_i)}$ in $\mathbb{T}^2$. We compute the area of each rectangle by dividing into two triangles and using cross product.

In order to realize an idea in Algorithm 8, several MATLAB functions are generated. See [1] . Note that all functions work in an n-dimensional setting as well.

[1] convhulln.m (MATLAB built-in): K=convhulln(X) returns the indices K of the points in X that comprise the facets of the convex hull of X. X is an m-by-n array representing m points in n-dimensional space.

verttocon.m: $[A\ b]$=verttocon(X) converts a set of points in X to the set of inequality constraints. If y satisfies $Ay \leq b$, then y is located inside of X. Moreover, for $Ay = b$, y is located at the boundary of X. Since there is always a mechanical precision error, very small perturbation to b is considered.

inpolyn.m: inpolyn(v,A) decides whether a point v is in A or not.

plinter.m: plinter($v, \vec{n}, p_1, p_2$) computes the intersection of a n-dimensional plane which is decided by normal $\vec{n}$ and a point v on it with a line segment p_1p_2.

3.4.2 Numerical examples

3.4.2.1 2-dimensional flat torus

A flow whose invariant measure is non trivial is given by below. We define a polynomial

$$p(x) = ax^4 - 2ax^3 + ax^2 + x \tag{3.4.33}$$

so that $p(0) = 0$, $p(1) = 1$ and $p'(0) = p'(1) = 1$. Using (3.4.33), we have a map associated invariant measure is non-uniform;

$$\varphi_t : \mathbb{R}^2 \to \mathbb{R}^2,\ \varphi_t(x, y) = \begin{bmatrix} p_1(p_1^{-1}(x) + \lambda_1 t \mod 1) \\ p_2(p_2^{-1}(y) + \lambda_2 t \mod 1) \end{bmatrix}. \tag{3.4.34}$$

where p_1 and p_2 have different constants a and λ_i are irrational so that the flow φ^t ergodic on $[0, 1]^2$. The reason why we consider (3.4.33) instead of an ODE is that we can analytically find the reference density function of (3.4.33). We will use this solution to benchmark our solutions.

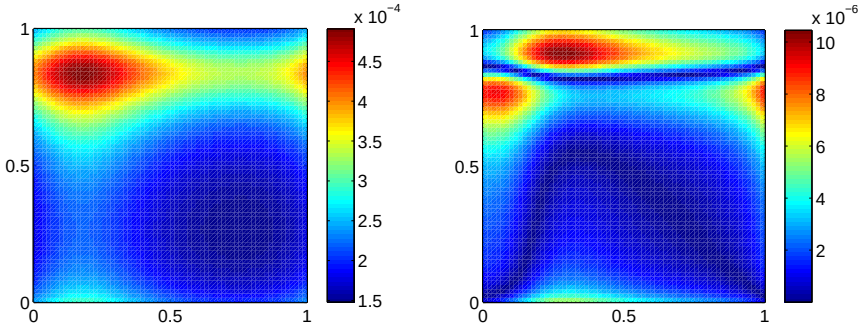

Figure 3.9: Approximate a non-uniform invariant measure with our method using $h = \frac{1}{64}$ and 4096 cells on $[0, 1]^2$. The L^1-error is $||\tilde{\mu} - u_h||_{L^1} = 0.0102$. The computational time is about 12.3s. The right plot is an error in each cell to the reference solution. If we use Monte-Carlo integration in this particular example, the error is $||\tilde{\mu} - u_h||_{L^1} = 0.1250$ and the computational time is about 210s with random 50 points in each box.

For this example our method is much more efficient than the method based on Monte-Carlo integration. Moreover, our algorithm shows $\mathcal{O}(h)$ convergence rate;

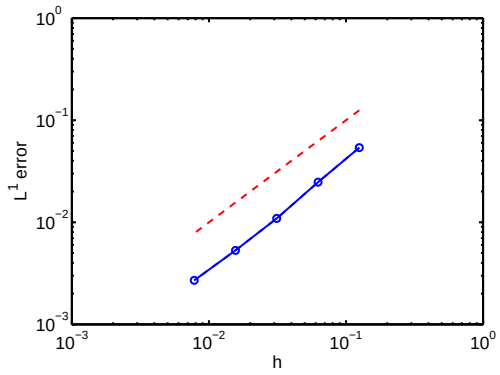

Figure 3.10: (flat 2-torus) Error plot of h vs $||\tilde{\mu} - u_h||_{L^1}$ using our method. The red line is slope with 1.

3.4.2.2 3-dimensional flat torus

A flow whose invariant measure is non trivial is given by below. We define a polynomial

$$\begin{cases} p_1(x) &= -x^4 + 2x^3 - x^2 + x, \\ p_2(x) &= 2x^4 - 4x^3 + 2x^2 + x \end{cases} \tag{3.4.35}$$

with $p_i(0) = 0$, $p_i(1) = 1$ and $p_i'(0) = p_i'(1) = 1$, $i = 1, 2$. Using (3.4.35), we have a map associated invariant measure is non-uniform in $\mathbb{T}^3$;

$$\varphi^t : \mathbb{T}^3 \to \mathbb{T}^3,\ \varphi_t(x, y, z) = \begin{bmatrix} p_1(p_1^{-1}(x) + \lambda_1 t \mod 1) \\ p_2(p_2^{-1}(y) + \lambda_2 t \mod 1) \\ z + \lambda_3 t \mod 1 \end{bmatrix} \tag{3.4.36}$$

where $\lambda_1 = \sqrt{7}$, $\lambda_2 = \sqrt{2}$ and $\lambda_3 = 1$ so that we make the flow φ^t ergodic on $\mathbb{T}^3$.

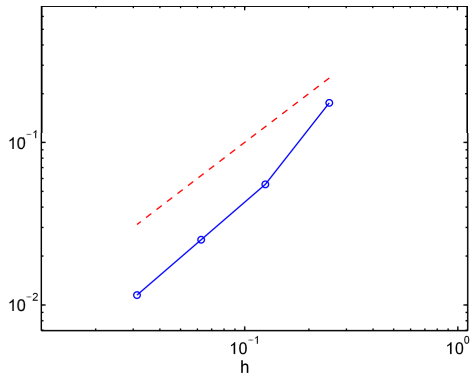

Figure 3.11: (flat 3-torus) Error plot of h vs $||\tilde{\mu} - u_h||_{L^1}$ using our method. The red line is slope with 1. $\eta = \frac{h}{2}$ is used.

3.4.2.3 Parallelization

One of the advantages of our algorithm is that it can be parallelized easily. On the other hand, the time-averaging aspect of the algorithm is serial which cannot be parallelized.

Table 3.5: Parallel performance of calculating the matrix P with size $Cells \times Cells$. A processor number is up to 6. $\eta = h/2$ is fixed. Only is the computational time to compute the matrix P considered.

h	Cells	Cpu time in sec (# of cpu)					
		# = 1	2	3	4	5	6
1/4	$4 \times 4 \times 4$	2.64	1.58	1.23	1.05	0.95	0.88
1/8	$8 \times 8 \times 8$	16.38	8.733	6.082	4.770	3.945	3.450
1/16	$16 \times 16 \times 16$	122.3	64.21	43.48	33.15	27.93	23.58
1/32	$32 \times 32 \times 32$	1321	728.2	523.6	438.7	375.5	330.7

3.4.2.4 Numerical methods for finding eigenvector

Suppose that we construct a stochastic $N \times N$ matrix P using the Frobenius-Perron method, i.e., its rows are summed to 1. Then P has the largest eigenvalue

equal to 1 and a real eigenvector x corresponding to this eigenvalue, i.e. $xP = x$ or equivalently $P^T x^T = x^T$. Finding this eigenvector is a basic problem in numerical analysis and in numerous applications using Markov chain. There are several approaches to achieve this:

- Null$(P^T - I)$: MATLAB uses the singular value decomposition. The computational cost is $\mathcal{O}(N^3)$. If one halves the step size $h \to h/2$, this cost increases by a factor of $(2^d)^3$ when an d-dimensional manifold is considered.

- Power method: In general, the asymptotic rate of convergence of the power method applied to a matrix depends on the ratio of the two eigenvalues that are largest in magnitude, denoted λ_1 and λ_2. Precisely, $\left|\frac{\lambda_2}{\lambda_1}\right|^k = |\lambda_2|^k \to 0$ where k is the number of iterations.

- Adaptive randomized algorithm for finding eigenvector of stochastic matrix with application to PageRank [88]: an adaptive randomized algorithm and provide an explicit upper bound for its rate of convergence $\mathcal{O}\left(\sqrt{\frac{\ln N}{k}}\right)$. If one halves the step size $h \to h/2$ in d-dimensional manifolds, this bound increases by a factor of $\mathcal{O}\left(\sqrt{\frac{d\ln 2 + \ln N}{\ln N}}\right)$ which is not large even for very high dimensions.

In the Frobenius-Perron algorithm, P is sparse with at most 3^d non-zero elements in each row, and from various numerical experiments, we observe that the Power method and adaptive randomized algorithm are much more efficient than SVD.

3.5 Numerical averaging over the embedded torus

3.5.1 Embedded torus

Recall an ODE system, formally written in the form

$$\dot{x} = \epsilon^{-1} f_1(x) + f_0(x), \tag{3.5.37}$$

with initial condition $\mathbf{x}(0) = \mathbf{x}_0 \in U \subset \mathbb{R}^d$. We assume that there exists a diffeomorphism $\Psi : x \to (\xi(x), \phi(x))$ separating slow and fast variables such that the dynamics satisfies an ODE of the form

$$\begin{cases} \dot{\xi} = g_0(\xi, \phi), & \xi(0) = \xi_0, \\ \dot{\phi} = \epsilon^{-1} g_1(\xi, \phi) + g_2(\xi, \phi), & \phi(0) = \phi_0, \end{cases} \tag{3.5.38}$$

where $(\xi, \phi) \in \mathbb{R}^{d-p} \times \mathbb{T}^p$ with $\xi \in \mathbb{R}^{d-p}$ and $\phi \in \mathbb{T}^p$. Here we emphasize that $\mathbb{T}^p$ is defined as the level sets of $\xi_1, \xi_2, \cdots, \xi_{d-p}$ which are slow variables with respect to $x(t)$. Thus, for each time t, we may identify the manifold as

$$\mathcal{M}(t) = \cap_{j=1}^{p} \{\mathbf{x} \in \mathbb{R}^d : x_j(\mathbf{x}) = x_j \circ \mathbf{x}(t)\}.$$

Due to the lower order perturbation in (3.5.37), $\mathcal{M}(t)$ changes as time goes by. Technically, approximating the slow behavior ξ in (3.5.38) is equivalent to track an evolution of $\mathcal{M}(t)$. From our multiscale strategy in Chapter 1, this can be done by using an algorithm which is equipped with averaging ξ' over $\mathcal{M}(t)$.

3.5.2 HMM with Frobenius-Perron algorithm

Motivated by the framework of HMM and the previous algorithm with Frobenius-Perron operator, we propose the HMM with Frobenius-Perron algorithm. Outline of the scheme can be summarized as below.

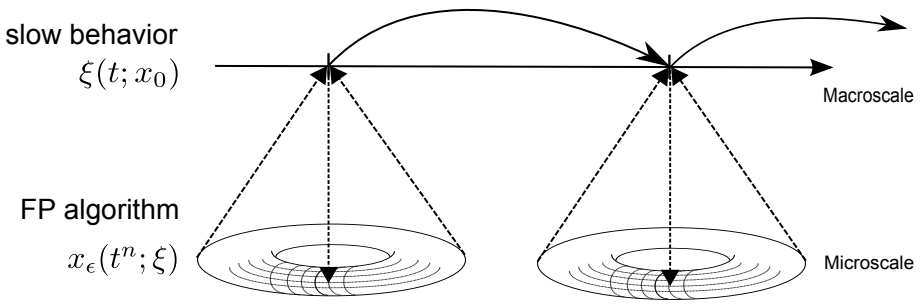

Figure 3.12: An illustration of a multiscale algorithm with averaging over the torus.

We present an algorithm aiming at d-dimensional manifold embedded on $\mathbb{R}^n$.

1. Determination of slow variables: Find $n-d$ independent slow variables $\xi_i(t) := \xi_i \circ x(t)$ evolving on the *slowest* time scale. We *do not* need to find a slow chart.

2. [Microscale simulation] Construct a coordinate system on lifted copies of the torus:

   At $t = t_n$, set $X_0 = x_n$. For $i = 1$ to k^{n-d} , $k = \eta_1/h_1$, one grid node is constructed by (1st order construction)

   (a) Set $X_i^f = X_j^1 = \cdots = X_j^{n-d-1} = X_i$.

   (b) (identifying hidden direction I) Find hidden directions τ^v, $v = 1, 2, \cdots, n-d-1$ orthogonal to $\{f(X_0), \nabla\xi(X_0)\}$ such that a system $[\tau^v, f(X_0), \nabla\xi(X_0)]$ is a square matrix of full rank.

   (c) (rotation for ergodicity) Set $\tilde{f} = \sqrt{\lambda_f} f + \sum_v \sqrt{\lambda_v}\tau^v$ where $\lambda_f + \sum_v \lambda_v = 1$ and $\lambda_f, \lambda_v > 0$.

(d) (identifying hidden direction II) Find hidden directions $\tilde{\tau}^v$, $v = 1, 2, \cdots, n-d-1$ orthogonal to $\{\tilde{f}(X_0), \nabla\xi(X_0)\}$ such that a system $\left[\tilde{\tau}^v, \tilde{f}(X_0), \nabla\xi(X_0)\right]$ is a square matrix of full rank.

(e) Set $X_{i+1}^v = X_i^v + h_1\tilde{\tau}^v$.

(f) Go (a) and repeat k times to each X_i^v to resolve each direction $\tilde{\tau}^v$.

(g) Set $X_0 = X_0 + h_1\tilde{f}^v$.

(h) End For

3. [Macroscale simulation] Use Frobenius-Perron operator algorithm using previously constructed grid points on the manifold. See Figure 3.13 for a graphical illustration.

4. Force estimation: approximate $\xi'(t_n)$, by the discrete integration

$$\left\langle \xi' \right\rangle (t_n) = \sum_i \xi'(x_i)\mu(B_i).$$

5. $x_{n+1} = x_n + H\delta x_0$ where δx_0 is the least squares solution to the linear system

$$\delta x_0 \cdot \nabla\xi = \left\langle \xi' \right\rangle.$$

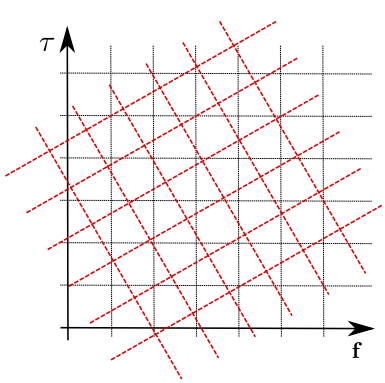

(a) (i) Coordinate rotation for ergodicity.

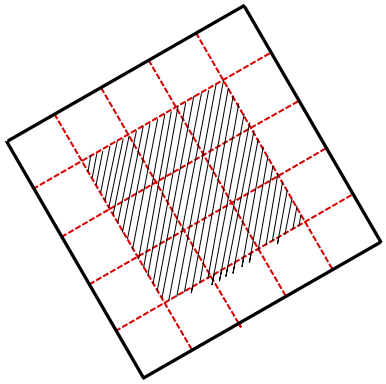

(b) (ii) A virtual torus – imposing an artificial boundary condition.

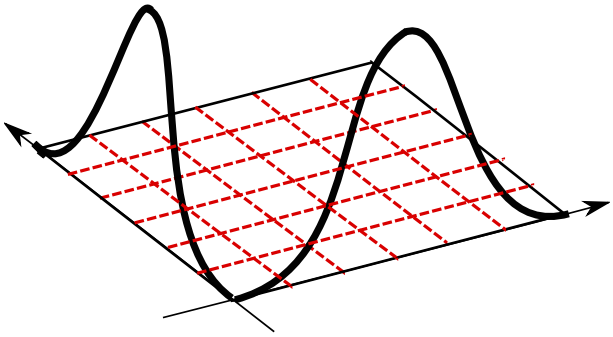

(c) (iii) Approximating the invariant density by multiplying 1D kernels.

Figure 3.13: Essential steps for approximating the invariant measure in Frobenius-Perron operator algorithm.

3.5.3 Numerical examples

3.5.3.1 Weakly coupled harmonic oscillator (averaging over the torus across ϵ^{-2} and $\epsilon^{-4/3}$ time scales)

Consider the following deterministic system describing two coupled fast harmonic oscillators and a slow dependent mode.

$$\begin{cases} x_1' &= -\epsilon^{-2}(1+0.5\sin y_2)x_2 + (1-z)(x_1^2+x_2^2)^{-1}x_1, \\ x_2' &= \epsilon^{-2}(1+0.5\sin y_2)x_1, \\ y_1' &= -\epsilon^{-4/3}y_2 - 0.5(1+x_1^2-z)y_1, \\ y_2' &= \epsilon^{-4/3}y_1, \\ z' &= -(1+0.5x_1^2)z + y_2^2, \end{cases}$$

with initial conditions $(x_1(0), x_2(0), y_1(0), y_2(0), z(0)) = (1, 0, 1, 1.5, 0.5)$. The numerical results are summarized in Figure 3.14.

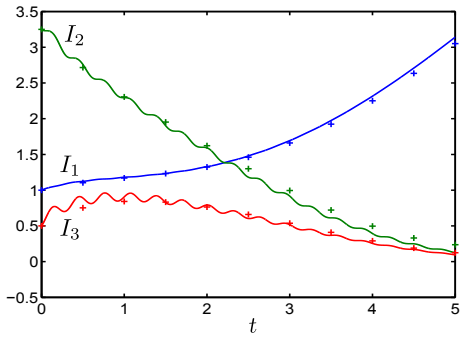

Figure 3.14: Numerical results of HMM with Frobenius-Perron operator algorithm, $\epsilon = 10^{-3}$, $\eta = 70\epsilon^2$, $h = \epsilon^2/10$ and $H = 1/2$. As $\epsilon \to 0$, we observe that plus signs are getting closer to the solid lines.

Chapter 4

Iterated averaging: A strategy for problems with more than two separated time scales

The main purpose of this chapter is twofold. First, we generalize the classical two-scale averaging theory to a class of highly oscillatory systems whose solutions possess slow variables or observables as well as fast oscillations with frequencies that are separated by two large spectral gaps. We shall call such systems three-scale oscillatory systems. Our generalization is along the lines of the so called iterated homogenization problem [14, 19, 22, 60, 81]. Similarly, we develop a theory of iterated averaging which is approached from three different points of view: (1) application of long time asymptotic and second order averaging theorems [93, 100]; (2) formal perturbation expansions applied to an associated SDE; and (3) a direct proof by repeated convolution with averaging kernels across different time scales. The latter is the foundation for a hierarchical numerical algorithm consisting of nested integrators, which is the second main objective of the paper. We demonstrate how tiers of two-scale numerical methods can be "stacked-up" in order to construct a consistent approximation of the effective slow dynamics in three-scale systems. To our knowledge, very few algorithms have been developed considering directly three or more scales. We develop our algorithm using the framework of the heterogeneous multiscale method (HMM) for highly oscillatory ODEs [3, 36].

4.1 Introduction

Averaging methods are some of the most widely used tools for the study and approximation of highly oscillatory ordinary differential equations (ODEs). In its most basic form, averaging means that following a change of variables that separates the system into slow coordinates and periodic fast ones, the effect of the fast oscillations can be integrated out, yielding an approximate effective equation. More precisely, consider the initial value problem

$$x' = f(x, \epsilon^{-1}t), \quad x(0) = x_0, \tag{4.1.1}$$

where $0 < \epsilon \leq \epsilon_0 \ll 1$ denotes the scale separation in the problem. It is assumed that a unique uniformly bounded solution $x(t) \in \mathbb{R}^d$ exists in a time segment $[0, T]$ which is independent of ϵ. Furthermore, $f(x, s)$ is sufficiently smooth and 1-periodic in s. See, for example [20, 93] for details. Then, $x(t)$ can be approximated by the effective averaged equation

$$\xi' = F(\xi), \quad \xi(0) = x_0, \tag{4.1.2}$$

where $F(\xi)$ is the average of $f(x, s)$ over one period of s

$$F(\xi) = \langle f(\xi, \cdot)\rangle_s \equiv \int_0^1 f(\xi, s)ds. \tag{4.1.3}$$

Furthermore, the approximation is of order ϵ in the sup norm, i.e.

$$\sup_{0\leq t\leq T} |x(t) - \xi(t)| = \mathcal{O}(\epsilon). \tag{4.1.4}$$

This elementary result has been generalized considerably to include, for example, chaotic and stochastic systems [12, 19, 20, 66, 69, 89, 91, 93]. From a computational

point of view, averaging methods inspire efficient numerical schemes for integrating the slow components of slow-fast systems without fully resolving all fast oscillations in $[0, T]$. See, for example [1, 3, 13, 24, 35, 36, 38, 40, 45, 49, 94, 98, 101] and references therein.

The main purpose of this paper is twofold. First, we generalize the classical two-scale averaging theory (4.1.1)-(4.1.4) to a model problem whose solutions possess slow variables or observables as well as fast oscillations with frequencies that are separated by two large spectral gaps. We shall call such systems three-scale oscillatory systems. Our generalization is along the lines of the so called iterated homogenization problem [14, 19, 22, 60, 81]. Similarly, we develop a theory of iterated averaging which is approached from three different views: (1) application of long time asymptotic and second order averaging theorems [93, 100]; (2) formal perturbation expansions applied to an associated stochastic differential equation (SDE); and (3) a direct proof by repeated convolution with averaging kernels across different time scales. The latter is the foundation for a hierarchical numerical algorithm consisting of nested integrators, which is the second main objective of the paper. We demonstrate how tiers of two-scale numerical methods can be "stacked-up" in order to construct a consistent approximation of the effective slow dynamics in three-scale systems. To our knowledge, very few algorithms have been developed considering directly three or more scales. We develop our algorithm using the framework of the heterogeneous multiscale method (HMM) for highly oscillatory ODEs [3, 36]. A proof of concept for the algorithm was previously suggested in [7] without the underlying mathematical theory of iterated averaging or proof of convergence.

To gain insight on the analysis of the numerical method described in [7], it is helpful to study the method when it is applied to an appropriately chosen and simpler problem which shows the similar features of the original model but is easier to analyze. We thus develop a simple model, motivated by Fermi, Pasta and Ulam (FPU) [46], which shows the multiscale behavior in time scales of integer powers of ϵ. The FPU model involves almost-periodic dynamics on the ϵ time scale, dynamics of the soft nonlinear springs on the time scale independent of ϵ, and the slow energy exchange among stiff springs on the ϵ^{-1} time scale; see e.g. [55]. We remark however that there of course exist dynamical systems whose multiscale features are not integer powers of ϵ, e.g. in weakly coupled, nearly resonant harmonic oscillators. A method for near-resonance is beyond the scope of this paper, but a new approach for these general systems will be reported in a forthcoming paper.

Consider ODE systems evolving on three well-separated time scales of the form

$$\begin{cases} x' = \epsilon^{-1}\tilde{f}_1(x,y,z) + \tilde{f}_0(x,y,z), & x(0) = x_0, \\ y' = \epsilon^{-1}\tilde{g}_1(x,y,z) + \tilde{g}_0(x,y,z), & y(0) = y_0, \\ z' = \epsilon^{-2}\tilde{h}_2(x,y,z), & z(0) = z_0, \end{cases} \tag{4.1.5}$$

where the separation into the three components x, y and z is according to the time-scale on which variables evolve, ϵ^2, ϵ and 1, respectively. Throughout this paper we assume the existence of a unique solution for each initial condition $(x_0, y_0, z_0) \in \mathcal{D}_0 \subset \mathbb{R}^{d_0} \times \mathbb{R}^{d_1} \times \mathbb{R}^{d_2}$ which is bounded independent of ϵ in a time segment $[0, T]$ also independent of ϵ. Since the time derivatives of $(x(t), y(t), z(t))$ are not uniformly bounded while solutions are, fast variables $y(t)$ and $z(t)$ are either dissipative (i.e., converge to a stable low dimensional manifold on an ϵ or ϵ^2 time scale), or highly

oscillatory. In this paper we concentrate on the highly oscillatory case. Accordingly, we assume the following,

- For fixed x and y, $z(t) \in \mathbb{R}^{d_2}$ is quasi-periodic (i.e., diffeomorphic to uniform rotations on a d_2 dimensional torus) with frequencies of order ϵ^{-2} over $t \in [0, T]$.

- For fixed x, $y(t) \in \mathbb{R}^{d_1}$ quasi-periodic with frequencies of order ϵ^{-1} over $t \in [0, T]$.

- The variable $x(t) \in \mathbb{R}^{d_0}$ is slow. More precisely, there exists a function $\xi(t)$ which is independent of ϵ such that

$$\sup_{0<\epsilon\leq\epsilon_0} \sup_{0\leq t\leq T} |x(t) - \xi(t)| \leq C\epsilon,$$

  for some constants ϵ_0, T and C independent of ϵ. In the following, it will be shown that a necessary condition for x to be slow is that the average of $\tilde{f}_1$ over z vanishes.

In many situations, one is only interested in the slowly changing quantity $x(t)$. Accordingly, our main objective is to investigate and approximate the effective dynamics $\xi(t)$, discarding the fast variables $y(t)$ and $z(t)$. When only looking for the effective dynamics $\xi(t)$ of the slow variable $x(t)$ in the time interval $[0, \epsilon T]$, one can simply truncate the $\tilde{f}_0$ term, and average over y and z. On the other hand, in case of $[0, T]$, we cannot neglect $\tilde{f}_0$ because its effect appears in this longer time interval.

In this paper, we focus on a a simplified version of (4.1.5) in which the fast scales associated with y and z are given explicitly as known time-dependent functions. Most of the analytical results will be proven in this simpler setup. However, in section 4.1.4 we explain heuristically why this simpler form keeps the essential multiscale features of the more general system (4.1.5) and why our suggested numerical method applies to the full three-scale problem (4.1.5). We consider ODE systems of the form

$$x' = \epsilon^{-1} f_1(x, \epsilon^{-1}t, \epsilon^{-2}t) + f_0(x, \epsilon^{-1}t, \epsilon^{-2}t), \quad x(0) = x_0, \tag{4.1.6}$$

where $f_1(x, s_1, s_2)$ and $f_2(x, s_1, s_2)$ are sufficiently smooth (e.g. C^1) and 1-periodic in s_1 and s_2. As before, it is assumed that a unique bounded solution exists for each $x_0 \in \mathcal{D}_1 \subset \mathbb{R}^d$ in a time segment $[0, T]$. Both the bound and T are independent of ϵ. The dynamics of (4.1.6) can be characterized across three well-separated time scales: a fast time scale involving time intervals with length of order ϵ^2, an intermediate scale of order ϵ and a slow $\mathcal{O}(1)$ scale. In Section 4.2 we will show that if the average of f_1 with respect to s_2 vanishes, then $x(t)$ effectively varies on the time scale of $\mathcal{O}(1)$, i.e., $x(t)$ is the slow variable. Moreover, effective equations for $x(t)$ will also be given.

In the following, we shall use s_1 and s_2 exclusively for the variables which will be scaled respectively to $\epsilon^{-1}t$ and $\epsilon^{-2}t$. Moreover, averages of a function $f(x, s_1, s_2)$ with respect to s_1 and s_2 with x fixed are denoted respectively by

$$\langle f(\xi, s_1, s_2)\rangle_1, \qquad \langle f(\xi, s_1, s_2)\rangle_2,$$

Accordingly, the double average of $f(x, s_1, s_2)$ over both s_1 and s_2 is denoted

$$\langle f(x, s_1, s_2)\rangle_{12}.$$

As motivation, we begin formally. Assuming that for fixed x and s_1 the average of f_1 with respect to s_2 vanishes, $x(t)$ can be written as a sum of a smooth function $w(t)$ whose first time derivative is bounded independent of ϵ, and fast oscillations around $w(t)$ whose amplitudes tend to zero as $\epsilon \to 0$ [87, 93]. As a motivation for identifying an ODE for $w(t)$, consider the form

$$x(t) = w(t) + \epsilon\phi(w(t), \epsilon^{-1}t, \epsilon^{-2}t).$$

Substituting into (4.1.6) yields

$$w' = \epsilon^{-1}(f_1 - \frac{\partial\phi}{\partial s_2}) + (\nabla_x f_1)\phi - \frac{\partial\phi}{\partial s_1} + f_0 + \mathcal{O}(\epsilon). \tag{4.1.7}$$

In order to have that $w'(t)$ is bounded independent of ϵ we require that $\partial\phi/\partial s_2 = f_1$. Consequently, ϕ should be taken to be the anti-derivative of f_1 with respect to s_2 and

$$w' = (\nabla_x f_1)\phi - \frac{\partial\phi}{\partial s_1} + f_0 + \mathcal{O}(\epsilon). \tag{4.1.8}$$

Since ϕ is periodic in s_1 and s_2, $\partial\phi/\partial s_1$ averages to zero and therefore does not contribute to the effective equation. In order to eliminate small oscillations in ϕ, the right hand side (RHS) of (4.1.8) should be averaged with respect to s_1 and s_2. This leads to the averaged equation

$$\xi' = F(\xi), \quad \xi(0) = x_0, \tag{4.1.9}$$

where

$$F = \langle (\nabla_x f_1)\phi + f_0 \rangle_{12},$$
$$\phi(\xi, s_1, s_2) = \int_0^{s_2} f_1(\xi, s_1, \tau) d\tau. \tag{4.1.10}$$

Remark 4.1.1. The definition of ϕ is not unique. For example, it is straightforward to verify that taking $\phi(\xi, s_1, s_2) = \int_0^{s_2} f_1(\xi, s_1, \tau) d\tau + a(\xi, s_1)$ where, for fixed ξ, $a(\xi, s_1)$ is periodic in s_1, one would arrive at the same averaged equation. Two canonical choices are either $a(\xi, s_1) = 0$ which is used in Sections 4.2 and 4.4, or $a(\xi, s_1)$ such that $\langle \phi \rangle_2 = 0$ which is used in Section 4.3.

Remark 4.1.2. Following the previous remark we note that in general, it is not true that writing $x = w + \epsilon\phi + \mathcal{O}(\epsilon^2)$.

The following theorem is proved in Section 4.2.

Theorem 4.1.1. Let $x(t)$ and $\xi(t)$ denote solutions of equations (4.1.6) and (4.1.9) respectively. If f_1 has a zero average with respect to s_2, then there exists a constant $C > 0$ independent of ϵ such that

$$\sup_{0 \le t \le T} |x(t) - \xi(t)| \le C\epsilon.$$

In fact, as will be seen later, the same theorem holds under weaker assumptions on the fast and intermediate time scales s_1 and s_2. The fast, ϵ^2 scale can be periodic, ergodic on a torus or almost periodic with frequencies that are bounded from below. On the intermediate $\mathcal{O}(\epsilon)$ scale, the only requirement is that for fixed ξ, the effective dynamics obtained after integrating the fastest ϵ^2 time scale is ergodic and that a two-scale averaging principle [93] holds. This includes oscillatory,

stochastic and chaotic dynamics. Such generalizations are further discussed in Section 4.5.

4.1.1 A simple example

Consider the ODE system

$$x' = 2\pi\epsilon^{-1}\left[x\sin(2\pi\epsilon^{-2}t) + \cos(2\pi\epsilon^{-2}t)\right], \quad x(0) = 0. \tag{4.1.11}$$

for $0 \leq t \leq 1$. By the method of variation of parameters, the exact solution of (4.1.11) is found to be

$$x(t) = 2\pi\epsilon^{-1}e^{-\epsilon\cos(2\pi\epsilon^{-2}t)}\int_0^t \cos(2\pi\epsilon^{-2}s)e^{\epsilon\cos(2\pi\epsilon^{-2}s)}ds. \tag{4.1.12}$$

Expanding in ϵ,

$$x(t) = \pi t + \epsilon\left[\sin(2\pi\epsilon^{-2}t) - \pi t\cos(2\pi\epsilon^{-2}t)\right] + \mathcal{O}(\epsilon^2). \tag{4.1.13}$$

Hence, $x(t) = \pi t + \mathcal{O}(\epsilon)$ for $t \in [0, 1]$.

A naive approach for obtaining an effective equation is to assume that in any sufficiently short time interval the solution of (4.1.11) can be approximated by integrating over the fast oscillations in the RHS of (4.1.11) while keeping x fixed. This yields

$$\tilde{x}(t) = 2\pi\epsilon^{-1}\int_0^t \left[X\sin(2\pi\epsilon^{-2}s) + \cos(2\pi\epsilon^{-2}s)\right] ds\Big|_{X=\tilde{x}(t)} = 2\pi\epsilon^{-1}\left[X\mathcal{O}(\epsilon^2) + \mathcal{O}(\epsilon^2)\right], \tag{4.1.14}$$

which implies that $\tilde{x}(t) = \mathcal{O}(\epsilon)$ only for $t \in [0, C\epsilon]$.

In contrast, Theorem 4.1.1 yields the correct averaged equation for x for $t \in [0,1]$:

$$X' = \pi, \quad X(0) = 0,$$

which clearly implies that

$$\sup_{t\in[0,1]} |x(t) - X(t)| \leq (1+\pi)\epsilon.$$

On the other hand, performing averages over fast oscillations can be approximated in a convenient and computationally efficient way by convolution of x' with appropriate compactly supported kernels. Inside the convolution, the value of x is not exactly fixed but varies following the correct dynamics. *This subtle change in the values of $x(t)$ allows for the kernel to capture the correct effective change of $x(t)$ in a longer time scale.* This can be demonstrated in the case of example (4.1.11). Consider a cosine kernel, which is particularly convenient in this example

$$K(t) = \frac{1}{2}\chi_{[-1,1]}(t)\left[1 + \cos(\pi t)\right],$$

where χ_A is the indicator function of a set A. Furthermore, for $\eta > 0$, let K_η denote a scaling of $K(t)$ to $[-\eta, \eta]$,

$$K_\eta(t) = \frac{1}{\eta}K\left(\frac{t}{\eta}\right).$$

Without loss of generality, we calculate the convolution of K_η with x' in (4.1.11) at $t = 0$

$$(K_\eta * x')(0) = \frac{2\pi}{\epsilon}\int_{-\eta}^{\eta} K_\eta(-s)\left[x(s)\sin(2\pi\epsilon^{-2}s) + \cos(2\pi\epsilon^{-2}s)\right] ds.$$

Substituting in the expansion of $x(s)$ shown in Eq. (4.1.13), and using $\eta = n\epsilon^2$ yields

$$\begin{aligned}(K_\eta * x')(0) =& \frac{\pi}{\eta\epsilon}\int_{-n\epsilon^2}^{n\epsilon^2}\left[1+\cos(\frac{\pi s}{\eta})\right]\left[\pi s\sin(\frac{2\pi ns}{\eta})+\cos(\frac{2\pi ns}{\eta})\right]ds \\ &+\frac{\pi}{\eta}\int_{-n\epsilon^2}^{n\epsilon^2}\left[1+\cos(\frac{\pi s}{\eta})\right]\left[\sin^2(\frac{2\pi ns}{\eta})-\frac{\pi s}{2}\sin(\frac{4\pi ns}{\eta})\right]ds+\mathcal{O}(\epsilon) \\ =&\pi+\mathcal{O}(\epsilon),\end{aligned}$$

which is, to leading order in ϵ, the correct derivative for the slow variable x for $t \in [0,1]$.

In Section 4.4 these ideas are generalized to oscillatory three-scale systems in which kernels are applied iteratively to the different time scales. This can then be exploited for construction of efficient multiscale numerical schemes.

4.1.2 Formal asymptotic expansions

Formal asymptotic expansions of singularly perturbed operators have been successfully applied to a wide variety of problems [19, 91]. Of particular relevance are the applications to SDEs [35, 82, 89, 101]. Consider SDE systems of the form

$$\begin{cases} dx_t = & \left[\epsilon^{-1}f_1(x_t,y_t)+f_0(x_t,y_t)\right]dt \\ dy_t = & \epsilon^{-2}a(x_t,y_t)dt+\epsilon^{-1}\beta(x_t,y_t)dB_t, \end{cases} \tag{4.1.15}$$

where B_t is a standard Brownian motion in $\mathbb{R}^d$. The variable $x_t \in \mathbb{R}^d$ is a slow process that evolves according to an ODE with a fast random coefficient $y_t \in \mathbb{R}^n$. Under some ergodicity, smoothness and growth assumptions, x_t can be approximated by an effective equation of the form

$$dX_t = F(X_t)dt + b(X_t)dB_t, \tag{4.1.16}$$

where F and b can be expressed as averages with respect to the fast process y_t with X_t fixed [89, 91]. One of the interesting consequences of (4.1.16) is that if the dynamics of y_t is mixing[1], then the effective diffusion $b(x)$ may be non-zero even if y_t is deterministic, i.e., $\beta = 0$. For details and examples, see [37, 45, 51, 52, 82, 84, 91].

Many oscillatory dynamics are not mixing, even though for fixed x_t the fast dynamics is ergodic on a low-dimensional invariant manifold. In Section 4.3 we show that the method of formal asymptotic expansions gives the correct vanishing effective diffusion coefficient, i.e., the effective slow dynamics is deterministic. Furthermore, the method reproduces the correct effective drift.

4.1.3 Numerical methods

The above discussion on applying averaging kernels across different time scales motivates a numerical method which applies our previous two-scale HMM algorithms [5, 6] hierarchically to multiple (> 2) timescale systems. We consider the time scales $\mathcal{O}(\epsilon^2)$, $\mathcal{O}(\epsilon)$ and $\mathcal{O}(1)$ and assume that both the ϵ and ϵ^2 scales are oscillatory.

The HMM to be constructed should evaluate the effective rate of change of $x(t)$. For three-scale problems this requires averaging over the $\mathcal{O}(\epsilon^2)$ as well as the $\mathcal{O}(\epsilon)$ scale oscillations, thus obtaining a numerical approximation for the effective equation. See [7] for further details.

[1] Loosely speaking, mixing means that for any two possible states of y_t, the occurrence of the states is independent if a sufficient amount of time t is given. For the precise definition and properties see [102].

The hierarchical HMM structure is illustrated in Fig. 4.1. The downward pointing arrows depict the determination of an initial condition for a lower, fast scale from data in an upper tier working on a slower time scale. The upward pointing arrows from 2nd tier to 1st tier and 1st tier to 0th tier relate the evaluation of averages with respect to s_2 and s_1, respectively. Below we detail the equations solved in each tier.

Let η_i and h_i denote the range of integration and step size used in the i-th tier, respectively. A chosen ODE solver in the 2nd tier numerically approximates the full ODE at the initial time $t_{n,m} = nh_0 + mh_1$.

$$x_2' = \epsilon^{-1} f_1(x_2, \epsilon^{-1}t, \epsilon^{-2}t) + f_0(x_2, \epsilon^{-1}t, \epsilon^{-2}t), \quad x_2(t_{n,m}) = X_1,$$

in a time segment $t \in [t_{n,m}-\eta_2, t_{n,m}+\eta_2]$ where $X_1(t_{n,m}; X_0(t_n))$ is an approximation of $x(t)$ at $t_{n,m}$ obtained from the 1st tier. Denote the solution by $x_2(t; X_1)$ and let

$$\mathcal{F}_1(t_{n,m}; X_1) = K_{\eta_2} * \left(\epsilon^{-1} f_1(x_2(\cdot; X_1), \epsilon^{-1}\cdot, \epsilon^{-2}\cdot) + f_0(x_2(\cdot; X_1), \epsilon^{-1}\cdot, \epsilon^{-2}\cdot)\right).$$

The 1st tier numerically approximates the effective ODE for the $\mathcal{O}(\epsilon)$ scale

$$x_1' = \mathcal{F}_1(t; X_1), \quad x_1(t_n) = X_0.$$

in the time interval $t \in [t_n - \eta_1, t_n + \eta_1]$ where $X_0(t_n)$ is an approximation of $x(t)$ at $t_n = nh_0$ obtained from the 0th tier. Denote the solution $x_1(t; X_0)$ and let

$$\mathcal{F}_0(t_n; X_0) = K_{\eta_1} * \mathcal{F}_1(\cdot).$$

Finally, the 0th tier numerically approximates the effective ODE for the $\mathcal{O}(1)$ scale

$$x' = \mathcal{F}_0(x), \quad x(0) = x_0$$

in $t \in [0, \eta_0] = [0, T]$.

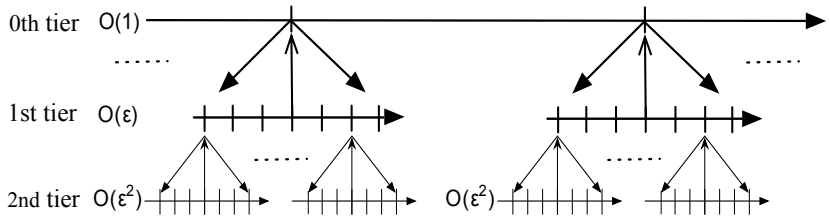

Figure 4.1: An illustration of a three scale algorithm.

4.1.4 Generalizing from (4.1.6) to (4.1.5)

In the following, we explain heuristically why the numerical method described above, which was motivated by the simple model (4.1.6) may be applied to a more general case (4.1.5) in which the fast and intermediate dynamics is periodic. Further generalizations to quasi and almost periodic systems are discussed in Section 4.5. As an analogy to the action-angle coordinates for mechanical systems, z and y can be considered as periodic angle-like coordinates with periods of order ϵ^2 and ϵ, respectively. In other words, we explicitly assume that $z(t)$ consists of a fast $\mathcal{O}(\epsilon^2)$ oscillation which is super-imposed on a slower $\mathcal{O}(\epsilon)$ oscillation and a slow $\mathcal{O}(1)$ drift. Similarly, $y(t)$ is an intermediate $\mathcal{O}(\epsilon)$ oscillation which is super-imposed on a $\mathcal{O}(1)$ drift. More precisely, recall the equation for z in (4.1.5),

$$z' = \epsilon^{-2}\tilde{h}_2(x, y, z).$$

On an $\mathcal{O}(\epsilon^2)$ time interval both x and y are, to leading order in ϵ, constant. Hence, $z(t)$ is oscillatory and satisfies an ODE of the form

$$z' = \epsilon^{-2}\tilde{h}_2(x(t_0), y(t_0), z) + \epsilon^{-1}\tilde{h}_1(x(t_0), y(t_0), z) + \mathcal{O}(1).$$

This implies that the solution, $z(t)$, can be generally written as

$$z(t) = \tilde{z}(t, \epsilon^{-1}t, \epsilon^{-2}t), \tag{4.1.17}$$

where $\tilde{z}(s_0, s_1, s_2)$ is quasi-periodic in s_2. Similarly, recall the equation for y in (4.1.5),

$$y' = \epsilon^{-1}\tilde{g}_1(x, y, z) + \tilde{g}_0(x, y, z).$$

Substituting in (4.1.17) and using the $\mathcal{O}(\epsilon^2)$ periodicity of z, y can be approximated by an averaged equation on a time segment of length $\mathcal{O}(\epsilon)$. The averaged equation takes the form

$$\bar{y}' = \epsilon^{-1}\bar{g}_1(x, \bar{y}) + \bar{g}_0(x, \bar{y}).$$

Hence, the solution of $y(t)$ can be written as

$$y(t) = \tilde{y}_0(t, \epsilon^{-1}t) + \epsilon\tilde{y}_1(t, \epsilon^{-1}t, \epsilon^{-2}t) + \mathcal{O}(\epsilon^2), \tag{4.1.18}$$

where $\tilde{y}_0(s_0, s_1)$ is quasi-periodic in s_1, and $\tilde{y}_1(s_0, s_1, s_2)$ is quasi-periodic in s_2. Substituting (4.1.17) and (4.1.18) into the equation for x in (4.1.5) yields the simplified form (4.1.6).

Finally, we note that HMM only requires integration on reduced time segments. Specifically, computing an approximation of the effective equation for x only requires solving for y on time segments of length $\mathcal{O}(\epsilon)$. Similarly, computing an approximation of the effective equation for y only requires solving for z on time segments of length $\mathcal{O}(\epsilon^2)$. Thus (4.1.17) and (4.1.18) are consistent with the requirements of the iterated kernel, nested HMM scheme. Furthermore, the form in which the microscopic scales are given – either (4.1.5) or (4.1.6) is not important for the HMM scheme to yield a converging approximation of the the averaged equation for the slow variable x. The only requirement is that all integrators across all time

scales are stable. We conclude that the tiered HMM scheme can be applied to the full three-scale problem (4.1.5).

Further evidence on the applicability of the nested-HMM framework to the general (4.1.5) comes from Section 4.3 which considers formal asymptotic expansions applied directly to (4.1.5).

4.1.5 Layout

The layout of the paper is as follows. Section 4.2 details a proof of Theorem 4.1.1 using the tools of averaging theory. In Section 4.3, the same result is derived using formal asymptotic expansions to singular perturbations of SDEs in which the white noise is turned off. Even though this method does not constitute a rigorous proof, its scope applies to the general system given in singular perturbation form (4.1.5). Section 4.4 proves that the effective dynamics of (4.1.6) can be approximated using convolution with respect to averaging kernels which are applied iteratively to the different time scales. The methods can be used in a numerical HMM scheme as described above. The HMM scheme suggests that the basic idea of iterated averaging can be applied in more general settings. Such generalizations are discussed in Section 4.5. A few examples of such generalizations are presented in Section 4.6.

4.2 A theory of iterated averaging

In this section we prove Theorem 4.1.1 which generalizes an averaging theorem for long time scales due to van der Burgh [93, 100]. Further generalizations are discussed in Section 4.5.

4.2.1 Basic estimate

As before, let $x(t)$ solve

$$x' = \epsilon^{-1} f_1(x, \epsilon^{-1}t, \epsilon^{-2}t) + f_0(x, \epsilon^{-1}t, \epsilon^{-2}t), \quad x(0) = x_0, \tag{4.2.19}$$

where $f_1(x, s_1, s_2)$ and $f_0(x, s_1, s_2)$ are sufficiently smooth and 1-periodic in s_1 and s_2. It is further assumed that the solution $x(t)$ exists, is unique and remains bounded independent of ϵ for a time segment $[0, T]$ independent of ϵ. When $\langle f_1 \rangle_2 = 0$, then $x(t)$ can be approximated by a slow trajectory and then our goal is to derive an approximate ODE for such a trajectory. As usual, by slow we mean that the first derivative of a time-dependent function is bounded independent of ϵ.

We consider two functions $w(t)$ and $y(t)$. Let $w(t)$ solve

$$w' = h(w(t), \epsilon^{-1}t, \epsilon^{-2}t) + f_0(w(t), \epsilon^{-1}t, \epsilon^{-2}t), \quad w(0) = x_0, \tag{4.2.20}$$

where h is defined by

$$\begin{aligned} h(x, s_1, s_2) =& (\nabla_x f_1)\phi(x, s_1, s_2) - \frac{\partial \phi}{\partial s_1}(x, s_1, s_2), \\ \phi(x, s_1, s_2) =& \int_0^{s_2} f_1(x, s_1, \tau) d\tau. \end{aligned} \tag{4.2.21}$$

Note that for fixed x, $h(x, s_1, s_2)$ and $\phi(x, s_1, s_2)$ are 1-periodic in s_1 and s_2.

Notation. We use the notation $(\nabla_x f_1)\phi(x, s_1, s_2)$ for the multiplication of ϕ by the derivative of f_1 with respect to x and both are evaluated at (x, s_1, s_2).

Let $y(t)$ solve

$$y' = G(y, \epsilon^{-1}t), \quad y(0) = x_0, \tag{4.2.22}$$

where G is given by

$$G(y, s_1) = \langle h(y, s_1, s_2) \rangle_2 + \langle f_0(y, s_1, s_2) \rangle_2. \tag{4.2.23}$$

We will show that for $t \in [0, T]$, there exist nonnegative constants C_0 and C_1 independent of ϵ such that

$$|x(t) - w(t)| \leq C_0 \epsilon \quad \text{and} \quad |w(t) - y(t)| \leq C_1 \epsilon.$$

Thus, we conclude by the triangle inequality for $t \in [0, T]$ that

$$|x(t) - y(t)| \leq C\epsilon.$$

We denote a generic positive constant by C whose value may change between expressions but is independent of ϵ.

Lemma 4.2.1. The solutions $x(t)$ and $w(t)$ defined above satisfy

$$|x(t) - w(t)| \leq \epsilon C e^{(L_{f_0} + L_h)t}$$

for $t \in [0, T]$ and $T > 0$ which is independent of ϵ. L_{f_0} and L_h are Lipschitz constants for f_0 and h, respectively.

Proof. From (4.2.19) and (4.2.20), integrating with respect to time yields that

$$x(t) - x_0 = \int_0^t \epsilon^{-1} f_1(x(\tau), \epsilon^{-1}\tau, \epsilon^{-2}\tau) d\tau + \int_0^t f_0(x(\tau), \epsilon^{-1}\tau, \epsilon^{-2}\tau) d\tau,$$
$$w(t) - x_0 = \int_0^t h(w(\tau), \epsilon^{-1}\tau, \epsilon^{-2}\tau) d\tau + \int_0^t f_0(w(\tau), \epsilon^{-1}\tau, \epsilon^{-2}\tau) d\tau.$$

This leads to

$$|x(t) - w(t)| \leq \left| \int_0^t \epsilon^{-1} f_1(x(\tau), \epsilon^{-1}\tau, \epsilon^{-2}\tau) - h(w(\tau), \epsilon^{-1}\tau, \epsilon^{-2}\tau) d\tau \right| + L_{f_0} \int_0^t |x(\tau) - w(\tau)| d\tau. \tag{4.2.24}$$

where L_{f_0} is a Lipschitz constant for f_0. We will show that the first integral in (4.2.24) is bounded by

$$L_h \int_0^t |x(\tau) - w(\tau)| \, d\tau + \mathcal{O}(\epsilon)$$

where L_h is a Lipschitz constant for h. Then, we have

$$|x(t) - w(t)| \leq (L_{f_0} + L_h) \int_0^t |x(\tau) - w(\tau)| \, d\tau + \mathcal{O}(\epsilon).$$

It follows from Gronwall's inequality that

$$|x(t) - w(t)| \leq \epsilon C e^{(L_{f_0} + L_h)t}.$$

To this end, let n denote the largest integer such that $\epsilon^2 n \leqq t$. We first consider $\int_0^1 \epsilon^{-1} f_1 d\tau$.

$$\int_0^t \epsilon^{-1} f_1(x(\tau), \epsilon^{-1}\tau, \epsilon^{-2}\tau) d\tau = \sum_{j=0}^{n-1} \int_{\epsilon^2 j}^{\epsilon^2 (j+1)} \epsilon^{-1} f_1(x(\tau), \epsilon^{-1}\tau, \epsilon^{-2}\tau) d\tau + \int_{\epsilon^2 n}^t \epsilon^{-1} f_1(x(\tau), \epsilon^{-1}\tau, \epsilon^{-2}\tau) d\tau.$$

Since f_1 is bounded and $0 \leq t - n\epsilon^2 < \epsilon^2$, the last term is $\mathcal{O}(\epsilon)$. Denoting $t_j = \epsilon^2 j$ and using the periodicity of f_1 in s_2, each term in the sum can be written as

$$\epsilon \int_0^1 f_1(x(t_j + \epsilon^2 s), \epsilon^{-1} t_j + \epsilon s, s) ds. \tag{4.2.25}$$

By the fundamental theorem of calculus, we write

$$\begin{aligned} x(t_j+\epsilon^2 s) &= x(t_j) + \int_{t_j}^{t_j+\epsilon^2 s} x'(\tau)d\tau \\ &= x(t_j) + \int_{t_j}^{t_j+\epsilon^2 s} \left[\epsilon^{-1} f_1(x(\tau),\epsilon^{-1}\tau,\epsilon^{-2}\tau) + f_0(x(\tau),\epsilon^{-1}\tau,\epsilon^{-2}\tau)\right] d\tau \\ &= x(t_j) + \int_{t_j}^{t_j+\epsilon^2 s} \epsilon^{-1} f_1(x(\tau),\epsilon^{-1}\tau,\epsilon^{-2}\tau)d\tau + \mathcal{O}(\epsilon^2) \end{aligned} \tag{4.2.26}$$

since f_0 is bounded independent of ϵ. After the substitution of (4.2.26) into (4.2.25) and using a Taylor expansion of $f_1(x(t_j+\epsilon^2 s),\epsilon^{-1}t_j+\epsilon s, s_2)$ around $s=0$ while keeping s_2 fixed,

$$\begin{aligned} &\epsilon\int_0^1 f_1(x(t_j+\epsilon^2 s),\epsilon^{-1}t_j+\epsilon s,s)ds \\ &\qquad = \epsilon\int_0^1 \left\{ f_1(x(t_j),\epsilon^{-1}t_j,s) + \left(\int_{t_j}^{t_j+\epsilon^2 s} x'(\tau)d\tau\right)\nabla_x f_1(x(t_j),\epsilon^{-1}t_j,s) \right. \\ &\qquad\quad \left. + \epsilon s\frac{\partial f_1}{\partial s_1}(x(t_j),\epsilon^{-1}t_j,s)\right\} ds + \mathcal{O}(\epsilon^3) \\ &\qquad = \int_0^1 \left(\int_{t_j}^{t_j+\epsilon^2 s} f_1(x(\tau),\epsilon^{-1}\tau,\epsilon^{-2}\tau)d\tau\right)\nabla_x f_1(x(t_j),\epsilon^{-1}t_j,s)ds \\ &\qquad\quad + \int_0^1 \epsilon^2 s\frac{\partial f_1}{\partial s_1}(x(t_j),\epsilon^{-1}t_j,s)ds + \mathcal{O}(\epsilon^3). \end{aligned}$$

where we used the fact that $\langle f_1\rangle_2 = 0$. Hence, for $\epsilon^{-1}\int_0^t f_1 d\tau$,

$$\begin{aligned} &\epsilon^{-1}\int_0^t f_1(x(\tau),\epsilon^{-1}\tau,\epsilon^{-2}\tau)d\tau \\ &\qquad = \sum_{j=0}^{n-1}\left[\int_0^1 \left(\int_{t_j}^{t_j+\epsilon^2 s} f_1(x(\tau),\epsilon^{-1}\tau,\epsilon^{-2}\tau)d\tau\right)\nabla_x f_1(x(t_j),\epsilon^{-1}t_j,s)ds \right. \\ &\qquad\quad \left. + \int_0^1 \epsilon^2 s\frac{\partial f_1}{\partial s_1}(x(t_j),\epsilon^{-1}t_j,s)ds\right] + \mathcal{O}(\epsilon^1). \end{aligned} \tag{4.2.27}$$

Next, changing of variables to $s = \epsilon^{-2}\tau$ in $\int_0^t h d\tau$ gives

$$\begin{aligned}\int_0^t h(w(\tau), \epsilon^{-1}\tau, \epsilon^{-2}\tau)d\tau =& \sum_{j=0}^{n-1}\left[\int_{t_j}^{t_{j+1}}\left(\int_0^{\epsilon^{-2}\tau} f_1(w(\tau), \epsilon^{-1}\tau, v)dv\right)\nabla_x f_1(w(\tau), \epsilon^{-1}\tau, \epsilon^{-2}\tau)d\tau\right.\\ &\left.-\int_{t_j}^{t_{j+1}}\int_0^{\epsilon^{-2}\tau}\frac{\partial f_1}{\partial s_1}(w(\tau), \epsilon^{-1}\tau, \tilde{v})d\tilde{v}d\tau\right] + \mathcal{O}(\epsilon^2).\\ =& \sum_{j=0}^{n-1}\left[\int_j^{j+1}\epsilon^2\left(\int_j^s f_1(w(\epsilon^2 s), \epsilon s, v)dv\right)\nabla_x f_1(w(\epsilon^2 s), \epsilon s, s)ds\right.\\ &\left.-\int_j^{j+1}\epsilon^2\left(\int_0^s\frac{\partial f_1}{\partial s_1}(w(\epsilon^2 s), \epsilon s, \tilde{v})d\tilde{v}\right)ds\right] + \mathcal{O}(\epsilon^2).\end{aligned}$$

Changing variables back to $\tau = \epsilon^2 v$ in the first integral and $\tilde{v} = \tau$ in the second integral,

$$\begin{aligned}\int_0^t h(w(\tau), \epsilon^{-1}\tau, \epsilon^{-2}\tau)d\tau =& \sum_{j=0}^{n-1}\left[\int_j^{j+1}\left(\int_{t_j}^{\epsilon^2 s} f_1(w(\epsilon^2 s), \epsilon s, \epsilon^{-2}\tau)d\tau\right)\nabla_x f_1(w(\epsilon^2 s), \epsilon s, s)ds\right.\\ &\left.-\epsilon^2\int_j^{j+1}\int_0^s\frac{\partial f_1}{\partial s_1}(w(\epsilon^2 s), \epsilon s, \tau)d\tau ds\right] + \mathcal{O}(\epsilon^2).\end{aligned} \tag{4.2.28}$$

We need to compare (4.2.27) and (4.2.28). Note that $w'(t)$ is bounded independent of ϵ and that $\tau \in [j, j+1]$.

$$\begin{cases} w(\epsilon^2 s) = w(\tau) + \mathcal{O}(\epsilon^2 s - \tau) = w(\tau) + \mathcal{O}(\epsilon^2),\\ w(\epsilon^2 s) = w(\epsilon^2 j) + \mathcal{O}(\epsilon^2 s - \epsilon^2 j) = w(t_j) + \mathcal{O}(\epsilon^2)\end{cases} \tag{4.2.29}$$

and

$$\begin{cases}\epsilon s = \epsilon^{-1}\tau + \mathcal{O}(\epsilon),\\ \epsilon s = \epsilon^{-1}t_j + \mathcal{O}(\epsilon).\end{cases} \tag{4.2.30}$$

Therefore, the first integration in (4.2.28) can be written as

$$\begin{aligned}&\int_j^{j+1}\left(\int_{t_j}^{\epsilon^2 s} f_1(w(\tau), \epsilon^{-1}\tau, \epsilon^{-2}\tau)d\tau\right)\nabla_x f_1(w(t_j), \epsilon^{-1}t_j, s)ds + \mathcal{O}(\epsilon^3)\\ =&\int_0^1\left(\int_{t_j}^{t_j+\epsilon^2 s} f_1(w(\tau), \epsilon^{-1}\tau, \epsilon^{-2}\tau)d\tau\right)\nabla_x f_1(w(t_j), \epsilon^{-1}t_j, s)ds + \mathcal{O}(\epsilon^3)\end{aligned}$$

which has the same form of the first term in (4.2.27) with an $\mathcal{O}(\epsilon^3)$ error.

Now compare the second integrals. Applying integration by parts to the second term in (4.2.27) and $\langle \frac{\partial f_1}{\partial s_1} \rangle = 0$ give

$$\begin{aligned}
&\int_0^1 \epsilon^2 s \frac{\partial f_1}{\partial s_1}(x(t_j), \epsilon^{-1}t_j, s)ds \\
&\qquad = \left[\epsilon^2 s \int_0^s \frac{\partial f_1}{\partial s_1}(x(t_j), \epsilon^{-1}t_j, \tau)d\tau\right]_{s=0}^1 - \epsilon^2 \int_0^1 \int_0^s \frac{\partial f_1}{\partial s_1}(x(t_j), \epsilon^{-1}t_j, \tau)d\tau ds \\
&\qquad = -\epsilon^2 \int_0^1 \int_0^s \frac{\partial f_1}{\partial s_1}(x(t_j), \epsilon^{-1}t_j, \tau)d\tau ds
\end{aligned} \tag{4.2.31}$$

On the other hand, in (4.2.28) using (4.2.29) and (4.2.30),

$$\begin{aligned}
-\epsilon^2 \int_j^{j+1} \int_0^s \frac{\partial f_1}{\partial s_1}(w(\epsilon^2 s), \epsilon s, \tau)d\tau ds &= -\epsilon^2 \int_j^{j+1} \int_0^s \frac{\partial f_1}{\partial s_1}(w(t_j), \epsilon^{-1}t_j, \tau)d\tau ds + \mathcal{O}(\epsilon^3) \\
&= -\epsilon^2 \int_0^1 \int_0^s \frac{\partial f_1}{\partial s_1}(w(t_j), \epsilon^{-1}t_j, \tau)d\tau ds + \mathcal{O}(\epsilon^3)
\end{aligned} \tag{4.2.32}$$

Thus, it is shown that (4.2.31) and (4.2.32) are different up to an $\mathcal{O}(\epsilon^3)$ error. Putting all estimates together and noting $n = \mathcal{O}(\epsilon^{-2})$, we conclude that

$$\left| \int_0^t \epsilon^{-1} f_1(x(\tau), \epsilon^{-1}\tau, \epsilon^{-2}\tau) - h(w(\tau), \epsilon^{-1}\tau, \epsilon^{-2}\tau)d\tau \right| \leq L_h \int_0^t |x(\tau) - w(\tau)|\, d\tau + \mathcal{O}(\epsilon) \tag{4.2.33}$$

where L_h is a Lipschitz constant for the function h. Substituting (4.2.33) into (4.2.24) yields the desired estimate. □

The following lemma gives an estimate of how much $w(t)$ and $y(t)$ can be apart in $0 \leq t \leq T$.

Lemma 4.2.2. Let $w(t)$ and $y(t)$ be defined as above. Then, the following estimate holds

$$|w(t) - y(t)| \leq \epsilon C e^{L_G t}, \tag{4.2.34}$$

for some constant $C > 0$ which is independent of ϵ, where L_G is a Lipschitz constant for G.

Proof. Consider $w' - y'$. Using (4.2.20) and (4.2.22) we have,

$$\begin{aligned} w' - y' =& f_0(w, \epsilon^{-1}t, \epsilon^{-2}t) - \langle f_0 \rangle_2(y, \epsilon^{-1}t) + h(w, \epsilon^{-1}t, \epsilon^{-2}t) - \langle h \rangle_2(y, \epsilon^{-1}t) \\ =& [G(w, \epsilon^{-1}t) - G(y, \epsilon^{-1}t)] + z(w, \epsilon^{-1}t, \epsilon^{-2}t), \end{aligned}$$

where

$$\begin{aligned} G(w, s_1) =& \langle h(w, s_1, s_2) \rangle_2 + \langle f_0(w, s_1, s_2) \rangle_2, \\ z(w, s_1, s_2) =& [f_0(w, s_1, s_2) - \langle f_0 \rangle_2(w, s_1)] + [h(w, s_1, s_2) - \langle h \rangle_2(w, s_1)]. \end{aligned}$$

Note that for fixed w and s_1, $z(w, s_1, s_2)$ is 1-periodic in s_2 with a zero average, $\langle z \rangle_2 = 0$. Integrating to the time t yields that

$$w(t) - y(t) = \int_0^t [G(w(\tau), \epsilon^{-1}\tau) - G(y(\tau), \epsilon^{-1}\tau)] d\tau + r(t; \epsilon),$$

where $r(t; \epsilon) = \int_0^t z(w(\tau), \epsilon^{-1}\tau, \epsilon^{-2}\tau) d\tau$. Taking absolute values

$$|w(t) - y(t)| \leq \int_0^t \left| G(w(\tau), \epsilon^{-1}\tau) - G(y(\tau), \epsilon^{-1}\tau) \right| d\tau + |r(t; \epsilon)|.$$

Let L_G denote a Lipschitz constant for G. Then,

$$|w(t) - y(t)| \leq L_G \int_0^t |w(\tau) - y(\tau)| d\tau + |r(t; \epsilon)|. \tag{4.2.35}$$

In order to evaluate $r(t; \epsilon)$, let n denote the largest integer such that $\epsilon^2 n \leq t$. We have

$$r(t; \epsilon) = \sum_{j=0}^{n-1} \int_{\epsilon^2 j}^{\epsilon^2 (j+1)} z(w(\tau), \epsilon^{-1}\tau, \epsilon^{-2}\tau) d\tau + \int_{\epsilon^2 n}^{t} z(w(\tau), \epsilon^{-1}\tau, \epsilon^{-2}\tau) d\tau. \tag{4.2.36}$$

Since z is bounded and $0 \leqq t - n\epsilon^2 < \epsilon^2$, the last term is $\mathcal{O}(\epsilon^2)$. As in the proof of Lemma 4.2.1, denoting $t_j = \epsilon^2 j$ and using the periodicity of z in s, each term in the sum can be written as

$$\epsilon^2 \int_0^1 z(w(t_j + \epsilon^2 s), \epsilon^{-1} t_j + \epsilon s, s) ds.$$

Expanding in ϵ yields,

$$\epsilon^2 \int_0^1 z(w(t_j), \epsilon^{-1} t_j, s) ds = \epsilon^2 \left[\langle z \rangle_2 (w(t_j), \epsilon^{-1} t_j) + \mathcal{O}(\epsilon) \right] = \mathcal{O}(\epsilon^3).$$

Therefore,

$$r(t;\epsilon) = \mathcal{O}(n\epsilon^3) = \mathcal{O}(\epsilon). \tag{4.2.37}$$

Substituting into (4.2.35) yields

$$|w(t) - y(t)| \leq L_G \int_0^t |w(\tau) - y(\tau)| d\tau + \mathcal{O}(\epsilon).$$

Using Gronwall's inequality we conclude Lemma 4.2.2. □

4.2.2 Proof of Theorem 4.1.1

Lemma 4.2.1 and 4.2.2 imply that

$$\sup_{0 \leq t \leq T} |x(t) - y(t)| \leq \epsilon C, \tag{4.2.38}$$

where $y(t)$ is the solution of

$$y' = G(y, \epsilon^{-1} t), \quad y(0) = x_0,$$

with

$$\begin{aligned} G(y, s_1) &= \langle h(y, s_1, s_2) \rangle_2 + \langle f_0(y, s_1, s_2) \rangle_2, \\ h(y, s_1, s_2) &= (\nabla_x f_1)\phi - \frac{\partial \phi}{\partial s_1}, \\ \phi(y, s_1, s_2) &= \int_0^{s_2} f_1(y, s_1, \tau) d\tau. \end{aligned} \tag{4.2.39}$$

Since the RHS of $G(y, s_1)$ is periodic in s_1, we are in a position to apply the two-scale averaging theorem [93], integrating out the intermediate $\mathcal{O}(\epsilon)$ time scale. Noting that since ϕ is 1-periodic in s_1, $\partial\phi/\partial s_1$ is also periodic and has zero average with respect to s_1. This leads to an averaged equation for $y(t)$:

$$\xi' = F(\xi), \quad \xi(0) = x_0, \tag{4.2.40}$$

where

$$F(\xi) = \langle (\nabla_x f_1)\phi(\xi, s_1, s_2)\rangle_{12} + \langle f_0(\xi, s_1, s_2)\rangle_{12}$$

and we have

$$\sup_{0\le t\le T} |y(t) - \xi(t)| \le \epsilon C. \tag{4.2.41}$$

Combining (4.2.38) with (4.2.41) completes the proof of Theorem 4.1.1.

Remark 4.2.1. It is not difficult to generalize this result to systems with non-commensurate and widely separated frequencies.

4.3 Formal asymptotic expansions

In this section we analyze the multiscale structure of a system using the operator formalism firstly developed by Papanicolaou et al. as a formal asymptotic expansion for singular perturbations of SDEs [19, 89]. This approach has been further generalized and applied to many different problems, for example, in [82, 91, 101]. For the case of Hamiltonian dynamics, including integrable periodic systems, a rigorous version of formalism is presented in [43, 44] and references therein. The derivation in this section is formal; nonetheless, it is instructive and provides intuitive explanation for Theorem 4.1.1.

4.3.1 Stochastic differential equations

For completeness, we begin by reviewing singular perturbation expansions of SDEs. The resulting effective equations are then considered in the case in which all diffusion coefficients are formally set to zero.

Consider SDE systems of the form

$$\begin{cases} dx_t = \left[\epsilon^{-1} f_1(x_t, y_t) + f_0(x_t, y_t)\right] dt, \\ dy_t = \epsilon^{-2} a(x_t, y_t) dt + \epsilon^{-1} \beta(x_t, y_t) dB_t, \end{cases} \tag{4.3.42}$$

where $x_t \in \mathbb{R}^d$ is a slow process that evolves according to an ODE with a fast random coefficient $y_t \in \mathbb{R}^n$. We assumed that $\beta(x,y)\beta^T(x,y)$ is uniformly positive definite in $\mathbb{R}^d \times \mathbb{R}^n$. Furthermore, we assume that for fixed x_t the dynamics of y_t is ergodic on an invariant set Σ_x with a unique invariant measure $d\mu_x$. The expectations with respect to the invariant measures are denoted $\langle \cdot \rangle_y$, in which the x dependence is suppressed. A necessary condition for x to be slow is that $\langle f_1 \rangle_y = 0$. Otherwise, x exhibits non-trivial dynamics on the $\mathcal{O}(\epsilon)$ time scale. It is well known that under some suitable conditions on (4.3.42), $x(t)$ satisfies an effective SDE that is independent of ϵ,

$$dX_t = F(X_t)dt + b(X_t)dB_t, \tag{4.3.43}$$

where F and b can be expressed as averages with respect to the fast process $y(t)$ with X fixed [19, 89, 91, 101]. We begin with a brief overview of the relevant results of [89]. For details the reader is referred to [91] and references therein.

The backwards equation that governs the evolution of a probability density, ϕ, of the initial conditions

$$\begin{cases} \partial_t u = \mathcal{L} u, \\ u(0, x, y) = \varphi(x, y), \end{cases}$$

where $\mathcal{L}$, the generator of (4.3.42) can be written as

$$\begin{aligned}
\mathcal{L} &= \epsilon^{-2}\mathcal{L}_2 + \epsilon^{-1}\mathcal{L}_1 + \mathcal{L}_0, \\
\mathcal{L}_0 &= f_0 \cdot \nabla_x, \\
\mathcal{L}_1 &= f_1 \cdot \nabla_x, \\
\mathcal{L}_2 &= a \cdot \nabla_y + \frac{1}{2}\beta\beta^T : \nabla_y \nabla_y^T,
\end{aligned} \tag{4.3.44}$$

where $A : B$ denotes formally the trace of the matrix AB^T. Next, consider a formal asymptotic expansion of u in ϵ

$$u(t, x, y) = u_0(x) + \epsilon u_1 + \epsilon^2 u_2 + \dots,$$

where we assumed that the leading order term u_0 only depends on the slow process. Substituting into the backwards equation yields

$$\mathcal{L}_2 u_0 = 0, \tag{4.3.45}$$

$$\mathcal{L}_2 u_1 = -\mathcal{L}_1 u_0, \tag{4.3.46}$$

$$\mathcal{L}_2 u_2 = \partial_t u_0 - \mathcal{L}_1 u_1 - \mathcal{L}_0 u_0. \tag{4.3.47}$$

The leading order equation (4.3.45) is automatically satisfied since u_0 only depends on x. Let $\mathcal{L}_2^*$ be the L^2 adjoint of $\mathcal{L}_2$, and assume that the Null space of $\mathcal{L}_2^*$ is a one dimensional subspace, spanned ρ_x, the density of the invariant measure $d\mu_x$. [2] Applying the Fredholm alternative, equation (4.3.46) has a solution if $f_1 \nabla_x u_0$ is perpendicular to the Null space of $\mathcal{L}_2^*$. In other words, the projection of $f_1 \nabla_x u_0$ on Null $\mathcal{L}_2^*$ should vanish. This projection amounts to averaging with respect to the

[2] The assumptions holds for the case of ergodic rotations on a torus in which we are interested

invariant measure of y (at fixed x), which is also equivalent to taking the standard L_2 inner product in Σ_x with ρ. This yields the condition

$$\langle f_1(x,y)\rangle_y = 0,$$

which implies the reasonable requirement that the average of f_1 vanishes. Otherwise, x oscillates with large amplitudes on the ϵ time scale and thus cannot be approximated by a slow variable. Then, (4.3.46) has a unique solution such that $\langle u_1\rangle_y = 0$. We formally write

$$u_1 = -\mathcal{L}_2^{-1}[\mathcal{L}_1 u_0].$$

Applying again the Fredholm alternative, equation (4.3.47) also has a solution if the RHS is perpendicular to the Null space of L_2^*, i.e.

$$\langle \partial_t u_0 - \mathcal{L}_1 u_1 - \mathcal{L}_0 u_0\rangle_y = 0$$

Substituting in $\mathcal{L}_0$, $\mathcal{L}_1$ and u_1 we obtain

$$\partial_t u_0 = F(x)\nabla_x u_0 + B(x) : \nabla_x \nabla_x u_0, \tag{4.3.48}$$

where

$$\begin{aligned} F(x) &= \langle -f_1 \cdot \nabla_x \mathcal{L}_2^{-1}[f_1] + f_0\rangle_y, \\ B(x) &= \langle -f_1 \mathcal{L}_2^{-1}[f_1]\rangle_y. \end{aligned} \tag{4.3.49}$$

We identify (4.3.48) as the backwards equation associated with the effective SDE (4.3.43) and $2B(x) = b(x)b(x)^T$.

If $\beta\beta^T$ is uniformly positive, then inverting $\mathcal{L}_2$ amounts to solving a uniformly elliptic cell problem

$$[a \cdot \nabla_y + \frac{1}{2}\beta\beta^T : \nabla_y \nabla_y] r(x,y) = f_1(x,y), \tag{4.3.50}$$

with appropriate boundary conditions, e.g., periodic on a torus. The equation indeed has a unique solution. See [91] for further details.

4.3.2 Periodic ODEs

We now formally set $\beta = 0$ and consider a case in which for fixed x the dynamics of y is periodic. Hence, we can think of y as an fast oscillator. Assume that $a(x, y)$ is uniformly positive in $\mathbb{R}^d \times \mathbb{R}^n$, $\inf_{x\in\mathbb{R}^d, y\in\mathbb{R}^n} |a(x, y)| > 0$. Loosely speaking, this means that the system remains highly oscillatory at all times. Therefore, for fixed x trajectories are closed loops and the invariant set Σ_x is a one-dimensional manifold in $\mathbb{R}^d$ that depends on the initial y and on x. The invariant measure $d\mu_x$, which is supported on Σ_x is absolutely continuous with respect to the Lebesgue measure on Σ_x. The ergodic assumption holds with respect to the same manifold and measure. A rigorous treatment of this problem is beyond the scope of this manuscripts. For two-scale systems the reader is referred to [43, 44] and references therein.

Instead, we continue formally trying to identify the effective equation for x_t. The main difference between the periodic and the stochastic cases can be seen from two complementary points of view. First, as a dynamical system, the fast process in the SDE (4.3.42) is mixing (for fixed x). This is no longer the case with periodic systems which are ergodic but not mixing. Second, as a homogenization problem, since $\beta\beta^T = 0$ the cell problem (4.3.50) is no longer elliptic.

For fixed x, consider the periodic solution of

$$\frac{d\zeta}{dt} = a(x, \zeta(t)),$$

with a suitable initial condition on Σ_x. The period is denoted τ_x. $\zeta(t)$ transverses the exact periodic trajectory of $y(t)$ and with the correct invariant measure. Therefore, averages with respect to $d\mu_x$ can be written as the time average over a single period of ζ

$$\langle h(x,y)\rangle_y = \frac{1}{\tau_x}\int_0^{\tau_x} h(x,\zeta(t))dt = \frac{1}{\tau_x}\int_{\Sigma_x} h(x,\zeta(t))\frac{1}{a(x,\zeta(t))}d\zeta.$$

Furthermore, recall the hierarchy of operators (4.3.44). Substituting $\beta = 0$, $\mathcal{L}_2$ takes the form

$$\mathcal{L}_2 = a(x,y)\cdot\nabla_y.$$

We note that, for any $y \in \Sigma_x$, $\mathcal{L}_2$ is the directional derivative of ζ along the tangent direction to Σ_x and that $|\mathcal{L}_2\zeta|$ is inversely proportional to the density of $d\mu_x$

$$\mathcal{L}_2 h(x,y) = a(x,y)\cdot\nabla_y h(x,y) = \frac{d}{dt}h(x,\zeta(t))\bigg|_{\zeta(t)=y}.$$

This implies that the inverse of $\mathcal{L}_2$ can be described in terms of integration with respect to time along the trajectory of $\zeta(t)$

$$H(x,y) = \mathcal{L}_2^{-1}h(x,y) = \int_0^{t(y)} h(x,\zeta(s))ds + C(x),$$

where $t(y)$ is the unique time in which $\zeta(t) = y$ within one period of ζ. Following the Fredholm alternative, we pick the unique inverse that is perpendicular to Null $\mathcal{L}_2^*$, i.e., we require

$$\langle H(x,y)\rangle_y = \frac{1}{\tau_x}\int_0^{\tau_x} H(x,\zeta(t))dt = 0.$$

This fixes the constant

$$C(x) = -\frac{1}{\tau_x}\int_0^{\tau_x}\int_0^t H(x,\zeta(s))dsdt.$$

In particular, we recognize that $\mathcal{L}_2^{-1}[f_1] = \phi$ as given by

$$\phi(x,y) = \int_0^y f_1(x,\tau)d\tau - \langle \int_0^y f_1(x,\tau)d\tau \rangle_y \tag{4.3.51}$$

so that $\langle \phi \rangle_y = 0$. Substituting into (4.3.49) yields

$$\begin{aligned} F(x) &= \langle -f_1 \cdot \nabla_x \phi + f_0 \rangle_y, \\ B(x) &= \langle -f_1 \phi \rangle_y. \end{aligned} \tag{4.3.52}$$

In order to identify (4.3.52) with the averaged equation (4.2.40), we need a simple Lemma.

Lemma 4.3.1. Let $h(s)$ denote an S-periodic function with zero average and let $H(s)$ be an anti-derivative of h, $H' = h$. Then,

$$\int_0^S h(s)H(s)ds = 0. \tag{4.3.53}$$

Proof. First, we note that since $h(s)$ has zero average, $\int_0^S h(\tau)d\tau = 0$, its anti-derivative is also S-periodic

$$H(S+s) = H(0) + \int_0^{S+s} h(\tau)d\tau = H(s).$$

Then, using integration by parts

$$\int_0^S h(s)H(s)ds = \left[H^2(s)\right]_0^S - \int_0^S H(s)h(s)ds.$$

The first term on the right vanishes, which proves (4.3.53). □

Since ϕ is the anti-derivative of f_1, an immediate consequence is that $B(x) = -\langle f_1(x,y)\phi(x,y)\rangle_y = 0$. Hence, the effective dynamics of x_t is deterministic. More precisely, the variance of the stochastic perturbation is of order ϵ. Furthermore,

$$0 = \nabla_x \langle f_1(x,y)\phi(x,y)\rangle_y = \langle \nabla_x f_1(x,y)\phi(x,y)\rangle_y + \langle f_1(x,y)\nabla_x \phi(x,y)\rangle_y.$$

We conclude that the effective drift and diffusion coefficient can be written as

$$\begin{aligned} F(x) &= \langle (\nabla_x f_1)\phi + f_0 \rangle_y, \\ B(x) &= 0. \end{aligned} \tag{4.3.54}$$

Thus, we obtain the consistent form of the effective drift as proven by Theorem 4.1.1. Note that since the fast process in (4.3.42) contains only $\mathcal{O}(\epsilon^2)$ time scale, $\frac{\partial \phi}{\partial s_1} = 0$ in (4.2.39).

4.4 Iterated averaging with multiple kernels

The goal of this section is to generalize the framework of averaging kernels studied in [3, 5, 6, 42] to include three or more time scales. In particular, we prove that averaging of three scale oscillatory problems can be approximated via convolution with respect to kernels with known support, differentiability properties and moments. Let $\mathbb{K}^{p,q}$ denote the space of normalized C^q functions, supported on $[-1, 1]$ that have p vanishing moments, i.e.,

$$\int_{[-1,1]} K(t) t^r dt = \begin{cases} 1, & r = 0, \\ 0, & 1 \leq r \leq p. \end{cases} \tag{4.4.55}$$

Recall that for $\eta > 0$, $K_\eta(t)$ denotes a rescaling of K as $K_\eta(t) = \eta^{-1} K(\eta^{-1} t)$.

We will have an error estimate for approximating the double average $\langle f \rangle_{12}$ with two convolutions $K_{\eta_1} * [K_{\eta_2} * f]$. Applied to the RHS of (4.1.6), the convolution approximates $F(\xi)$ of Theorem 4.1.1. The proposition below establishes the accuracy of iterated averaging with multiple kernels under the scaling condition $\epsilon^2 \ll \eta_2 \ll \epsilon \ll \eta_1 \ll 1$.

Proposition 4.4.1. Let $K \in \mathbb{K}^{p,q}$ and $f_0, f_1 \in C^{\max\{q,p+1\}}$. Then, for $K \in \mathbb{K}^{p,q}$, there exists a constant $C > 0$ such that

$$\left|K_{\eta_1} * \{K_{\eta_2} * \left(\epsilon^{-1} f_1 + f_0\right)(\cdot)\}(t) - F(\xi(t))\right| \leq C \left(\frac{\epsilon^{2q-1}}{\eta_2^q} + \frac{\epsilon^q}{\eta_1^q} + \frac{\eta_2^{p+1}}{\epsilon^{p+2}} + \eta_1^{p+1} \right) \max_{j=0\ldots q} ||K^{(j)}||_1 \tag{4.4.56}$$

for some constant $C > 0$, where F is given by (4.2.39) as in *Theorem* 4.1.1, $K^{(j)}(\cdot)$ denotes the j-th derivative of K and $||\cdot||_1$ is the L_1 norm.

Throughout, C denotes a generic positive constant whose value may change between expressions.

4.4.1 Estimation of the effective force

Let $f : \mathbb{R}^{n+1} \to \mathbb{R}$ denote a scalar function of the vector argument $(x, s_1, s_2, \cdots, s_n)$ and 1-periodic in $s_1, \cdots, s_n$. To be consistent with previous notation, averaging with respect to s_k is respectively denoted by

$$\langle f \rangle_k = \int_0^1 f(x, \cdots, s_k, \cdots) ds_k, \quad k = 1, 2, \cdots, n. \tag{4.4.57}$$

Motivated by the averaging techniques in [3], we approximate $\langle f \rangle_n$ using a kernel. First let us prove the following lemma.

Lemma 4.4.2. If $f(t, s_1, s_2, \cdots, s_n) = a(t, s_1, s_2, \cdots, s_{n-1}) b(s_n)$, where $n \in \mathbb{N}$, $b(s_n + 1) = b(s_n)$, $\int_0^1 b(s_n) ds_n = 0$, $a \in C^q(\mathbb{R}^n)$ and $\max\limits_{0 \leq j \leq q} ||a^{(j)}||_\infty \leq M$, then for any $K \in \mathbb{K}^{p,q}$ and $\eta = \mathcal{O}(\epsilon^k)$, $k > n - 1$,

$$\left|K_\eta * f(\cdot, \epsilon^{-1}\cdot, \epsilon^{-2}\cdot, \cdots, \epsilon^{-n}\cdot)\right| \leq CM \left(\frac{\epsilon^n}{\eta}\right)^q \max_{j=0\ldots q} ||K^{(j)}||_1.$$

Proof. Let $\tilde{K}_\eta(x,y) = K_\eta(x-y)a(y,\epsilon^{-1}y,\epsilon^{-2}y,\cdots,\epsilon^{-n+1}y)$.

$$|K_\eta * f| = \left| \int \tilde{K}_\eta(t,s) b(\epsilon^{-n}s) ds \right| \leq \epsilon^{nq} \int \left| \partial_y^q \tilde{K}_\eta(t,s) b^{[q]}(\epsilon^{-n}s) \right| ds$$

where $b^{[j]}(t) = \int_0^t b^{[j-1]}(s)ds - \int_0^1 \int_0^t b^{[j-1]}(s)dsdt$ and $||b^{[j]}(t)||_\infty \leq ||b||_\infty$. For the kernel part,

$$\begin{aligned}
\int \left| \partial_y^q \tilde{K}_\eta(t,s) \right| ds = \int \Bigg| & \sum_{k_1+k_2+\cdots+k_{n+1}=q} \begin{pmatrix} q \\ k_1, k_2, \cdots, k_{n+1} \end{pmatrix} \\
& \cdot (-\eta^{-1})^{k_1} \cdot K_\eta^{(k_1)}(t-s) \cdot \prod_{i=1}^{n} \frac{1}{\epsilon^{k_{i+1}(i-1)}} \partial_i^{k_{i+1}} a(s, \epsilon^{-1}s, \epsilon^{-2}s, \cdots, \epsilon^{-n+1}s) \Bigg| ds \\
\leq & \frac{C}{\eta^q} \max_{j=0\ldots q} ||a^{(j)}||_\infty \max_{j=0\ldots q} ||K^{(j)}||_1
\end{aligned}$$

where $\begin{pmatrix} q \\ k_1, k_2, \cdots, k_{n+1} \end{pmatrix}$ is the multinomial coefficient and defined by $\frac{q!}{k_1!k_2!\cdots k_{n+1}!}$.

□

Lemma 4.4.3. For $r = (r_1, r_2, \cdots, r_n) \in \mathbb{Z}_+^n$ an ordered n-tuple of nonnegative integers, assume $\partial^r f(t, s_1, \cdots, s_n)$ is continuous and bounded by C_f for $r = 0, \cdots, \sigma$, and $\sigma \geq 1$. [3] Then, for any $K \in \mathbb{K}^{p,q}$ and $\eta = \mathcal{O}(\epsilon^k)$ with $k > n-1$, there exists $C > 0$ such that

$$\left| K_\eta * (f(\cdot, \epsilon^{-1}\cdot, \epsilon^{-2}\cdot, \cdots, \epsilon^{-n}\cdot) - \langle f \rangle_n) \right| \leq C \left(\frac{\epsilon^{nq}}{\eta^q} + \frac{\eta^\sigma}{\epsilon^{(n-1)\sigma}} \right) \max_{j=0\ldots q} ||K^{(j)}||_1. \tag{4.4.58}$$

Proof. Let

$$g(t, s_1, s_2, \cdots, s_n) = f(t, s_1, s_2, \cdots, s_n) - \langle f \rangle_n .$$

[3] $|r| = r_1 + r_2 + \cdots + r_n$ and $\partial^r = (\partial_{x_1})^{r_1}(\partial_{x_2})^{r_2} \cdots (\partial_{x_n})^{r_n}$.

g is 1-periodic with respect to s_i and $\partial^r g(t, s_1, s_2, \cdots, s_n)$ are continuous and bounded for $r \in \mathbb{Z}_+^n,\ |r| = 0, \cdots, \sigma$. In considering

$$K_\eta * g = \int_{t-\eta}^{t+\eta} K_\eta(t - s_n) \cdot g(s_n, \epsilon^{-1}s_n, \epsilon^{-2}s_n, \cdots, \epsilon^{-n}s_n) ds_n,$$

we expand $g(s_n, \epsilon^{-1}s_n, \epsilon^{-2}s_n, \cdots, \epsilon^{-(n-1)}s_n, t)$ around $s_n = 0$ while keeping t fixed. We denote $\partial_{x_i} g$ by the partial derivative with respect to the i-th component of g respectively.

$$\begin{aligned} g(s_n, \epsilon^{-1}s_n, \epsilon^{-2}s_n, \cdots, \epsilon^{-n}s_n) =& \sum_{j=0}^{\sigma-1} \frac{1}{j!} \left[\sum_{i=1}^{n} \frac{s_n}{\epsilon^{i-1}} \partial_{x_i} \right]^j g(0, \cdots, 0, \epsilon^{-n}s_n) \\ &+ \frac{1}{\sigma!} \left[\sum_{i=1}^{n} \frac{s_n}{\epsilon^{i-1}} \partial_{x_i} \right]^\sigma g(\mu_1, \epsilon^{-1}\mu_2, \cdots, \epsilon^{-n+1}\mu_n, \epsilon^{-n}s_n) \end{aligned}$$

where $(\mu_1, \mu_2, \cdots, \mu_n)$ is in the open line segment joining $\vec{0}$ and $(s_n, \epsilon^{-1}s_n, \cdots, \epsilon^{-n+1}s_n)$ in $\mathbb{R}^n$. The key idea consists of in writing the expansion as a sum of two parts. Without loss of generality, we set $t = 0$ and write $K_\eta * g$ as $I_1 + I_2$ where

$$\begin{aligned} I_1 &= \sum_{j=0}^{\sigma-1} \int_{-\eta}^{\eta} K_\eta(-s_n) \cdot \frac{1}{j!} \left[\sum_{i=1}^{n} \frac{s_n}{\epsilon^{i-1}} \partial_{x_i} \right]^j g(0, \cdots, 0, \epsilon^{-n}s_n) ds_n, \\ I_2 &= \int_{-\eta}^{\eta} K_\eta(-s_n) \cdot \frac{1}{\sigma!} \left[\sum_{i=1}^{n} \frac{s_n}{\epsilon^{i-1}} \partial_{x_i} \right]^\sigma g(\mu_1, \epsilon^{-1}\mu_2, \cdots, \epsilon^{-n+1}\mu_n, \epsilon^{-n}s_n) ds_n. \end{aligned}$$

By using Lemma 4.4.2, I_1 is estimated by

$$|I_1| \leq C(\frac{\epsilon^n}{\eta})^q \cdot \max_{j=0\cdots q} ||K^{(j)}||_1 \cdot \sum_{j=0}^{\sigma-1} \frac{1}{j!} [\sum_{i=1}^{n} \frac{\eta}{\epsilon^{i-1}}]^j.$$

Finding the leading order term in the summation, I_2 is estimated by

$$|I_2| \leq C(\frac{\eta}{\epsilon^{n-1}})^\sigma \sup_{t, s_1, s_2, \cdots, s_n} \sup_{|r| = \sigma} |\partial^r f(t, s_1, \cdots, s_n)| \cdot ||K||_1$$

Putting these estimates together, we find that there exists a positive constant C such that

$$|K_\eta * g| \leq C\left(\frac{\epsilon^{nq}}{\eta^q} + \frac{\eta^\sigma}{\epsilon^{(n-1)\sigma}}\right) \max_{j=0\ldots q} ||K^{(j)}||_1.$$

□

We now compare iterated averaging of (4.1.6) with the averaged equation (4.1.9). Before we move on to the next step, we simplify our notation of the forces by writing $f(t, \epsilon^{-1}t, \epsilon^{-2}t)$ instead of $f(x(t), \epsilon^{-1}t, \epsilon^{-2}t)$. This is possible since, after solving (4.1.6) at the 1st tier, $x(t)$ is known up to a prescribed accuracy Δ. Theorem 4.4.1 shows that the error between x and x_1 (solution of the 1st tier) is $\mathcal{O}(\Delta)$.

Theorem 4.4.1. Let $x_1(t)$ denote an approximation of $x(t)$ in the 1st tier using a two-scale HMM in the time interval $t \in [t_n - \eta_1, t_n + \eta_1]$. Given $0 < \epsilon < \epsilon_0$ and a prescribed accuracy Δ, there exists $C > 0$ such that

$$\sup_{t\in[t_n-\eta_1,t_n+\eta_1]} |x(t) - x_1(t)| \leq C\Delta. \tag{4.4.59}$$

Proof. By considering 1st and 2nd tiers as the two-scale HMM solver, we generalize the error analysis discussed in [5, 42]. We denote the order of accuracy, step size and length of integration in i-th tier by m_i, h_i and η_i respectively.

At the 1st tier, the global accuracy of integrating the original ODE (4.1.6) to time $\eta_1 (\ll \epsilon)$ is given by

$$C \max\left\{\frac{\eta_1 h_1^{m_1}}{\epsilon^{m_1}}, \frac{\eta_1\eta_2 h_2^{m_2}}{h_1\epsilon^{2m_2+1}}, \frac{\eta_1\epsilon^{2q}}{h_1\eta_2^{q+1}}\right\}$$

for some $C > 0$. The errors from each evaluation at the 2nd tier accumulate by taking $h_1^{-1}\eta_1$ steps. Thus we can balance the required accuracy Δ with different sources of errors. Note that the maximal possible accuracy is $\Delta = \epsilon^2$ since this error is introduced by simulating the averaged equation instead of the original equation.

□

Next, by iterated use of Lemma 4.4.3, we show that $\langle f(t, s_1, s_2)\rangle_{12}$ is well approximated by $K_{\eta_1} * [K_{\eta_2} * f](t)$.

Lemma 4.4.4. Let $f_0(t, s_1, s_2)$ be 1-periodic in s_1 and s_2. For $r = (r_1, r_2) \in \mathbb{Z}_+^2$, assume that $\partial^r f_0(t, s_1, s_2)$ is continuous and bounded for $|r| = 0, \cdots, \sigma$, and $\sigma \geq 1$. Then, for any $K \in \mathbb{K}^{p,q}$ and suitable choice of $\eta_1,\ \eta_2$ such that $\epsilon^2 \ll \eta_2 \ll \epsilon \ll \eta_1 \ll 1$, there exists a constant $C > 0$ such that

$$\left|K_{\eta_1} * \left[K_{\eta_2} * \left(f_0(\cdot, \epsilon^{-1}\cdot, \epsilon^{-2}\cdot) - \langle f_0(t, s_1, s_2)\rangle_{12}\right)(\cdot)\right](t)\right| \leq C\left(\frac{\epsilon^{2q}}{\eta_2^q} + \frac{\epsilon^q}{\eta_1^q} + \frac{\eta_2^\sigma}{\epsilon^\sigma} + \eta_1^\sigma\right) \max_{j=0\ldots q} ||K^{(j)}||_1.$$

Proof. Let

$$g(t, s_1, s_2) = f_0(t, s_1, s_2) - \langle f_0\rangle_{12}(t). \tag{4.4.60}$$

Note that $\langle g\rangle_{12} = \int_0^1 \int_0^1 (f_0(t, s_1, s_2) - \langle f_0\rangle_{12})\, ds_2 ds_1 = 0$ and that $g(x, s_1, s_2)$ is 1-periodic with respect to $s_1,\ s_2$ and $\partial^r g(x, s_1, s_2)$ is continuous and bounded for $r \in \mathbb{Z}_+^2,\ |r| = 0, \cdots, \sigma$. Iterated convolution with two kernels yields

$$K_{\eta_1} * \left[\left(K_{\eta_2} * g(\cdot, \epsilon^{-1}\cdot, \epsilon^{-2}\cdot)\right)(\cdot)\right](t) = \int_{t-\eta_1}^{t+\eta_1} K_{\eta_1}(t - s_1) \underbrace{\left[\int_{s_1-\eta_2}^{s_1+\eta_2} K_{\eta_2}(s_1 - s_2) \cdot g(s_2, \epsilon^{-1}s_2, \epsilon^{-2}s_2) ds_2\right]}_{=I_1(s_1)} ds_1.$$

We iterate the argument in Lemma 4.4.3. First, there exists $C > 0$ such that

$$\left|I_1(s_1) - \langle g\rangle_2(s_1, \epsilon^{-1}s_1)\right| \leq C\left(\frac{\epsilon^{2q}}{\eta_2^q} + \frac{\eta_2^\sigma}{\epsilon^\sigma}\right)\max_{j=0\ldots q}||K^{(j)}||_1. \tag{4.4.61}$$

Recalling that $\langle g\rangle_{12} = 0$,

$$I_1 = I_1 - \langle g\rangle_2(s_1, \epsilon^{-1}s_1) + \langle g\rangle_2(s_1, \epsilon^{-1}s_1) - \langle g\rangle_{12}. \tag{4.4.62}$$

Thus

$$\begin{aligned}
&\left|\int_{t-\eta_1}^{t+\eta_1} K_{\eta_1}(t-s_1)\cdot I_1 ds_1\right| \\
&\quad= \left|\int_{t-\eta_1}^{t+\eta_1} K_{\eta_1}(t-s_1)\left(I_1 - \langle g\rangle_2(s_1, \epsilon^{-1}s_1) + \langle g\rangle_2(s_1, \epsilon^{-1}s_1) - \langle g\rangle_{12}\right) ds_1\right| \\
&\quad\leq C\left(\frac{\epsilon^{2q}}{\eta_2^q} + \frac{\eta_2^\sigma}{\epsilon^\sigma}\right)\max_{j=0\ldots q}||K^{(j)}||_1 + \left|\int_{t-\eta_1}^{t+\eta_1} K_{\eta_1}(t-s_1)\left(\langle g\rangle_2(s_1, \epsilon^{-1}s_1) - \langle g\rangle_{12}\right) ds_1\right|.
\end{aligned} \tag{4.4.63}$$

Second, define $\hat{g}(\hat{s}_1, s_1) = \langle g\rangle_2(\hat{s}_1, \epsilon^{-1}s_1) - \langle g\rangle_{12}$. Hence, $\hat{g}(\hat{s}_1, s_1)$ is 1-periodic in the second variable and the average over s_1 is zero. A second application of Lemma 4.4.3 yields existence of $C_2 > 0$ such that

$$\left|\int_{t-\eta_1}^{t+\eta_1} K_{\eta_1}(t-s_1)\hat{g}(\hat{s}_1, s_1) ds_1\right| \leq C_2\left(\frac{\epsilon^q}{\eta_1^q} + \eta_1^\sigma\right)\max_{j=0\ldots q}||K^{(j)}||_1. \tag{4.4.64}$$

Hence, we can find a positive constant C such that

$$\left|K_{\eta_1} * \left[K_{\eta_2} * \left(f_0(\cdot, \epsilon^{-1}\cdot, \epsilon^{-2}\cdot) - \langle f_0(t, s_1, s_2)\rangle_{12}\right)(\cdot)\right](t)\right| \leq C\left(\frac{\epsilon^{2q}}{\eta_2^q} + \frac{\epsilon^q}{\eta_1^q} + \frac{\eta_2^\sigma}{\epsilon^\sigma} + \eta_1^\sigma\right)\max_{j=0\ldots q}||K^{(j)}||_1.$$

This concludes the proof of the theorem. □

Recall the three scale problem (4.1.6) and its averaged equation (4.1.9):

$$x' = \epsilon^{-1}f_1(x, \epsilon^{-1}t, \epsilon^{-2}t) + f_0(x, \epsilon^{-1}t, \epsilon^{-2}t), \quad x(0) = x_0,$$

$$\xi' = \langle(\nabla_x f_1)\phi(\xi, s_1, s_2)\rangle_{12} + \langle f_0(\xi, s_1, s_2)\rangle_{12}, \quad \xi(0) = x_0.$$

Key to the following theorem is the vanishing of $\langle f_1(x(t), s_1, s_2)\rangle_2$.

Theorem 4.4.2. Let $f_1(x(t), s_1, s_2)$ be 1-periodic in s_1 and s_2, and have a zero average with respect to s_2. For $r = (r_1, r_2) \in \mathbb{Z}_+^2$, assume $\partial^r f_1(x(t), s_1, s_2)$ are continuous and bounded for $|r| = 0, \cdots, \sigma + 1$, and $\sigma \geq 1$. Then, for any $K \in \mathbb{K}^{p,q}$ and $\epsilon^2 \ll \eta_2 \ll \epsilon \ll \eta_1 \ll 1$, the following estimate holds.

$$\begin{aligned}\left|K_{\eta_1} * \left[K_{\eta_2} * \left(\epsilon^{-1} f_1(x(\cdot), \epsilon^{-1}\cdot, \epsilon^{-2}\cdot) - \langle h\rangle_{12}(\xi)\right)(\cdot)\right](t)\right| \\ \leq C\left(\frac{\epsilon^{2q-1}}{\eta_{2q}} + \frac{\epsilon^q}{\eta_1^q} + \frac{\eta_2^\sigma}{\epsilon^{\sigma+1}} + \eta_1^{\sigma-1}\right) \max_{j=0\ldots q} ||K^{(j)}||_1\end{aligned}$$

where

$$\begin{aligned}h(\xi, s_1, s_2) &= (\nabla_x f_1)\phi(\xi, s_1, s_2), \\ \phi(\xi, s_1, s_2) &= \int_0^{s_2} f_1(\xi, s_1, \tau) d\tau.\end{aligned}$$

Proof. We begin with the first convolution $K_{\eta_2} * (\epsilon^{-1} f_1 - \langle h\rangle_{12})$. Lemma 4.2.1 allows ones to write $x(t)$ as

$$x(t) = w(t) + \epsilon\psi(t) + \epsilon\phi(t) \tag{4.4.65}$$

where $\psi(t) = \psi(w(t), \epsilon^{-1}t, \epsilon^{-2}t)$, $\phi(t) = \phi(w(t), \epsilon^{-1}t, \epsilon^{-2}t)$, and $\psi(t)$ is bounded independent of ϵ.

$$\begin{aligned}&K_{\eta_2} * \left(\epsilon^{-1} f_1 - \langle h\rangle_{12}\right)(s_1) \\ =&\int_{s_1-\eta_2}^{s_1+\eta_2} K_{\eta_2}(s_1 - s_2) \cdot \left(\epsilon^{-1} f_1(w(s_2) + \epsilon\psi(s_2) + \epsilon\phi(s_2), \epsilon^{-1}s_2, \epsilon^{-2}s_2) - \langle h\rangle_{12}\right) ds_2 \\ =&I_1 + I_2 + \mathcal{O}(\epsilon)\end{aligned}$$

where we set

$$\begin{aligned}I_1 &= \int_{s_1-\eta_2}^{s_1+\eta_2} K_{\eta_2}(s_1 - s_2) \cdot \left(\epsilon^{-1} f_1(w(s_2) + \epsilon\psi(s_2), \epsilon^{-1}s_2, \epsilon^{-2}s_2)\right) ds_2 \\ I_2 &= \int_{s_1-\eta_2}^{s_1+\eta_2} K_{\eta_2}(s_1 - s_2) \cdot \left(\nabla_x f_1(w(s_2) + \epsilon\psi(s_2), \epsilon^{-1}s_2, \epsilon^{-2}s_2)\phi(s_2) - \langle h\rangle_{12}\right) ds_2.\end{aligned} \tag{4.4.66}$$

Each term in the integrations is estimated in a similar way. Before we move on, recall from Theorem 4.4.1 that we identify $f_1(x(s_2), \epsilon^{-1}s_2, \epsilon^{-2}s_2)$ with $f_1(s_2, \epsilon^{-1}s_2, \epsilon^{-2}s_2)$. In (4.4.66), this simplification is also allowed since by solving the 1st and 2nd tier, we know $x(t)$ over $[t-\eta_1, t+\eta_1]$ and thus $w(t)+\epsilon\psi(t)$ as well. First, applying Lemma 4.4.3 to I_1 with $\langle f_1\rangle_2 = 0$ yields

$$|I_1| \leq \left(\frac{\epsilon^{2q-1}}{\eta_2^q} + \frac{\eta_2^\sigma}{\epsilon^{\sigma+1}}\right) \max_{j=0\cdots q} ||K^{(j)}||_1. \tag{4.4.67}$$

Second, for I_2, we now return to consider convolving with K_{η_1} and K_{η_2}. Note that $\langle h\rangle_{12}$ is a function of $\xi(\cdot)$. Theorem 4.1.1 yields that

$$\sup_{0\leq t\leq T} |w(t)-\xi(t)| \leq \sup_{0\leq t\leq T} (|w(t)-x(t)| + |x(t)-\xi(t)|) \leq C\epsilon.$$

Then we have $\langle(\nabla_x f_1)\phi - \langle h\rangle_{12}\rangle_{12} = 0 + \mathcal{O}(\epsilon)$, and this allows us to use Lemma 4.4.4 and thus to get an estimate for $|K_{\eta_1} * I_2(\cdot)|$.

$$|K_{\eta_1} * I_2(\cdot)| \leq \; C\left(\frac{\epsilon^{2q}}{\eta_2^q} + \frac{\epsilon^q}{\eta_1^q} + \frac{\eta_2^\sigma}{\epsilon^\sigma} + \eta_1^\sigma\right) \max_{j=0\cdots q} ||K^{(j)}||_1. \tag{4.4.68}$$

Since we differentiate f_1 with respect to x, $\partial^r \nabla_x f_1 \cdot \phi$ are continuous and bounded for $|r| = 0, \cdots, \sigma$. Putting estimates (4.4.67) and (4.4.68) together, Theorem 4.4.2 follows. □

We conclude this section by proving Proposition 4.4.1 which is the cornerstone of our numerical method.

Proof. (Proposition 4.4.1) The RHS of the estimate in Theorem 4.4.2 dominates that of Lemma 4.4.4. Therefore, having p $(< \sigma)$ vanishing moments yields (4.4.56). □

Remark 4.4.1. Theorem 4.1.1 is only valid up to times T independent of ϵ. However, in special cases in which additional cancellation or self averaging occurs, iterated averaging with kernels may give an consistent approximation for the effective behavior of ODEs for longer time intervals.

4.5 Generalizations

This paper is focused on three scale problems modeled by

$$x' = \epsilon^{-1} f_1(x, \epsilon^{-1}t, \epsilon^{-2}t) + f_0(x, \epsilon^{-1}t, \epsilon^{-2}t), \quad x(0) = x_0,$$

restricting $\langle f_1 \rangle_2 = 0$. However, the discussions at the preceding sections suggest several possible generalizations.

4.5.1 Almost-periodic dynamics

The three-scale averaging theorem can be generalized to include dynamics in which the fast $\mathcal{O}(\epsilon^2)$ or $\mathcal{O}(\epsilon)$ time scales are not necessarily periodic but rather ergodic on a torus. The periodicity of s_2 is only taken into account when evaluating the remainder term $r(t;\epsilon)$ in (4.2.36). In the case of a torus, $r(t;\epsilon)$ can be written as a finite sum of periodic functions whose periods are incommensurable. Thus, estimate (4.2.37) still holds. A similar generalization can be obtained for almost-periodic functions whose spectrum is bounded away from zero. See, for example [23, 93].

4.5.2 The 3-tier HMM using slow charts

In the proof of Theorem 4.1.1, as well as while applying the expansion formalism, it was necessary to assume that the average of the singular $\mathcal{O}(\epsilon^{-1})$ part in x' vanishes, $\langle f_1 \rangle_2 = 0$. Nonetheless, it can be shown that the estimate of section 4.2.1 does hold, but only on a short time segment of $\mathcal{O}(\epsilon)$ length, i.e.

$$\sup_{0 \le t \le \epsilon T} |x(t) - \xi(t)| = \mathcal{O}(\epsilon).$$

In addition, the HMM procedure which utilizes the iterated averaging estimate indicates that in fact, in order to generate a consistent approximation of a slow variable, one only needs to evaluate its derivative on a short time segment of order ϵ. Then, if the dynamics on the intermediate $\mathcal{O}(\epsilon)$ is again oscillatory (i.e. periodic or as above), additional averaging on the ϵ time scale may average this divergence out. This self averaging property can be captured by the iterated averaging procedure.

To this end, we first need to define slow variables. Formally, slow variables of a dynamical system involving three or more time scales are defined as below [7].

Definition 4.5.1. A smooth time dependent function $\alpha : [0, T] \mapsto \mathbb{R}$ is said to *evolve on the ϵ^k time scale in* $[0, T]$ for some integer k and for $0 < \epsilon \le \epsilon_0$, if there exists a smooth function $\beta : [0, T] \mapsto \mathbb{R}$ and constants C_0 and C_1 such that

$$\sup_{t \in [0,T]} \left| \frac{d}{dt} \beta(t) \right| \le C_0 \epsilon^{-k} \quad \text{and} \quad \sup_{t \in [0,T]} |\alpha(t) - \beta(t)| \le C_1 \epsilon.$$

Definition 4.5.2. A function $\xi(x)$ is said to *evolve on the ϵ^k time scale along the trajectories of* (4.1.6) *in* $[0, T]$ if the time dependent function $\xi(x(t; \epsilon, x_0))$ evolves

on the ϵ^k time scale in $[0, T]$. For brevity, we will refer to variables that evolve on the ϵ^0 time scale as slow.

The 3-tier HMM using slow variables shares a similar strategy described in Section 4.1.3, which implements a recursive two-level solver, but the fast oscillations we need to average over are not explicitly given. As [5], with the need for identifying hidden slow variables, we approximate an averaged equation for slow variables by time averaging the microscopic evolution using a suitable kernel. Recall that since the time scales $\mathcal{O}(\epsilon^2)$, $\mathcal{O}(\epsilon^1)$, and $\mathcal{O}(1)$ are considered, we need to identify three sets of variables which evolve on each time scale respectively.

Suppose we obtain such a coordinate system using, e.g., the method described in [7]. We denote this system of coordinates $\xi = (\xi_0, \xi_1, \xi_2)$, where $\xi_i = (\xi_i^1, \ldots, \xi_i^{d_i})$ are the variables evolving on the ϵ^i time scale, and $\sum_{i=0}^{2} d_i = d$. One should take the coordinates of ξ as slow as possible, i.e., if ϕ evolves on both ϵ^0 and ϵ^1 time scales, then $\phi \in \xi_0$. In terms of the new coordinates the ODE system takes the form

$$\begin{aligned} \xi_0' &= \epsilon^{-1} f_1(\xi_0, \xi_1, \xi_2) + f_0(\xi_0, \xi_1, \xi_2), \quad \langle f_1 \rangle_2 = 0, \\ \xi_1' &= \epsilon^{-1} g_1(\xi_0, \xi_1, \xi_2) + g_0(\xi_0, \xi_1, \xi_2), \quad \langle g_1 \rangle_2 > C_1 > 0, \\ \xi_2' &= \epsilon^{-2} h_2(\xi_0, \xi_1, \xi_2), \end{aligned} \tag{4.5.69}$$

where $\langle \cdot \rangle_2$ denotes averaging with respect to the invariant measure for ξ_2 on fixed ξ_0 and ξ_1 and C_1 is independent of ϵ, i.e., $\langle g_1 \rangle_2$ is bounded away from 0 independent of ϵ. Note that (4.5.69) is of the similar form as (4.1.5). We assume that no resonances, passage through resonances or turning points exists as these may cause hidden slow

variables and the decomposition of states into time scales may not be trivial, as discussed in [7, 75].

Then outline of the 3-tier HMM with slow variables is as follows. For simplicity of notation, we suppress the superscript in ξ_i. As before, we denote the descretized time $t_{n,m} = nh_0 + mh_1$ and $t_n = nh_0$. We concentrate on the forward Euler and a symmetric kernel.

1. Determination of slow variables:

   Find a coordinate system $\xi(x) = (\xi_0(x), \xi_1(x), \xi_2(x))$ where ξ_i are the variables evolving on the ϵ^i time scale. See [7] for details. Set $n = 0$.

2. Multilevel evolution:

   - (0th tier) At $t = t_n$, set $\tilde{X}_0 = x_{1,0} = x_n$.

     (a) (1st tier) For $m = 0$ to k $(= \eta_1/h_1)$,

     set $t = t_{n,m} = nh_0 + mh_1$,

     i. (2nd tier) Solve the full ODE (4.1.6) in $t \in [t_{n,m} - \eta_2, t_{n,m} + \eta_2]$ with initial conditions $\tilde{X}_0$.

     ii. (2nd tier) Force estimation in $\mathcal{O}(\epsilon^1)$ scale: approximate $\xi_i'(t_{n,m})$, $i = 0, 1$ by

     $$\langle \xi_i' \rangle_{\eta_2}(t_{n,m}) = (K_{\eta_2} * \xi_i')(t_{n,m}). \tag{4.5.70}$$

     (b) (1st tier) $x_{1,m+1} = x_{1,m} + h_1 \delta x_1$, where δx_1 is the least squares solution to the linear system

     $$\delta x_1 \cdot \nabla \xi_i = \langle \xi_i' \rangle_{\eta_2}, \tag{4.5.71}$$

for all $i = 0, 1$. Redefine $\tilde{X}_0 = x_{1,m+1}$.

(c) End FOR

(d) (1st tier) Force estimation in $\mathcal{O}(1)$ scale: approximate $\xi_0'(t_n)$, by

$$\langle \xi_0' \rangle_{\eta_1}(t_n) = K_{\eta_1} * \left(\langle \xi_0' \rangle_{\eta_2}(\cdot) \right)(t_n). \tag{4.5.72}$$

- (0th tier) $x_{n+1} = x_n + h_0 \delta x_0$, where δx_0 is the least squares solution to the linear system

$$\delta x_0 \cdot \nabla \xi_0 = \langle \xi_0' \rangle_{\eta_1}. \tag{4.5.73}$$

Set $\tilde{X}_0 = x_{n+1}$.

3. $n = n + 1$ and repeat 2.

A rigorous proof of Section 4.5.2 is beyond the scope of the current paper. However, we refer the reader to [3, 5] for designing multiscale algorithms that compute the effective behavior of two-scale highly oscillatory dynamical systems by using slow variables. A related example is presented in Section 4.6.2.

4.5.3 Stochastic effects

The theory of asymptotic expansions and the nested-HMM integrators approach can be extended to a setting in which the intermediate scale is stochastic. In fact, the only requirements for applying the numerical method 4.1.3 is that the fastest $\mathcal{O}(\epsilon^2)$ scale is oscillatory - thus ensuring that the effective slow scale is deterministic, and that the intermediate $\mathcal{O}(\epsilon)$ time scale is ergodic. Consider (4.5.69). If the dynamics of ξ_1 is stochastic, then, on the $\mathcal{O}(1)$ time scale averaging with kernels

needs to be replaced by an alternative method such as stochastic HMM [37, 101]. Such an example is presented in Section 4.6.3.

4.6 Numerical examples

In this section, we numerically apply the iterated HMM approach described in Section 4.1.3 to deterministic and stochastic systems with three scales. A basic example which has the form of (4.1.6) is studied in Section 4.6.1. Following that, we concentrate on examples which demonstrate the applicability of our method to the generalizations discussed in the previous section. The classical example of two coupled harmonic oscillators in resonance is illustrated in Section 4.6.2. In this example, one of the slow variables has formally unbounded derivatives as $\epsilon \to 0$, but it evolves on the ϵ^0 time scale due to a zero-average of ϵ^{-1} term. Section 4.6.3 is a deterministic example for the generalization discussed in Section 4.5. The period of the fast oscillator on the $\mathcal{O}(\epsilon^2)$ time scale changes according to the ϵ scale variable. Lastly, an interesting stochastic system whose period of the fastest oscillator changes randomly on the ϵ scale is given in Section 4.6.4.

Our multiscale algorithm is constructed as a family of multilevel (>2) solvers which resolve the different time scales and use kernels to estimate the effective force of the slower scales. In Section 4.6.1 through 4.6.3, we use a symmetric C^∞ kernel. We see that for a smooth kernel the computational cost is independent of ϵ — see [7] for discussions about accuracy and efficiency. In the stochastic example 4.6.4, a $\mathbb{K}^{2,7}$ kernel is used.

4.6.1 Example 1

We begin with a simple example of a three-scale system, which is similar to (4.1.12)

$$x' = \epsilon^{-1}\left[x\sin(\epsilon^{-2}t) + \cos(\epsilon^{-2}t)\sin^2(\epsilon^{-1}t)\right] + \cos^2(x) + \cos(\epsilon^{-1}t), \quad x(0) = 1. \tag{4.6.74}$$

Applying Theorem 4.1.1 to (4.6.74), we have an averaged equation for $x(t)$,

$$\bar{x}' = 1/4 + \cos^2(\bar{x}), \quad \bar{x}(0) = 1. \tag{4.6.75}$$

The different three-time scales of (4.6.74) are illustrated in Figures 4.2 and 4.3. The solution $x(t)$ undergoes small-amplitude fast oscillations around the slow trajectory over the interval $[0, 10]$. As proved in Section 4.2 and 4.4, the 3-tier HMM approximates $\bar{x}(t)$ which remains close (of order ϵ) to the slow trajectory of $x(t)$. We apply an exponential kernel $K^{\exp} \in \mathbb{K}^{1,\infty}([-1, 1])$. See [5, 42] for details. In Figure 4.3, we compare the results of 3-tier HMM with both $\bar{x}(t)$ and $x(t)$ obtained by the explicit Runge-Kutta 4th order method. HMM is about 12 times faster than RK4 applied to (4.6.74) directly with the step size $h = \epsilon^2/5$. The computational effort of HMM is independent of ϵ once η_i and h_i are fixed. However, for classical numerical methods moving from $\epsilon = 10^{-3}$ to $\epsilon = 10^{-4}$ multiplies the computational effort by 100.

Table 4.1: (Section 4.6.1) Parameters for the 3-tier HMM of example 1.

$\epsilon = 10^{-3}$	η_i	h_i	Method	Kernel
2nd tier	$18\epsilon^2$	$\epsilon^2/5$	RK4	$K^{\exp} \in \mathbb{K}^{1,\infty}([-1, 1])$
1st tier	18ϵ	$\epsilon^1/5$	RK2	$K^{\exp} \in \mathbb{K}^{1,\infty}([-1, 1])$
0th tier	10	1/3	RK2	-

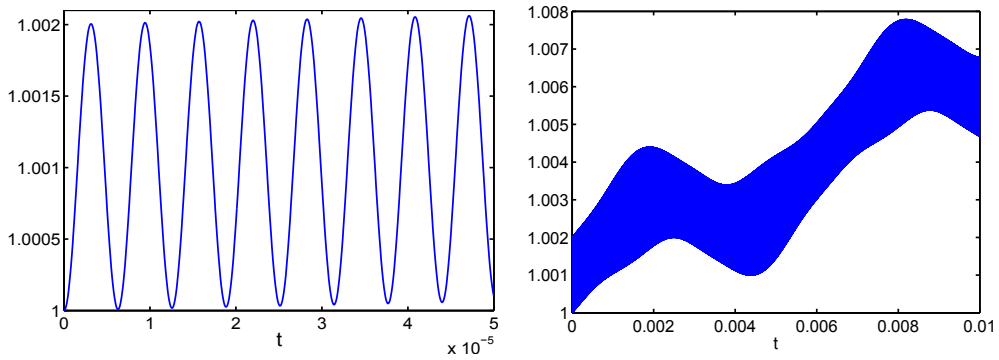

Figure 4.2: (Section 4.6.1) The dynamics of (4.6.74) on the (Left) ϵ^2 time scale and (Right) ϵ^1 time scale ($\epsilon = 10^{-3}$). Plots are obtained by RK4 with $h = \epsilon^2/100$.

4.6.2 Example 2

Consider the following system describing two coupled harmonic oscillators in resonance [7].

$$\begin{cases} x_1' &= -\epsilon^{-2} y_1 + \epsilon^{-1} y_2^2 - 3 x_1 x_2^2, \\ y_1' &= \epsilon^{-2} x_1 + y_1/2, \\ x_2' &= -\left(\epsilon^{-2} + \epsilon^{-1}\right) y_2 - x_2, \\ y_2' &= \left(\epsilon^{-2} + \epsilon^{-1}\right) x_2 - y_2 + 2 x_1^2 y_2. \end{cases} \tag{4.6.76}$$

with initial conditions $(x_1(0), y_1(0), x_2(0), y_2(0)) = (0, 1, 0, 1)$. As depicted in Figure 4.4, all four state variables oscillate with a period which is of the order of ϵ^2. Hence, x_1, y_1, x_2 and y_2 evolve on the ϵ^2 time scale.

In order to find a slow coordinate system, we change to polar coordinates $(x_i, y_t) \mapsto (I_i, \varphi_i)$, $i = 1, 2$ and introduce a polynomial variable θ that describes the

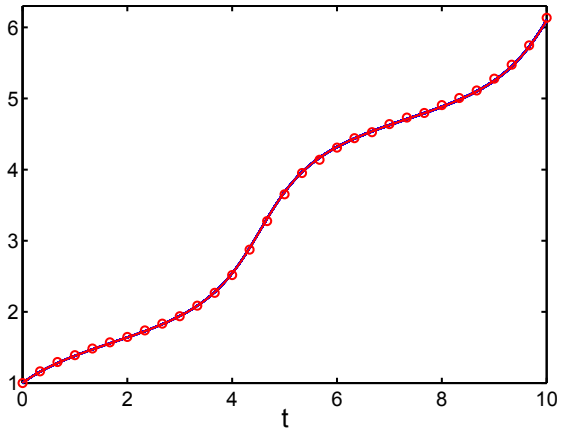

Figure 4.3: (Section 4.6.1) The dynamics of (4.6.74) on the ϵ^0 time scale. $x(t)$ and $\bar{x}(t)$ are represented by a full line where both are almost indistinguishable. The results of 3-tier HMM are indicated by circles.

1:1 resonance between the oscillators

$$I_1 = x_1^2 + y_1^2,$$

$$I_2 = x_2^2 + y_2^2,$$

$$\theta = x_1 x_2 + y_1 y_2,$$

$$\cos\varphi_1 = x_1/\sqrt{I_1}.$$

The corresponding time derivatives are

$$I_1' = 2\epsilon^{-1} x_1 y_2^2 - 6x_1^2 x_2^2 + y_1^2,$$

$$I_2' = -2I_2 + 4x_1^2 y_2^2,$$

$$\theta' = \epsilon^{-1}(x_2 y_2^2 + y_1 x_2 - x_1 y_2) + (-0.5 y_1 y_2 - x_1 x_2 - 3x_1 x_2^3 + 2x_1^2 y_1 y_2),$$

$$\varphi_1' = \epsilon^{-2}.$$

It appears as if $(I_1, I_2, \theta, \varphi_1)$ is a chart in which φ_1 evolves of the ϵ^2 time scale, I_1 and θ evolve on the ϵ time scale while I_2, which has a bounded derivative, evolves on the $\mathcal{O}(1)$ scale. The dynamics of the three slow variables I_1, I_2 and θ on the $\mathcal{O}(\epsilon)$

scale is depicted on the right in Figure 4.4. The figure suggests that both I_1 and I_2 are practically constant on the ϵ scale. Indeed, it can be shown that the average of $x_1 y_2^2$ on any segment of length $\mathcal{O}(\epsilon)$ and larger is of order ϵ^2. Therefore, the ϵ^{-1} term in I_1' has a zero average. As a result, the averaged I_1' is bounded independent of ϵ and I_1 evolves on the $\mathcal{O}(1)$ time scale, rather than the expected $\mathcal{O}(\epsilon)$.

The time evolution of I_1 and I_2 on the slowest $\mathcal{O}(1)$ time scale is depicted in Figure 4.5. In addition, the figure shows the results of the 3-tier HMM integrator described in Section 4.1.3. We refer to the solver integrating the ϵ^i scale as the i-th tier. The step-size and length of integration of the i-th tier are denoted h_i, η_i, respectively. The HMM algorithm approximates the slow $\mathcal{O}(1)$ dynamics using macroscopic steps which are independent of ϵ. The integration is done using a fourth order method (in the macroscopic step size) and its efficiency is essentially independent of ϵ. Simulation parameters are detailed in Table 4.2.

Table 4.2: (Section 4.6.2) Parameters for the 3-tier HMM of example 2.

$\epsilon = 10^{-3}$	η_i	h_i	Method	Kernel
2nd tier	$70.1\epsilon^2$	$\epsilon^2/10$	RK4	$K^{exp} \in \mathbb{K}^{1,\infty}([-1,1])$
1st tier	$70.1\epsilon^1$	$\epsilon^1/10$	RK4	$K^{exp} \in \mathbb{K}^{1,\infty}([-1,1])$
0th tier	10	1/3	RK4	-

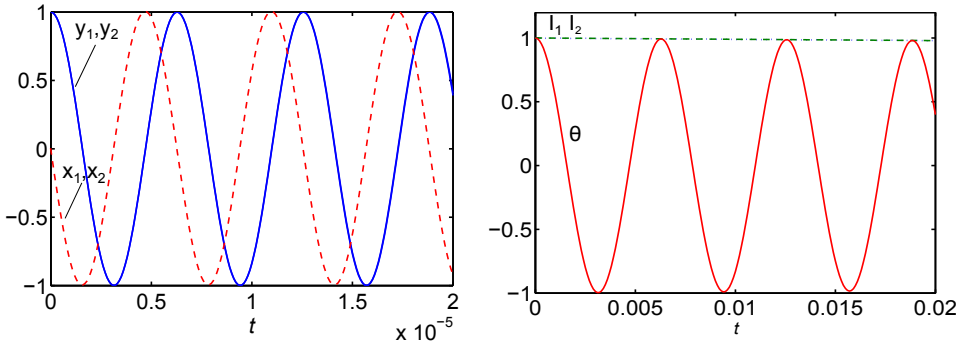

Figure 4.4: (Section 4.6.2) The dynamics of (4.6.76) on the (Left) ϵ^2 time scale and (Right) ϵ^1 time scale. $\epsilon = 10^{-3}$.

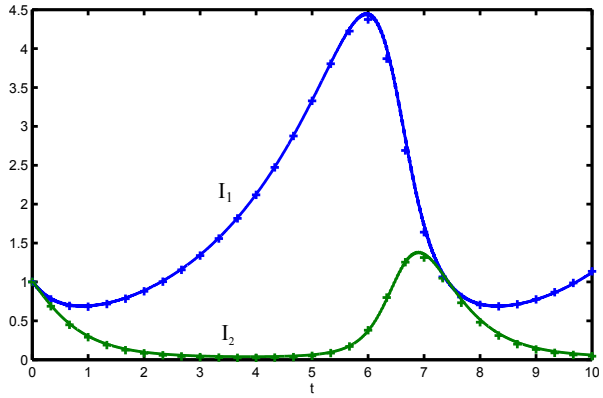

Figure 4.5: (Section 4.6.2) The dynamics of (4.6.76) on the ϵ^0 time scale. Plus signs are results of the 3-tier HMM.

4.6.3 Example 3

Consider the following deterministic system describing two coupled fast harmonic oscillators and a slow dependent mode.

$$\begin{cases} x_1' = -\epsilon^{-2}(1 + 0.5\sin y_2)x_2 + (1-z)(x_1^2 + x_2^2)^{-1}x_1, \\ x_2' = \epsilon^{-2}(1 + 0.5\sin y_2)x_1, \\ y_1' = -\epsilon^{-1}y_2 - 0.5(1 + x_1^2 - z)y_1, \\ y_2' = \epsilon^{-1}y_1, \\ z' = -(1 + 0.5x_1^2)z + y_2^2 \end{cases} \tag{4.6.77}$$

with initial conditions $(x_1(0), x_2(0), y_1(0), y_2(0), z(0)) = (1, 0, 1, 1.5, 0.5)$. The system describes two coupled harmonic oscillators (x_1, x_2) and (y_1, y_2) with $\mathcal{O}(\epsilon^2)$ and $\mathcal{O}(\epsilon)$ periods, respectively. However, the period of the fastest $\mathcal{O}(\epsilon^2)$ oscillator depends on y_2 and is therefore changing on the slower ϵ scale. Figure 4.6 (Left) demonstrates the different period of x_1 and x_2 over 2.5×10^{-7} duration with $\epsilon = 10^{-4}$. This is an example for the first generalization suggested in Section 4.5 in which the fastest oscillation exhibits non-trivial dynamics of the intermediate ϵ scale.

The system admits three slow variables that evolve on the ϵ^0 scale: z, and the square amplitudes of the harmonic oscillators, $I_1 = x_1^2 + x_2^2$ and $I_2 = y_1^2 + y_2^2$. A numerical algorithm for identifying polynomial slow variables is described in [5]. Hence, we have a coordinate system (ξ_0, ξ_1, ξ_2) in which ξ_i evolves on the ϵ^i time scale:

$$\begin{aligned} \xi_0 &= \{I_1, I_2, z\}, \\ \xi_1 &= \{y_2\}, \\ \xi_2 &= \varphi \in S^1. \end{aligned}$$

As before, we refer to the solver integrating the ϵ^i scale as the i-th tier. The step-size and length of integration of the i-th tier are denoted h_i, η_i, respectively. The dynamics of the slow variables I_1, I_2 and z, as well as the 3-tier HMM approximation is depicted in Fig. 4.6 (Right). See Table 4.3 for simulation parameters.

Table 4.3: (Section 4.6.3) Parameters for the 3-tier HMM of example 3.

$\epsilon = 10^{-4}$	η_i	h_i	Method	Kernel
2nd tier	$75.1\epsilon^2$	$\epsilon^2/10$	RK4	$K^{exp} \in \mathbb{K}^{1,\infty}([-1,1])$
1st tier	$75.1\epsilon^1$	$\epsilon^1/10$	RK2	$K^{exp} \in \mathbb{K}^{1,\infty}([-1,1])$
0th tier	10	1/2	RK2	-

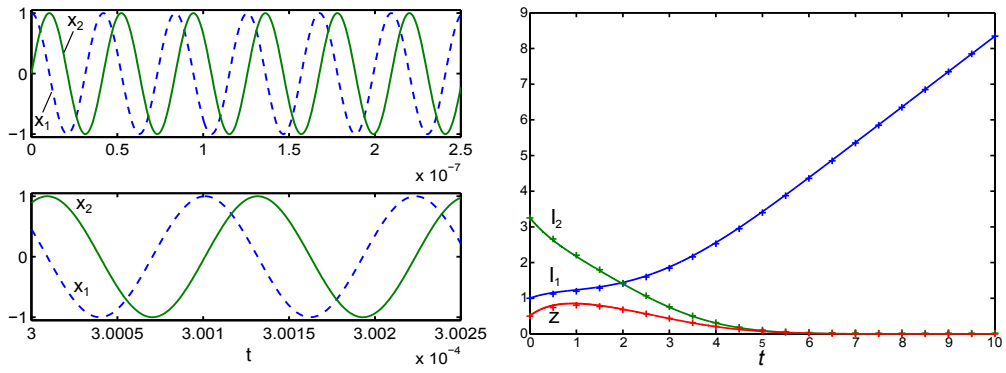

Figure 4.6: (Section 4.6.3) (Left) The period of the fastest $\mathcal{O}(\epsilon^2)$ oscillator is changing on the slower ϵ scale. (Right) The dynamics of (4.6.77) on the ϵ^0 time scale. Plus signs: 3-tier HMM. Solid line: a reference solution using the RK4 method with step size $h = \epsilon^2/50$. HMM runs about 1150 times faster. $\epsilon = 10^{-4}$.

4.6.4 Example 4

Consider the following system in which a fast harmonic oscillator has a randomly changing period.

$$\begin{cases} dx_1 = -(\epsilon^{-2}(1 + 0.5\sin y)x_2 + x_1(1 - z))dt, \\ dx_2 = \epsilon^{-2}(1 + 0.5\sin y)x_1 dt, \\ dy = -\epsilon^{-1} y dt + \epsilon^{-1/2} z d\mathrm{B}_t, \\ dz = -((1 + x_1^2)z - y)dt \end{cases} \tag{4.6.78}$$

with initial conditions: $(x_1(0), x_2(0), y(0), z(0)) = (2, 0, 1, 1)$. In this example, (x_1, x_2) is a harmonic oscillator with an $\mathcal{O}(\epsilon^2)$ period. However, the period changes

randomly through a random variable y which is an Ornstein–Uhlenbeck process evolving on the $\mathcal{O}(\epsilon^1)$ time scale. The system has two slow variables that evolve on the $\mathcal{O}(\epsilon^0)$ scale: z and $I_1 = x_1^2 + x_2^2$. Thus, we find a coordinate system; $\xi_0 = \{I_1, z\}$, $\xi_1 = \{y\}$ and $\xi_2 = \varphi \in S^1$ in which ξ_i evolve on the $\mathcal{O}(\epsilon^i)$ scale.

In order to demonstrate that the effective dynamics of z and I_1 is indeed deterministic, Figure 4.7 (Left) shows the standard deviations of I_1 and z as a function of ϵ. As expected, it is of order $\sqrt{\epsilon}$.

Fig. 4.7 (Right) compares the results computed by the proposed HMM with those by the semi-implicit Euler method [79]. The sample averages of I_1 and z against t are plotted with a solid line (Euler) and plus signs (HMM). We estimate the errors of the method by comparing the standard deviation of sample paths. Taking $\epsilon = 10^{-4}$, for the semi-implicit Euler, we take 1,000 paths over [0, 4] and decrease step size until the desired accuracy is reached, $(\max\{\sigma(I_1)\}+\max\{\sigma(z)\})/2 = 0.1$. This requires $h = \epsilon^2/100$. For the 3-tier HMM, we compute 100 independent paths with h_0=0.5 and calculate the standard deviation for each. The kernel was constructed from Chebyshev polynomials to have exactly seven continuous derivatives and two vanishing moments:

$$K^{2,7}(t) = 4157010\ \chi_{[0,1]}(t)(42t^2 - 44t + 11)t^8(t-1)^8$$

where $\chi_{[0,1]}$ is the characteristic function of the interval $[0, 1]$. HMM parameters are shown in Table 4.4. With these parameters, HMM achieves $(\max\{\sigma(I_1)\}+\max\{\sigma(z)\})/2 = 0.025$. Even if HMM has four times less standard deviation, it runs about 1,000 times faster than the semi-implicit Euler. In addition, we note that the dominant error of

3-tier HMM comes from h_0 and decreases with smaller h_0.

Table 4.4: (Section 4.6.4) Parameters for the 3-tier HMM of example 4

$\epsilon = 10^{-4}$	η_i	h_i	Method	Kernel
2nd tier	$50\epsilon^2$	$\epsilon^2/10$	semi-implicit Euler	$K^{2,7} \in \mathbb{K}^{2,7}([0,1])$
1st tier	$50\epsilon^1$	$\epsilon^1/10$	Euler	$K^{2,7} \in \mathbb{K}^{2,7}([0,1])$
0th tier	10	1/10	RK2	-

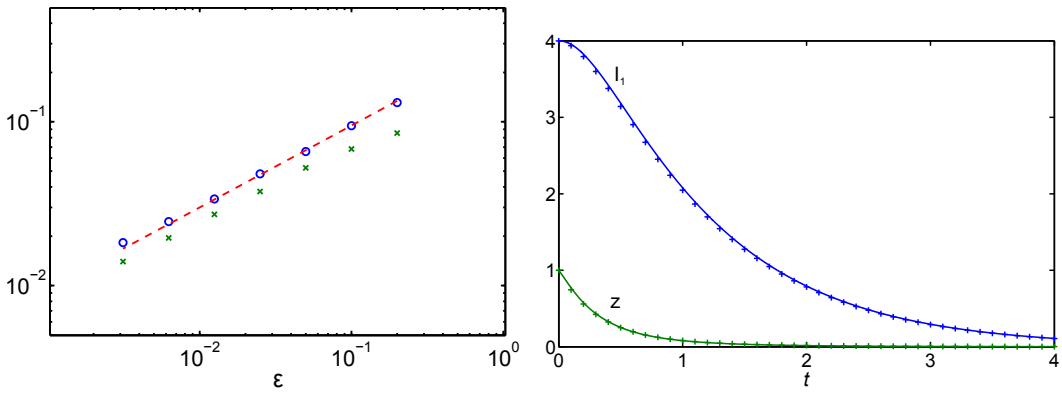

Figure 4.7: (Section 4.6.4) (Left) o-markers are $\max_{t\in[0,4]}\{\sigma(I_1)\}$. x-markers are $\max_{t\in[0,4]}\{\sigma(z)\}$. The dashed line is a guide for the eye with slope 1/2. (Right) The evolution of the slow variables in example 3. Plus signs: HMM. The solid line is a reference solution calculated as explained in the text.

4.7 A comprehensive multiscale algorithm and FPU

Motivated from the iterated averaging, the method of approximating the invariant measure and the Backward Forward HMM, we propose a comprehensive hierarchical method which may be applicable to the Fermi-Pasta-Ulam problem. We have the following equations of motion

$$\begin{cases} \dot{y}_i = u_i, \\ \dot{x}_i = \epsilon^{-1} v_i, \\ \dot{u}_i = -(y_i - \epsilon x_i - y_{i-1} - \epsilon x_{i-1})^3 + (y_{i+1} - \epsilon x_{i+1} - y_i - \epsilon x_i)^3, \\ \dot{v}_i = -\epsilon^{-1} x_i + (y_i - \epsilon x_i - y_{i-1} - \epsilon x_{i-1})^3 + (y_{i+1} - \epsilon x_{i+1} - y_i - \epsilon x_i)^3. \end{cases} \tag{4.7.79}$$

Both fixed ends yield $y_0 = x_0 = y_{k+1} = x_{k+1} = 0$ and we choose $k = 2$ for an illustration. Initial conditions are $[y_1, x_1, u_1, v_1, y_2, x_2, u_2, v_2] = [1, 1, 0, 1.2, 1, 1, 1, 0]$. Total energies of the stiff springs are given by

$$I_i = x_i^2 + v_i^2, \quad i = 1, 2 \tag{4.7.80}$$

where $I_i : \mathbb{R}^8 \to \mathbb{R}$. The system admits 7 slow variables:

$$\begin{aligned} \mathcal{O}(1) &= \{y_1, u_1, y_2, u_2\}, \\ \mathcal{O}(\epsilon^{-1}) &= \{I_1, I_2, \phi\}. \end{aligned}$$

The averaging theorem cannot be generally extended to the ϵ^{-1} time scale. However, in this case, due to the oscillatory nature of the soft degrees of freedom, the dynamics undergoes additional averaging. In this section, after rescaling in time, we use our algorithm to average over the invariant tori in $\mathcal{O}(\epsilon)$ time scale. Simulation parameters are used as follows: $\epsilon = 10^{-3}$,

- from $\mathcal{O}(\epsilon^2)$ time scale to $\mathcal{O}(\epsilon)$ time scale: Midpoint rule BF HMM with z-structure – $h_2 = \epsilon^2/10$, $\eta_2 = 20.4\epsilon^2$ and over 2ϵ delta amount of the time, $h_1 = 2\epsilon$, and
- from $\mathcal{O}(\epsilon)$ time scale to $\mathcal{O}(10)$ time scale: HMM with Frobenius-Perron algorithm – $H = 0.05$, $\eta_1 = 70\epsilon$.

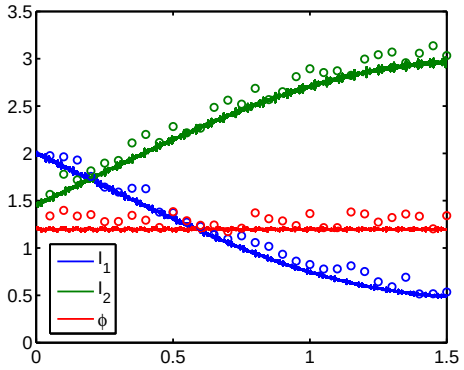

Figure 4.8: FPU with Frobenius-Perron operator algorithm. Circles are results of our algorithm. Solid lines are computed by a geometrical integrator with very small time step. This numerical simulation is experimental. There has been efforts in trying to understand where the leading error comes from.

Chapter 5

Conclusions

5.1 Summary

We discuss a methodology to design efficient and novel numerical algorithms for a class of deterministic and stochastic dynamical systems with multiple time scales. The traditional numerical methods for such problems need a very small step size to resolve the finest scale and become, therefore, inefficient when we are interested in the slow behavior over the much longer time intervals.

In Chapter 2, we have introduced the BF HMM scheme, a novel, accurate and fast approach for computing the effective behavior of a class of highly oscillatory ODEs and SDEs which does not rely on any explicitly derived slow variables. The main idea is *to exploit a nonstandard splitting of the vector field and construct effective paths in the state space whose projection onto the slow subspace has the correct dynamics.* A suitable set of slow and fast variables provides a new coordinate system for the state space of system

Chapter 3 involves averaging over suitable tori at different time scales due to different types of near resonances in the system. This is motivated by the near resonance structure in the Fermi-Pasta-Ulam (FPU) system. The tori in question are defined by the slow variables of the oscillatory dynamical systems. We classify

two kinds of near resonances – weak near resonances for the case $\delta = C\epsilon^q, q < 1$ and strong near resonances for $\delta = C\epsilon^p,\ p > 1$ with non-negative constant C. This separation is related to the speed of the flow to cover an invariant torus:

- **weak near resonance** the trajectories cover an invariant torus in a time interval $[0, T]$ independent of ϵ and we need to average over a torus.
- **strong near resonance** the system is effectively in resonance for the time interval $[0, T]$. We only need to average the flow over a suitable sub-torus which is embedded on the invariant torus.

We have proposed new algorithms for efficiently computing averages over the invariant tori using Frobenius-Perron operator.

In Chapter 4, we developed an iterated averaging theory for oscillatory dynamical systems involving three widely separated time scales and the relevant multiscale method for computing the effective behavior. In such multiple time scale problems, we identified a new type of slow variables which do not have formally bounded derivatives. The effective behavior for such variables are studied intensively in two ways: one is a formal approach via the tools of averaging theory, and the other involves homogenization techniques based on singular perturbation expansions and consequent matching of variables. We showed that the results of the developed averaging theory can be efficiently approximated computationally via convolutions of the dynamical system's solutions with a smooth compactly supported kernel. With the developed averaging strategies, we proposed an HMM which is built hierarchically

from our previously developed HMMs for two-scale problems. Several numerical examples were presented that demonstrate the efficacy of the proposed algorithms.

We conclude by emphasizing that there is a very similar philosophy between averaging over a torus in Chapter 3 and iterated averaging in Chapter 4. In Chapter 3 and 4, new directions orthogonal to the flow are corresponding to the fast variables and intermediate variables, respectively. The former constructs orthogonal vector fields on the torus as in 3.3.2, and the latter finds the maximally slow chart in order to devise efficient algorithms. See Figure 5.1.

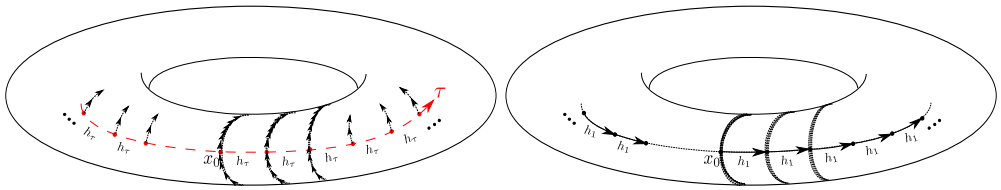

Figure 5.1: Comparison with numerical averaging over the torus (left) Averaging over the torus in Chapter 3 (right) Iterated averaging method presented in Chapter 4.

5.2 Future works

Built on previous approaches with my collaborators to multiscale problems, there are many exciting possibilities for future research which I plan to explore in the next few years.

Applications and problems related to the BF HMM

The BF HMM has great potential for generalizations to high order accurate multiscale integrators for a wider class of problems: (1) stochastic differential

equations – each γ_k^* shall be considered as an ensemble average of independent evaluations of x with respect to different initial conditions, and then the possible variance reduction in computation will be studied, (2) molecular dynamics – it is generally believed that ergodicity holds for some systems in molecular dynamics, such as liquid argon simulated via Lennard–Jones potential. In view of statistical physics, one needs to solve an equation for many initial conditions to take an ensemble average [21]. By using the BF HMM approaches, I will study the construction of methods which accelerate the computation of averages and get effective estimates of the error in numerically computed averages, and (3) nonlinear relaxation oscillator – this is caused by the stiff dissipation in the system. In this case, the Assumptions in BF HMM should be relaxed to allow eigenvalues with large negative real parts. We shall employ the structure described in Figure 2.2, but in the construction of γ_k^* the backward in time integration is removed.

Upscaling microscale models

A new multiscale algorithm which couples pore-scale network models and effective continuum conservation laws has been introduced in [25]. The missing quantities and data in the macroscopic model are obtained by solving an accurate pore-scale network model locally over small domains. The main idea is very similar to what I have done with dynamical systems. I am interested in applying this coupling idea to many different problems in material sciences and engineering, including the mechanical properties of composite materials, heat conduction in heterogeneous media, and flow in porous media.

Long time simulation with averaging over the invariant tori

Currently, our algorithm computes averages over a hypercube identified with the invariant tori and considers dynamical systems with two-time scales. It would be of practical interest to extend it to the embedded tori in the Euclidean space and to the three or more time scale systems.

The HMM procedure which utilizes the iterated averaging estimate indicates that in fact, in order to generate a consistent approximation of a slow variable in $\mathcal{O}(\epsilon^{-1})$ time scale, one only needs to evaluate its derivative on a short time segment of order $\mathcal{O}(1)$. If the dynamics on the $\mathcal{O}(1)$ time scale are again ergodic on tori, an additional averaging can be performed. A typical application is the FPU problem which shows the multiscale behavior in time scales of $\mathcal{O}(\epsilon)$, $\mathcal{O}(1)$ and $\mathcal{O}(\epsilon^{-1})$ [55]. We are expecting a hierarchical algorithm consisting of nested integrators equipped with the method to average over the tori. Since the key here is to average over the embedded tori, I plan to improve our algorithm to achieve this.

Bibliography

[1] G. Ariel, B. Engquist, S. Kim, Y. Lee, and R. Tsai. A Multiscale Method for Highly Oscillatory Dynamical Systems Using a Poincaré Map Type Technique. *J. Sci. Comput.*, 54(2-3):247–268, 2013.

[2] G. Ariel, B. Engquist, S. Kim, and R. Tsai. Iterated averaging for three-scale oscillatory systems. To appear.

[3] G. Ariel, B. Engquist, H.-O. Kreiss, and R. Tsai. Multiscale computations for highly oscillatory problems. In *Multiscale modeling and simulation in science*, volume 66 of *Lect. Notes Comput. Sci. Eng.*, pages 237–287. Springer, Berlin, 2009.

[4] G. Ariel, B. Engquist, and R. Tsai. Numerical multiscale methods for coupled oscillators. *Multiscale Model. Simul.*, 7(3):1387–1404, 2008.

[5] G. Ariel, B. Engquist, and R. Tsai. A multiscale method for highly oscillatory ordinary differential equations with resonance. *Math. Comp.*, 78:929–956, 2009.

[6] G. Ariel, B. Engquist, and R. Tsai. A reversible multiscale integration method. *Comm. Math. Sci.*, 7:595–610, 2009.

[7] G. Ariel, B. Engquist, and R. Tsai. Oscillatory systems with three separated time scales – analysis and computation. In *Numerical analysis of multi scale*

computations, volume 82 of *Lect. Notes Comput. Sci. Eng.*, pages 23–45. Springer, Berlin, 2011.

[8] G. Ariel and E. Vanden-Eijnden. Accelerated simulation of a heavy particle in a gas of elastic spheres. *Multiscale Model. Simul.*, 7(1):349–361, 2008.

[9] A. Armaou and I. G. Kevrekidis. Equation-free optimal switching policies for bistable reacting systems. *Internat. J. Robust Nonlinear Control*, 15(15):713–726, 2005.

[10] V. I. Arnold, V. V. Kozlov, and A. I. Neishtadt. *Mathematical aspects of classical and celestial mechanics*, volume 3 of *Encyclopaedia of Mathematical Sciences*. Springer-Verlag, Berlin, third edition, 2006. [Dynamical systems. III], Translated from the Russian original by E. Khukhro.

[11] V.I. Arnol'd. *Mathematical methods of classical mechanics*. Springer-Verlag, New York, 1989.

[12] Z. Artstein. A young measures approach to averaging. in differential equations, chaos and variational problems. volume 75 of *Progress in Nonlinear Differential Equations and Their Applications*, pages 15–28. Birkhüser Verlag, Basel, 2007.

[13] Z Artstein, J. Linshiz, and E. S. Titi. Young measure approach to computing slowly advancing fast oscillations. *Multiscale Model. Simul.*, 6(4):1085–1097, 2007.

[14] M. Avellaneda. Iterated homogenization, differential effective medium theory and applications. *Comm. Pure Applied Math.*, 150:527–554, 1987.

[15] J. Avigad, P. Gerhardy, and H. Towsner. Local stability of ergodic averages. *Trans. Amer. Math. Soc.*, 362(1):261–288, 2010.

[16] D. Bambusi and A. Ponno. On metastability in FPU. *Comm. Math. Phys.*, 264(2):539–561, 2006.

[17] D. Bambusi and A. Ponno. Resonance, metastability and blow up in FPU. In *The Fermi-Pasta-Ulam problem*, volume 728 of *Lecture Notes in Phys.*, pages 191–205. Springer, Berlin, 2008.

[18] G. Benettin and A. Ponno. On the numerical integration of fpu-like systems. *Physica D: Nonlinear Phenomena*, 240(7):568–573, 2011.

[19] A. Bensoussan, J.L. Lions, and G. Papanicolaou. *Asymptotic Analysis for Periodic Structures*, volume 5 of *Studies in mathematics and its applications*. North-Holland, Amsterdam, New York, Oxford, 1978.

[20] N. N. Bogoliubov and Yu. A. Mitropolski. *Asymptotic Methods in the Theory of Nonlinear Oscillations*. Gordon and Breach, New York, 1961.

[21] S. D. Bond and B. J. Leimkuhler. Molecular dynamics and the accuracy of numerically computed averages. *Acta Numer.*, 16:1–65, 2007.

[22] A. Braides and D. Lukkassen. Reiterated homogenization of integral functionals. *Mathematical Models and Methods in Applied Sciences*, 10(01):47–71, February 2000.

[23] I. Bright. Tight estimates for general averaging applied to almost-periodic differential equations. *J. Diff. Eqn.*, 246:2922–2937, 2009.

[24] Y. Cao, D.T. Gillespie, and L.R. Petzold. The slow-scale stochastic simulation algorithm. *J. Chem. Phys.*, 122:014116, 2005.

[25] J. Chu, B. Engquist, M. Prodanovic, and R. Tsai. A multiscale method coupling network and continuum models in porous media I – single phase flow. *Under review*, 2011.

[26] J. Chu, B. Engquist, M. Prodanovic, and R. Tsai. A multiscale method coupling network and continuum models in porous media II – single and two phase phase flow. *Under review*, 2011.

[27] D. Cohen, T. Jahnke, K. Lorenz, and C. Lubich. Numerical integrators for highly oscillatory hamiltonian systems: A review. In *Analysis, Modeling and Simulation of Multiscale Problems*, pages 553–576. Springer Berlin Heidelberg, 2006.

[28] M. Condon, A. Deaño, and A. Iserles. On second-order differential equations with highly oscillatory forcing terms. *Proc. R. Soc. Lond. Ser. A Math. Phys. Eng. Sci.*, 466(2118):1809–1828, 2010.

[29] M. Dellnitz and O. Junge. On the approximation of complicated dynamical behavior. *SIAM J. Numer. Anal.*, 36(2):491–515, 1999.

[30] P. Deuflhard. A study of extrapolation methods based on multistep schemes without parasitic solutions. *Z. Angew. Math. Phys.*, 30(2):177–189, 1979.

[31] J. Ding, Q. Du, and T. Y. Li. High order approximation of the Frobenius-Perron operator. *Appl. Math. Comput.*, 53(2-3):151–171, 1993.

[32] J. Ding and A. Zhou. Finite approximations of Frobenius-Perron operators. A solution of Ulam's conjecture to multi-dimensional transformations. *Phys. D*, 92(1-2):61–68, 1996.

[33] J. R. Dorfman. *An introduction to chaos in nonequilibrium statistical mechanics*, volume 14 of *Cambridge Lecture Notes in Physics*. Cambridge University Press, Cambridge, 1999.

[34] W. E. Analysis of the heterogeneous multiscale method for ordinary differential equations. *Commun. Math. Sci.*, 1(3):423–436, 2003.

[35] W. E. *Principles of multiscale modeling*. Cambridge University Press, Cambridge, UK, 2011.

[36] W. E, B. Engquist, X. Li, W. Ren, and E. Vanden-Eijnden. Heterogeneous multiscale methods: A review. *Comm. Comput. Phys.*, 2:367–450, 2007.

[37] W. E, D. Liu, and E. Vanden-Eijnden. Analysis of multiscale methods for stochastic differential equations. *Commun. on Pure and Applied Math.*, 58:1544–1585, 2005.

[38] W. E, D. Liu, and E. Vanden-Eijnden. Nested stochastic simulation algorithms for chemical kinetic systems with multiple time scales. *J. Comput. Phys.*, 221:158–180, 2007.

[39] W. E, W. Ren, and E. Vanden-Eijnden. A general strategy for designing seamless multiscale methods. *J. Comput. Phys.*, 228(15):5437–5453, 2009.

[40] B. Engquist, A. Fokas, E. Hairer, and A. Iserles, editors. *Highly Oscillatory Problems*, volume 366 of *London Mathematical Society Lecture Notes Series*. Cambridge University Press, Cambridge, UK, 2009.

[41] B. Engquist, H. Holst, and O. Runborg. Multi-scale methods for wave propagation in heterogeneous media over long time. In B. Engquist, O. Runborg, and R. Tsai, editors, *Numerical analysis of multiscale computations*, volume 82 of *Lect. Notes Comput. Sci. Eng.* Springer-Verlag, 2011.

[42] B. Engquist and Y.-H. Tsai. Heterogeneous multiscale methods for stiff ordinary differential equations. *Math. Comp.*, 74(252):1707–1742, 2005.

[43] L.C. Evans and D. Gomes. Effective hamiltonians and averaging for hamiltonian dynamics i. *Arch. Rational Mech. Anal.*, 157:1–33, 2001.

[44] L.C. Evans and D. Gomes. Effective hamiltonians and averaging for hamiltonian dynamics ii. *Arch. Rational Mech. Anal.*, 161:271–305, 2002.

[45] I. Fatkullin and E. Vanden-Eijnden. A computational strategy for multiscale chaotic systems with applications to Lorenz 96 model. *J. Comp. Phys.*, 200:605–638, 2004.

[46] E. Fermi, J. Pasta, and S. Ulam. Studies of the nonlinear problems, i. *Los Alamos Report LA-1940*, 1955. Later published in *Collected Papers of Enrico Fermi*, ed. E. Segre, Vol. II (University of Chicago Press, 1965) p.978.

[47] B. García-Archilla, J. M. Sanz-Serna, and R. D. Skeel. Long-time-step methods for oscillatory differential equations. *SIAM J. Sci. Comput.*, 20(3):930–963, 1999.

[48] C. W. Gear and I. G. Kevrekidis. Projective methods for stiff differential equations: problems with gaps in their eigenvalue spectrum. *SIAM J. Sci. Comput.*, 24(4):1091–1106 (electronic), 2003.

[49] C. W. Gear and I. G. Kevrekidis. Projective methods for stiff differential equations: problems with gaps in their eigenvalue spectrum. *SIAM J. Sci. Comput.*, 24(4):1091–1106 (electronic), 2003.

[50] C. W. Gear and I. G. Kevrekidis. Constraint-defined manifolds: a legacy code approach to low-dimensional computation. *J. Sci. Comput.*, 25(1-2):17–28, 2005.

[51] D. Givon, I.G. Kevrekidis, and R. Kupferman. Strong convergence of projective integration schemes for singularly perturbed stochastic differential systems. *Comm. Math. Sci.*, 4:707–729, 2006.

[52] D. Givon, R. Kupferman, and A.M. Stuart. Extracting macroscopic dynamics: model problems and algorithms. *Nonlinearity*, 17:R55–R127, 2004.

[53] V. Guillemin and A. Pollack. *Differential topology*. AMS Chelsea Publishing, Providence, RI, 2010. Reprint of the 1974 original.

[54] E. Hairer and C. Lubich. On the energy distribution in Fermi-Pasta-Ulam lattices. *Arch. Ration. Mech. Anal.*, 205(3):993–1029, 2012.

[55] E. Hairer, C. Lubich, and G. Wanner. *Geometric numerical integration*, volume 31 of *Springer Series in Computational Mathematics*. Springer-Verlag, Berlin, 2002. Structure-preserving algorithms for ordinary differential equations.

[56] E. Hairer, S. P. Nørsett, and G. Wanner. *Solving ordinary differential equations. I*, volume 8 of *Springer Series in Computational Mathematics*. Springer-Verlag, Berlin, second edition, 1993. Nonstiff problems.

[57] E. Hairer and G. Wanner. *Solving ordinary differential equations. II*, volume 14 of *Springer Series in Computational Mathematics*. Springer-Verlag, 1996.

[58] G. Halász. Remarks on the remainder in Birkhoff's ergodic theorem. *Acta Math. Acad. Sci. Hungar.*, 28(3-4):389–395, 1976.

[59] M. Hochbruck and A. Ostermann. Exponential integrators. *Acta Numer.*, 19:209–286, 2010.

[60] A. Holmbon, N. Svanstedt, and N. Wellander. Multiscale convergence and reiterated homogenization of parabolic problems. *Applications of Math.*, 50:131–151, 2005.

[61] F. Y. Hunt. A Monte Carlo approach to the approximation of invariant measures. *Random Comput. Dynam.*, 2(1):111–133, 1994.

[62] A. Iserles, H. Z. Munthe-Kaas, S. P. Nørsett, and A. Zanna. Lie-group methods. In *Acta numerica, 2000*, volume 9 of *Acta Numer.*, pages 215–365.

Cambridge Univ. Press, Cambridge, 2000.

[63] A. Katok and B. Hasselblatt. *Introduction to the modern theory of dynamical systems*, volume 54 of *Encyclopedia of Mathematics and its Applications*. Cambridge University Press, Cambridge, 1995. With a supplementary chapter by Katok and Leonardo Mendoza.

[64] M. Keane, R. Murray, and L.-S. Young. Computing invariant measures for expanding circle maps. *Nonlinearity*, 11(1):27–46, 1998.

[65] J. Kevorkian and J. D. Cole. *Perturbation methods in applied mathematics*, volume 34 of *Applied Mathematical Sciences*. Springer-Verlag, New York, 1981.

[66] J. Kevorkian and J. D. Cole. *Multiple Scale and Singular Perturbation Methods*, volume 114 of *Applied Mathematical Sciences*. Springer-Verlag, New York, Berlin, Heidelberg, 1996.

[67] J. Kevorkian and J. D. Cole. *Multiple scale and singular perturbation methods*, volume 114 of *Applied Mathematical Sciences*. Springer-Verlag, New York, 1996.

[68] I. G. Kevrekidis, C. W. Gear, J. M. Hyman, P. G. Kevrekidis, O. Runborg, and C. Theodoropoulos. Equation-free, coarse-grained multiscale computation: enabling microscopic simulators to perform system-level analysis. *Commun. Math. Sci.*, 1(4):715–762, 2003.

[69] Y. Kifer. Random perturbations of dynamical systems. volume 16 of *Progress in Probability and Statistics*. Birkhüser Boston Inc., Boston, 1988.

[70] H.-O. Kreiss. Problems with different time scales for ordinary differential equations. *SIAM J. Numer. Anal.*, 16(6):980–998, 1979.

[71] H.-O. Kreiss. Problems with different time scales. In *Acta numerica, 1992*, pages 101–139. Cambridge Univ. Press, 1992.

[72] H.-O. Kreiss and J. Lorenz. Manifolds of slow solutions for highly oscillatory problems. *Indiana Univ. Math. J.*, 42(4):1169–1191, 1993.

[73] U. Krengel. On the speed of convergence in the ergodic theorem. *Monatsh. Math.*, 86(1):3–6, 1978/79.

[74] U. Krengel. *Ergodic theorems*, volume 6 of *de Gruyter Studies in Mathematics*. Walter de Gruyter & Co., Berlin, 1985. With a supplement by Antoine Brunel.

[75] M. Krupa, N. Popović, and N. Kopell. Mixed-mode oscillations in three time-scale systems: a prototypical example. *SIAM J. Appl. Dyn. Syst.*, 7(2):361–420, 2008.

[76] J. D. Lambert. *Numerical methods for ordinary differential systems*. John Wiley & Sons Ltd., Chichester, 1991. The initial value problem.

[77] A. Lasota and M. C. Mackey. *Chaos, fractals, and noise*, volume 97 of *Applied Mathematical Sciences*. Springer-Verlag, New York, second edition, 1994. Stochastic aspects of dynamics.

[78] B. Leimkuhler and S. Reich. *Simulating Hamiltonian dynamics*, volume 14 of *Cambridge Monographs on Applied and Computational Mathematics*. Cambridge University Press, Cambridge, 2004.

[79] B. Leimkuhler and S. Reich. *Simulating Hamiltonian dynamics*, volume 14 of *Cambridge Monographs on Applied and Computational Mathematics*. Cambridge University Press, Cambridge, 2004.

[80] P. Lochak and C. Meunier. *Multiphase averaging for classical systems*, volume 72 of *Applied Mathematical Sciences*. Springer-Verlag, New York, 1988. With applications to adiabatic theorems, Translated from the French by H. S. Dumas.

[81] D. Lukkassen and G.W. Milton. On hierarchical structures and reiterated homogenization. In *Function spaces, interpolation theory and related topic*, pages 355–368. de Gruyter, Berlin, 2002.

[82] A.M. Majda, I. Timofeyev, and E. Vanden-Eijnden. Stochastic models for selected slow variables in large deterministic systems. *Nonlinearity*, 19:769–794, 2006.

[83] J.E. Marsden and M. West. Discrete mechanics and variational integrators. *Acta Numerica*, pages 357–514, 2001.

[84] I. Melbourne and A. M. Stuart. A note on diffusion limits of chaotic skew product flows. *Nonlinearity*, 24:1361, 2011.

[85] C. Meyer. *Matrix analysis and applied linear algebra.* Society for Industrial and Applied Mathematics (SIAM), Philadelphia, PA, 2000.

[86] J. A. Murdock. *Perturbations: Theory and Methods.* A Wiley-Interscience Publication. John Wiley & Sons Inc., New York, 1991.

[87] J.A. Murdock. *Perturbations. Theorey and methods.* Wiley-Interscience, New York, 1991.

[88] A. Nazin and B. Polyak. Adaptive randomized algorithm for finding eigenvector of stochastic matrix with application to pagerank. In *Decision and Control, 2009 held jointly with the 2009 28th Chinese Control Conference. CDC/CCC 2009. Proceedings of the 48th IEEE Conference on*, pages 127–132, 2009.

[89] G. Papanicolaou. Introduction to the asymptotic analysis of stochastic equations. In *Modern modeling of continuum phenomena*, volume 16 of *Lectures in Applied Mathematics*, pages 47–109. Amer. Math. Soc., Providence, RI, 1977.

[90] G. A. Pavliotis and A. M. Stuart. *Multiscale methods*, volume 53 of *Texts in Applied Mathematics.* Springer, New York, 2008. Averaging and homogenization.

[91] G. A. Pavliotis and A. M. Stuart. *Multiscale Methods: Averaging and Homogenization.* Number 53 in Texts in Applied Mathematics. Springer-Verlag, New York, 2008.

[92] L. R. Petzold, L. O. Jay, and J. Yen. Numerical solution of highly oscillatory ordinary differential equations. In *Acta numerica, 1997*, volume 6 of *Acta Numer.*, pages 437–483. Cambridge Univ. Press, Cambridge, 1997.

[93] J. A. Sanders and F. Verhulst. *Averaging Methods in Nonlinear Dynamical Systems*, volume 59 of *Applied Mathematical Sciences*. Springer-Verlag, New York, Berlin, Heidelberg, Tokyo, 1985.

[94] J. M. Sanz-Serna. Modulated fourier expansions and heterogeneous multiscale methods. *IMA J. Numer. Anal.* to appear.

[95] J. M. Sanz-Serna and M. P. Calvo. *Numerical Hamiltonian problems*, volume 7 of *Applied Mathematics and Mathematical Computation*. Chapman & Hall, London, 1994.

[96] Z. Schuss. *Theory and applications of stochastic processes*, volume 170 of *Applied Mathematical Sciences*. Springer, New York, 2010. An analytical approach.

[97] R. Sharp, Y.-H. Tsai, and B. Engquist. Multiple time scale numerical methods for the inverted pendulum problem. In *Multiscale methods in science and engineering*, volume 44 of *Lect. Notes Comput. Sci. Eng.*, pages 241–261. Springer, Berlin, 2005.

[98] M. Tao, H. Owhadi, and J Marsden. Nonintrusive and structure preserving multiscale integration of stiff odes, sdes, and hamiltonian systems with hidden slow dynamics via flow averaging. *Multi. Model. Simul.*, 8:1269–1324, 2010.

[99] M. Tao, H. Owhadi, and J. E. Marsden. Nonintrusive and structure preserving multiscale integration of stiff ODEs, SDEs, and Hamiltonian systems with hidden slow dynamics via flow averaging. *Multiscale Model. Simul.*, 8(4):1269–1324, 2010.

[100] A.H.P. van der Burgh. On the higher order asymptotic approximations for the solutions of the equations of motion of an elastic pendulum. *J. of Sound and Vibrations*, 42:463–475, 1975.

[101] E. Vanden-Eijnden. Numerical techniques for multi-scale dynamical systems with stochastic effects. *Comm. Math. Sci.*, 1:385–391, 2003.

[102] P. Walters. *An Introduction to Ergodic Theory.* Number 79 in Graduate Texts in Mathematics. Springer, October 2000.

Vita

Seong Jun Kim was born in Seoul, South Korea on June 30, 1984. He graduated from Chungnam Science High School in 2002, and received a Bachelor of Science degree in Applied Mathematics from the Korea Advanced Institute of Science and Technology in 2006. Before he entered the Mathematics Ph.D. program at the University of Texas at Austin in 2008, he fulfilled his mandatory two-year military service duty in the Korean Augmentation To the United States Army.

Email address: skim at math.utexas.edu

This dissertation was typeset with LaTeX[†] by the author.

[†]LaTeX is a document preparation system developed by Leslie Lamport as a special version of Donald Knuth's TeX Program.